SUPPORTED METAL CATALYSTS FOR THE PREFERENTIAL OXIDATION OF CARBON MONOXIDE AND PARTIAL OXIDATION OF METHANE

A THESIS

SUBMITTED TO THE

UNIVERSITY OF PUNE

FOR THE DEGREE OF

DOCTOR OF PHILOSOPHY

IN CHEMISTRY

BY

SACHIN S. MALWADKAR

CATALYSIS AND INORGANIC DIVISION

NATIONAL CHEMICAL LABORATORY

PUNE - 411008

INDIA

Dr. C. V. V. SATYANARAYANA

(RESEARCH GUIDE)

MARCH 2008

...Dedicated to
My Beloved Mother...

"Experiments are the only means of knowledge at our disposal. The rest is poetry, imagination."

Max Planck

CERTIFICATE

Certified that the work incorporated in the thesis

"Supported metal catalysts for the preferential oxidation of carbon monoxide and partial oxidation of methane"

submitted by **Mr. Sachin S. Malwadkar**, for the Degree of **Doctor of Philosophy**, was carried out by the candidate under my supervision in the Catalysis Division, National Chemical Laboratory, Pune – 411 008, India. Materials obtained from other sources have been duly acknowledged in the thesis.

Dr. C.V.V. Satyanarayana

(Research Supervisor)

DECLARATION BY RESEARCH SCHOLAR

I hereby declare that the thesis entitled "Supported metal catalysts for the preferential oxidation of carbon monoxide and partial oxidation of methane" submitted for the Degree of Doctor of Philosophy in chemistry to the University of Pune, has been carried out by me at the Catalysis and Inorganic Chemistry Division, National Chemical Laboratory, Pune – 411 008, India, under the supervision of Dr. C. V. V. Satyanarayana. The work is original and has not been submitted in part or full by me for any other degree or diploma to this or any other University.

Date:

Sachin S. Malwadkar
Catalysis and Inorganic Chemistry Division
National Chemical Laboratory
Pune - 411008
India.

… ACKNOWLEDGEMENTS…

It gives me great pleasure to express my heartfelt gratitude to my research supervisor, ***Dr. Satyanarayana Chilukuri,*** *for his unending support and invaluable guidance throughout the period of this investigation. I sincerely thank him for the care and affection that I received from him in the entire period.*

I take this opportunity to express my deepest sense of gratitude towards Dr. B. S Rao, Dr. Anil Kinage, Dr. S. P. Mirajkar, Ms. Violet Samuel, Mr. S. C. Jha Dr. S. Umbarkar, Mr. V. V. Bokade and Dr. Nandini Devi for their timely help, constant support and valuable guidance during the entire period.

I am very much grateful, Head, Catalysis and Inorganic Chemistry Division, NCL, who is very kind and generous and the help I received from him is gratefully acknowledged.

I express my gratitude to Dr. S. Siva Sankar, Dr. A. V. Ramaswamy and Dr. Rajiv Kumar former HOD's of the Catalysis Division for their support and help during the period of my research work.

I would like to thank Dr. S. B. Halligudi, Dr. Veda Ramaswamy, Dr. T. Raja, Dr. Manikandan, Ms. Agashe, Mrs. Nalini Jacob and Dr. Belhekar for their valuable help and cooperation given to me in completing my research work successfully. I am also grateful to Mr. Ramkrisna Gholap and Mr. Shriniwas Dev, Mr. A. B. Gaikwad (CMC, NCL) for his generous help in carrying out my research studies.

I also thank Dr. Selvaraj, Dr. R. A. Shaikh Mr. Purushotham for their help on various occasions. I would like to acknowledge the help recieved from Mr. Madhu, Mr. Milind and Mr. Katti.

I sincerely thank my labmates Ganesh, Koteswar rao, Sivaram, Satyanarayana Reddy, Shivanand, Shiju, Thomas, Anjali, Richa, Pravin, Reji, Atul, Pankaj, Rituraj, Sebastian, Upendra and Praful for their friendly help and kind cooperation during the period of my work. I also thank all my friends in the division Pallavi, Devendra, Maitri, Trupti, Lakhi, Mahesh, Atul, Rohit, Ankush, Ganpati and Shankar in NCL for their help and support in one way or other, which made my work much easier. I specially thank all my friends Shekhar, Manish, Sanjay, Sharad, Dushant, Bhalchandra, Bhaskar, Santosh,

Prashant, Sudhir and Devidas many of them are abroad now, for their love, support and help. They made my life in NCL enjoyble and lively.

I would like to thank all my teachers for the love and encouragement that I received from them. I would like to acknowledge specially my teachers at B.Sc level, who really created interest in Chemistry in me. Also I thank all well-wishers and friends whose names are not mentioned here.

I specially thank my professors, in the Department of Chemistry, University of Kohlaapur and University of Pune who really shaped my curiosity towards research. I take this opportunity to express my gratitude to Prof. Maldar, Dr. Lonikar, Dr. More, Dr. Suresh Waghmode and Prof. Nikumbh. I also thank my M. Sc friends who really made my life memorable in Solapur.

I am sure that this work would not have been completed successfully without the support of my near and dear friends and well-wishers at various stages of my life. I thank Prashant, Jayprakash, Sanjay, Mangesh and Sujit.

I would like to thank Director, NCL for allowing me to carryout the research work at NCL. I thank CSIR, New Delhi, India, for the financial support in the form of senior research fellowships.

Words are not enough to express my love and gratitude to my family members. It is their love, blessings and prayers that helped me throughout my life. I am very much indebted to them. I specially thank my brothers Amarjeet, Ambadas, Avinash, Abhijeet, Rahul and sisters Ashwini, Rupali, Dipali, Vandana, Uma and Aaprna for their cooperation during my research work and writing this thesis.

Above all, I thank God for his blessings, for forgiving my mistakes, for leading me in the right path and for being there whenever I needed.

Sachin S. Malwadkar

CONTENTS

LIST OF FIGURE

Chapter - 4

Chapter – 5

LIST OF TABLES

LIST OF ABBREVIATIONS

BE	**Binding energy**
B/L ratio	**Bronsted to Lewis acidity ratio**
BET	**Brunauer-Emmett-Teller**
CT	**Charge transfer**
DRS	**Diffuse reflectance spectroscopy**
FID	**Flame ionization detector**
FWHM	**Full width at half maximum**
FTIR	**Fourier transform infrared**
GHSV	**Gas hour space velocity**
GC	**Gas chromatography**
HRTEM	**High resolution transmission electron microscopy**
ICP-AES	**Inductively coupled plasma atomic emission spectroscopy**
I.D.	**Internal diameter**
LRS	**Laser Raman spectroscopy**
MFC	**Mass flow control**
PID	**Proportional integral derivative**
PrOx	**Preferential oxidation**
POx	**Partial oxidation**
P-IR	**Pyridine infrared**
P-XRD	**Powder X-ray diffraction**
PGM	**Platinum group metal**
RWGS	**Reverse water gas shift**
SEM	**Scanning electron microscopy**
SAED	**Selected area electron diffraction**
TEM	**Transmission electron microscopy**
TPD	**Temperature programmed desorption**
TPR	**Temperature programmed reduction**
TOS	**Time on stream**
TCD	**Thermal conductivity detector**
WGSR	**Water gas shift reaction**
XPS	**X-ray photoelectron spectroscopy**

Chapter - 1

INTRODUCTION AND LITERATURE SURVEY

1.1. SUPPORTED METAL OXIDE CATALYSTS IN HETEROGENEOUS CATALYSIS

1.1.1. Introduction

Transportation fuels, petrochemicals, bulk chemicals, lubricants, chlorine-free refrigerants, high-strength polymers, plastics, removal of the pollutants emitted from various sources and many thousands of other products required by modern societies would not be possible without the help of catalysts and catalysis technologies. Human body even depends on catalysts for its functioning and growth. Catalyst is a compound, which alters the rate of a chemical reaction, but neither consumed nor chemically changed at the end of reaction. This definition allows for the possibility that small amount of the catalyst may be lost in the reaction or that the catalytic activity may slow down. However, the catalyst affects only the rate of the reaction, but does not change the thermodynamics of the reaction or the equilibrium composition.

Catalysis is crucial and important for the chemical industry as it enables to produce various products efficiently [1]. The number of catalysts applied in industry is very large and catalysts come in many different forms, heterogeneous catalysts in the form of porous solids to soluble homogeneous catalysts in the liquid reaction mixture to biological catalysts in the form of enzymes.

One of the most challenging in the field of chemical engineering and catalysis is the direct conversion of methane to methanol or other oxygenates like formaldehyde [2]. The reaction products usually comprise of CO, CO_2, and H_2O with only trace amounts of CH_3OH and CH_2O. The later two form the group of important chemical intermediates used for the production of industrial chemicals.

There are many new catalysts, which have been discovered and broadly classified either into homogeneous or heterogeneous catalysis systems. Though homogeneous catalyst systems possess several advantages such as better selectivity, activity and reproducibility, they are associated with several drawbacks like low thermal stability, recovery, recyclability and short catalyst lifetime [3]. Hence, finding heterogeneous catalyst systems to replace the existing homogeneous ones has become a challenging task in the field of catalysis.

1.1.2. Heterogeneous catalysis

Heterogeneous catalysis is crucial to chemical technology. Innumerable reactions are facilitated through heterogeneous catalysis. Chemical bonds are broken and new chemical bonds are formed during the catalytic process, usually without significant changes in the catalyst. These are most commonly modeled as surface reactions with adsorption and desorption as additional steps. The first industrially important heterogeneous catalytic process introduced in 1875, used platinum to oxidize SO_2 to SO_3, for the synthesis of sulfuric acid [4]. Heterogeneous catalysis is gaining increasing importance in the production of fine chemicals and pharmaceuticals due to its definite advantages, like enhanced production processes, competitiveness and economics. The main advantage of a heterogeneous catalytic process is that it can be operated continuously in a reactor for long duration, at times up to few years. Since the catalyst is present in a phase different from that of reactants and the products, the separation of the catalyst from the final reaction mass is quite easy.

Inorganic oxides and zeolites play extremely important role in heterogeneous catalysis. The article entitled "Heterogeneous Base Catalysis" by H. Hattori provides a review of the development and current understanding of base-catalyzed reaction [5]. Corma et al provided an overview of acid-catalyzed reactions in a review "Inorganic solid acids and their use in acid-catalyzed hydrocarbon reactions" [6].

1.1.3. Oxides

Oxides as catalysts are quite complex since they involve a variety of crystal systems of different compositions with a wide range of physico-chemical properties. They are either poor electrical conductors or good conductors. Insulator oxides are those in which the cationic material has a single oxidation state, so they have stoichiometric M: O ratios. The simple oxides, MgO, Al_2O_3 and SiO_2 and the more complex zeolites, which are aluminosilicates, fall into this category. These materials are not effective as oxidation catalysts, but mostly useful as solid acids or bases [5, 7]. Semiconductor and conducting oxides are most commonly used in oxidations. They are materials in which the metal ion species is relatively easily switched between two different valence states. There can be two or more different oxidation states under reaction conditions as in Fe_2O_3, V_2O_5, TiO_2, CuO

or NiO, or the interconversion between the positive ion and neutral metal as with the more easily reduced oxides such as ZnO and CdO. Semiconductor oxides can be either n-type (e.g., Fe_2O_3, V_2O_5, TiO_2, CuO etc) or p-type (e.g., NiO, CoO, Cu_2O etc). In general, oxides are prepared as single component or as multiple components; they may be crystalline or amorphous and they may be supported or unsupported. While simple oxides show activity for some oxidations, they are more commonly used as solid acids or bases.

1.1.3.1. Mixed metal oxides

Oxides of two or more different kinds of cations are known as mixed metal oxides. They can be further classified based on whether they are crystalline or amorphous. If the oxides are crystalline, the crystal structure can determine the oxide composition. For instance, perovskites have the general formula ABO_3, scheelites are ABO_4, spinels are AB_2O_4 and palmeirites are $A_3B_2O_8$ [8]. For mixed oxide catalysts it is not always evident which of the constituent elements play a role as active center. Although the industrial catalysts are usually multiphase systems, the presence of one phase, appears usually be indispensable to render the systems active in a given reaction. One of the most important results of the studies on monophasic systems is the demonstration of different catalytic properties of different crystallographic faces in an oxide, which provided an experimental proof for structure sensitivity phenomenon in the oxide systems. For mixed oxide catalysts it is not always evident which of the constituent elements play a role of active centers.

Supported metal catalysts: The early concept of support was that of an inert substance, which provide a means of spreading out the expensive catalyst ingredient for its most effective use, or a means of improving the mechanical strength of an inherently weak catalyst. Multiphase catalysts are non-uniform solids at the molecular or crystalline level and usually consist of an active phase dispersed on a carrier support. Most catalysts consist of nanometer-sized particles dispersed on a high-surface-area support. Support plays very important role because metals used in industrial catalysis are often expensive and they are mostly used in a highly dispersed form on a high surface area porous support. Most catalyst supports have pores that allow reactants and products to be transported into and out of the interior volume; the pores provide high-area internal platforms for the metal. Common supports are amorphous metal oxides such as γ-Al_2O_3 and SiO_2. Powders of these

solids consist of particles that are aggregates of small primary particles of the metal oxide, held together by interparticle interactions or sometimes by binders. The surfaces of metal oxide powders are highly nonuniform, exposing faces with various crystal planes and defects. Naphtha reforming catalyst, platinum - rhenium on γ-Al_2O_3 is a classic example of this kind. In the case of catalyst for oxidation reaction the metal is highly dispersed on the support, in aggregates so small that many or most of the atoms are present on the surface. The relative rates of parallel or sequential reactions are affected by the number and arrangement of the sites on the catalyst. These in turn may be affected by the particle size, crystal imperfection and blockage of some of the sites by deliberately added poisons.

1.1.3.2. Acid-base and redox properties of metal oxides

The exposed cations and anions on oxide surfaces have been described as acid-base site pairs [9]. In metal oxide systems, oxide ions act as Lewis base site and metal cations as Lewis acid sites. Hydroxyl groups bound at certain oxide surfaces may exhibit considerable Brønsted acidity. Strong Brønsted acidity usually arises in mixed oxides rather than pure oxides due to charge imbalance and/or coordination changes occurred due to incorporation of a second cation. Exposed coordinatively unsaturated cations may act as acceptors for free electron pairs of adsorbed species.

The strength of the acid sites in metal oxides depends on the charge and size of the cations, both of which may vary with the oxidation number of the cation. In general, according to the concept of hard and soft acids, cations of higher oxidation are harder. For cations in the same group and of the same oxidation state, those in later period are softer. Harder cations are smaller and polarizable. These will adsorb or bind hard bases stronger than soft or polarisable bases. Surface hydroxyl groups may act as Brønsted acid sites, which may dissociate to protonate-adsorbed bases. The resultant conjugate acid and bases are stabilized on the surface by electrostatic interaction with each other and with oxide. Thus one may expect such surfaces would be active for dissociative adsorption of Bronsted acids.

Redox properties

In catalytic oxidation, oxide catalysts have to undergo oxidation-reduction cycles. In selective oxidation reactions, gaseous oxygen is consumed to form oxygenates. In oxidation reactions, the introduction of oxidant into reactant molecule takes place in two ways. (i) The electrons may be transferred to adsorbed oxygen to form any of the species like O^-, O_2^{2-} and O^{2-} from reduced cations or anion vacancies with trapped electrons. After the incorporation of oxygen in to a product molecule, which is then desorbed, the electrons return to the solid. (ii) Direct incorporation of lattice oxygen of oxide in to product molecule takes place, the site of adsorption of oxide and incorporated lattice oxide into the molecule may be different. The migration of oxide ion between these two sites would occur; this is referred as Mars - van Krevelan mechanism. This mechanism which involves lattice oxide will cause some changes in local structure on the surface of oxide. The cations in metal oxides that undergo redox cycle would change the local cation-anion ratio in the solid. The oxide catalysts must be able to accommodate these changes reversibly and easily. Some of the important factors that influence the redox cycle during the oxidation reactions are metal-oxygen bond strength, presence of cation vacancies, ability to form shear structures, optimal density of active oxygen, acid base properties, electron binding energy of lattice oxygen and crystallographic plane [10]. This thesis is mainly aimed to exploit acid-base and redox properties of mixed metal oxide catalysts for acid-base and redox catalyzed chemical reactions.

1.1.4. Zeolites

1.1.4.1. Zeolites and Historical background

Zeolites offer advantages over conventional catalysts in acid, acid-base, oxidation and reduction reactions. The major properties such as well-defined structure, uniform pores, high thermal stability, high surface area, easy regeneration, well-defined micro-pores etc. make zeolites unique heterogeneous catalysts. Zeolites are crystalline aluminosilicates, with highly ordered structures [11 -18]. They consist of SiO_4 and AlO_4^- tetrahedra, which are interlinked through shared oxygen atoms to give a three dimensional network. They consist of channels and in some cases cavities. The interior of these

channels contain adsorbed water molecules and exchanged alkali metal ions, the latter can be exchanged with other metal cations. These cations compensate for the excess negative charge in the framework resulting from the substitution of aluminum in the lattice. The interior of the pore system, with its atomic-scale dimensions is the active surface of the zeolites. The inner pore structure depends on the zeolite type, composition and the cations. Thus, zeolites are represented by the general formula:

$$\mathbf{M_{y/n}\,[(SiO_2)_x\,(AlO_2)_y].zH_2O}$$

where, M is the charge compensating cation with valency 'n'. While, M represents the exchangeable cation (eg. alkali or alkaline earth metals or organic cations). The ratio x/y may have the value 1 to α. According to Lowenstein's rule no two aluminum tetrahedra can exist adjacent to one another. The Si/Al molar ratio corresponds to the acid sites in the zeolites. **z** represents the number of water molecules, which can be reversibly adsorbed in the pores, while **y** represents the exchange capacity. Zeolites are also popularly known as *'molecular sieve*s' due to their ability to differentiate between molecules of different shapes and size. Zeolites have found widespread application as adsorbents, ion exchange materials, detergent builders and catalysts, especially in petroleum refining, petrochemicals, and as fluidized catalytic cracking catalysts (FCC) [17]. Furthermore, zeolite functionality has also been compared with catalytic antibodies [19] and metalloenzymes [20]. The characteristic features of zeolites, which make them effective catalysts are: High surface area and adsorption properties, active acid sites, shape selectivity (result of uniform pores and channels), easy regeneration, high thermal stability and eco friendliness.

Axel Fr. Cronstedt [21] (1756), a Swedish mineralogist, observed that certain rock minerals, when heated sufficiently, appeared as were boiling. He named them *'zeolite*s' (zeo means to boil and lithos means stone). Damour [22] observed that zeolites could be reversibly dehydrated without changes in the structure or morphology. The role of water as a mineralizing agent, aided by alkaline conditions, drew the attention of mineralogists towards hydrothermal reaction conditions for the synthesis. The first claim, to have synthesized a zeolite named levynite, was made by St. Claire Deville and Thompson in 1862 [23, 24]. In 1962, the commercialization of natural zeolites namely chabazite, erionite, mordenite and clinoptillotite started for a number of applications [25]. McBain

introduced the term *molecular sieve* to describe a class of materials that exhibited selective adsorption properties [26]. Molecular sieves separate components of a mixture on the basis of molecular size and shape differences. However, Barrer [27] was the first to demonstrate the molecular sieve behavior of zeolites and their potential in separation techniques. ZK-5 [28 - 30] was the first known synthetic zeolite (no natural counterpart) crystallized under hydrothermal conditions. Hydrogen forms of zeolites were also made for the first time in the year 1949, by heating ammonium-exchanged forms of mordenite [31].

1.1.4.2. Active Sites: Acidity

Each zeolite type can be easily obtained over a wide range of compositions directly by synthesis and/or after various post synthesis treatments. Moreover, various compounds can be introduced or even synthesized within the zeolite pores (ship in a bottle synthesis).

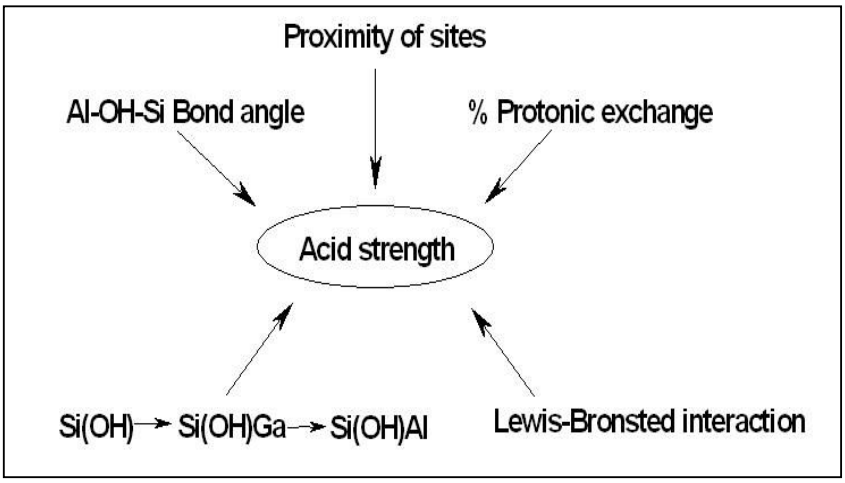

Fig. 1.1: *Parameters determining the acid strength of the zeolite protonic sites*

This explains why zeolites can be used in acid, base, acid-base, redox and bifunctional catalysis. Most of the hydrocarbon reactions as well as many transformations of functionalised compounds are catalysed by protonic sites [32]. In zeolites, they are associated with bridging hydroxyl groups attached to framework oxygens linking tetrahedral Si and Al atoms: (Al (OH) Si). The maximum number of protonic sites is equal to the number of framework aluminium atoms, the actual number being smaller due to limitations in cation exchange, dehydroxylation and dealumination during activation at

high temperatures. The parameters controlling the other features of the protonic sites and particularly their acid strength (Fig. 1.1) have also been assessed in order to design the zeolite catalysts.

The acidity of zeolites is mainly due to the presence of Brönsted acid sites. But, some Lewis acid sites may be present especially when zeolites are treated at high temperature. The measurement of the number, type and strength of acid sites provides the key experimental data regarding zeolite acidity. For a complete characterization of zeolite acidity, it is, therefore, necessary to determine number and strength of both types of acid sites. Several methods have been developed for this purpose, most important among them are

(i) Titration methods
(ii) Adsorption and desorption of bases
(iii) IR spectroscopy of – OH groups
(iv) IR spectroscopy of adsorbed species
(v) NMR spectroscopy of – OH groups
(vi) NMR spectroscopy of adsorbed species

1.1.4.3. Modifications

The use of zeolites can further be enhanced by altering various properties. Zeolites can be modified either by isomorphous substitution, cation exchange, dealumination or silylation.

Isomorphous substitution: Modification of zeolites by isomorphous substitution induces variation in acidic properties and unit cell volume, which may lead to interesting catalytic properties. Goldsmith [33] was the very first to report isomorphous substitution of Si^{4+} by Ge^{4+} in the lattice. This was followed by isomorphous substitution of Si^{4+} or Al^{3+} by elements such as B [34 - 38], Fe [35, 36], Ga [35 - 37], Ti [39], V [40], etc. Barrer [40] classified four types of substitution in zeolites namely, (i) cation exchange, (ii) framework substitution, (iii) isomorphous substitution of isotopes and (iv) substitution of intracrystalline salts and molecular water. Isomorphous substitution can be achieved by direct hydrothermal synthesis or by post synthesis methods.

Cation exchange: The ion exchange capacity of a zeolite is dependent upon the amount of aluminum present in the framework of zeolite. Majority of the zeolites synthesized are in their cationic forms, wherein, positively charged cations neutralize the charge created by the aluminum tetrahedra in the framework. These extra framework cations are exchangeable and the degree of cation exchange depends on the type of cation being exchanged, its size as well as its charge, the nature, size and strength of any cation coordination complex, the temperature of the ion-exchange treatment, the thermal treatment of the parent zeolite before and after exchange, the structural properties of the zeolites and its silica to alumina ratio, the location of the cations in the zeolite structure, the concentration of the cation exchange solution, the prior treatment of the zeolite.

1.1.4.4. Characterization of Zeolites

X-ray powder diffraction and adsorption measurements are very important techniques employed in the zeolite characterization. Infrared spectroscopy, UV-vis, NMR and ESR spectroscopy have also been applied to obtain structural information about zeolites. For modified zeolites, TEM, XPS and other related techniques are applied.

1.1.5. Supported transition metals for selective oxidation

Transition metals are widely used in the field of catalysis due to their high activity. These metals have variable oxidation states, because of difference between (n-1) d and ns orbital is very small and electron from both the energy levels can be used for bonding. And also one of the theories of catalytic activity is based on formation of unstable intermediate compounds. Transition elements on account of variable valances are able to form unstable intermediate compounds. The large-scale selective oxidation processes like epoxidation of ethylene, oxidative dehydrogenation of methanol to formaldehyde are based on heterogeneous metallic catalysis. The reaction temperature for these reaction are moderate, whereas oxidation of NH_3 to NO and CH_4 to synthesis gas requires temperatures higher than 600 ^{0}C and catalyzed by noble metals like Pt or Rh [41]. Among these applications, use of transition metal oxides as catalysts is the most important technology. The activities of oxides or modified zeolites are mainly due to partially coordinated surface atoms, redox nature and average oxidation state of metal on the surface. Surface coordination

environment can be controlled by the choice of crystal plane exposed and by the preparation procedure for materials. In addition to being used as catalysts, transition metals are also applied as important supports and promoters.

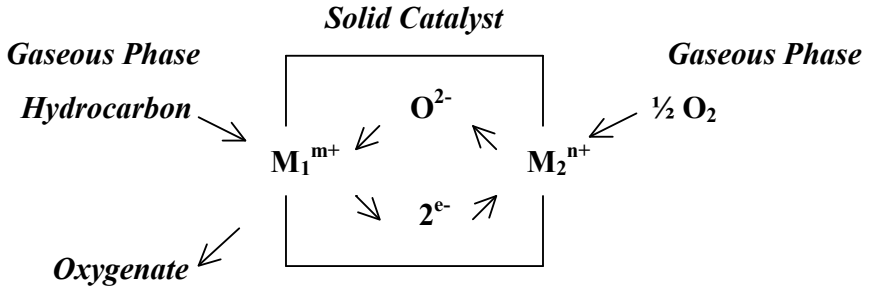

The oxidation reaction in gas phase heterogeneous catalysis according to the redox process usually proceeds via Mars and van Krevelen mechanism. According to this mechanism the substrate is oxidized by the solid and not directly by molecular oxygen of gaseous phase. The role of such dioxygen is to regenerate or maintain the oxidized state of the catalyst. The mechanism involves the presence of two types of distinct active sites; one active site that oxidizes the substrate and another site active for oxygen reduction.

1.1.6. The importance of platinum, molybdenum and copper in catalysis

Platinum:

Platinum-group metals (PGMs) are the chosen catalysts for many modern gas-phase processes, in both the clean production and the clean destruction of chemicals. These metals are inherently stable, even when highly dispersed, and yet they have enough surface reactivity to activate a range of different molecular species. Traditionally used to catalyze single reactions under steady-state conditions, they are increasingly being applied to more complex processes. Their ability to catalyze two energetically opposing reactions means that energy-consuming and energy-wasting processes can be combined in a single efficient reactor. Furthermore, the electronic properties of PGMs can be exploited in M-MO composites, in which the metal does not provide the active sites, but modifies the solid-state chemistry of the metal oxide to make it catalytically productive.

In case of PGM catalysts, a high number of active sites can be created by dispersing the metal on a stable support with high surface area (e.g. Al_2O_3, ZrO_2, SiO_2 or zeolite), which is then dried and heat-treated at a high enough temperature to decompose the metal salt, leaving a uniform covering of nano-sized metallic particles. The durability of the resultant catalyst largely depends on the resilience of the metal particles, particularly to restructuring, sintering, and poisoning.

Platinum catalysts are widely used in reactions like reforming, supported on aluminium oxide together with various promoters to make the catalyst more efficient. It is also widely applied in isomerization, cracking, oxidation of hydrocarbons and in many industrially important reactions.

Molybdenum:

Molybdenum is also a very important metal particularly as oxidation catalyst. Different procedures may be used such as impregnation of oxides or zeolites with molybdate salt or molybdenum chloride or organometallic compounds of Mo like carbonyls on the hydroxyl groups of the support. A parameter important for impregnation is the pH of molybdanate solution. As a matter of fact the following equilibrium has been established:

$$Mo_7O_{24}^{6-} + 4H_2O \leftrightarrow 7MoO_4^{2-} + 8H^+$$

The monomeric tetrahedral MoO_4^{2-} species is favored at higher pH and vice versa for polymeric heptamolybdate anion. Moreover one defines the so-called isoelectric point of support (ieps) or zero point charge (zpc) of support by the pH value for which the surface charge turn from anionic to cationic i.e. will allow cations or anions from the liquid phase to be adsorbed. One has the value of 2 for silica, 5-6 for titania, 8 for allumina etc, clearly shows that the size of adsorbed anion (monomeric or polymeric) adsorbed on support will depends on ieps (zpc) value i.e. on the support itself.

Copper:

Copper is one of the most widely used metals in modern industry as well as for catalysts. It has been the most active transition metal oxides extensively used to catalyze

variety of organic reactions. Copper-chromite catalysts have been used for years in various industrial processes such as partial hydrogenation of vegetable oils and fatty acids as well as decomposition or dehydration of alcohols [42]. These catalysts are utilized in selective hydrogenation reactions due to their capability to hydrogenate carbonyl bonds while leaving unsaturated C = C bonds virtually untouched. The mechanistic studies on copper-chromite catalysts reveal that Cu^{1+} is the active species in various hydrogenation reactions [43]. The copper-zinc-aluminum oxides catalysts are used in many industrial processes including the low-pressure methanol synthesis [44], low-temperature shift reaction [45], dehydration/dehydrogenation of alcohols [46] and for the production of hydrogen from oxidative steam reforming of methanol [47]. Apart from this, it is applied for selective catalytic reduction of nitrogen oxides by hydrocarbons [48], CO oxidation [49] etc.

Despite superior activity of copper catalysts in several chemical reactions, its utility is often limited by rapid deactivation and poor mechanical stability under reaction conditions. One of the probable reasons for deactivation of copper catalyst is sintering due to the low melting point of bulk copper. Thus, instead of bulk copper, supported copper catalysts have been the focus of current research and appropriate support is extremely necessary for distributing copper particles to avoid or, at least, retard the occurrence of sintering. A catalyst support may also serve as an active species in some reacting systems, in addition to playing the role of an inert material for increasing the degree of metal dispersion, promoting thermal stability and for modifying mechanical properties.

1.1.7. Preparation methods in catalysis

Catalytic materials exist in various forms and their preparation involves different protocols with a multitude of preparation schemes. Different methods applied for catalyst manufacture to produce a commercial product which can be used as a stable, active, and selective catalyst, the best preparative solution is sought which results in sufficiently high surface area, good porosity, and suitable mechanical strength [50, 51]

Some of the most important common preparation techniques along with their advantages and disadvantages will be discussed briefly in this section.

1.1.7.1. Co-precipitation

A scientific approach to the preparation of catalysts by precipitation route was introduced by Marcilly [52, 53]. The formation of the precipitate from a homogeneous liquid phase may occur as a result of physical transformations (change of temperature or of solvent, solvent evaporation) but most often is by chemical processes (addition of bases or acids, use of complex forming agents). In almost all cases, the formation of a new solid phase in a liquid medium results from two elementary processes which occur simultaneously or sequentially: (1) nucleation, i.e., formation of the smallest elementary particles of the new phase which are stable under the precipitation conditions; and (2) growth or agglomeration of the particles. Marcilly stressed the importance of supersaturation, among other factors such as pH, temperature, nature of reagents, presence of impurities, and method of precipitation in determining the morphology, the texture and the structure of the precipitates. For example, under conditions of high supersaturation, the rate of nucleation of solid particles is much higher than the rate of crystal growth and leads to the formation of numerous but very small particles. Under the condition when the critical nucleation size is very small, only a metastable and poorly organized phase can develop; this may further change to a more stable phase during the hydrothermal treatment of the precipitates.

In the synthesis of multicomponent systems, the problems are even more complex. Co-precipitation rarely allows one to obtain good macroscopic homogeneity. In a system with two or more metallic compounds, the composition of the precipitate depends on the differences in solubility between the components and the chemistry occurring during precipitation. Generally, under the conditions of either a slow precipitation rate or poor mixing within the reaction medium, co-precipitation is selective and the coprecipitate is heterogeneous in composition. The formations of the coprecipitate followed by hydrothermal treatments are used to transform amorphous precipitates to crystalline materials with improved thermal stability to prepare molecular sieves [54].

1.1.7.2. Ion exchange

The method of ion exchange allows for the introduction, in a controlled way, of a precursor from aqueous solution onto the support. The term ion exchange has been used to

describe all processes where ionic species from aqueous solution are attracted electrostatically by charged sites on the support surface. Catalyst systems, which require charge compensating ions that received the most attention as versatile materials suitable for ion exchange include zeolites, cationic clays, and layered double hydroxides. These are ideal ion exchangers because the crystalline lattice bears electric charges. Zeolites are cationic exchangers. They combine the unique features of high ion exchange capacity, crystalline structure, and uniform pore sizes. The catalytic properties of noble and transition metals and steric constraints imposed by the zeolite structure have provided a strong incentive for developing reliable procedures to prepare highly selective supported-metal catalysts with narrow particle size distributions [55]. Preparation of zeolite-supported metals by ion exchange [56] involves the exchange of complex amine cations of Pt or Pd with K^+, Na^+, or NH_4^+ ions:

$$Pt(NH_3)_4{}^{2+}{}_{(aq)} + 2Cl^-{}_{(aq)} + Na^+{}_{Zeol} \leftrightarrow 2Na^+{}_{(aq)} + Cl^-{}_{(aq)} + Pt(NH_3)_4{}^{2+}{}_{Zeol}$$

Na^+ and $C1^-$ are removed by filtration and washing. On the other hand, if incipient wetness impregnation is employed, these ions remain in the zeolite. The next step is the destruction of the NH_3 ligands by calcination, which produces PtO particles and Pt^{2+} ions, coordinated to zeolite walls whereas an unknown distribution of Pt^{4+} and Pt^{2+} is obtained by incipient wetness [57]. Complications arise from side phenomena, which accompany the calcination and reduction step [56, 58, 59] migration of metal ions into smaller zeolite cages leading to their reduction at higher temperatures, causing agglomeration of larger particles. Proton generation during metal reduction changes the acidity of the catalyst. These undesired processes can be controlled by reduction of zeolite-encaged Co^{2+}, Ni^{2+}, and Fe^{2+} in the presence of noble metal (Pd, Pt). Alloy particles encaged in NaY zeolite were obtained after simultaneous ion exchange with $Pd(NH_3)_4{}^{2+}$ and Ni^{2+}. Blocking small size channels with less reducible, high charge density ions (Ca^{2+}, Sr^{2+}, Mn^{2+}) forces Co^{2+} and Ni^{2+} to remain in super cage [60, 61].

1.1.7.3. Impregnation

Impregnation is the simplest and widely used preparation technique for the preparation of catalysts. The mounting of dissolved aqueous precursors on oxide or zeolite

supports is generally called impregnation method. This term denotes a procedure whereby a certain volume of solution containing the precursor of the active element of the catalyst is contacted with the solid support. If the volume of solution either equals or is less than the pore volume of the support, the technique is referred to as incipient wetness [62]. In the wet impregnation technique (also called soaking or dipping), an excess of solution is used. After a certain time, the solid is separated from solution, and the excess solvent is removed by drying [63 - 67]. Depending on the nature of the required finished catalyst, the impregnated support may or may not be calcined further.

1.1.7.4. Deposition precipitation

This method can provide a well-dispersed and homogeneous active precursor even for the high metal content [68, 69]. This method found its greatest utility when applied either for deposition of nicke1 [68 - 71] or copper [72 - 75] on either alumina, ceria or silica. The chemical processes occurring involve a reactant, which transforms the catalyst precursor into an insoluble form, which is generated slowly in solution, and its concentration is raised homogeneously. When nucleation first occurs, the precipitate is deposited exclusively (adsorbed) onto the support. It would appear that, of the techniques discussed above, incipient wetness impregnation and deposition-precipitation are specific for systems with weak interaction or without any interaction at all between precursor and support. Changes in metal concentration, pH and precipitating agent dramatically affected the dispersion of metal. For example with reagents such as $Ni(NO_3)_2$, an increase in solution concentration decreases the pH which influence the dissolution of the support [76] In this system, the metal dispersion and the partitioning between surface Ni and Ni incorporated depended on the crystallinity of the support, a factor which determines its dissolution properties [77]. When there is weak or no interaction between the precursor and the support, and when washing step after deposition is not used, the result is that the counter ions introduced with the main component remain in the catalyst and can take part in unwanted physico-chemical processes. During drying, catalyst redistribution may occur within the pore network of the support. Calcination is usually required in order to transform the metal salt into oxide, and this is sometimes accompanied by chemical bonding at the oxide/support interface.

1.1.7.5 Sol-gel

The sol-gel method is a homogeneous process, which results in a continuous transformation of solution into a hydrated solid precursor (hydrogel). Sol-gel methods have been recognized for their versatility, which allows control of the texture, composition, homogeneity and structural properties of the finished solids. The applications of catalysts prepared by the sol-gel method were reviewed [78 - 81]. The method is based on the hydrolysis and gelation (for instance by controlled addition of water) of alkoxides or other reactive compounds in alcoholic solution [82, 83]. The chemistry of the processes, that occur during the formation of porous structure are controlled by changing of various parameters during preparation, such as pH, solvent and amount of water added for reaction.
Hydrolysis (hydroxylation) of the metal alkoxides

$$M\text{-}OR + H_2O \rightarrow M\text{-}OH + R\text{-}OH \quad (M = \text{metal or Si; } R = \text{alkyl})$$

Olation (condensation with formation of hydroxy bridges)

$$M\text{-}OH + M\text{-}OHX \rightarrow M\text{-}OH\text{-}M + X\text{-}OH \ (X = H \text{ or } R)$$

Oxolation (condensation with formation of oxygen bridges)

$$M\text{-}OH + M\text{-}OX \rightarrow M\text{-}O\text{-}M + X\text{-}OH \ (X = H \text{ or } R)$$

1.2. PREFERENTIAL OXIDATION (PrOx) OF CO IN H_2 RICH STREAM

1.2.1. Introduction to fuel cells

The developments leading to an operational fuel cell can be traced back to the early 1800's with Sir William Grove recognized as the discoverer in 1839. Throughout the remainder of the century, scientists attempted to develop fuel cells using various fuels and electrolytes. Further work in the first half of the 20th century served as the foundation for systems eventually used in the Gemini and Apollo space flights. Fuel cell systems are usually compared to internal combustion engines and batteries and offer unique advantages as well as disadvantages with respect to them. Fuel cells do not require recharging. Rather, fuel cell systems must be re-fueled, which is faster than charging a battery and can provide greater range depending on the size of the storage tank

A fuel cell is an energy conversion device that converts the chemical energy of a fuel into electricity without any intermediate thermal or mechanical processes. The basic

physical structure or building block of a fuel cell consists of an electrolyte layer in contact with a porous anode (H_2) and cathode (air) on either side. In a typical fuel cell, gaseous fuels are continuously fed to the anode compartment and an oxidant (i.e., O_2 from air) is fed continuously to the cathode compartment; the electrochemical reactions take place at the electrodes to produce an electric current [84].

In the hydrogen case, the electrochemical oxidation can be simply written as, assuming an acidic electrolyte.

$$H_2 \rightarrow 2H^+ + 2\,e^-$$

The electron flows through the external circuit, while proton sustains the current in solution. At cathode electrons and protons combine again with oxidizing agent (oxygen in air). The reduction reaction can be written as

$$O_2 + 4H^+ + 4e^- \rightarrow 2H_2O$$

The overall reaction, $2H_2 + O_2 \rightarrow 2H_2O$, corresponds exactly to the direct combustion of hydrogen.

Fuel cells are a viable alternative for clean energy generation [85 - 87]. At present the major commercial markets are in residential applications and public/private transportation. A variety of applications for fuel cell technology range from portable/micro power and transportation [88 - 91]. A variety of fuel cells for different applications are under development [92 - 95], these types mainly depend on the electrolyte used and the operating temperature of fuel cell. In short they are discussed below:

	Type of fuel cell	Electrolyte	Operating Temperature (^{0}C)
1	Alkaline fuel cell (AFC)	Potassium hydroxide	50 - 90
2	Polymer electrolyte membrane fuel cell (PEMFC)	Proton conducting polymer	70 - 80
3	Phosperic acid fuel cell (PAFC)	Orthophosperic acid	180 - 200
4	Molten carbonate fuel cell (MCFC)	Li/K carbonate mixture	600 - 650
5	Solid oxide fuel cell (SOFC)	Stabilized zirconia	800 - 1000
6	Direct methanol fuel cell (DMFC)	H_2SO_4/Solid polymer	50 - 120

PEMFC is one of the promising candidate, as it can be applied for stationary as well as mobile applications. It works at low temperatures and tolerant to CO_2. Absence of solution phase electrodes compared to AFC and PAFC, which reduce the complicity and also corrosion. These factors promote the use of air as oxidant and various reformates as fuel. It operates at low temperature, which simplifies material issues, facilitates quick start up and safe operation. The only disadvantage is that it does not tolerate CO. It needs H_2 that is free from CO. For this purpose hydrocarbon has to be reformed and the reformate has to processed through water gas shift (WGS) and preferential oxidation (PrOx) steps.

1.2.1.1. Reforming:

Hydrogen is an attractive fuel for several reasons. However, H_2 is not found in usable form on earth. Some of the techniques that have been developed to produce hydrogen include electrolysis of water and steam reforming of hydrocarbons [96]. Hydrogen can be generated from ethanol, methanol natural gas, LPG and the hydrocarbon sources by means of an appropriate catalytic process.

Steam reforming of methane (SRM): It is a highly endothermic process in which a hydrogen rich syn gas is produced. It is typically described for methane as primary fuel,

$$CH_4 + H_2O \rightarrow CO + 3H_2 \qquad \Delta H = 206 \text{ kJ/mole}$$

As per stoichiometry of equation one mole of water is required per mole of methane, but under these conditions carbon deposition is thermodynamically favored. Therefore, steam is usually fed in excess to reduce coke formation and H_2O/CH_4 ratios of 2.5 – 3.0 are commonly used.

Partial oxidation (POX): Burning hydrocarbons with reduced access to oxygen is called partial oxidation. In the development of syngas technology, noncatalytic partial oxidation with oxygen was also considered because it does not need external heat. It can be described in general as [97].

$$C_xH_y + x/_2\, O_2 \rightarrow x\ CO + y/_2\, H_2$$

This reaction can be initiated by a simple combustion process leading to a quick start, once the system is running it then requires little external heating. Partial oxidation is preferred where there is less access to natural gas or where there is an abundance of oil.

Autothermal Reforming (ATR): Autothermal reforming combines the endothermic steam reforming process with the exothermic partial oxidation reaction [97, 98], balancing the heat flow into and out of the reactor. This system can be highly productive, fast starting and compact and has been demonstrated with methanol, gasoline and natural gas. One example of this technology is the Johnson Matthey HotSpot reformer.

1.2.2. H_2 enrichment and CO clean up

1.2.2.1. Water gas shift (WGS) reaction

Reaction of CO with water producing H_2 and CO_2 is called water gas shift (WGS) reaction. WGS reaction is one of the critical steps in fuel processor for preliminary CO clean up and for the production of additional hydrogen, prior to CO preferential oxidation or methanation step. WGS reaction is given as follows,

$$\mathbf{CO\,(g) + H_2O\,(g) \leftrightarrow CO_2\,(g) + H_2\,(g)} \qquad \mathbf{\Delta H = -\,41.2\ kJ/mol,\ \Delta G = -\,28.6\ kJ/mol}$$

It is a reversible exothermic reaction, thermodynamically unfavorable at elevated temperatures. Since, it is an exothermic reaction, lower temperature is favored for higher CO removal. In general, it is in operation in the temperature zone of 200-400 ^{0}C. In industrial applications, for continuous operation, high temperature shift (HTS) catalyst that consist of Fe_2O_3-Cr_2O_3 oxide and low temperature shift (LTS) catalyst Cu-ZnO-Al_2O_3 in subsequent stage are used. [99], for obtaining good conversion of CO under steady state conditions. Many studies have been reported focusing on catalyst preparation [100, 101], kinetics or reaction mechanism [99, 102, 103]. Most of the work was in the mechanistic area particularly for Cu-ZnO-Al_2O_3 catalyst. The investigation pertains to the mechanism whether it is associative, taking place through intermediates such as formates or associated with formation of surface species such as carbonate, hydroxycarbonates [103 - 104]. The use of Fe-Cr and Cu-Zn oxide catalysts has some disadvantages like low activity, sensitivity towards air (LTS) or temperature excursion and the length of pre-conditioning of the catalyst. These HTS and LTS catalysts are therefore unsuitable for use in either residential or automotive applications, where fast start-ups require small catalyst volumes. In trying to find the best compromise between activity and cost, non precious metal catalysts are usually active at higher temperatures, whereas precious metals are active over

a larger temperature range. Among precious metals, gold has been regarded as a potentially useful catalyst if it is highly dispersed on a suitable support for low temperature WGS reaction [105]. Also Au/Fe_2O_3 [106], $Au\text{-}TiO_2$, $Au\text{-}ZrO_2$ [107], Au/ZnO and Au/Al_2O_3 [108] are reported. Platinum is another precious metal, which has been studied on different supports like $Pt\text{-}CeO_2$ [109].

1.2.2.2. Preferential oxidation (PrOx) of CO

Preferential oxidation of CO is one of the important and most preferred reaction, to reduce the residual CO in the reformate to desired level [110 - 112, 113] without excessive hydrogen consumption. PrOx reaction is exothermic.

$$\mathbf{CO + \tfrac{1}{2}\, O_2 \rightarrow CO_2} \qquad \mathbf{\Delta H = -\,283.6\ kJ/mol,\ \Delta G = -\,63\ kJ/mol}$$

Trace amount of CO in H_2 can deteriorate the efficiency of the PEM fuel cell Pt catalyst via CO poisoning. More CO tolerant fuel cell anode catalysts are being developed [114 - 116]. A good PrOx catalyst should have the following characteristics:

(i) High CO oxidation activity, preferably at lower temperatures.
(ii) High selectivity for CO oxidation without the undesired H_2 oxidation.
(iii) Stable activity even in the presence of CO_2 and water.

PrOx catalyst should be active and selective to only CO oxidation, without oxidizing hydrogen. It is usually placed between the outlet temperature of the WGS reactor and inlet temperature of PEM fuel cell (60 - 80 ^{0}C). Depending on the nature of the catalyst, the extent of hydrogen oxidation varies influencing the end quality of product gas. The selectivity of the process goes down with increase in O_2/CO. Moreover secondary reactions such as reverse water gas shift reaction, hydrogen oxidation and methanation of CO may occur depending upon the catalyst and reaction conditions.

$$CO + 3H_2 \rightarrow CH_4 + H_2O$$
$$CO_2 + H_2 \rightarrow CO + H_2O$$
$$H_2 + \tfrac{1}{2}\, O_2 \rightarrow H_2O$$

The low temperature CO oxidation has been reviewed and documented in the literature. However, the number of reports on selective CO oxidation in the presence of hydrogen has only recently increased as a result of interest in PEM fuel cells. Early work was reported by Engelhard using platinum supported on alumina, silica and diatomaceous earth [117]. A variety of materials among which Pt, Pd, Rh and Ru at low metal loading and in diluted feed has been studied [118]. Improved selectivity for zeolite supported platinum over platinum alumina [119] was observed which may depend on temperature and water content in the feed, water adsorption may, however, be the issue for these materials [119, 120]. Korotkikh and Farrauto [121, 122] reported selective oxidation of CO in the absence of CO_2, on Pt and Fe promoted Pt catalyst. Fe promoted catalyst performed better than that of unpromoted. The role of Fe as a promoter was interpreted based on the ability to provide additional sites for O_2 adsorption/dissociation, the close contact with Pt and Fe believed to induce electron rich Pt surface and provide the readily available oxygen by means of duel-site mechanism [122]. Ceria [123] gold [124] and cobalt [125] were also used as promoter with platinum for selective CO oxidation.

Number of papers published on Au catalysts [126, 127 - 129] indicate that they are potential candidates for selective oxidation of CO than WGS, based on low operating temperature. But these catalysts have some drawbacks such as high metal loading (~2 wt %), not capable of handling high space velocities and rapid deactivation in the presence of CO_2.

Apart from precious metals, Cu/CeO_2 mixed oxides have been reported as a promising candidate for PrOx [130, 131]. The well-known enhancement of the total oxidation activity of CuO when supported on oxides like CeO_2 was attributed to a "synergistic" effect [132, 133]. It is proposed that well dispersed CuO on CeO_2, which is reducible at lower temperature vis-a-vis bulk CuO, could easily absorb CO. As a consequence, this catalyst exhibited high activity/selectivity for low temperature CO oxidation [125, 134, 135]. The information gained may aid the development of these catalysts, which may replace precious metal catalysts for low temperature CO oxidation. Additionally, it was demonstrated that the redox processes during the CO oxidation involved the reduction and oxidation of both the copper and the ceria phases [136 - 139]. It

was also postulated that the presence of copper enhances the redox behavior, the oxygen storage capacity and thermal stability of ceria [140, 141].

1.2.3. Other processes to remove CO from hydrogen stream

Apart from PrOx of CO there are other process, which are used for removal of CO from hydrogen rich stream that are given below:

Methanation:

Some of the hydrogen plants use simple and convenient methanation reaction to remove traces of CO from the process gas. Even very low levels of CO or CO_2 can often adversely affect downstream hydrogen consuming processes. Methanation is the final stage in the purification of hydrogen and residual amounts of carbon oxides (0.1-1.0 mole % total) are removed by reaction with hydrogen using a nickel catalyst, usually to less than 5ppm. Methane formed during methanation does not cause problems in the downstream hydrogen consuming processes and simply acts as an inert diluent. The conversion of carbon oxide to methane and water by using nickel or other catalyst is called as methanation.

$$CO + 3H_2 \leftrightarrow CH_4 + H_2O$$

$$CO_2 + 4H_2 \leftrightarrow CH_4 + 2H_2O$$

Almost all industrial methanation catalysts are based on NiO supported on various refractory oxides, such as alumina-silica-lime-magnesia, often strengthened with calcium aluminate cement. Nickel oxide must be reduced to nickel metal in the reactor before use. Successful catalysts must, therefore, be easily reduced, have a high, stable activity and retain activity for long periods Although the major use of methanation catalysts is in ammonia synthesis and hydrogen plant purification, several other important applications have been developed. The methanation reactions are strongly exothermic. The temperature rise for typical methanator gas compositions in hydrogen plants is about 74 ^{0}C (133 ^{0}F) for each 1 mole % of CO converted and 60 ^{0}C (108 ^{0}F) for 1 mole % of CO_2 converted [142]

Pressure swing adsorption (PSA):

A variety of commercial PSA processes for the production of H_2 with or without a by-product, as well as PSA processes for direct production of ammonia from synthesis gas are reviewed [143 - 145]. The equilibrium adsorption / desorption characteristics of the components feed gas on an activated carbon, a zeolite, and a silica gel are reported [146], and the criteria for adsorbent selection in these PSA processes are discussed. The process is carried out by passing feed gas at pressure *P*F through an adsorber and an essentially pure H_2 stream is produced through the product end at the feed gas pressure. A part of this gas is withdrawn as the primary H_2 product stream. The step is stopped when the impurity mass transfer zones are somewhere in the middle of the adsorber and the rest of the adsorber is essentially clean.

Membrane separation:

PSA process features very high product purity (99 mole % +) and moderate hydrogen recovery (65 – 90 mole %) depending on the tail gas pressure. Polymeric membrane systems recover hydrogen at moderate purity (90 – 95 mole %) and moderate recovery (85 – 90 mole %) [147]. As compared with PSA process, a polymeric membrane system has no moving parts and is extremely reliable. Additional modules can be added for expansion or increased recovery. Also instead of polymeric membranes, Pd membranes have been used for many years for the production of extremely pure hydrogen for specific purpose. Ceramic materials including alumina or glass have been used as the porous supports [148 - 153]. However, from the viewpoint of a practical application porous stainless steel has the merit of getting more easily connected into commercial unit. Lot of work has been done using porous stainless steel tube as a support to investigate the characteristics and performance of supported Pd membrane [154 - 156].

1.2.4. Limitations of PrOx:

As compared to other processes that are used to remove CO from hydrogen rich stream, PrOx has some limitation like;

(i) Catalysts are very sensitive towards temperature

(ii) Presence of water and CO_2 usually has adverse effect on most of the catalysts reported.

(iii) At higher space velocity catalyst gets deactivated.

(iv) As the CO from WGS reaction keeps on changing, it is very difficult to maintain the oxygen required for oxidation of CO. Excess oxygen leads to hydrogen oxidation, whereas decrease in the oxygen reduces the CO conversion.
(v) Precious metal catalysts are used, which increases the cost of the fuel cell power pack.

1.2.5. Mechanism of PrOx reaction

CO oxidation over metals is believed to follow a competitive Langmuir-Hinshelwood mechanism where CO and O_2 adsorb on the same site. However, there were also reports suggesting Eley-Rideal mechanism, in which, gas phase CO directly reacts with adsorbed oxygen.

The mechanism for CO oxidation over the metals supported on reducible metal oxides is different. In fact, it is assumed that it occurs in two steps, according to the mechanism suggested by Mars and van Krevelen [157]. First, the CO adsorbed on metal site is oxidized by the lattice oxygen from the active metal oxide. As a result, an oxygen vacancy is created and the neighboring metal atom gets reduced. In a second step, the surface metal atom is re-oxidized by the gas phase oxygen. In such a scheme, H_2 and CO compete for the same adsorption site but the hydrogen oxidation is suppressed due to stronger CO adsorption. Furthermore, active supports, such as ceria-based ones, were shown to store hydrogen at low temperatures [158]. Such capacity would potentially reduce hydrogen partial pressure above the catalyst, lowering the hydrogen coverage and enhance the catalyst selectivity.

The nature of the active site for CO oxidation on supported Au catalysts and the reaction mechanism are also subjects of great research interest. Although active catalysts commonly contain small, 2 - 5 nm Au crystallites, size alone does not seem to be a factor for higher activity [159]. The other parameters, which include gold-support interface, small Au clusters that possess nonmetallic electronic properties due to a quantum-size affect, shape of Au catalyst and strain defects, affect the reaction.

Many of the reported observations can be understood on the basis of a model in which the active catalyst contains *both* gold atoms *and* ions, and that the latter form the 'chemical glue', which binds the particle to the support. Each particle is, therefore, bounded by a ring of Au^{III} ions. The structure is not, however, fixed: the Au^{III}/Au^{0} ratio

may change (i) during calcination, (ii) during reduction by hydrogen and (iii) during reaction. Initial changes in reactivity may reflect changes in this ratio, *complete* reduction, due to excessive calcination or use of hydrogen, is harmful because the glue is lost from the interface and sintering can then occur easily. The total absence of Au^0 is undesirable, as it is needed to provide a locus for the chemisorption of the carbon monoxide, and a partially reduced support surface may contain anion vacancies, which assist oxygen adsorption.

$$Au^0 + CO \rightarrow Au^0...CO \quad (1)$$

$$Au^{III} + OH_S^- \rightarrow Au^{II}...OH \quad (2)$$

$$Au^0...CO + Au^{II}...OH \rightarrow Au^{II}...COOH + Au^0 \quad (3)$$

$$O_2 + \square_S^- \rightarrow O_2^-...\square_S \quad (4)$$

$$Au^{II}...COOH + O_2^-...\square_S \rightarrow Au^{II} + CO_2 + HO_2^-...\square_S \quad (5)$$

$$Au^{II}...COOH + HO_2^-...\square_S \rightarrow Au^{II} + CO_2 + 2OH_S^- + \square_S \quad (6)$$

$$Au^{II} + \square_S \rightarrow Au^{III} + \square_S^- \quad (7)$$

It has been suggested in the case of magnesia, that the mechanism may start by a support hydroxyl ion attacking a CO molecule on the gold (Au^0...CO). This may occur more generally and propose a 'periphery' mechanism as follows. The Au^0...CO is attacked by a hydroxyl group either on a support cation or on a peripheral Au^{III} ion, forming a carboxylate group attached to the latter. This is in turn attacked by a superoxide ion, which must be responsible for oxidizing two carboxylate ions: the hydroxyl group returns whence it came and is ready to re-engage in the catalytic cycle [160].

The mechanism might not be the same on all catalysts. If mobile support hydroxyls do not exist, reactions (2) and (3) will not take place, and the mechanism may entail direct reaction of a chemisorbed carbon monoxide with an oxygen molecule or a superoxide ion.

1.3. PARTIAL OXIDATION OF METHANE

1.3.1. Introduction:

Methane is a colourless, odourless gas widely found in nature. Methane is a greenhouse gas, with second greatest impact on climate, after carbon dioxide. Methane is

the major component in natural gas, currently an important energy source. Nonetheless, only part of the methane uptake in the atmosphere is due to industrial activities connected to energy production and use. The increase of methane in the atmosphere is due to so-called "biogenic" sources, e.g., rice cultivation or due to rumination of domestic cattle.

Natural gas is a mixture containing about 90 – 95 mole % CH_4, rest being CO_2 and other hydrocarbons such as C_2H_6, C_3H_8 and C_4H_{10}. The "firedamp" of coal mines is chiefly methane. Anaerobic bacterial decomposition of plant and animal matter, which occurs under water, produces marsh gas, which is also methane. At room temperature, methane is a gas less dense than air. It melts at –183 ^{0}C and boils at –164 ^{0}C. Methane is combustible, and mixtures of about 5 to 15 percent in air are explosive. Methane is not toxic when inhaled, but it can produce suffocation by reducing the concentration of oxygen inhaled. Trace amount of smelly organic sulfur compounds (mercaptans and dimethyl sulfide) are added to give natural gas a detectable odor, for easy detection of leaks.

$$\mathbf{CH_4(g) + 2\ O_2(g) \rightarrow CO_2(g) + 2\ H_2O(l)} \qquad \mathbf{\Delta H = -\ 891\ kJ}$$

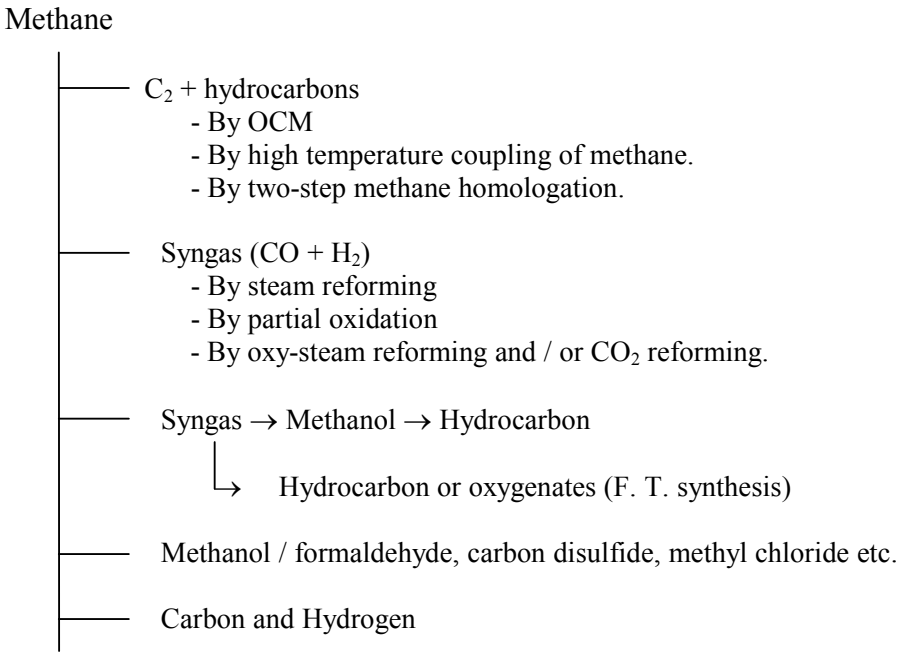

Fig. 1.2: *Different routes for methane conversion*

In the chemical industry, methane is a raw material for the manufacture of methanol, formaldehyde, nitromethane, chloroform, carbon tetrachloride (CCl_4), and some freons. The reactions of methane with Cl and F are triggered by light. When exposed to bright visible light, mixtures of methane with Cl or F react explosively. Figure 1.2 gives general view for methane to useful chemicals through different routes.

The principal use of methane is as a fuel. The combustion of methane is highly exothermic. Energy released by the combustion of methane (natural gas), is used directly in homes and commercial buildings. It is also used in the generation of electric power.

Natural gas occurs in reservoirs beneath the surface of the earth. It is often found in conjunction with petroleum deposits. Before it is distributed, natural gas usually stripped off heavier hydrocarbons (propane and butane) and marketed separately. Non-hydrocarbon gases, such as hydrogen sulfide are also removed. The cleaned gas is then distributed throughout the country through thousands of miles of pipeline. Local utility companies add an odorant before delivering the gas to their customers.

Natural gas is classified as non-associated gas (dissolved gas) and associated gas (free gas). Non-associated natural gas is found in reservoirs in which there is no or, at best, minimum amount of crude oil and usually richer in methane but markedly leaner in terms of the higher paraffinic hydrocarbons and condensate material. It can be kept underground as long as required unlike associated gas.

Associated gas is usually leaner in methane than non-associated gas but will be richer in higher molecular weight hydrocarbon.

1.3.2. Natural gas technology

Natural gas technology involves production of natural gas, processing (purification, separation, odourization), transportation and storage of natural gas or liquid, utilization for domestic, industrial and commercial application and chemical transformation into value added and easily transformable product.

For effective utilization, the major problems faced are transportation and storage of very large volumes of natural gas. The transportation is highly capital intensive and also the presence of CO_2 with water and sulpher components are corrosive. Generally absorption processes are used for removal of carbon dioxide and hydrogen sulphide.

Hence, alternative efforts are being made for chemical transportation of natural gas into easily transportable product by converting it to products like methanol, light hydrocarbons etc.

Methanol is one of the potential products of natural gas, which can be directly used as a fuel or can be converted to other useful intermediates form methane.

$CH_4 + H_2O \rightarrow CO + H_2$ (Steam reforming)

$CO + 2H_2 \rightarrow CH_3OH$ (F-T synthesis)

$CH_3OH \rightarrow$ Useful products such as formaldehyde, olefins etc.

1.3.3. Natural gas as feedstock for production of value added chemicals

Apart from its use as fuel and as a source of hydrogen, natural gas also finds applications as a feedstock in chemical industries for producing various syngas based products (Fig. 1.2). It is supposed as a future feed stock for petrochemicals industry and for manufacture of aromatics and fuels like gasoline, middle distillates etc. There are several chemicals like chloromethane, carbon black, HCN are commercially produced from methane. The process conditions employed in the manufacture are summarized below. In recent years, direct conversion of methane to methanol got momentum as an alternative to storage and transportation of gas.

Products	***Reaction***	***Condition***
Synthesis gas	$CH_4 + H_2O \rightarrow CO + 3H_2$	20-30 bar, 800-950 ^{0}C, supported Ni catalyst
HCN	$CH_4 + NH_3 \rightarrow HCN + 3H_2$ $CH_4 + NH_3 + 3/2O_2 \rightarrow HCN + 3H_2O$	1bar, 1000-1300 ^{0}C, Pt Catalyst.
Chloromethane CH_3Cl, CH_2Cl_2, $CHCl_3$, CCl_4	$CH_4 + xCl_2 \rightarrow CH_{4-x}Cl_x + xHCl$ x = 0- 4	T: 400 ^{0}C, non catalytic gas phase reaction
Carbon disulphide (CS_2)	$CH_4 + 2S_2 \rightarrow CS_2 + H_2S$	2 - 5 bar, 600 ^{0}C.
Acetylene, Ethylene	$2CH_4 \rightarrow C_2H_2 + H_2$	a) Electric arc process b) Partial combustion

1.3.3.1. Oxidative coupling of methane to hydrocarbons

Methane can be converted to hydrocarbons (ethane and ethylene) by oxidative coupling in the following way.

- ✓ *-Catalytic oxidative coupling of methane in the presence of free oxygen.*
- ✓ *-Catalytic oxidative coupling of methane in the absence of free oxygen using redox catalyst system.*
- ✓ *-Homogeneous (Non catalytic) oxidative methane pyrolysis.*
- ✓ *-Oxidative pyrolysis of natural gas.*

1.3.3.2. Conversion of methane to methanol by syngas route

The established technology for production of methanol is based on the syngas, produced by steam reforming (SR) or partial oxidation (PO) of methane.

Natural Gas (CH_4) $\rightarrow$ Syngas ($CO + H_2$) $\rightarrow$ Methanol (CH_3OH).

The SR is carried out over nickel catalyst at 800 - 950 ^{0}C at a pressure about 20-30 bars. Syngas to methanol conversion is carried out over Cu-ZnO-Al_2O_3 catalyst at a pressure of 50-70 atm. The major drawback of this process is the step for methane to syngas conversion which is a highly energy intensive process.

1.3.3.3. Direct conversion of methane to methanol / formaldehyde

The technology is well established for the production methanol via syngas. A direct conversion of methane to methanol, where the oxidation is interrupted at the initial stage of oxidation, not only yield a liquid product in one step but also preferred because it will be energetically more efficient.

The recent demand for the methanol as a fuel and as a starting material for many industrial processes has increased that new technology must be developed for commercial production of methanol. Because of the above limitation of the process based on syngas route, efforts are being made for direct conversion of methane to methanol. However, so far little success has been achieved for selective oxidation of methane using acidic metal oxides (transition metal oxide) as catalysts. Although, high selectivity of about 80 mole %

was achieved but very low conversion levels, not acceptable for commercial purpose were reported [161]. The high-pressure selective oxidation of methane to methanol was studied by Pichler and Reder [162] at 160 atm and 350 ^{0}C. K. Newitt and haffner reported [163] formaldehyde and formic acid also produced as condensable products along with methanol. The reaction was carried out in a static system at 360 - 393 ^{0}C and at pressure 50 - 180 atm. Partial oxidation is widely used process to convert hydrocarbon and alcohols to valuable oxygen containing chemicals. But due to the favourable deep oxidation, the partial oxidation of methane to oxygenate selectively is still far away from commercial realization.

Moreover methanol and formaldehyde are susceptible for oxidation to oxides of carbon at high reaction temperatures. However, work is going on for improvement in the catalyst activity and selectivity. Catalysts based on MoO_3 have been most widely studied for the partial oxidation of methane [164]. Use of different zeolite, alumina, silica, and metal oxides are also attempted for the partial oxidation of methane to methanol or formaldehyde. Comparative studies on the methane oxidation using nitrous oxide and oxygen as an oxidizing agent indicates that the partial oxidation products favoured by high CH_4/O_2 ratio and low CH_4/N_2O ratio. The presence of hydrocarbon, especially ethane, in small quantities seems to have a favorable influence on methane to methanol. The direct oxidation reaction needs further work for optimizing methanol or formaldehyde production. This would include determination of optimum operating conditions (pressure, temperature, residence time, CH_4/O_2 ratio), presence of other hydrocarbons and the catalytic activity of various materials.

1.3.3.4. Current industrial process for methanol / formaldehyde production

Formaldehyde became a chemical of major industrial importance, current world annul production capacity is estimated to be almost 5 million tones as 100 % formaldehyde. The main industrial use of formaldehyde is in the production of urea-phenolic and melamine resins, which are used in the manufacture of chipboard and plywood. Other well established applications are in the production of paint, cosmetics, explosive, fertilizers, dyes, textiles and papers.

Commercially, formaldehyde is produced in three steps involving H_2/CO synthesis gas and methanol as intermediate. Sixty percent cost of this intermediate arise from the high temperature SR of methane to produce syngas [165].

Currently in the chemical industry methane is converted by SR process into synthesis gas using NiO/Al_2O_3

$$CH_4 + H_2O \rightarrow CO + 3H_2$$

The synthesis gas is used for manufacture methanol over $Cu\text{-}ZnO\text{-}Al_2O_3$

$$CO + 2H_2 \rightarrow CH_3OH$$

And the production of formaldehyde from methanol is based on its oxidation and dehydrogenation over silver or iron molybdate catalysts

Oxidation

$CH_3OH + ½\ O_2 \rightarrow HCHO + H_2O$ $\quad\quad \Delta H = -157\ kJ\ mol^{-1}$

Dehydrogenation

$CH_3OH \rightarrow HCHO + H_2$ $\quad\quad \Delta H = +\ 85\ kJ\ mol^{-1}$

1.3.4. Methane activation

1.3.4.1. Thermodynamics of methane reaction

Simple dehydrogenative coupling of methane is thermodynamically unfavorable (Eq.1) whereas all reactions involving oxygen such as partial oxidation of methane to formaldehyde (Eq.2) or methanol (Eq.3) are thermodynamically favored.

	ΔG (kcal mol^{-1}) at 427 ^0C	
$2CH_4 \rightarrow C_2H_6 + H_2$	+ 71	Eq. 1
$CH_4 + O_2 \rightarrow HCHO + H_2O$	– 70	Eq. 2
$CH_4 + ½\ O_2 \rightarrow CH_3OH$	– 22	Eq. 3
$CH_4 + 3/2\ O_2 \rightarrow CO + 2H_2O$	– 136	Eq. 4
$CH_4 + 2O_2 \rightarrow CO_2 + 2H_2O$	– 189	Eq. 5

However much larger decrease in the Gibbs free energy accompanies the total oxidation of methane to CO, CO_2 and H_2O (Eq. 4 and 5). Therefore one can expect that eventually the

reaction lead to formation of CO_2. The main problem in this reaction is how to achieve high conversion without significant loss of methane in complete combustion [166].

Methane is extremely stable and activation of the C – H bond requires stringent reaction conditions. The direct conversion of methane into valuable chemicals, i.e., CH_3OH and HCHO, involve partial oxidation under specific reaction conditions [167 - 174]. As a general rule, these conversion processes use fuel rich mixtures with an oxidant to minimize the extent of combustion reactions. Under these conditions, purely gas-phase oxidation reactions require high temperatures, which determine the control of selectivity to the desired products. Thermodynamic and kinetic studies reveal that the rate-limiting step of the partial oxidation of methane (POM) is the first H-abstraction from the C-H bond. Thus, initiators and sensitizers have been examined in order to decrease the energy barrier of this H-abstraction. So far, activation methane in liquid phase has not made an appreciable progress, although methane into various complexes has been reported [175].

1.3.4.2. Catalyst systems for methane activation

Silica as support

Silica and silica-supported oxide catalysts exhibit a superior functionality in the POM [176, 177]. Several authors pointed out that SiO_2 itself has measurable activity for CH_4 conversion to HCHO, although at lower levels than most other catalysts. At the same reaction conditions, alumina and magnesia produced only CO and CO_2, confirming the specificity of silica for the partial oxidation. One of the few explanations offered concerning the mechanism of methane activation over silica comes from the surface chemistry of reactive silicas. The term “reactive silica” is a trivial name coined by Morterra and Low [178] to designate high surface area silica, which after activation becomes remarkably active in chemisorbing a variety of gases [179]. The available spectroscopic information suggests that activity of silica comes probably from the presence of unusual reaction centers. Kobayashi et al. [180] reported that doping fumed silica with Fe^{3+} ions strongly enhances HCHO productivity and Fe loading, its dispersion and the coordination of the Fe^{3+} ions with oxygen are critical parameters governing the partial oxidation reaction. Fe^{3+}sites in several oxide systems enhanced the formation of peroxide (O_2^{+2}) species, which were responsible for the selective activation of the CH_4 molecule.

Promotion of silica surfaces by deliberately adding Fe^{3+} ions enhances the partial oxidation of CH_4 due to the creation of more isolated (or in small oxidic clusters) Fe^{3+} sites at the surface. However, if large ferric oxide particles are developed, total combustion of methane becomes the dominant reaction.

Molybdenum based systems

Molybdenum-containing catalysts belong to one of the categories of oxides widely used for the partial oxidation of CH_4 into C_1-oxygenates. Most of the catalysts employed for this purpose include molybdena either alone [181] or with various oxide substrates (ZnO, Fe_2O_3, UO_2, VO_2) [181, 182], molybdena dispersed on silica [183, 184] or on zeolites [185, 186] and molybdenum oxometalates [187, 188].

The involvement of the different Mo species, in MoO_3/SiO_2 catalysts prepared with varying surface concentrations of Mo atoms. In methane partial oxidation, CH_4 conversion and HCHO selectivity were found to depend on both Mo-loading and the pH of impregnation, which in turn governed the dispersion of molybdenum oxide. It was shown that the oxygen was incorporated into HCHO from the lattice molybdenum oxide and not from the gas phase molecular O_2, whereas CO_2 came from CH_4; the role of molecular oxygen was to restore the oxidation state of molybdenum, while the catalyst worked in a redox Mars–van Krevelen cycle. Smith and Ozkan [189, 190] proposed that the Mo = O sites present in the MoO_3 crystals were catalytically active while the Mo – O – Mo bonds accelerate the deep oxidation of methane. However, the reactivity of supported molybdenum oxide differs from bulk MoO_3 and no direct extrapolation can be done [191]. Zeolites, instead of silica, have also been used as carriers to prepare molybdenum oxide catalysts for the CH_4 oxidation. On account of the specific activity of the monomeric molybdenum species, a few attempts have been made to deposit highly dispersed Mo species in HY [185] and HZSM-5 [186] zeolites. Banares et al. working with HY zeolite, [185] found that highly dispersed MoO_3 species could be obtained by different methods: (i) a solid-state reaction between $MoCl_5$ and the hydroxyl groups of the zeolite; (ii) adsorption-decomposition on the $Mo(CO)_6$ complex; and (iii) conventional impregnation with ammonium heptamolybdate, followed by thermal decomposition under very low pressure for long periods of time.

Vanadia based systems

A large amount of work has been reported concerning CH_4 oxidation into CH_3OH and HCHO over vanadia catalysts [191]. Using O_2 as an oxidant at 1 bar and temperatures in the range of 300–350 ^{0}C, a sequential reaction path was proposed, where HCHO formed from CH_4, CO from HCHO and CO_2 from CO. This contrasted with MoO_3/SiO_2 catalysts where CO_2 was formed in a parallel way either completely [183] or partially [184] from CH_4. The reactivity of MoO_3/SiO_2 and V_2O_5/SiO_2 catalysts was found to be quite different [191]. The selectivity to HCHO was always lower for the vanadium catalyst. The observed differences between both catalysts appeared to be related to their different abilities to activate oxygen but not to their redox properties [191, 192].

Methane conversion increased with vanadium loading and then decreased slightly. These results suggest that catalytic activity is related to the appearance of dispersed vanadia on the silica surface. It has no effect on its structure below its monolayer capacity [193]. However, the interaction among the surface vanadia species under reducing environment becomes increasingly important. Because the probability of this interaction increases with the coverage, it is expected that under reaction conditions the catalysts with higher vanadia coverage would have a greater capacity to release oxygen.

Zeolites

ZSM zeolites were used [194] to oxidize CH_4 with nitrous oxide into aromatic hydrocarbons. As a general trend, the conversion of N_2O, and the formation of aromatics and carbon oxides increased with the Al content in the ZSM zeolite. The catalytic activity increased with the increase in the concentration of their decationized sites, i.e., with the increase in the number of acid centers. HZSM-5 zeolite was also used for the direct oxidation of CH_4 with oxygen and N_2O oxidants in a flow reactor. Reaction with oxygen over a wide range of experimental conditions gave CO_2 as the only C-containing molecule. However, reaction with N_2O resulted in the production of carbon oxides, CH_3OH, HCHO, lower olefins and $C_6 - C_{12}$ aromatics. The conversion decreased rapidly with time and was paralleled with darkening of the catalyst bed, due to catalyst deactivation by coke.

Other systems

Most work on CH_4 partial oxidation has used metal oxides. Metals are generally too specific towards combustion, although Cullis et al. [195] tested Pd/ThO_2 and Mann and Dosi [196] with Pd/Al_2O_3 were able to inhibit combustion by adding halocarbons to the CH_4/O_2 reactor feed. Residual activity was high for HCHO formation, with yields of 7.5 % HCHO at 34 mole % selectivity [196]. Unfortunately, no further work was pursued on this type of modifications for CH_4 conversion. Taking into account that the standard industrial catalysts for oxidizing CH_3OH into HCHO were based either on Ag or on $Fe_2(Mo_4)_3$ systems, several studies were concentrated not only on Mo but also on Cr and W oxides. A large number of metal oxides (Mox) were tested by Otsuka and Hatano [197] with a view to correlating activity with the electronegativity of the respective cation.

1.3.4.3. Non-catalytic processes

In all the catalytic systems reviewed in the literature evident that the selectivities of CH_3OH and HCHO are exceedingly low and not of commercial significance. However, higher selectivities for CH_3OH have been found under non-catalytic conditions [199 - 201]. Reactor inertness, which is crucial for obtaining high CH_3OH selectivity, was achieved by using quartz-lined reactor.

The presence of higher hydrocarbons in natural gas leads to a lower oxidation reaction temperature, compared to that observed in the oxidation of pure CH_4 [199]. These higher molecular weight hydrocarbons are assumed to “sensitize” the oxidation of methane by virtue of their lower C-H bond strength, thus easily providing free radicals.

On surveying the literature on the POM, a few studies that focus on the influence of reaction parameters (temperature, pressure, oxygen concentration, residence time) on the conversion and the selectivity were found [199, 201]. When looking at the effect of the reaction variable parameters on selectivity to the products, this cannot be viewed separately without examining the dependence on conversion levels. This is rather difficult because CH_4 conversion always depends on the reaction conditions.

1.3.4.4. Methane activation by N_2O

During the last decade a growing concern is about nitrous oxide, which is identified as a contributor to the destruction of ozone in the stratosphere and also a relatively strong greenhouse gas. Nitrous oxide is not only formed as a by-product in industrial plants from the production of adipic and nitric acid but also from the combustion of fossil fuels and biomass. It is also formed from land cultivation, the regeneration of coked fluid cracking catalysts and also as a consequence of measures to control the emission of other environmentally harmful species, like in the nonselective catalytic reduction of NO. Though the concentration seems to be low, N_2O is strongly involved in the atmospheric greenhouse effect because each molecule of N_2O present in the atmosphere is characterized by an average lifetime of about 150 years and a net greenhouse effect of about 300 times greater than that of CO_2 [198]. The emission of N_2O can be reduced by catalytic decomposition into N_2 and O_2 or by utilizing it as a mild oxidizing agent in selective oxidation of hydrocarbons; it is a potential alternative because of its mild oxidizing nature.

The catalytic effects of the addition of nitrogen oxides for the partial oxidation of methane with O_2 both in the presence/absence of catalysts have been reported [201 - 210].

1.4. Scope of the thesis

After a thorough literature survey, it was found that there are large gaps in terms of basic understanding and technology development in the areas of preferential oxidation of CO in presence of excess hydrogen and partial oxidation/selective oxidation of methane to oxygenates. By developing novel catalysts, that have less concentration of Pt, for PrOx reaction, there is scope for reducing the cost of hydrogen production for fuel cells. Similarly, conversion of methane/natural gas to useful chemical intermediates in single step is a technological challenge. Any improvement in per pass yield of oxygenates during partial oxidation of methane has very high commercial significance.

This thesis describes preparation, characterization and catalytic activity studies of mixed metal oxides and modified zeolites for the above two reactions. Mixed metal oxides of Cu-Co-Ce-O mixed oxides and Pt supported on NaY were prepared and preferential oxidation (PrOx) of CO in hydrogen rich stream was carried out which is an important reaction to avoid the CO poisoning of Pt-electrode used in proton exchange fuel cell. Pt-

NaY catalyst, which has a good activity towards CO conversion and oxidation selectivity, used as PrOx catalyst in on-going project of fuel cell. Here we are able to explore and develop a catalyst, which is comparable with commercial PrOx catalyst with low metal loading and operate at low temperature than commercial catalyst i.e. Pt-Al_2O_3 which has metal loading of ~ 2 wt % Pt and operate at 175 ^{0}C whereas our catalyst has metal loading of ~ 0.75 and work at 135 ^{0}C. Second reaction was partial oxidation of methane to formaldehyde, considerable efforts have been devoted to developing active and selective catalysts but, however, neither the achieved yield of nor the thorough mechanism of reactions has been clarified. Here we tried to develop a catalyst with good conversion and selectivity. For this reaction Mo/Fe-ZnO and Mo/Hβ has been used.

The thesis has been divided into six chapters.

Chapter-1 gives a general introduction to supported metal catalysts, particularly mixed oxides, modifications and preparation of zeolite supported metals. Various methods of their preparation and their use in catalysis has been described. The chapter also presents an introduction to preferential oxidation of CO in hydrogen rich streams. In addition, it contains a general introduction to partial oxidation of methane to oxygenates like formaldehyde and methanol.

Chapter - 2 describes the preparation and characterization of Pt-NaY, modified Pt-NaY and Cu-Co-Ce-O mixed oxide catalysts. The principles behind various characterization techniques that are used for this study have been described in this chapter. This chapter also contains details of preparation of Cu-Co-Ce-O mixed oxides and their characterization. The characterization of these materials was carried out using powder XRD, BET suface area, SEM, TEM, TPR/TPD, IR, UV-vis and Laser Raman spectroscopy.

Chapter - 3 presents the catalytic activity data of preferential oxidation of CO in the presence of hydrogen in fixed bed down flow reactor. This chapter is divided into three parts. Part - A presents the catalytic activity for PrOx on Pt-NaY, the effect of different reaction parameters like Pt content, operating temperature, space velocity, O_2/CO ratio, CO concentration, water and time on stream on PrOx activity.

Part - B describes the investigation of PrOx of CO in excess of hydrogen on Pt promoted NaY catalyst. Pt-NaY catalysts were modified by using second metal like Fe, Co and Au. The detail study like metal composition, activation temperature and time on stream was carried out on PtFe-NaY and compared with Pt-NaY catalyst.

Part - C gives detail study on Cu-Co-Ce-O mixed oxide catalysts. The synergetic effect of copper and cobalt on ceria has been studied in detail on these catalyst having general formula $Cu_xCo_{(1-x)}Ce_2O_{4-\delta}$ with x = 0, 0.15, 0.25, 0.50, 0.75, 1.0.

Chapter - 4 describes the preparation and characterization results for Mo/Hβ and Mo/Fe-ZnO. The calcined samples were characterized by powder XRD, BET surface area, SEM, UV, IR, P-IR, TPD/TPR, laser Raman and XPS studies. These characterization results were carried out to identify the molybdenum species and other properties, which were found to be differing with the molybdenum content.

Chapter - 5 is divided in two Parts for partial oxidation of methane to formaldehyde by using air as an oxidant. Part - A presents the catalytic activity data over Mo/Hβ catalysts by using fixed bed down flow reactor. The effect of metal content, reaction temperature, space velocity, Air/Methane ratio, different oxidants and time on stream was carried out.

Part - B gives the partial oxidation of methane to formaldehyde by using air over Mo/Fe-ZnO catalyst. The effect of Fe as a promoter for synthesis of formaldehyde on Mo/Fe-Zn-O catalysts was studied for this reaction.

Chapter - 6 summarizes the conclusion reached in this thesis and gives suggestion for further research.

1.5. REFERENCES

[1] S. M. George, Chem. Rev., 95 (3) (1995) 475.

[2] N. D. Parkyns, C. I. Warburton and J. D. Wilson, Catal. Today, 18 (1993) 385.

[3] D. J Cole-Hamilton and R. P. Tooze (eds.), Catalyst Separation, Recovery and Recycling, 1- 8.

[4] Introduction: Heterogeneous catalysis, Chem. Review, 95 (1995) 3.

[5] H. Hattori, Stud. Surf. Sci. Catal., 78 (1993) 35.

[6] A. Corma, V. Fornes, R.H. Martin-Aranda, H. Garcia, J. Primo, Appl. Catal., 59 (1990) 237.

[7] M. Thomas, Sci. Am., 266 (1992) 112.

[8] W. R. Moser and J. Happel, Eds, Ann. N. Y. Acad. Sci., 272 (1976) 1.

[9] Jr. R. L. Burwell, G. L Haller, K. C. Taylor, J. F. Read, Adv. Catal., 29 (1969) 1.

[10] R. A. Sheldon, R. A. Van Santen, Catalytic Oxidation: Principles and Applications, World Scientific, (1995) 53.

[11] R. M. Barrer, Hydrothermal Chemistry of Zeolites academic press, New York (1982).

[12] R. M. Barrer, J. Chem. Soc., (1961) 971.

[13] D. W. Breck, Zeolites Molecular Sieves, Wiley, New York (1974).

[14] N. Y. Chen, W. W. Kaedly and F .G. Dwyer, J. Am. Chem. Soc., 101 (1979) 6783.

[15] F. Liebau, Zeolites, 3 (1983) 191.

[16] R. Szostak, Molecular Sieves: Principles of Synthesis and Identification, Van Nostrand Reinhold, New York (1989).

[17] L. V. C. Rees, Nature, 296 (1992) 492.

[18] J. W. McBain, The Sorption of gases and vapours by solids, Ritledge and Sons, London, (1932) Ch. 1.

[19] P. G. Szhultz, Angew Chem. Int. Ed. Engl., 28 (1989) 1283.

[20] M. E. Davis, Acc. Chem. Res., 26 (1993) 111.

[21] A. F. Cronstedt, Kongl Vetenskaps, Acad. Handl. Stockholm, 17 (1756) 120.

[22] A. Damour, Ann. Mines, 17 (1840) 191.

[23] St. Claire Deville, Compt. Rend., 54 (1862) 324.

[24] H. S. Thomson, J. Roy. Agric. Soc., 11 (1862) 68.

[25] D. W. Breck, Molecular Sieves Zeolites, Adv. Chem. Ser., (American Chemical Society, Washington DC) 101 (1971) 251.

[26] J. W. McBain, The Sorption of gases and vapors by solids, Pub. Rutledge and Sons London, (1932) Ch. 5.

[27] R. M. Barrer, Proc. Roy. Soc. (London) 162 A (1938) 393, Trans. Far. Soc., 40 (1944) 559.

[28] R. M. Barrer, J. Chem. Soc., (1984) 127.

[29] R. M. Barrer, and C. Marcilly, J. Chem. Soc., A (1970) 2735.

[30] R. M. Barrer and D. J. Robinson, Zeit. Krist, 135 (1972) 374.

[31] R. M. Barrer, Nature, 164 (1949) 112.

[32] Zeolites for cleaner technologies. Guisnet, M., and Edimbourg in Supported Catalysts and their Applications, Ed. D. C. Sherrington and A. P. Kybett (The Royal Society of Chemistry, Cambridge, 2001) 55.

[33] T. R. Goldsmith, Min. Mag., 29 (1952) 952.

[34] K. Becker, H. John, K Steinburg, M. Weber, and K. Nestler, Catalysis on Zeolites (Kallo. D and Minachev, Kh. M., Eds.), Akademia Kiado, Budapest (1988) 515.

[35] C. Naccache, and Y. Ben Tarrit, Zeolite Science and Technology, Riberio, F. R., Rodrigues, A. E., Rollmann, L. D. and Naccache, E. Eds.) Martinus Nijhoff, The Haque (1984) 373.

[36] A. N. Kotasthane, V. P. Shiralkar, S. G. Hegde and S. B Kulkarni, Zeolites, 6 (1986) 233.

[37] G. N. Rao, V. P. Shiralkar, A. N. Kotasthane, and P. Ratnasamy, Molecular Sieves; Synthesis of Microporous Materials, Vol. 1, Ed. M. L. Occelli and H. E. Robson, Van Nostrand Reinhold-New York.

[38] Kh. M. Minachev, V. V. Khariamov and V. I. Garanin, Catalysis on Zeolites (Kallo. D and Minachev, Kh. M., Eds.), Akademia Kiado, Budapest (1988) 489.

[39] G. Pergo, G. Bellusi, C. Corono, M. Taramasso and F. Buonomo, Stud. Surf. Sci. Catal., 28 (1986) 129.

[40] J. Kornatowki, M. Sychev, V. Goncharuk and W-H. Bauer, Stud. Surf. Sci. Catal., 65 (1991) 581.

[40] R. M. Barrer, J. W. Bayhans, F. W. Bultitude and W. M. Meier, J. Chem. Soc., (1995) 195.

[41] R. A. Sheldon, R. A. van Sheldon, Catalytic Oxidation Principle and Application.

[42] C. L. Thomas, "Catalytic Processes and Proven Catalysts," Academic Press, New York (1970).

[43] T. Hubaut, M. Daage, J. P. Bonnelle, Appl. Catal., 22 (1986) 231.

[44] E. M. Calverly, K. J. Smith, J. Catal., 130 (1991) 616.

[45] C. T. Cambell, K. A. Daube, J. Catal., 104 (1987) 109.

[46] J. Cunningham, G. H. Al-Sarred, J. A. Cronin, J. L. G. Fierro, C. Healy, W. Hirshwald, M. Ilyas, J. P. Tobin, J. Catal., 102 (1986) 160.

[47] S. Velu, K. Suzuki, M. Okazaki, M. P. Kapoor, T. Osaki, F. Ohashi, J. Catal., 194 (2000) 373.

[48] H. Praliaud, S. Mikhailenko, Z. Chajar, M. Primet, Appl. Catal., B 16 (1998) 359.

[49] A. Martinez-Arias, M. Fernandez-Garcia, O. Galvez, J. M. Coronado, J. A. Anderson, J. C. Conesa, J. Soria, G. J. Munuera, J. Catal., 195 (2000) 207.

[50] James A**.** Schwarz, Cristian Contescu and Adriana Contescu, Chem. Rev., 1995, 95,477-510.

[51] G. Ertl, H. Knozinger, J. Weitkamp, Handbook of Heterogeneous Catalysis, Weinheim, VCH, (1997) 49.

[52] C. Marcilly, Rev. Inst. Fr. Pet., 39 (1984) 189.

[53] Courty, Ph.; Marcilly, Ch. In Preparation of Catalysts III; G. Poncelet, P. Grange, J. A. Jacobs, Eds. Stud. Surf. Sci. Catal., 16 (1983) 485.

[54] S. Cheng, S. Y. Cheng, J. Catal., 122 (1990) 1.

[55] W. M. H. Sachtler, Catal. Today, 15 (1992) 419.

[56] W. M. H. Sachtler, Adu. Zhang, J. Catal., 39 (1993) 129.

[57] D. J. Ostgard, L. Kustov, K. R. Poppelmeier, W. M. H. Sachtler, J. Catal., 133 (1992) 342.

[58] S. T. Homeyer, W. M. H. Sachtler, J. Catal., 117 (1989) 91.

[59] S. T. Homeyer, W. M. H. Sachtler, J. Catal., 118 (1989) 266.

[60] H. J. Jiang, M. S. Tzou, W. M. H. Sachtler, Catal. Lett., 1 (1988) 99.

[61] Z. Zhane, T. T. Wong, W. M. H. Sachtler. J. Catal., 128 (1991) 13.

[62] R. L. Augustine, Heterogeneous Catalysis for the Synthetic Chemist, Marcel Dekker, New York, (1996) 277.

[63] S. Y. Lee, R. Aris, Catal. Rev. Sci. Eng., 27 (1985) 207.

[64] M. Baltes, P. Van Der Voort, O. Collart, E. F. Vansant, J. Porous Mater., 5 (1998) 357.

[65] M. Baltes, O. Collart, P. Van Der Voort, E. F. Vansant, Langmuir 15 (1999) 5841.

[66] P. Van Der Voort, M. Baltes and E. F. Vansant, Catal. Today, 68 (2001) 121.

[67] P. Van Der Voort, M. G. White, E. F. Vansant. Langmuir, 14 (1998) 106.

[68] J. W. Geus, In Preparation of catalysts III. G. Poncelet, P. Grange, P. A. Jacobs, Eds. Stud. Surf. Sci. Catal., 16 (1983) 1.

[69] P. C. M. van Stiphout, H. Donker, C. R. Bayense, J. W. Geus, F. Versluis, In Preparation of Catalysts N. Delmon, B., Grange, P., Jacobs, P. A, Poncelet, G., Eds. Stud. Surf. Sci. Catal., 31 (1987) 55.

[70] J. W. E. Coenen, In Preparation of Catalysts II. B. Delmon, P. Grange, P. A. Jacobs, G. Poncelet, Eds. Stud. Surf. Sci. Catal., 3 (1979) 113.

[71] O. Clause, L. Bonneviot, M. Che, H. Dexpert, J. Catal., 130 (1991) 21.

[72] Ch. Sivaraj, P. Kanta Rao, Appl. Catal., 45 (1988) 103.

[73] C. J. G. Van der Grift, A. F. H. Wielers, A. Mulder, J.W. Geus, Thermochim. Acta., 171 (1990) 95.

[74] X. Tang, B. Zhang, Y. Li, Y. Xu, Q. Xin, W. Shen, Appl. Catal., A 288 (2005) 116

[75] V. K. Kaushik, Ch. Sivaraj, P. Kanta Rao, Appl. Surf. Sci., 51 (1991) 27.

[76] Y. J. Huang, J. A. Schwarz, Appl. Catal., 32 (1987) 45.

[77] S. L. Chen, H. L. Zhane, J. Hu, Cr. Contescu, J. A. Schwarz, Appl.Catal., A. 73 (1991) 289.

[78] H. D. Gesser, P. C. Goswami, Chem. Rev., 89 (1989) 765.

[79] S. J. Teichner, G. A. Nicolaon, M. A. Vicarini, G. E. E. Gardes, Adv. Colloid Interface Sci., 1976,5, 245.

[80] A. Livage, J. Lemerle, Annu. Rev. Mater. Sci., 12 (1982) 103.

[81] J. Fricke, Sci. Am., (1988) 92.

[82] C. J. Brinker, G. W. Sherer, Sol-Gel Science, Academic Press, San Diego, 1990.

[83] L. L. Hench, J. K. West, Chem. Rev., 90 (1990) 33.

[84] J. H. Hirschenhofer, D. B. Stauffer, R. R. Engleman and M. G. Klett, Fuel Cell Handbook, Forth addition 1998.

[85] P. G. Gray, M. I. Petch. Catal. Lett., 51 (1998) 149.

[86] S. Golunski, Platinum Metals Rev., 42 (1) (1998) 2.

[87] N. Edwards, S. R. Ellis, J. C. Frost, S. E. Golunski, A. N. J. van Keulen, N. G. Lindewald, J. Power Sources, 71 (1998) 123.

[88] I. Carpenter, N. Edwards, S. Ellis, J. Frost, S. Golunski, N. van Keulen., SAE Tech Paper Ser, 1 (1999) 1320.

[89] P. G. Gray, J. C. Frost. 12 (1998) 1121. AIChE J 46(6) (2000) 1260.

[90] A. Docter, A. Lamm, J. Power Sources, 84 (1999) 194.

[91] D. R. Brown. PEM fuel cells for commercial building. Office of Building Technology, State and Community Programs, Document Number PNNL-12-51, prepared for the US Department of by the Pacific Northwest National Laboratory, November 1998.

[92] 5th ed, Fuel cells handbook, EG&G Services, Parson, Science Applications International Corporation–US Department of Energy, Office of Fossil Energy, National Energy Technology Laboratory, 2000;193:203 -14.2000.

[93] G. J. K. Acres, J. C. Frost, G. A. Hards, R. J. Potter, T. R. Ralph, D. Thompsett, Catal Today 38 (1997) 393.

[94] T. R. Ralph, G. Hards, Fuel cells: clean energy production for the new millennium. Chem Ind Lond 1998;8:334–5; TR. Ralph, G. Hards, Powering the cars and homes for tomorrow. Chem. Ind. Lond. 8 (1998) 337.

[95] C. Song, Catal. Today, 77 (2002) 17.

[96] P. Ferreira-Aparicio and M. J. Benito, Catal. Rev., 47 (2005) 491.

[97] L. Pettersson, R. Westerholm, Int. J. Hydrogen Energy, 26 (2000) 243.

[98] C. Perrire, R. Wilkenhoener, S. Ahmed, M. Krumplet, 1999 DOE Hydrogen Program Technical Peer Review, Golden, CO, 4 - 6 May 1999.

[99] M. V. Twigg, editor, 2nd ed, Catalyst handbook, London: Wolfe Press, 1989, Chapter 6, Water-gas shift.

[100] X. D. Hu, J. P. Wagner. US 5,990,040, November 23 (1999).

[101] M. Schneider, I. Pohl, K. Kochloefl, O. Boch. US 4598062, July 1, 1986.

[102] C. V. Ovesen, B. S. Clausen, B. S. Hammershoi, G. Steffensen, T. Askgaard, I. Chorkendorff, J. Catal., 158 (1996) 170.

[103] C. Rhodes, G. J. Hutchings, A. M. Ward. Catal. Today, 23 (1995) 43.

[104] A. F. Ghenciu, Curr. Opinion Solid State Mater. Sci., 6 (2002) 389 –399.

[105] D. Andreeva, Gold Bull., 35 (2002) 82.

[106] D. Andreeva, T. Tabakova, V. Idakiev, P. Christov, R. Giovanoli, Appl. Catal., A 169 (1998) 9

[107] T. Tabakova, V. Idakiev, D. Andreeva, in: L. Petrov, Ch. Bonev, G. Kadinov (Eds.), Proceedings of the 9th International Symposium Heterogeneous Catalysis, Varna, (2000) 489.

[108] H. Sakurai, A. Ueda, T. Kobayashi, M. Haruta, Chem. Commun., (1997) 271.

[109] W. Keim in Ullman's encyclopedia of industrial chemistry, VCH, Weinheim 1985, Vol. A1, p.197.

[110] P. G. Gray, M. I. Petch, Platinum Metals Rev., 44 (3) (2000) 108.

[111] S. Golunski, Platinum Metals Rev, 42 (1) (1998) 2.

[112] N. Edwards, S. R. Ellis, J. C. Frost, S. E. Golunski, A. N. J. van Keulen, N. G. Lindewald, J. Power Sources, 71 (1998) 123.

[113] G. W. Skala, M. A. Brundage, R. L. Borup, W. H. Pettit, K. Stukey, D. J. Hart-Predmore, J. Fairchok. US 6,132,689, October 17, 2000.

[114] G. J. K. Acres, J. C. Frost, G. A. Hards, R. J. Potter, T. R. Ralph, D. Thompsett, Electrocatalysts for fuel cells. Catal Today, 38 (1997) 393.

[115] A. G. Gunner, I. Hyde, R. I. Potter, D. Thompsett. US 5,939,220, August 17 (1999).

[116] B. Rohland, V. Plazak, J. Power Sources, 84 (1999) 183.

[117] J. G. E. Cohn. Process for selectively removing carbon monoxide from hydrogen-containing gases. US patent 3,216,783, Nov. 9, 1965.

[118] G. K. Bethke, H. H. Kung. Appl. Catal., A 194 (2000) 43.

[119] H. Igarashi, H. Uchida, M. Suzuki, Y. Sasaki, M. Watanabe. Appl. Catal., A 159 (1997) 159.

[120] G. G. Xia, Y. G. Yin, W. S. Willis, J. Y. Wang, S. L. Suib. J. Catal., 185 (1999) 91.

[121] X. Liu, O. Korotkikh, R. Farrauto. Appl. Catal., A 226 (2002) 293.

[122] O. Korotkikh, R. Farrauto, Catal. Today, 62 (2000) 249.

[123] H. Son, AM. Lane. Catal. Lett., 76 (3 - 4) (2001) 151

[124] S. Chilukuri, T. Joseph, S. Malwadkar, S. B. Halligudi, M Sastry and P. Ratnasamy, Stud. Surf. Sci.Catal., 146 (2003) 573.

[125] M. Haruta, S. Yamada, T. Kobayashi, S. Iijima, J. Catal., 115 (1989) 301.

[126] M. Haruta, M. Date. Appl. Catal., A 222 (2001) 427.

[127] G. C. Bond and D. T. Thompson, Cat. Rev. - Sci. Eng., 41 (1999) 319.

[128] G. J. Hutchings, Catal Today, 72 (2002) 72.

[129] N. A. Hodge, C. J. Kiely, R. Whyman, M. R. H. Siddiqui, G. J. Hutchings, Q. A. Pankhurst. Catal Today, 72 (2002) 133.

[130] G. Avgouropoulos, T. Joannides, Ch. Papadopoulou, J. Batista, S. Hicevar, H. K. Matralis, Catal Today, 75 (2002) 157.

[131] P. Ratnasamy, D. Srinivas, C. Satyanarayana, P. Manikandan, R. Senthil Kumaran, M. Sachin, V. Shetti, J. Catal., 221 (2004) 455.

[132] A. Luengnaruemitchai, S. Osuman, E. Gulari, Int. J Hydrogen Energy, 30 (2005) 981.

[133] J. B. Wang, W. H. Shih, T. J. Huang, Appl. Catal. A 203 (2000) 191.

[134] J. Xiaoyuan, L. Guanglie, Z. Renxian, M. Jianxin, C. Yu, Z. Xiaoming, Appl. Surf. Sci., 173 (2001) 208.

[135] M. Luo, Y. Zhong, X. Yuan, X. Zheng, Appl. Catal., A 162 (1997) 121.

[136] A. Martinez-Arias, M. Fernandez-Garcıa, J. Soria, J. Conesa, J. Catal., 182 (1999) 367

[137] A. Martinez-Arias, M. Fernandez-Garcıa, O. Galvez, J. Coronado, J. Anderson, J. Conesa, J. Soria, G. Munuera, J. Catal., 195 (2000) 207.

[138] J. Wang, S. Lin, T. Huang, Appl. Catal., A 232 (2002) 107.

[139] G. Jernigan, G. Somorjai, J. Catal., 147 (1994) 567.

[140] S. Kacimi, J. Barbier Jr., R. Taha, D. Duprez, Catal. Lett., 22- 4 (1993) 343.

[141] G. Avgouropoulos, T. Ioannides, H.K. Matralis, J. Batista, S. Hocevar, Catal. Lett., 73 (2001) 33.

[142] Methanation catalyst for hydrogen production, Johnson Matthey Group 2003.

[143] A. Fuderer, "Selective Adsorption Process for Production of Ammonia Synthesis Gas Mixtures," US Patent 4, 375, 363 (1983).

[144] S. Sircar, "Production of Nitrogen, Hydrogen and Carbon Dioxide from Hydrocarbon Reformate," US Patent 4, 813, 980 (1989).

[145] S. Sircar, Sep. Sci. Technol., 25 (1990) 1087.

[146] A. Malek and S. Farooq, AIChE J. 44 (9) (1998) 1985.

[147] S. Peramanu, B. G. Cox, B. B. Pruden, Int. J. Hydrogen Energy, 24 (1999) 405.

[148] J. P. Collins, J. D. Way, Ind. Eng. Chem. Res., 32 (1993) 3006.

[149] E. Kikuchi, Catal. Today, 25 (1995) 333.

[150] S. Uemiya, Separ. Purif. Methods, 28 (1999) 51.

[151] S. Uemiya, N. Sato, H. Ando, Y. Kude, T. Matsuda, E. Kikuchi, J. Membr. Sci., 56 (1991) 303.

[152] S. N. Paglieri, K.Y. Foo, J. D. Way, J. P. Collins, D. L. Harper-Nixon, Ind. Eng. Chem. Res., 38 (1991) 1925.

[153] J. Shu, B. P. A. Grandjean, S. Kaliaguine, P. Ciavarella, A. Giroir-Fendler, J. A. Dalmon, Can. J. Chem. Eng., 75 (1997) 712.

[154] P. P. Mardilovich, Y. She, Y. H. Ma, M. H. Rei, AIChE J.44 (1998) 310.

[155] J. Shu, B. P. A. Grandjean, E. Ghali, S. Kaliaguine, J. Membr. Sci., 77 (1993) 181

[156] A. Li, W. Liang, R. Hughes, J. Membr. Sci., 165 (2000) 135.

[157] P. Mars, D. Van Krevelen, Chem, Eng. Sci., 3 (1954) 41.

[158] S. Bernal, J. J. Calvino, G. A. Cifredo, J. M. Rodriguez-Izquierdo, V. Perrichon, A. Laachir, J. Catal., 137 (1992) 1.

[159] H. S. Oh, J. H. Yang, C. K. Costello, Y. Wang, S. R. Bare, H. H. Kung, M. C. Kung, J. Catal., 210 (2002) 375.

[160] G. C Bond, and D. T. Thompson, Gold Bull, 2000, 33(2).

[161] G. A. Fould, B. F. Gray, Fuel Process Technol, 42 (1995) 129.

[162] H. Pichler and R. Reder, Angew. Chem., 46 (1933) 161.

[163] D. M. Newitt, A. E. Haffner, Proc. Roy. Soc. London, Ser A 134 (1932) 591.

[164] H. T. Lin, R. S. Lin, K. J. Liew, R. J. Johnson, and J. H. Lunsford, J. Am. Chem. Soc., 106 (1984) 4117.

[165] M. Bistolfi, G. Fornasari, M. Molinari, S. Palmery, M. Dente, E. Ranzi, Chem Eng Sci., 47(9 –11) (1992) 2647.

[166] Oxygen in catalysis by Adam Bielanski, Jerzy Haber.

[167] H. D. Gesser, N. R. Hunter, C. B. Prakash, Chem. Rev., 85 (1985) 235.

[168] N. R. Foster, Appl. Catal., 1(1985) 19.

[169] V. S. Arutyunov, V. Y. Vasevich, V. I. Vedeneev, Y. V. Parfenov, O. V. Sokolov, Russ. Chem. Bull., 45 (1996) 45.

[170] H. D. Gesser, N. R. Hunter, Catal. Today, 42 (1998) 183.

[171] J. C. MacKie, Catal. Rev.-Sci. Eng., 33 (1991) 169.

[172] M. J. Brown, N. D. Parkyns, Catal. Today, 8 (1991) 305.

[173] Y. Wang, K. Otsuka, J. Catal., 155 (1995) 256.

[174] M. M. Bhasin, D. W. Slocum, (Eds.) Methane, Alkane Conversion Chemistry; Plenum Press: New York, 1995.

[175] J. A. Labinger, Fuel Processing Technology, 42 (1995) 325-338.

[176] O. V. Krylov, Catal. Today, 18 (1993) 209.

[177] R. C. Herman, Q. Sun, C. Shi, K. Klier, C. B. Wang, H. Hu, I. E. Wachs, M. M. Bashin, Catal. Today, 37 (1997) 1.

[178] C. Morterra, M. J. D. Low. J. Chem. Soc., Chem. Commun., 1968, 203.

[179] M. J. D. Low, J. Catal., 103 (1987) 496.

[180] T. Kobayashi, N. Gilhaume, J. Miki, N. Kitamura, M. Haruta, Catal. Today, 32 (1996) 171.

[181] D. A. Dowden, G. T. Walker, Oxygenated Hydrocarbons Production. Br. Pat. 11,244,001, 1971.

[182] V. I Atrosshchenko, Z. M Shchedrinskaya, N. A Gavrya, J. Appl. Chem. URSS 1985, 38, 643.

[183] N. D. Spencer, C. J Pereira, J. Catal., 116 (1989) 399.

[184] M. A. Banares, J. L. G. Fierro, Catalytic Selective Oxidation; S. T. Oyama, J. W. Hightower, Eds, American Chemical Society: Washington, 1992; 354.

[185] M. A. Banares, B. Pawelec, J. L. G. Fierro, Zeolites, 12 (1992) 882.

[186] A. Antinolo, P. Canizares, F. Carrillo, J. Fernandez-Baeza, F. J. Funez, A. de Lucas, A. Otero, L. Rodriguez, L. Valverde, J. Appl. Catal., A 193 (2000) 139.

[187] S. Kasztelan, E. Payen, J. B. Moffat, J. Catal., 112 (1988) 320.

[188] S. Kasztelan, J. B. Moffat, Proceedings of the Ninth International Congress Catalysis, Calgary, 1988; M. J. Philips, M. Ternan, Eds; Chemical Institute of Canada: Otawa,

1988.

[189] M. R. Smith, U.S. Ozkan, J. Catal., 141 (1993) 124.

[190] M. R. Smith, L. Zhang, S. A. Driscoll, U.S. Ozkan, Catal. Lett., 19 (1993) 1.

[191] M. Faraldos, M. A. Banares, J. A. Anderson, H. Hu, I.E. Wachs, J. L. G. Fierro, J. Catal., 160 (1996) 214.

[192] M. J. Brown, N. D. Parkyns, Catal. Today, 8 (1991) 305.

[193] M.A. Banares, J. H. Cardoso, F. Agullo-Rueda, J. M. C. Bueno, J. L. G. Fierro, Catal. Lett., 64 (2000) 1191.

[194] S. S. Shepelev, K. G. Ione, React. Kinet. Catal. Lett., 23 (1983) 319.

[195] C. F Cullis, D. E. Keene, D. L. Trimm, J. Catal., 19 (1970) 378.

[196] R. S. Mann, M. K Dosi, J. Chem. Technol. Biotechnol., 29 (1979) 467.

[197] K. Otsuka, M. Hatano, J. Catal., 108 (1987) 252.

[198] N.R. Hunter, H.D. Gesser, L.A. Morton, P.S. Yarlagadda, Appl. Catal., 57 (1990) 45.

[199] Y. Wang, K. Otsuka, J. Catal., 155 (1995) 256.

[200] J. W. Chun, R. G. Anthony, Ind. Eng. Chem. Res., 32 (1993) 796.

[201] G. A. Foulds, B. F. Gray, S. A. Miller, G. S. Walker, Ind. Eng. Chem. Res., 32 (1993) 780.

[202] H. Bibb, H. J. Lucas, Ind. Eng. Chem., 21 (1929) 633.

[203] C. H. Bibb, Ind. Eng. Chem., 24 (1932) 10.

[204] D. F. Smith, R. T. Milner, Ind. Eng. Chem., 23 (1931) 357.

[205] B. H. McConkey, P. R. Wilkinson, I. E. C. Process Design Dev., 6 (1967) 436.

[206] Y. Teng, K. Tabata, F. Ouyang, L. Dai, H. Sakurai, T. Karasuda, Y. Yamaguchi, E. Suzuki, Chem. Lett., 1991, 991.

[207] Y. Teng, K. Tabata, E. Suzuki, Appl. Catal., A 190 (2000) 283.

[208] P. G. Ashmore, K. F. Preston, Combust. Flame, 11 (1967) 125.

[209] E. A. Dorko, D.M. Bass, R.W. Crossley, K. Scheller, Combust. Flame, 24 (1975) 173.

[210] E. K. Dabora, Combust. Flame, 24 (1975) 181.

Chapter - 2

PREPARATION AND CHARACTERIZATION OF Pt-NaY, PtFe-NaY AND Cu-Co-Ce-O CATALYSTS

2.1. INTRODUCTION

Metal based catalysts are very important, as they are used on a large scale in treating automobile exhaust, petroleum refining, carbon monoxide hydrogenation, hydrogenation of fats and for applications in many other processes. Precious metals are often expensive and may constitute only about 1 wt % of the catalyst material, being finely dispersed as particles on a high-surface area porous metal oxide or a zeolite. Hence, it is very important to apply a suitable method for the preparation and characterization of these catalysts.

The characterization of catalytic materials is a very important step in the process of catalyst development, as it provides insight into the relation between physical and chemical properties of the catalyst and its activity. If the structure and composition of the catalyst can be correlated with its activity and the desired product selectivity, the working of the catalyst is considered to be understood.

In this work for PrOx reaction, the catalysts were prepared by ion exchange and co-precipitation method, characterized by various physico-chemical methods such as powder X-ray diffraction, ICP-AES, infrared spectroscopy, surface area measurements, SEM, TEM, TPR-TPD, XPS, FTIR etc. The theory and experimental procedures of various characterization techniques used in the present study have been briefly described in the current chapter.

2.2. PHYSICOCHEMICAL CHARACTERIZATION - THEORY AND PRACTICE

Catalytic materials are usually characterized to correlate the structure and composition of the catalyst with their activity selectivity to a particular product. By applying these techniques one can get information of their crystallinity, surface structure, nature of active sites, particle size and morphology, acidity and other characteristic features.

2.2.1. Powder X-ray diffraction (PXRD)

PXRD is used to identify bulk phases, if desired under *in situ* conditions and is also used to monitor the kinetics of bulk transformations and to estimate particle sizes. In catalyst characterization, diffraction patterns are mainly used to identify the

crystallographic phases that are present in a catalyst [1]. The PXRD method involves the interaction between the incident monochromatized X-rays (like Cu or Mo Kα) with the atoms of a periodic lattice. X-rays scattered by atoms in an ordered lattice interfere constructively in directions given by Bragg's law:

$$n\lambda = 2\ d\ \sin\theta; \qquad n = 1, 2, 3\ldots \qquad (2.1)$$

where λ is the wavelength of the X-rays, d is the distance between two lattice planes, θ is the angle between the incoming X-rays and the normal to the reflecting lattice plane and n is the integer called order of the reflection. Bragg's peaks are measured by observing the intensity of the scattered radiation as a function of scattering angle 2θ. The angles of maximum intensity enable one to calculate the spacings between the lattice planes, which facilitates phase identification. The width of the diffraction peaks carries information on the dimensions of the reflecting planes. Diffraction lines from the perfect crystals are very narrow. For crystals with size below 100 nm, line broadening occurs due to incomplete destructive interference in scattering directions where the X-rays are out of phase. The width of the diffraction lines can be used to estimate the crystal size by using Debye-Scherrer formula [2],

$$L = k\lambda / \beta\cos\theta \qquad (2.2)$$

where, L, λ, β and θ are the volume averaged particle diameter, X-ray wavelength, full width at half maximum (FWHM), diffraction angle respectively, whereas k is a constant, often taken as 1. One important limitation of PXRD is that this technique requires samples, possessing sufficient long-range order. Amorphous phases and small particles give either broad and weak diffraction lines or no diffraction at all which makes them virtually invisible for XRD. Powder X-ray diffraction patterns of catalysts reported in this thesis were obtained on a Rigaku Miniflex X-ray diffractometer with a monochromatic Cu Kα radiation (λ = 0.15406 nm, 30 kV, 15 mA). Samples were scanned in the 2θ range of 10 to 90 ^{0} for mixed oxide materials, 5-50 for zeolite samples, at a step size of 0.02.

2.2.2. Infrared spectroscopy (IR)

Infrared spectroscopy is one of the most important technique in catalysis. The most common application of IR in catalysis is to identify adsorbed species and to study the way

in which these species are chemisorbed on the surface of a catalyst. More specifically, IR spectroscopy has been used to study the adsorption of typical probe molecules like ammonia, pyridine or other bases, hydrocarbons and carbon dioxide to monitor either the acidic or basic sites on oxide catalysts. Investigation of adsorbed species in relation to their behavior in catalytic reactions is the main field of application of IR spectroscopy. IR studies, if performed under conditions where some intermediates are actually detectable can give valuable information on reaction mechanisms.

The Fourier transform-infrared spectra of the catalysts reported here were recorded on Shimadzu 8300 FT-IR spectrometer under ambient conditions. The spectra were recorded using either thin self-supporting discs or discs made by pressing the mixture of a catalyst sample and KBr.

IR spectroscopy of adsorbed bases:

It is possible to determine the acidity by studying the adsorption of bases on acid sites of the zeolites and other solid acids using IR spectroscopy. Chemisorption of pyridine is a good technique to estimate the acidity of zeolites but not so suitable for oxides. Pyridine can react with Bronsted (B) as well as Lewis (L) acid sites of a zeolite. The chemisorption on the Bronsted acid sites results in the formation of pyridinium ion while the pyridine molecule also can coordinatively bound to the Lewis acid sites. Both the pyridinium ion and the coordinatively bound pyridine have characteristic IR absorption bands. The intensity of these bands corresponds to the number of sites; however, it is not possible to obtain quantitative information of the acid sites. The presence of the absorption bands shows that acid-sites are present with an acid-strength sufficient enough to react with the basic probe molecule pyridine. FTIR analysis of adsorbed pyridine allows a clear distinction between Brönsted and Lewis acid sites, the absorption bands appearing at 1545 and 1455 cm^{-1} in the IR spectra are assigned to adsorbed pyridinium ions and pyridine coordinated to Lewis acid sites, respectively [3 - 5].

A Thermo Nicolet (model Nexus 870) FTIR Spectroscopy was used for the acidity study by employing a high-temperature vacuum stainless steel cell, fitted with water-cooled CaF_2 windows. A high number of scans were averaged for obtaining better quality spectra.

2.2.3. Diffuse reflectance UV-visible spectroscopy (DR - UV)

Diffuse reflectance spectroscopy (DRS) is a technique based on the reflection of light in the ultraviolet (UV), visible (VIS) and near-infrared (NIR) region by a powdered sample. In a DRS spectrum, the ratio of the light scattered from an "infinitely thick" closely packed catalyst layer and the scattered light from an infinitely thick layer of an ideal non-absorbing (white) reference sample is measured as a function of the wavelength λ. The scattered radiation, emanating from the sample, is collected in an integration sphere and detected.

DRS is particularly suitable for studying the speciation of supported transition metal ions (TMI), because it measures both their d-d transitions and charge transfer bands. The obtained information is directly chemical since the outer shell electrons are probed. The DRS technique can be used under *in situ* conditions. DRS technique can be applied at different levels of sophistication, from merely detecting the presence of a certain oxidation state of a supported TMI up to a detailed distribution of different oxidation states and co-ordination environments under catalytic conditions. If the spectra are complex, encompassing several broad and overlapping bands, chemometrical techniques need to be employed for correct spectral analysis [6].

Diffuse reflectance UV-visible spectra of the present samples were recorded using a Shimadzu UV-2550 spectrophotometer. The spectra were measured in the range of 200-800 nm in air at room temperature.

2.2.4. Surface area by BET method (SA)

The Brunauer-Emmett-Teller (BET) method is the most widely used procedure for the determination of surface area of solid materials and involves the use of the BET equation (3).

$$P/V_{ads}\,(P_0-P) = 1/V_mC + [(C-1)/V_mC] \times (P/P_0) \qquad (3)$$

where P = adsorption equilibrium pressure, P_0 = standard vapour pressure of the adsorbent, V_{ads} = volume at STP occupied by molecules adsorbed at pressure P, V_m = volume of adsorbate required for a monolayer coverage, C = constant related to heat of adsorption. A plot of $P/V_{ads}\,(P_0-P)$ Vs (P/P_0) will yield a straight line usually in the range $0.05 \le P/P_0 \le 0.35$. The slope (s) and intercept (i) of the BET plot are $s = (C-1)/V_mC$ and $i = 1/V_mC$.

Solving these equations permits the calculation of Vm. Then the specific surface area of the catalyst can be calculated as,

$$\textbf{Specific surface area in } m^2g^{-1}\textbf{cat.} = [(V_mN_a)/22414xWt]xA_m \qquad (4)$$

Am = mean cross sectional area occupied by adsorbate molecule (16.2 A^2 for N_2), Wt = weight of the catalyst sample, Na = Avogadro number, Vm = monolayer volume in ml at STP. To differentiate between the adsorption mechanism in micropore and that occurring in meso and macropores, the t-plot analysis developed by Lippens and de Boer was applied [7]. The method consists of plotting the adsorption isotherm in terms of the volume of the gas adsorbed versus the statistical film thickness, t. The pore size distribution is obtained from the analysis of the desorption isotherms by applying the BJH model [8] which involves the area of the pore walls and uses the Kelvin equation to correlate the partial pressure of nitrogen in equilibrium with the porous solid to the size of the pores where the capillary condensation takes place.

The BET surface area and pore volume of the catalysts were determined by N_2 adsorption-desorption method at liquid N_2 temperature (77K) using Quantachrome Nova-1200 adsorption unit. About 200 mg of sample was degassed at 300^0C for about 4 hours till the residual pressure was $<10^{-3}$ Torr. The isotherms were analyzed in a conventional manner, that includes the BET surface area in the region of the relative pressure P/P_0 = 0.05 to 0.3 with the assumption for the nitrogen molecular area in an adsorbed monolayer of w = 0.162 nm^2. The pore size distribution was calculated via the BJH method. The total pore volumes were taken at P/P_0 = 0.95.

2.2.5. Scanning electron microscopy (SEM)

Scanning electron microscopy is a straightforward technique to study overall topography of a material [9]. SEM scans over a sample surface with probe of electrons (5-50 kV) and detects the yield of either secondary or back-scattered electrons as a function of the position of the primary beam. Parts of the surface facing the detector appear brighter than parts of the surface with their surface normal pointing away from the detector. Magnifications of 20 - 50,000 times is possible with a resolution of about 5 nm. Particle shape, size and distributions are easily obtained for particles larger than 5 nm. The

crystallite size and morphology of the catalysts of the present study were examined using a JEOL JSM-840A scanning electron microscope.

2.2.6. Transmission electron microscopy (TEM)

Direct visual information of size, shape, dispersion and structure of nanoparticles is generally obtained by TEM and more specifically by employing high-resolution transmission electron microscopy (HRTEM). Potential drawbacks of this technique include, (a) electron beam-induced structural rearrangements, aggregations or decompositions; (b) the inherent problems in interpreting two-dimensional images of 3D samples and (c) problems with sampling (only a small number of clusters can be analyzed and counted, which may not be representative of the sample as a whole). Despite these limitations, TEM has been the technique of choice due to atomic-level resolution and the attendant benefits of possible selected area electron diffraction (SAED). In SAED, an aperture is used to define the area from which a diffraction pattern is formed in a TEM specimen. The resulting patterns contain information about phases present (lattice spacing measurement) and sample orientation.

A TEM works much like a slide projector. A projector shines a beam of light through (transmits) the slide, as the structures and objects on the slide affect the light passing through it. These effects result in only certain parts of the light beam being transmitted through certain parts of the slide. This transmitted beam is then projected onto the viewing screen, forming an enlarged image of the slide. TEM works the same way except that they shine a beam of electrons (like the light) through the specimen (like the slide). Whatever part is transmitted is projected onto a phosphor screen for the user to see.
TEM measurements were made on a JEOL model 1200EX instrument operated at an accelerating voltage of 120 kV. Samples for TEM studies were prepared by placing a drop of the solutions on carbon-coated copper grids by dispersing minute quantity of crushed powder of the catalyst in IPA (isopropyl alcohol) that is ultra-sonicated for 30 min.

2.2.7. Temperature programmed techniques: TPR and TPD

Temperature programmed reduction (TPR), temperature programmed oxidation (TPO), temperature programmed desorption (TPD) and temperature programmed reaction

spectroscopy (TPRS) form a class of techniques in which a chemical reaction is monitored while the temperature is increased linearly. The basic set up for TPR, TPO and TPD consists of a reactor in a furnace that can be temperature programmed and a thermal conductivity detector to measure the hydrogen content in TPR or the oxygen content in TPO, of the gas mixture before and after reaction. In case of TPD, the desorption of the probe molecule is monitored with respect to temperature. The TPR/TPO/TPD methods are used for qualitative and quantitative analysis. All these techniques are applicable to practical catalysts as well as single crystals. Interpretation on a qualitative basis is rather straightforward, however quantitative analysis is more complicated.

In the TPR technique, the catalyst material is subjected to a programmed temperature rise, while a reducing gas mixture is flowing over it (usually, hydrogen diluted in some inert gas like argon). The reduction rate of the sample is continuously measured by monitoring the change in composition of the gas mixture after passing through the reactor. The decrease in H_2 concentration in the effluent gas with respect to the initial percentage is monitored with the linear increase in temperature.

TPD is a technique for studying the kinetics of adsorbates on solid surfaces. The data are collected under well-controlled flow or vacuum conditions. After analysis, it yields kinetic parameters as a function of adsorbate surface coverage. An evolved gas analyzer such as quadruple mass spectrometer is tuned to monitor one or more mass fragments simultaneously that can be correlated to the desorbing species with respect to sample temperature. The desorption temperature, the shape of the desorption peak, and how these changes are related to initial surface coverage and heating rate are analyzed to provide information about the binding character of the adsorbate/substrate system.

Desorption of bases: Temperature programmed desorption (TPD)

When an acid is neutralized by reaction with a base, the heat of neutralization is evolved. The higher the heat of neutralization, stronger is the acid strength and so it can be used to characterize acid-strength. This principle can be used to characterize the acid sites present on a solid acid by TPD of probe molecules like ammonia and pyridine. This is a popular method for the determination of acidity of solid acids as well as acid strength because it is an easy and reproducible method. Ammonia is used frequently as a probe molecule because of its small molecular size, stability and strong basic strength [10]. First

the zeolite is contacted with a base (NH_3 or pyridine) to neutralize the acidic sites present. Then the temperature is raised at a constant rate and the amount of desorbed base is monitored and recorded. In short, TPD consists of heating a sample at a constant rate and measuring the quantity of material desorbed at each temperature. TPD data provide a partially averaged value for acid strength. It is a simple and rapid method to characterize zeolite acidity. NH_3-TPD is one of the most often used methods [11-13]. In principle, the concentration of sites having similar acid strength and the average heat of adsorption or activation energy of NH_3 desorption can be determined using the TPD method. Often the temperature of maximum desorption rate, i.e., the temperature of a TPD peak (T_{max}), is used as a rough measure of the acid strength of the sorption sites. Among the limitations of this method is that it can distinguish sites by sorption strength only, but not Lewis and Bronsted type-sites. Moreover, desorption may proceed simultaneously from sites of different types resulting in composite curve consisting of overlapping TPD peaks. In a NH_3-TPD spectrum for solid acids, generally two peaks are observed, one at low temperature (LT) corresponding to NH_3 desorbing from the weaker acidic sites (also observed for nonacidic silicates) and another one at higher temperature (HT) corresponding with the stronger acidic sites. The area under these peaks gives information about the amount of these strong acid sites whereas the peak-maximum-temperature (T_{max}) gives information about its acid-strength.

The temperature programmed reduction experiments were carried out with a Micromeritics Autochem 2910 catalyst characterization system, equipped with a TCD detector.

2.2.8. X- ray photoelectron spectroscopy (XPS)

The X-ray photoelectron spectroscopy [14-16] is based on the photoelectric effect, which involves the bombardment of a sample surface with X rays and the measurement of the concomitant photoemitted electrons. The photoemitted electrons have discrete kinetic energies that are characteristic of the emitting atoms and their bonding states. The kinetic energy, E_k, of these photoelectrons is determined by the energy of the X-ray radiation, $h\nu$, and the electron binding energy, E_b, as given by:

$$E_k = h\nu - E_b \qquad (5)$$

The experimentally measured energies of the photoelectrons are given by:

$$E_k = h\nu - E_b - E_w \qquad (6)$$

where, E_w is the work function of the spectrometer.

The binding energies of the peaks are characteristic of each element. The peak areas can be used (with appropriate sensitivity factors) to determine the composition of the materials surface. The shape of each peak and the binding energy can be slightly altered by the chemical state of the emitting atom, which provide chemical bonding information as well. XPS and the related Auger electron spectroscopy (AES) can provide elemental analysis for essentially the entire periodic table. Because the electrons whose energies are analyzed arise from a depth of no greater than about 5 nm, the technique is surface-sensitive.

X-ray photoelectron spectra of the present study were acquired on a VG Microtech Multilab ESCA 3000 spectrometer using a non-monochromatized MgKa X-ray source ($h\gamma$ = 1253.6 eV) at room temperature. Base pressure in the analysis chamber was maintained at 3-6 x 10-10 Torr range. The energy resolution of the spectrometer was determined from the full width at half maximum of metallic gold and the value obtained is better that 0.8 eV for MgKα radiation and 1.1 eV for AlK α radiation respectively, at a pass energy of 20 eV. The error in the BE values [17] reported is ± 0.1 eV.

2.2.9. H_2-Chemisorption

Hydrogen chemisorption occurs readily on n-type semiconductor oxides and negligible on p-type semiconducting oxides. There are two possible modes of chemisorptions one rapid, week and tending to predominate at low temperatures and the other slower, stronger and predominant at high temperature. There is evidence to show that in both cases hydrogen molecule is dissociated.

2.2.10. Laser Raman spectroscopy (LRS)

Raman spectroscopy is based on the inelastic scattering of photons, which loose energy by exciting vibrations in the sample. A vibration is Raman active if it changes the polarizability of the molecule. Raman and infrared spectroscopies complement each other, particularly for highly symmetrical molecules.

Raman spectroscopy can widely be used for investigations of metals oxides, and metals supported on oxides/mixed oxides and at the water-solid interface and has found steadily increasing applications in the characterization of supported transition metal oxide catalysts since the early work of Villa et al [18] in 1974. Laser Raman spectroscopy (LRS) is particularly powerful for investigations of the structure of supported oxide catalysts. All characteristic vibrational features of oxides of the transition metals like Mo, W, Cr, V and Re fall into a frequency range below 1100 cm^{-1}. These oxides have high Raman scattering cross-sections because of their relatively high covalent bond character. The usual support materials (particularly alumina and silica) have very low Raman scattering cross-sections and only show weak absorption bands in the 700–1100 cm^{-1} region. Hence LRS has the advantage that the normal modes of the minority components, namely the transition metal oxides dispersed on the supports, can most frequently be detected by LRS with relative ease in the frequency region 50 to 100 cm^{-1}. It should be also mentioned that titania and zirconia oxides possess strong Raman absorption bands in the region below 700 cm^{-1}. The surface vanadium oxide structure has been studied during the adsorption and oxidation of methanol and methane, and during the selective catalytic reduction of nitrogen oxides. There are some major problems that may be encountered in LRS like the heating effects of the laser beam, low sensitivity of the technique and background fluorescence.

Laser Raman spectra reported in this thesis were obtained at room temperature using a Spex 1403 spectrometer. The samples were heated at 473 K in air for 2 h and cooled to room temperature before recording the spectra. The 514.5 nm line of an argon ion laser (Spectra Physics 165) was used for excitation. The laser power at the sample was approximately 40 mW. The scattered light was collected in the backscattering geometry and detected with a thermoelectrically cooled photomultiplier.

2.3. PREPARATION OF Pt-NaY AND PtFe-NaY CATALYSTS

The Pt-NaY samples with different platinum loadings (0.2, 0.5, 0.75, 1.0) were prepared by simple ion exchange method as discussed in preparation method of catalyst in chapter 1. The catalysts were prepared by exchange of Na in NaY-type zeolite (SiO_2/Al_2O_3 = 5, surface area 683 m^2/g) obtained from Zeolyst International. Aqueous $Pt(NH_3)_4(NO_3)_2$ solution was used for ion exchange at 80 ^0C for 3 h. The same procedure was applied for

promoted Pt NaY catalysts by using salts of Au, Co and Fe. After exchange, the samples were filtered and washed by distilled water to remove chloride, dried at 100 ^{0}C for 10-12 h followed by calcination in air at 350 ^{0}C for 3 h. The filtrate of the sample after exchange was analyzed by AAS for estimation of the Pt content that remained un-exchanged.

2.4. CHARACTERIZATION RESULTS OF Pt-NaY AND PtFe-NaY CATALYSTS

Table 2.1 gives the surface area, aimed platinum content vs actual Pt content, platinum dispersion and hydrogen consumption (H_2 - TPR) of platinum and modified platinum NaY samples. Platinum contents were determined by AAS analysis. The catalysts were calcined at 350 ^{0}C in air for 4h before analysis.

Fall in surface area was noticed with increase in platinum loading. Better dispersion of platinum was observed for 0.2Pt-NaY and PtFe-NaY catalyst.

Table 2.1 Structural results of Pt and Pt promoted NaY catalysts

Sample name	Pt content (wt%)	Pt content by AAS (wt%)	Surface area m^2/g*	H_2 consumption By H_2-TPR µmoles/g	Pt Dispersion (%)**
NaY	-----	-----	683	-----	-----
0.2Pt-NaY	0.20	0.21	670	-----	80
0.5Pt-NaY	0.50	0.49	650	45.23	47
0.75Pt-NaY	0.75	0.73	642	67.45	56
1Pt-NaY	1.00	0.99	631	53.27	45
(0.75:0.38) PtFe-NaY	0.75	0.74	593	70.24	65

** Calculated through BET method.*

** * Calculated from hydrogen chemisorption.*

2.4.1. Powder X- ray diffraction

PXRD analysis was performed to study the stability of NaY zeolite to various treatments and also to investigate the nature of the metal oxide deposited on the zeolite. The crystalline structures of modified as well as spent catalyst samples were substantially preserved, as shown in Fig. 2.1. and 2.2. Absence of diffraction peaks related to Pt as well as Fe, Au and Co in these samples indicates fine dispersion of these metals on the support.

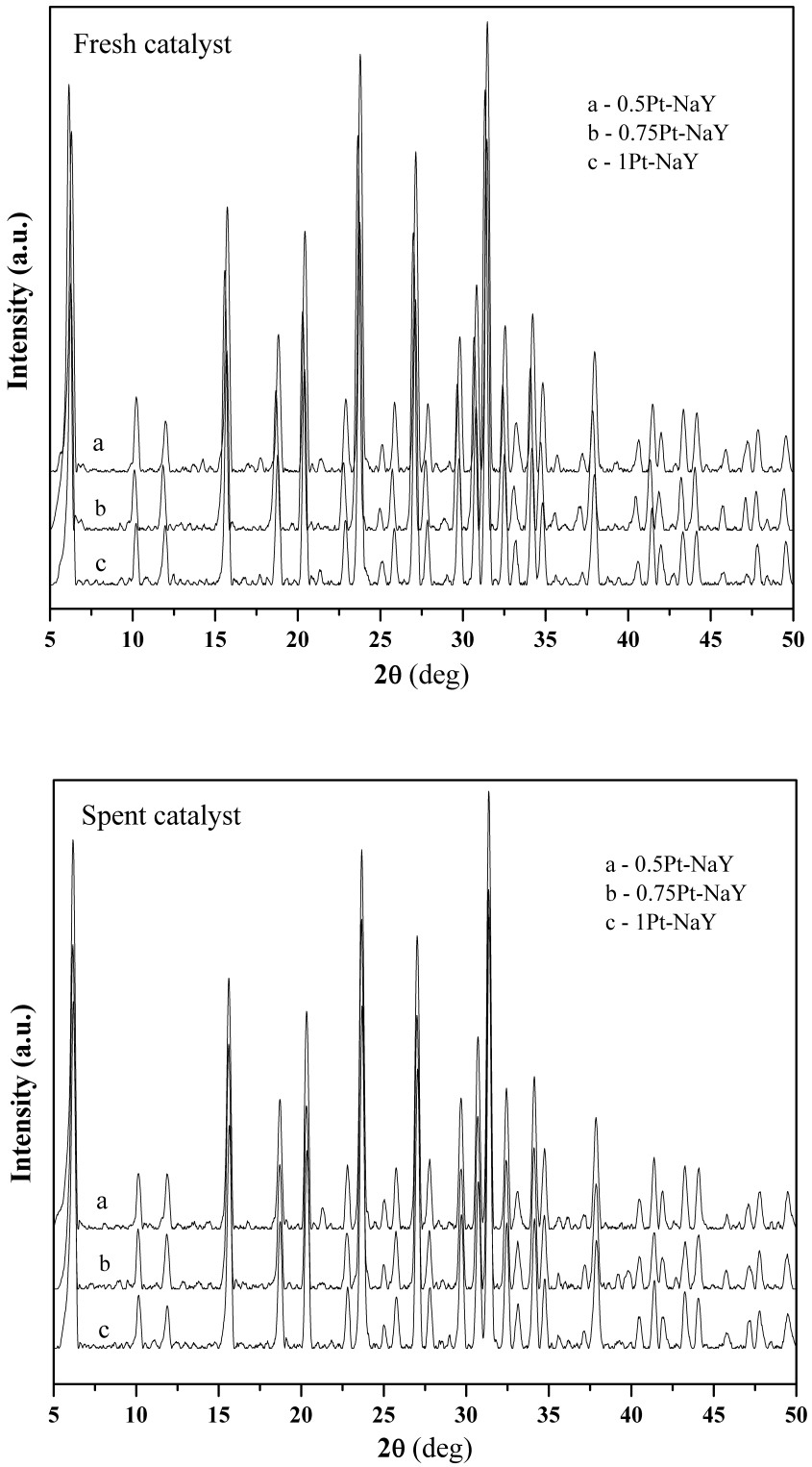

Fig. 2.1: *Powder X-ray diffraction pattern of Pt-NaY, fresh and spent samples.*

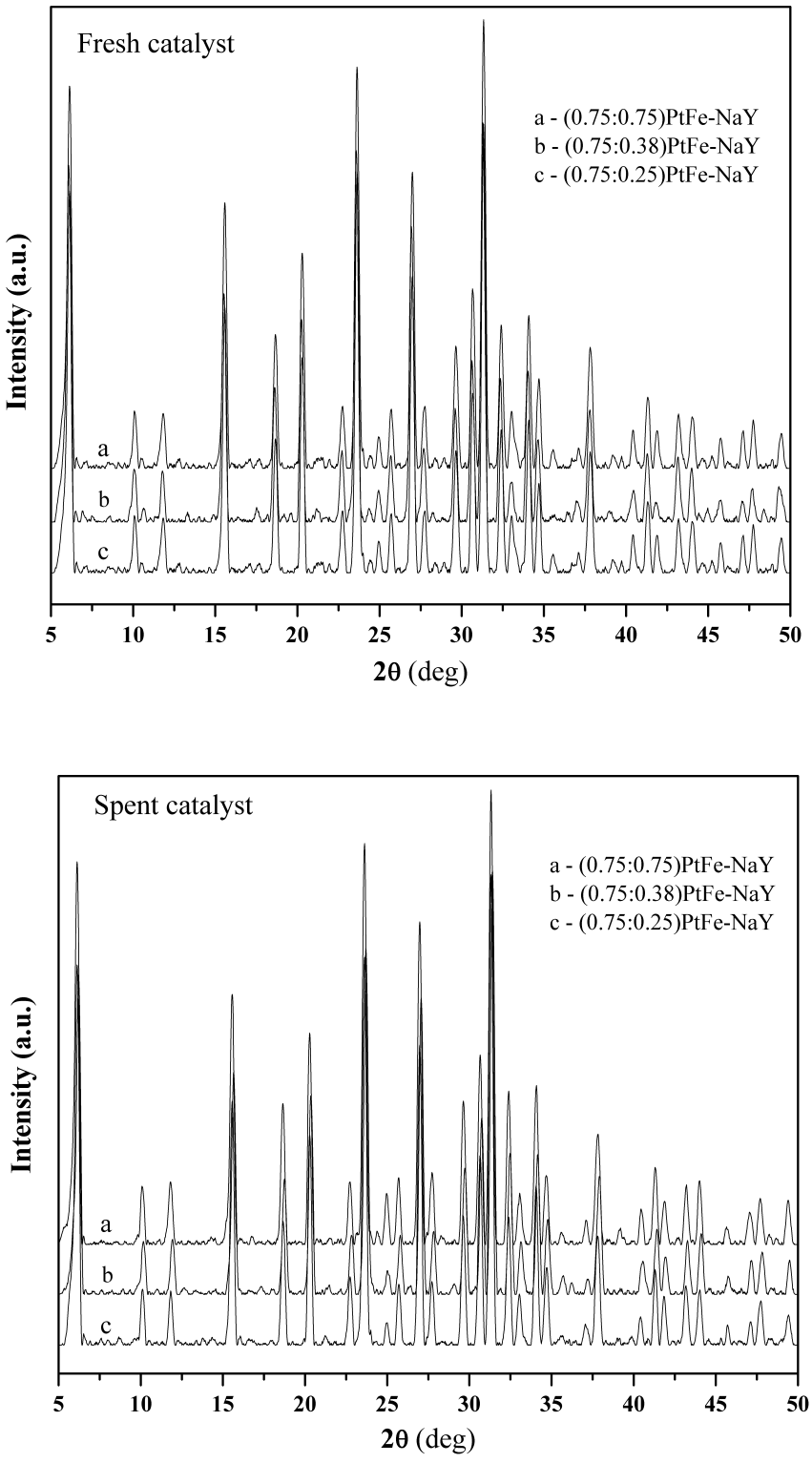

Fig. 2.2: *Powder X-ray diffraction pattern of PtFe-NaY, fresh and spent samples.*

A small degradation in the structure of the sample was observed when water was added to the feed stream during the PrOx reaction [19]. From these results it is assumed that there is not much change in the fresh and spent samples, which may be due to the low metal loading or might be due to high dispersion of these metals [19 - 21]. These results are in good agreement with hydrogen chemisorption results presented in table 2.1.

2.4.2. Temperature programmed reduction

TPR profiles of Pt loaded NaY samples with different metal catalysts calcined at 350 ^{0}C are presented in the Fig. 2.3. A TPR spectrum of blank NaY was also recorded (not shown) which shows the absence of any reduction peak in the temperature region (50-950 ^{0}C) of the present study.

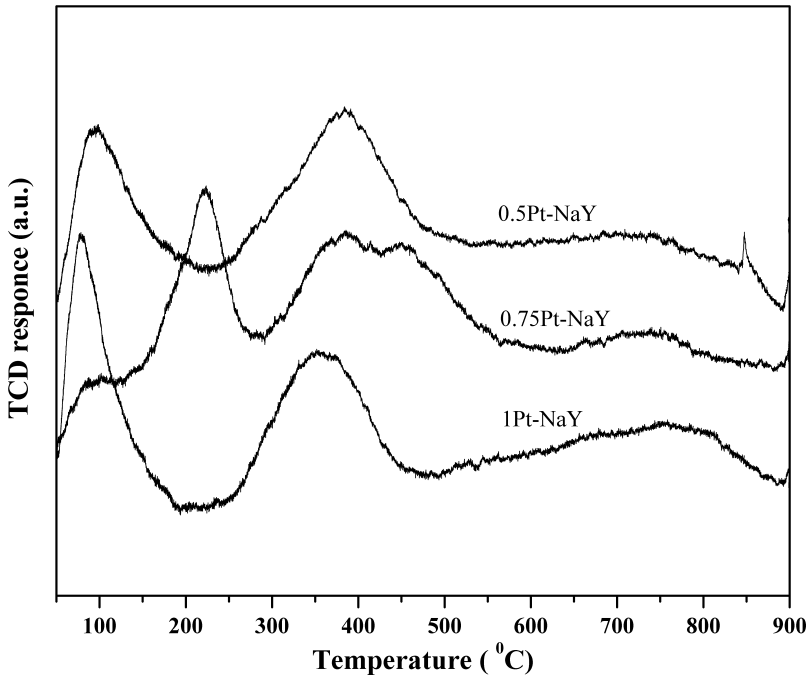

Fig. 2.3: *TPR profiles of Pt-NaY with different platinum contents.*

Two peaks were observed for 0.5Pt-NaY (78 and 357 ^{0}C) and 1Pt-NaY (95 and 386 ^{0}C), while three peaks were seen for 0.75Pt-NaY (84, 224 and 388 ^{0}C) as shown in Fig. 2.3. The three peaks correspond to the reduction of three hypothetical surface oxides of platinum on 0.75Pt-NaY. These results are in agreement with those reported for supported metals by Lieske et al [22, 23]. They observed two reduction peaks in the temperature zone

100 and 300 ^{0}C. From the quantity of H_2 consumed it was concluded that platinum must have been present as PtO_2 and the peaks were attributed to the reduction of two modifications of hypothetical surface oxide.

Figure 2.4 shows TPR spectra of the samples that contain Pt and Fe. The spectra of PtFe-NaY are obviously not linear combinations of Pt-NaY and Fe-NaY. A shift in the temperature of reduction was noticed, which may be due to the mixed oxide particles formed during the calcination process. The peak at 367 ^{0}C in Fe-NaY is due to the reduction of Fe^{3+} to Fe^{2+} [22], whereas peak at 872 ^{0}C may be attributed to Fe^{2+} to Fe [23, 24]. There is a significant peak at lower temperature for PtFe-NaY, which strongly suggests that iron ion migrated to smaller cages [25] and due to the blocking by iron ions a large fraction of Pt^{2+} ions remain in the supercages, which is easily reduced at lower temperature. Also, as seen in Fig. 2.4, the intensity of the low temperature peak increases with increasing iron content that supports our interpretation. Hydrogen consumption of these samples is summarized in table 2.1, hydrogen consumption increases with increase in platinum content, but not linearly.

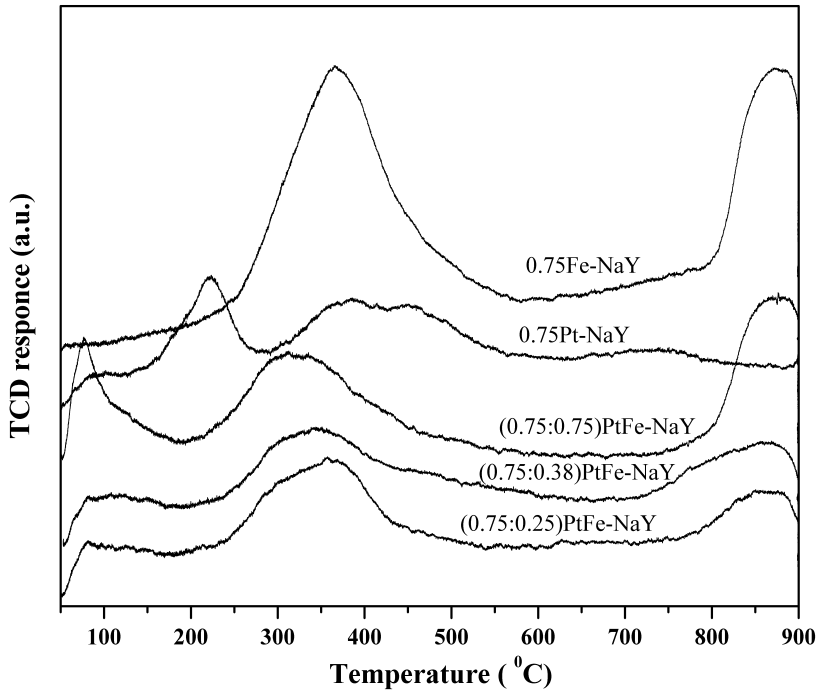

Fig. 2.4: *TPR profiles of 0.75Pt, Fe-NaY and Pt: Fe with different metal ratio.*

2.4.3. Transmission electron microscopy studies

Particle size and dispersion of Pt on the support (NaY) plays a vital role in the preferential oxidation of CO. For obtaining small particles and higher dispersion, different studies like metal composition, calcination temperatures were studied. Transmission electron microscopy studies of 0.5, 0.75 and 1.0 Pt-NaY are shown in Fig. 2.5 whereas Fig. 2.6 and 2.7 gives photographs of modified Pt-NaY samples. Samples were prepared by dispersing in isopropyl alcohol (sonicated for 30 min and dried on coated Cu grids). The TEM results show particles with good contrast, presumably of platinum, scattered on the NaY matrix. Crystals of platinum are expected to yield a highly contrasted and morphologically resolved images compared to the faintly contrasted images of the support i.e. NaY. A number of well-dispersed platinum particles on the support can be seen in the TEM picture with a fairly even size distribution. The average particle size of the platinum was found to be 8 nm (± 2 nm) for samples with only platinum, whereas 4 nm (± 2 nm) for PtFe-NaY samples that have 0.75 % Pt and 0.38 % Fe. From Fig. 2.5 it is clearly seen that the dispersion increased initially with metal content giving a better dispersion for the sample containing 0.75 % platinum than 0.5 or 1.0 % sample.

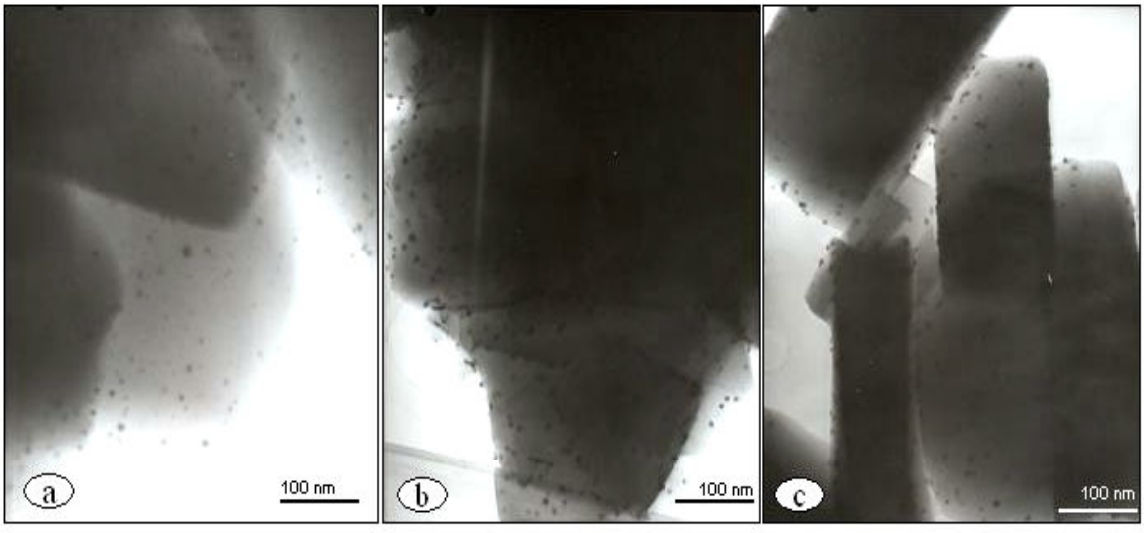

Fig. 2.5: *TEM images of different platinum loaded sample activated at 400 ^{0}C (a) 0.5Pt-NaY, (b) 0.75Pt-NaY (c) 1Pt-NaY.*

In Fig. 2.6 the TEM images of PtFe-NaY (0.75:0.38) samples calcined and reduced at different temperatures (300, 400, 500 ^{0}C) are given, which are useful to monitor the metallic particles on NaY. This particular ratio was chosen for detail study due to its relatively better PrOx activity.

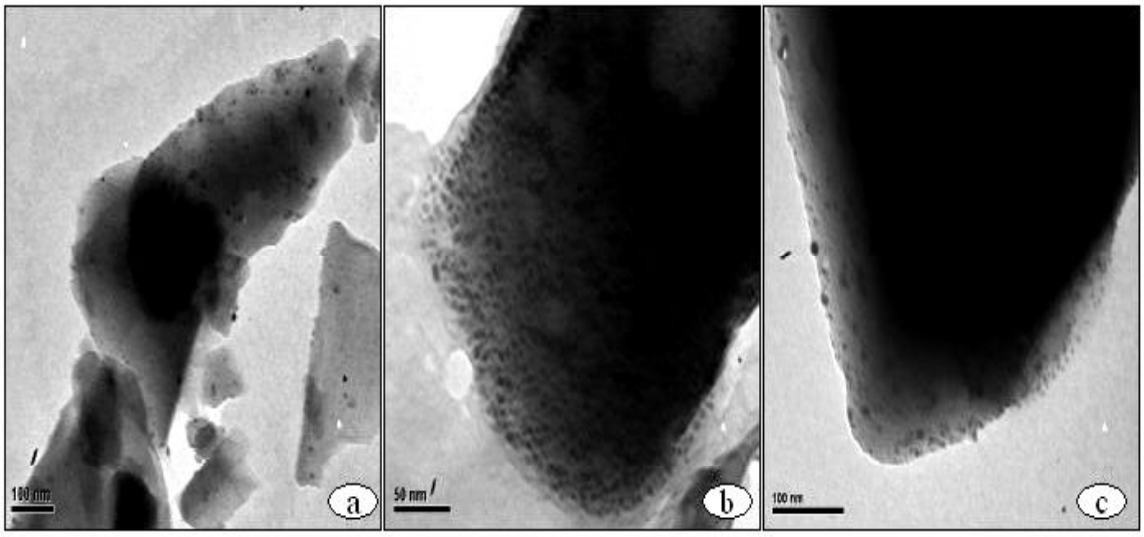

Fig. 2.6: *TEM images PtFe-NaY (0.75:0.38) sample activated at (a) 300 ^{0}C, (b) 400 ^{0}C, (c) 500 ^{0}C.*

For the samples treated at 300 ^{0}C most of the metallic particles were well dispersed with almost similar size except for few large particles (2.6 a). But, sample activated at 400 ^{0}C (2.6 b) shows better dispersion with very small and uniform particle size of platinum as compared to 500 ^{0}C activated sample (Fig. 2.6 c). The small particles may be obtained under conditions that does not aid diffusion of ion-exchanged Pt and Fe, thereby arresting the growth of metallic particles, as a result of low temperature (400 ^{0}C) treatment [26, 27]. Large metallic particles with varying sizes can be observed in the sample activated at 500 ^{0}C (2.6 c). Similar images were observed for 6 % Pt/ZSM-5 [28] and Pt-Fe/Mordenite [26]. Large metallic particles were presumably formed as a result of the diffusion of Pt and Fe cationic species, which could be facilitated due to high pretreatment temperature. A few particles of size about 8-9 nm are also observed along with agglomerated Pt particles of size of 15-20 nm, indicating that a small fraction of the platinum particles remained unaffected on the support (NaY). Figure 2.7 shows the TEM images of samples with

different Fe (0.25, 0.38, 0.75 %) content on 0.75Pt-NaY. Sample with 0.38 % iron gave better results as per the reasons cited above. Fe was not detected in Fe containing samples by TEM observation as well as PXRD. However, the presence of Fe was clearly seen by AAS analysis and its influence was clearly seen PrOx reaction.

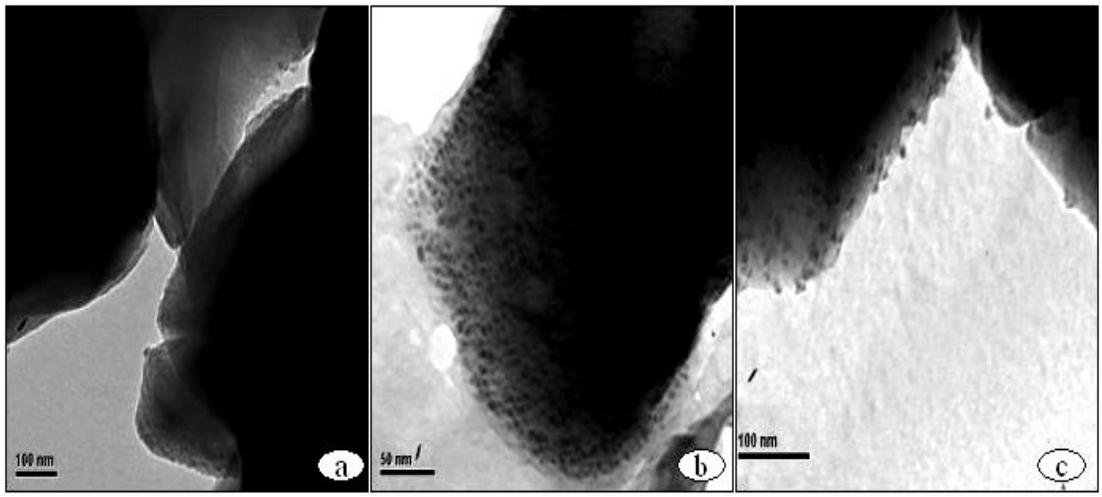

Fig. 2.7: *TEM images of different iron loaded 0.75Pt-NaY sample (a) 0.25%, (b) 0.38%, (c) 0.75% iron containing samples activated at 400 ^{0}C.*

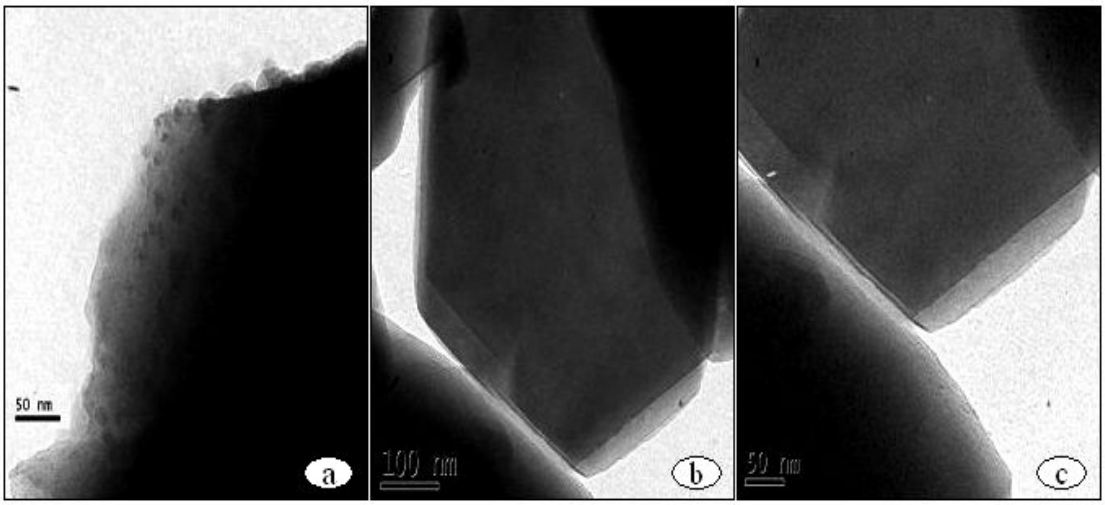

Fig. 2.8: *TEM images of (a) Fe-NaY, (b & c) NaY without any metal loading*

The TEM images of NaY and Fe-NaY are shown in Fig. 2.8. We were unable to take the diffraction pattern of the platinum and iron due to charging of the sample, thereby

making the image un-stable. Iron sample shows small particles of around 12 nm, whereas clean surface of the NaY can be seen in b and c of Fig. 2.8.

2.4.4. H_2-Chemisorption

Pt dispersion was measured by volumetric H_2 chemisorption uptake at 40 ^{0}C using a Quantachrom chemisorption analyzer assuming a 1:1 H/Pt adsorption stiochiometry. Prior to this study, the samples were treated in H_2 at 300 ^{0}C for 2 h and then evacuated at 350 ^{0}C for 30 minutes. Followed by it, the sample was cooled to 35 ^{0}C and H_2 chemisorption isotherms were measured at 5-50 kPa H_2; physic sorption isotherm also was recorded by repeating this procedure after evacuating the sample at 35 ^{0}C for 20 min. These two isotherms were extrapolated to zero H_2 pressure, and their difference was measured to obtain strong chemisorbed hydrogen and utilized for calculation of Pt dispersion.

Dispersion of platinum and platinum-iron loaded NaY samples is listed in table 2.1. Better dispersion was observed for samples that have less amount of platinum. Pt dispersion was found to be better on alkali exchanged NaY, as it has been reported to aid metal dispersions [29-32]. Alkali increases the zero point charge of SiO_2 surfaces from pH 3.2 to ~ 8 [33-36] due to this Pt amine complex interact more strongly with SiO_2 surface of the NaY.

2.5. PREPARATION OF Cu-Co-Ce-O MIXED OXIDE CATALYSTS

Cu-Co-Ce-O mixed oxide samples were prepared by simple co-precipitation method that was described in chapter-1. Copper and cobalt supported on ceria having general formula of $Cu_xCo_{(1-x)}Ce_2O_{4-\delta}$ with x = 0, 0.15, 0.25, 0.50, 0.75, 1.0 were prepared using aqueous potassium hydroxide as precipitating agent. Appropriate amounts of $Cu(NO_3)_2$, $Co(NO_3)_2$, $Ce(NO_3)_3$ and KOH were dissolved in distilled water to prepare 0.2M solutions of each salts. The salt solutions of copper, cobalt and ceria were mixed together and added slowly to 0.2M solution of potassium hydroxide in 2 liter round bottom flask placed in heating mental under continuous stirring. Addition was done at 80 ^{0}C with while maintaining the pH in the range of 9.5-10. Subsequently, the precipitate was digested, cooled to room temperature, filtered and washed with distilled water to remove

potassium. Followed by this, it was dried at 100 ^{0}C for 8 h, crushed to powder and calcined at 500 ^{0}C for 5 h to obtain the corresponding oxide.

2.6. CHARACTERIZATION RESULTS OF Cu-Co-Ce-O MIXED OXIDE CATALYSTS

Support plays an important role in any oxidation reaction, particularly if it provides oxygen for the reaction. Here in this system we have applied ceria, which has a high oxygen storage capacity, as a support for copper and cobalt.

Table 2.2 gives metal concentration in weight percentage of different Cu-Co-Ce-O mixed oxide samples along with their BET surface areas and PXRD parameters. Not much deviation in metal percentage of the projected and actual concentration was observed. Usually samples prepared by co-precipitation does not show much deviation.

Table 2.2. Surface properties of $Cu_xCo_{(1-x)}Ce_2O_{4-\delta}$ samples

Catalyst Composition (x)	Metal Content (Wt %) by AAS *			Crystalline size of CeO_2 (nm)**	a (A^0)	Surface area m^2/g	H_2 Consum. #	NH_3 Desorb. Φ
	Cu	Co	Ce				μmoles/g	
0	0.00	14.60	85.4	6.9	5.405	101	4270	120
0.15	2.40	11.1	86.5	5.4	5.410	101	5770	300
0.25	3.90	10.9	85.2	4.7	5.411	105	6060	200
0.50	7.84	7.30	84.9	10.6	5.411	113	5010	900
0.75	11.7	3.60	84.7	7.8	5.410	131	5060	400
1.00	15.6	0.00	84.4	7.6	5.411	144	4980	300

* *Analyzed by AAS.*
** *Calculated using Debye-Scherrer equation.*
\# *Estimated by H_2-TPR.*
Φ Calculated by NH_3 -TPD.

Surface areas of the ceria and ceria-supported samples are usually 60 m^2/g [37]; we were successful in preparing high surface area mixed oxide samples. The surface area of the samples increased from 101 to 144, with the in crease in copper content. This shows that, there is drop in surface area of the sample with increase in cobalt content. The drop in surface area for samples with higher Co content may be due to the formation of new phases of cobalt [38]. It is tempting to attribute the drop in surface area to blocking pores of ceria

by clusters of cobalt. [39]. The major phase obtained was of CeO_2 with separate phases of CuO and Co_3O_4, so the lattice constant (CeO_2) obtained for these sample shows not much deviation as given in table 2.2. This small deviation in x = 0 and others is due to the presence of extra phases in the samples.

2.6.1. Powder X-ray diffraction

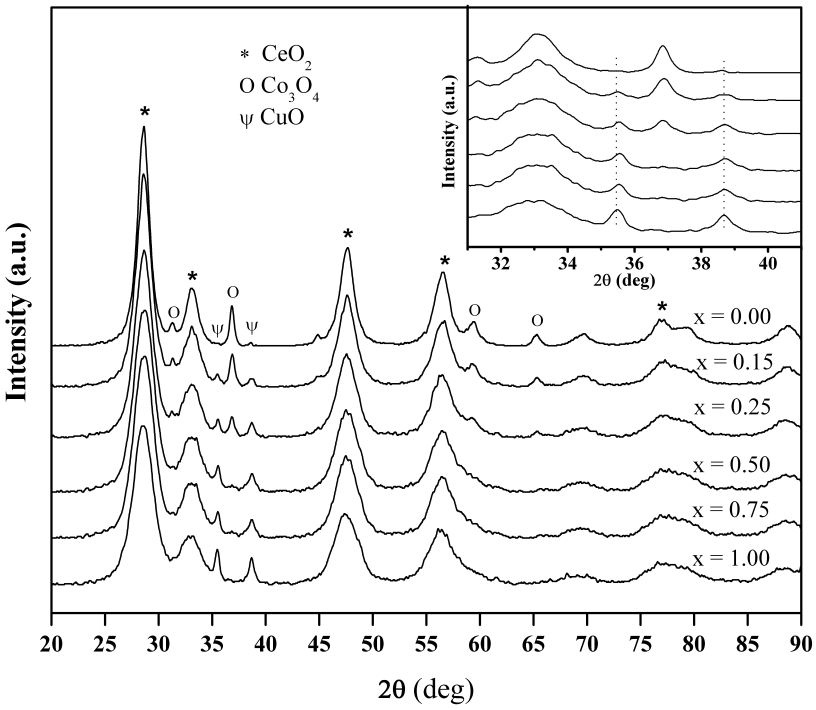

Fig. 2.9: *Powder X-ray diffraction pattern of $Cu_xCo_{(1-x)}Ce_2O_{4-\delta}$ calcined at 500 ^0C.*

Figure 2.9 shows X-ray diffraction pattern of various Cu-Co-Ce-O mixed oxide samples calcined at 500 ^{0}C. The broad peaks seen in PXRD pattern indicate the formation of small particles in contrast to sharp peaks obtained by other than co-precipitation method. The crystalline sizes of the samples (table 2.2) were estimated by using the most intense CeO_2 peak using Debye-Scherrer equation [39]. The four strong peaks observed in the 2θ range 28-60 ^{0} corresponds to cubic structure of fluorite type of ceria (*) [40, 41], while no other phases of ceria were observed in any of these samples. Whereas well dispersed separate CuO and Co_3O_4 phases were observed, no solid solution formation was

recorded by PXRD except two apparent CuO diffraction peaks at 2θ = 35.6 and 38.8 indicating that a change of CuO dispersion state had taken place.

2.6.2. Infrared spectroscopy

The FTIR spectra of calcined Cu-Co-Ce-O mixed oxide samples as a function of copper content are shown in Fig. 2.10. Since, the cobalt oxide is X-ray amorphous, its IR spectrum could provide valuable information about its structure. The spectra of these samples show that oxygen is bound to the Co metal ions. The IR spectra of Co_3O_4 shows two distinct broad bands at 659 - 662 and 562 - 569 cm^{-1} that originate from stretching of the metal to oxygen band [42]. Whereas, CoO does not show any intense bands in the vibrational spectra and hence difficult to identify using FTIR.

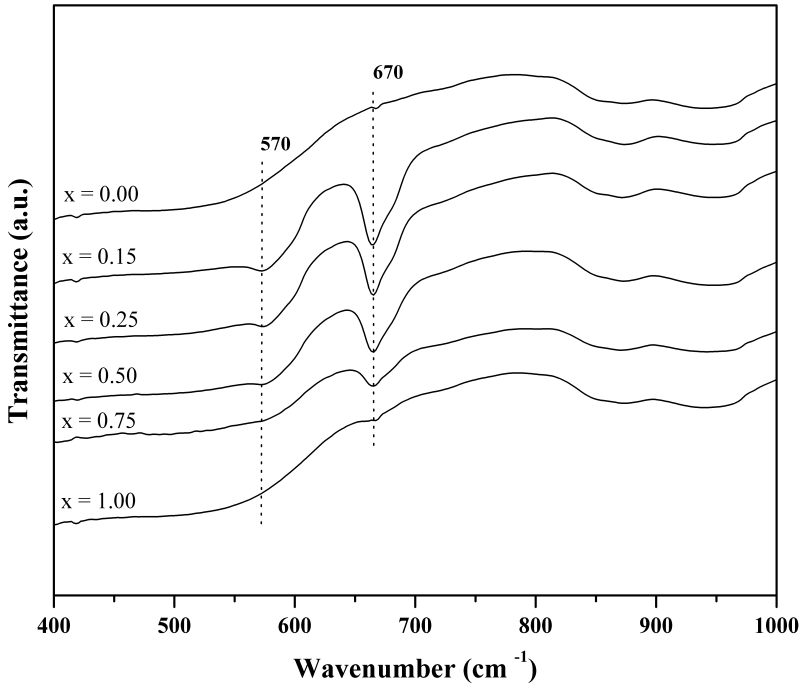

Fig. 2.10: *Diffuse reflectance IR (DR-IR) of $Cu_xCo_{(1-x)}Ce_2O_{4-\delta}$ at room temperature.*

The IR spectra of present mixed oxide system (Cu-Co-Ce-O) shows two characteristic bands [43, 44] at 570 and 670 cm^{-1}, interpreted for stretching vibrations of the metal to oxygen bond in Co_3O_4. These two bands can be ascribed to the vibration of

low spin Co(III) in octahedral sites [45 - 50]. Hence, based on the above results one can say that cobalt is present as Co^{3+} and in octahedral holes.

2.6.3. Diffuse reflectance UV-visible spectroscopy

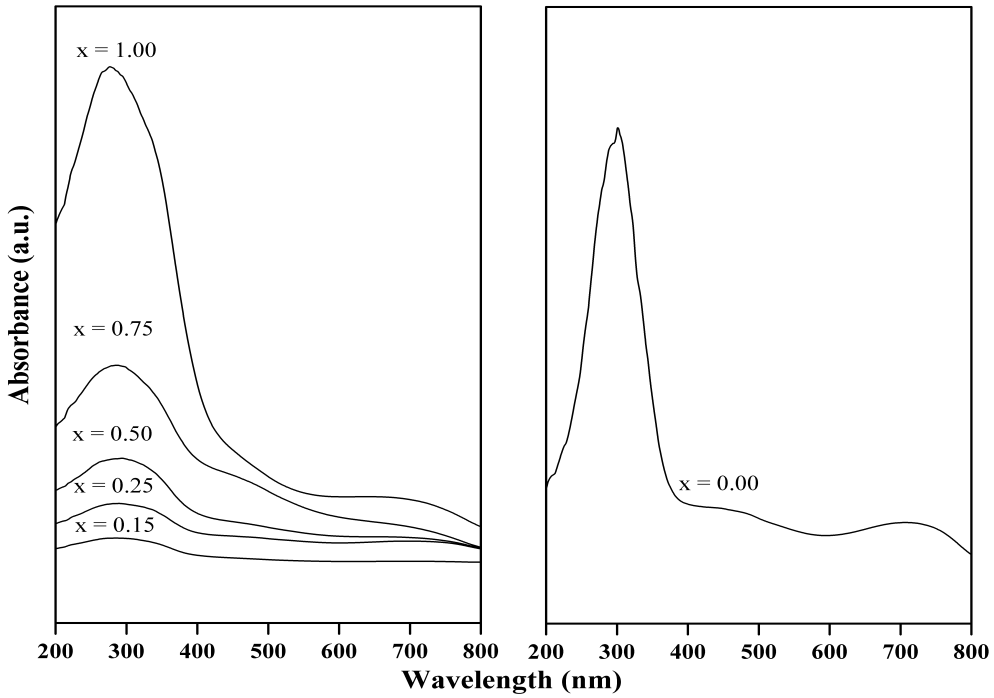

Fig. 2.11: *Diffuse reflectance UV-visible spectra of* $Cu_xCo_{(1-x)}Ce_2O_{4-\delta}$.

Diffuse reflectance spectra of Cu-Co-Ce-O mixed oxides is shown in Fig. 2.11. As pure ceria shows strong absorption band in the UV range, the diffuse reflectance (DR) spectrum for $\lambda < \lambda g$ is affected by specular reflectance; this phenomenon explains two UV bands at 275 and 350 nm attributable to $O^{2-} \rightarrow Ce^{4+}$ charge transfer (CT) transitions. First band is arising from the surface site and latter from bulk ceria [51]. The CT band shifted to higher wavelength (lower energy) i.e. from 276 to 293 nm, with the addition of copper. The observed shift towards lower wavelength with the increasing copper content reveals a decrease in the crystalline size of ceria. These observations further emphasize the results of PXRD data. These catalysts showed a broad *d-d* band in the visible region (Fig. 2.11). The shift from 625 to 729 nm was observed with increase (x = 0.15 to 1.0) in the CuO content. Absorbance decreases with addition of cobalt whereas only cobalt shows high absorbance

and CT band shift was observed at 300 to 450 nm. Cobalt containing ceria (x = 0) shows a broad *d* - *d* band which shift in the visible region at 713 nm, indicating that the type of copper and cobalt species in these materials is influenced by both the support and their concentration.

2.6.4. Scanning electron microscopy studies

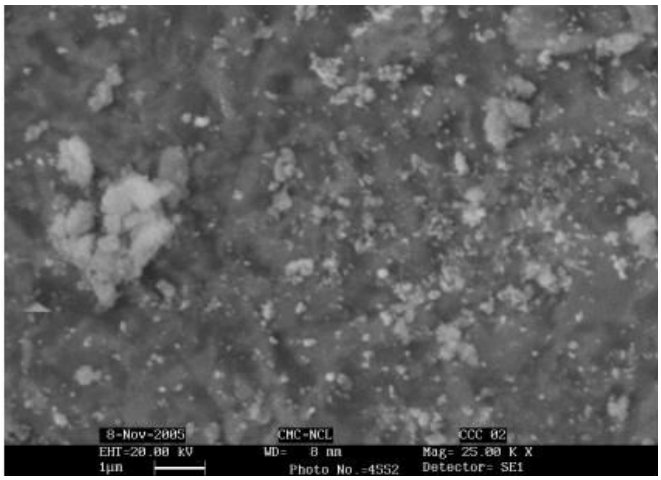

(a)

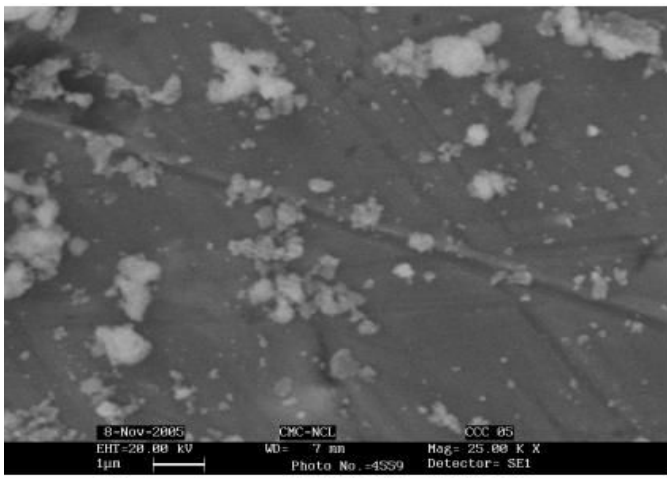

(b)

Fig. 2.12: *SEM photographs of $Cu_xCo_{(1-x)}Ce_2O_{4-\delta}$ sample (a) x = 0.25, (b) x = 1.00.*

Scanning electron microscopy of $Cu_xCo_{(1-x)}Ce_2O_{4-\delta}$ catalysts, with x = 0.25 and 1, calcined at 500 ^{0}C are shown in Fig. 2.12. From these images we can say that the morphology of the particles depends on the copper content in the sample. The sample with

x = 1 shows particles of non-uniform size and shape as compared to that of the sample with x = 0.25. This is probably due to the aggregation of particles with increase in copper content. Infact, we can see the well-dispersed particles in sample with x = 0.25.

2.6.5. Transmission electron microscopy studies

Figure 2.13 shows TEM images of Cu-Co-Ce-O mixed oxide samples along with electronic diffraction. The TEM image shows well dispersed particles with uniform shape and size of CeO_2. The electronic diffraction shows that the particles observed in the sample are of ceria only. The average particle size of the samples was around 6 nm for x = 0.25, whereas around 8 nm for x = 1.0. These results are further supported by PXRD. It has been reported that the average size of ceria is around 30 nm for sample prepared by different methods [52].

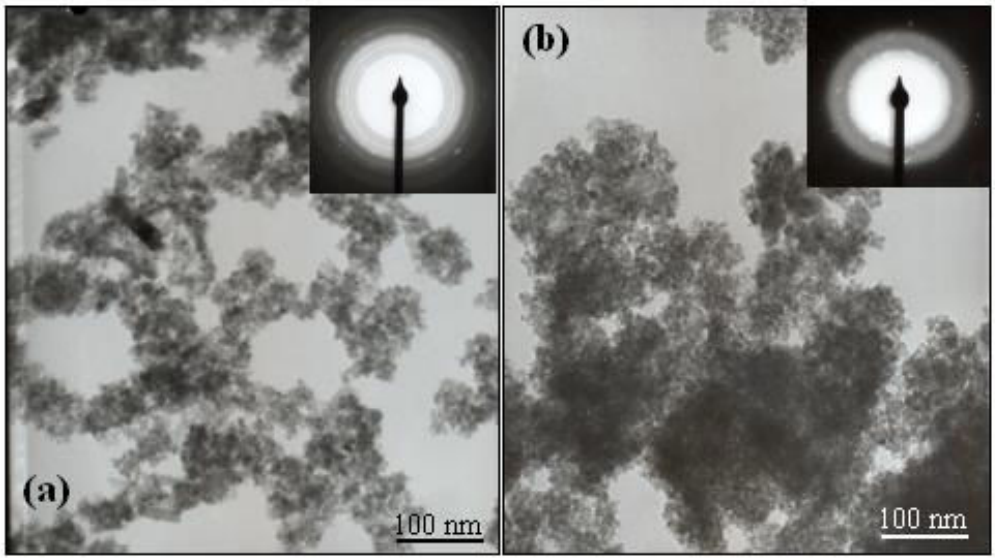

Fig. 2.13: *TEM photographs of $Cu_xCo_{(1-x)}Ce_2O_{4-\delta}$ (a) x = 0.25, (b) x = 1.0.*

Because of the amorphous character and the higher dispersion of copper and cobalt oxides on ceria, even the lateral resolution of high-resolution TEM is unable to accurately determine the copper distribution. These attributes though challenging for characterization can lead to high catalytic activity of these samples [53 - 56]. It was generally observed that sample with low content of copper generally exhibit small ceria particles.

2.6.6. High resolution transmission electron microscopy (HRTEM) studies

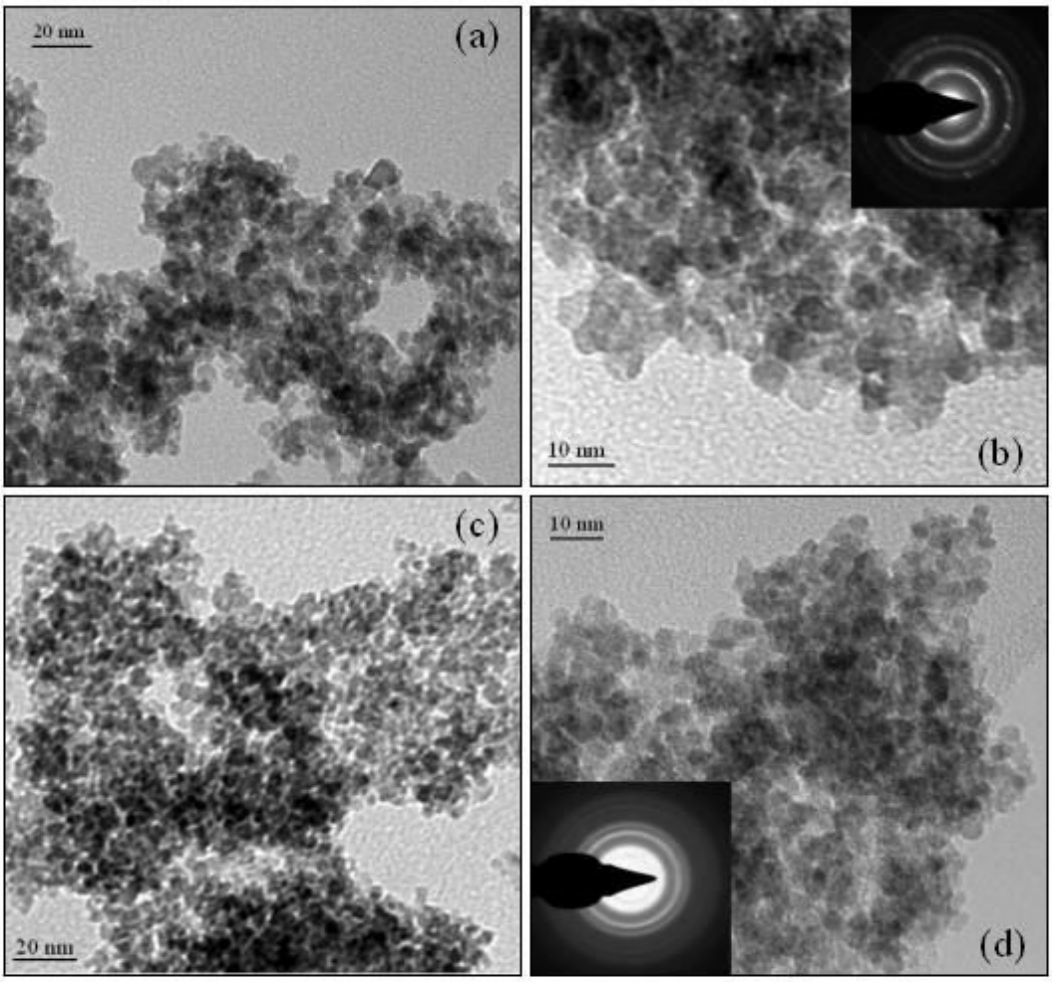

Fig. 2.14: *HRTEM photographs of $Cu_xCo_{(1-x)}Ce_2O_{4-\delta}$ samples x = 0.25 (a and b); x =1.0 (c and d).*

Figure 2.14 illustrates the HRTEM images of the $Cu_xCo_{(1-x)}Ce_2O_{4-\delta}$ mixed oxide samples with x = 0.25 (a and b) and x = 1 (c and d). From Fig. 2.14 we can see well dispersed regular spherical shaped particles with particle size of 3 to 5 nm for x = 1 and 6 to 8 nm for x = 0.25. The selective area electron diffraction (SAED) pattern in the Fig. 2.14 indicate that the particles belong to ceria, where as the dots in SAED pattern of the sample x = 0.25 indicates the particles are uniformly distributed as compared to x = 1.0. These results are similar to those obtained using low resolution TEM.

2.6.7. Temperature programmed reduction studies

The H_2-TPR profiles of the $Cu_xCo_{(1-x)}Ce_2O_{4-\delta}$ mixed oxides with x = 0, 0.15, 0.25, 0.5, 1.0, are given in Fig. 2.15. For comparison, profiles of copper, cobalt and cerium oxides, which were prepared by a similar method, are also included in the same figure. Reduction of bulk CuO gave a peak at 268 ^{0}C, whereas it was reported at 294 ^{0}C [57] and 392 ^{0}C [58] respectively in the literature.

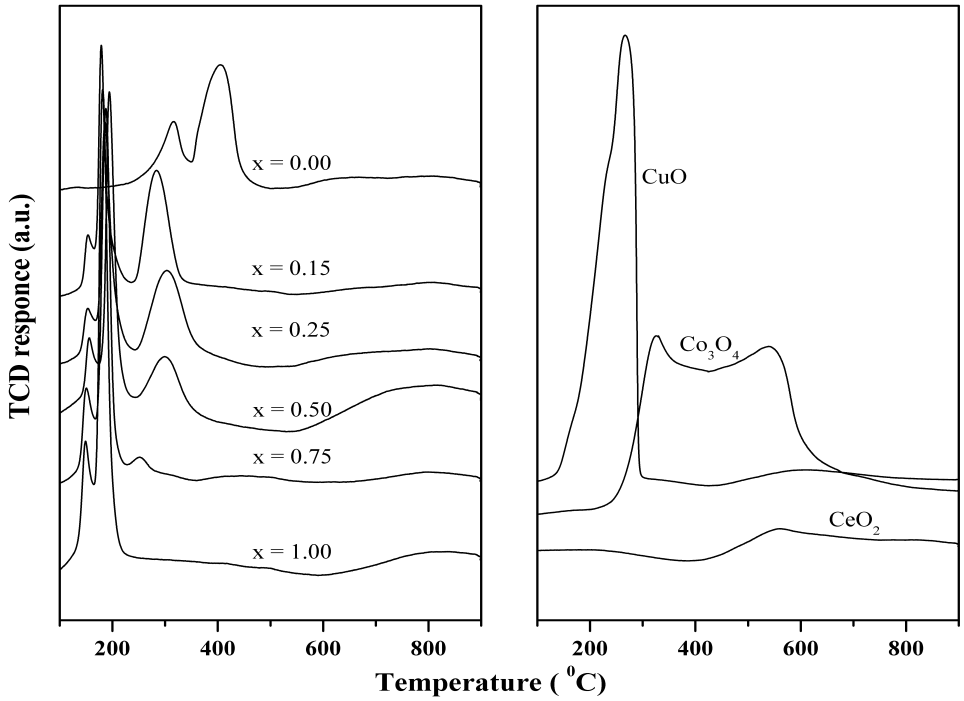

Fig. 2.15: *TPR profiles of $Cu_xCo_{(1-x)}Ce_2O_{4-\delta}$ and CuO, Co_3O_4 and CeO_2.*

Two sharp reduction peaks were observed for all Cu-Co-Ce-O mixed oxide samples, indicating the existence of two types of CuO species. One reduction maximum (temperature) could be assigned to small CuO crystallies that are highly dispersed reducing at lower temperature. Another reduction peak may be assigned to bulk CuO species, which reduce at higher temperature [59]. These results can be seen in Fig. 2.15 (x = 0.15 to 1). The low temperature peak was at 152 ^{0}C for x = 0.15 & 0.25, which is shifted to higher temperature for x = 0.5 at 156 ^{0}C, while the same is shifted to lower temperature (150 & 148 ^{0}C) when x = 0.75 & 1.0. A Similar trend was observed for high temperature peak, as

it was observed at 178, 181, 194, 187, 185 ^{0}C for x = 0.15, 0.25, 0.50, 0.75, 1.0 respectively. In combination with PXRD analysis, it can be said that there were two apparent CuO diffraction peaks at 2θ = 35.6 and 38.8 indicating that a change of CuO dispersion state had taken place.

Co_3O_4 gives two reduction peaks at 327 and at 540 ^{0}C. Reported TPR studies demonstrated that oxides of cobalt in different environments undergo reduction at different temperatures. For cobalt supported on alumina, four different reduction regimes have been observed: (i) Co_3O_4 undergoes reduction at ca. 327 ^{0}C (ii) well-dispersed surface Co^{3+} ions at ca. 477 ^{0}C (iii) surface Co^{2+} ions at ca. 627 ^{0}C and (iv) subsurface Co^{2+} ions or phases such as $CoAl_2O_4$ undergo reduction at ca. 877 ^{0}C [60, 61]. The temperature at which reduction of cobalt occurs is strongly influenced not only by the oxidation state of the cobalt, but also by the nature of neighboring metal cations and/or metal oxide phases. The presence of neighboring Cu and Ce ions should influence the reducibility of Co cations strongly, which can be seen by the lower reduction temperature of cobalt species of only cobalt and copper-cobalt containing ceria samples. All catalysts exhibit one reduction peak attributed to cobalt oxide, but for x = 0 that is $CoCeO_2$ two peaks are observed; the peaks may be attributed to stepwise reduction of various cobalt oxides $Co^{3+} \rightarrow Co^{2+} \rightarrow Co^0$ [62, 63]. Presence of copper may be assisting the reduction of cobalt oxide species. It was reported that the higher the dispersion of a metal oxide, the lower the peak temperature of the metal oxide in the TPR pattern [59].

CeO_2 reduction is expected to give two peaks at 430 and 570 ^{0}C, respectively. It is presumed that the low temperature peak is due to the reduction of CeO_2 surface oxygen, and the high-temperature peak is due to the reduction of bulk oxygen. In our studies, we observe only one peak at 555 ^{0}C [60, 64]. Hydrogen uptake is given in the table 2.12, which shows increase in hydrogen uptake with increase in copper content.

2.7. SUMMARY

A series of platinum loaded NaY catalysts were prepared by simple ion exchange method. These materials were characterized by using various physico-chemical techniques such as PXRD, BET surface area, H_2-TPR, TEM, AAS and H_2-chemisorption. No diffraction peaks of platinum were observed in PXRD, which may be the result of lower

metal loading. Platinum containing NaY samples gives two reduction peaks, one at low temperature and other one at high temperature. From the quantity of H_2 consumed it was concluded that platinum must have been present as PtO_2 and attributes the TPR peaks to the reduction of two surface oxide species. But 0.75Pt-NaY show three peaks, which may be due to reduction of platinum in three steps. Shift in the temperature was noticed among Pt-NaY, Fe-NaY and PtFe-NaY, which may be as a result of mixed oxide particles formed during calcination process. The peak at 367 ^{0}C in Fe-NaY is due to the reduction of Fe^{3+} to Fe^{2+}, whereas peak at 872 ^{0}C may be attributed to reduction of Fe^{2+} to Fe. There is a significant peak at lower temperature for PtFe-NaY, this strongly suggest that iron ion migrated to smaller cages. Due to the blockage by iron ions, a higher fraction of Pt^{2+} ions remain in the supercages. The intensity of the low temperature peak increases with increase in iron content, this supports the above explanation. A number of well-dispersed platinum particles were observed in the TEM pictures with a fair even size distribution of platinum particles. Better dispersion of 0.75% the platinum metal loaded sample was observed compared to 0.5 and 1.0 % metal loaded samples. Effect of calcinations temperature and iron loading on particle size of 0.75Pt-NaY was studied. The particle size increases with increase in calcination temperature. Calcination at 400 ^{0}C gives better dispersion and uniform particle sizes of platinum were observed in TEM. PtFe-NaY with 0.75 and 0.38 percentage of platinum and iron calcined at 400 ^{0}C showed better dispersion and small particle size, because base metal like Fe helps aid dispersion of platinum. These results were supported by H_2-Chemisorption.

Copper and cobalt containing ceria with general composition $Cu_xCo_{(1-x)}Ce_2O_{4-\delta}$ were prepared by simple co-precipitation method and characterized by techniques such as PXRD, BET surface area, H_2-TPR, NH_3-TPD, TEM, UV-visible, IR, AAS and XPS. The four strong peaks observed in the 2θ range 28-60^0 for powdered XRD corresponds to cubic structure of fluorite type of ceria with fine particles. No other phases of ceria were observed, whereas separate phases of CuO and Co_3O_4 were observed in all the compositions of Cu-Co-Ce-O mixed oxides. Higher BET surface areas were observed with increase in copper content, as copper may be facilitating formation of small crystallites of ceria. Not much deviation is noticed in the lattice constant of these samples. FTIR spectra shows two bands at 570 and 670 cm^{-1}, these stretching vibrations corresponds to metal to

oxygen bond in Co_3O_4. These two bands can be ascribed to the vibration of low spin Co (III) in octahedral sites. From the FTIR results, it is clear that cobalt is present in Co^{3+} and in octahedral holes. Two UV bands at 275 and 350 nm attributable to $O^{2-} \rightarrow Ce^{4+}$ charge transfer (CT) transitions were observed. First band must be arising from the surface sites of ceria, while the later is from bulk ceria. Shift in the CT band towards lower energy was noticed with addition of copper, which is due to decrease in crystalline size of ceria. These catalysts showed a broad, *d–d* band in the visible region. Cobalt containing ceria i.e. x = 0 shows a broad *d-d* band shift in visible region to 713 nm, indicating that the type of copper and cobalt species in these catalysts is influenced by both the support and their concentration. The average particle size of the sample was around 6 nm for x = 0.25, whereas it was around 8 nm for x = 1.0 based on TEM studies. Two temperature programmed reduction peaks were observed for Cu-Co-Ce-O series of mixed oxide samples, indicating the existence of two types of CuO species. One was represented by small CuO particles at around 150 ^{0}C, which was highly dispersed and reduced at lower temperature. Another peak may be due to larger particle of CuO that reduce at higher temperature (170 ^{0}C).

2.8. REFERENCES

[1] J. W. Niemantsverdriet, Spectroscopic methods in Heterogeneous catalysis, VCH, Weinheim, 1993.

[2] J. M. Thomas, W. J. Thomas, Principles and Practice of Heterogeneous catalysis, VCH, Weinheim, 1997.

[3] T. Barzetti, E. Selli, D. Moscotti, L. Forni, J. Chem. Soc., Faraday Trans, 92 (1996) 1401.

[4] T. R. Hughes, H. M. White, J. Phys. Chem., 71 (1967) 2192.

[5] C. A. Emeis, J. Catal., 141 (1993) 347.

[6] B. M. Weckhuysen, R. A. Schoonheydt, Catal. Today, 49 (1999) 441.

[7] B. C. Lippens and J. H. de Boer, J. Catal., 4 (1965) 319.

[8] E. P. Barret, L. G. Joyner and P. H. Halenda, J. Am. Chem. Soc., 73 (1951) 373.

[9] C. Villette, Ph. Tailhades and A. Rousset, J. Solid State Chem., 117 (1995) 64.

[10] A. Satsuma, Y. Kamiya, Y. Westi. T. Hattori, Appl. Catal., A 194 (2000) 253.

[11] A. Martin, U. Wolf, H. Berndt, B. Lucke, Zeolites, 13 (1993) 309.

[12] H. Sato, Catal. Rev. Sci. Eng., 39 (1997) 395.

[13] C. V. Hidalgo, H. Itoh, T. Hattori, M. Niwa, Y. Murakami, J. Catal., 85 (1984) 362.

[14] T. A. Carlson, X-ray Photoelectron Spectroscopy, Dowden, Hutchinson & Ross: Stroudsburg, PA, 1978.

[15] Practical Surface Analysis, Vol. 1: Auger and X-ray Photoelectron Spectroscopy, 2nd ed., D. Briggs, M. P. Seah, Eds., Wiley, New York, 1990.

[16] S. Hufner, Photoelectron Spectroscopy, Springer-Verlag: Berlin, 1995.

[17] V. L. J. Joly, P. A. Joy, S. K. Date and C. S. Gopinath, J. Phys. Condens. Matt., 13 (2001) 649.

[18] P. L. Villa, F. Trifiro, I. Pasquon, React. Kinet. Catal. Lett., 1 (1974) 341.

[19] J. Mikulova, J. Barbier Jr., S. Rossignol, D. Mesnard, D. Duprez, C. Kappenstein, J. Catal., 251 (2007) 172.

[20] E. Y. Ko, E. D. Park, K. W. Seo, H. C. Lee, D. Lee and S. Kim, Korean J. Chem. Eng., 23(2), (2006) 182.

[21] J. Peng, S. Wang, Appl. Catal., B 73 (2007) 282.

[22] H. Lieske, G. Lietz, H. Spindler and J. Volter, J. Catal., 81 (1983) 8.

[23] S. H. Park, M. S. Tzou and W. M. H. Sachtler, Appl. Catal., 24 (1986) 85.

[24] H. J. Jiang, M. S. Tzou and W. M. H. Sachtler, Appl. Catal., 39 (1988) 255.

[25] R. L.Garten, W. N. Delglass and M. Boudart, J. Catal., 18 (1970) 90.

[26] M. Kotobuki, A. Watanabe, M. Watanabe. Appl. Catal., A 307 (2006) 275.

[27] M. Watanabe, H. Uchida, K. Ohkubo, H. Igarashi, Appl. Catal., B 46 (2003) 595.

[28] M. Kotobuki, A. Watanabe, H. Uchida, H. Yamashita, M. Watanabe, Chem. Lett., 34 (2005) 866.

[29] M. Konsolakis, I. V. Yentekakis, Appl. Catal., B 29 (2001) 103.

[30] J. S. Rieck, A. T. Bell, J. Catal., 100 (1986) 305.

[31] M. McLaughlin, M. M. McClory, R. D. Gonzalez, J. Catal., 89 (1984) 392.

[32] C. Pedrero, T. Waku, E. Iglesia, J. Catal., 233 (2005) 242.

[33] J. Korah, W. A. Spieker, J. R. Regalbuto, Catal. Lett., 85 (2003) 123.

[34] M. Schreier, J. R. Regalbuto, J. Catal., 225 (2004) 190.

[35] W. A. Spieker, J. R. Regalbuto, Stud. Surf. Sci. Catal., 130 (2000) 203.

[36] K. Ch. Akratopulu, L. Vordonis, A. Lycourghiotis, J. Catal., 109 (1988) 41.

[37] M. Kang, M. W. Song, C. H. Lee, Appl. Catal., A 251 (2003) 143.

[38] H. Idrris, C. Diagne and M. A. Barteau, J. Catal., 155 (1995) 219.

[39] N. F. M. Henry, J. Lipson and W. A. Wooster, "The interpretation of x-ray diffraction photographs" Macmillan and Co Ltd., London, 1951.

[40] A. Martínez-Arias, M. Fernández-García, J. Soria, J.C. Conesa, J. Catal., 182 (1999) 367.

[41] P. Ratnasamy, D. Srinivas, C. Satyanarayana, P. Manikandan, R. Senthil Kumaran, M. Sachin, V. Shetti, J. Catal., 221 (2004) 455.

[42] C. B. Wanga, C. W. Tanga, S. J. Gaua and S. H. Chien, Catal. Lett., 101 (2005) 59.

[43] C. W. Tang, C. C Kuo, M. C. Kuo, C. B. Wang, S. H. Chien, Appl. Catal., A 309 (2006) 37.

[44] D. Stoyanova, M. Christova, P. Dimitrova, J. Marinova, N. Kasabova, D. Panayotov, Appl. Catal., B 17 (1998) 233.

[45] B. Lal, N.K. Singh, S. Samuel, R.N. Singh, J. New Mater. Electrochem. Syst., 2 (1999) 59.

[46] T. Andrushkevich, G. Boreskov, V. Popovskii, L. Pliasova, L. Karakchiev, A. Ostankovitch, Kinet. Catal., 6 (1968) 1244.

[47] St. G. Christoskova, M. Stoyanova, M. Georgieva, D. Mehandjiev, Mater. Chem. Phys., 60 (1999) 39.

[48] R. N. Singh, J. P. Pandey, N. K. Singh, B. Lal, P. Chartier, J. F. Koenig, Electrochim. Acta., 45 (2000) 1911.

[49] H. K. Lin, H. C. Chiu, H. C. Tsai, S. H. Chien, C. B. Wang, Catal. Lett., 88 (2003) 169.

[50] J. L. Martin, S. E. Vidales, O. Gracia-Martinez, E. Vila, R. N. Rojas, M. J. Torralvo, Mat. Res. Bull., 28 (1993) 1135.

[51] A. Bensalem, F. Bozon-Verduraz, M. Delamar, G. Bugli, Appl. Catal., A 121 (1995) 81.

[52] P. Bera, K. R. Priolkar, P. R. Sarode, M. S. Hegde, S. Emura, R. Kumashiro and N. P. Lalla, Chem. Mater., 14 (2002) 3591.

[53] E. A. Shaw, T. Rayment, A. P. Walker, R. M. Lambert, T. Gauntlett, R. J. Oldman, A. Dent, Catal. Today, 9 (1991) 197.

[54] S. Hocevar, U. O. Krasovec, B. Orel, A. S. Arico, H. Kim, Appl. Catal., B 28 (2000) 113.

[55] Harrison, P. G. Ball, I. K. Azalee, W. Daniell, W. Goldfarb, D. Chem Mater., 12 (12) (2000) 3715.

[56] P. W. Park, Ledford, J. S. Langmuir, 12 (1996) 1794.

[57] G. Avgouropoulos, T. Ioannides, H. matralis, Appl. Catal., B 56 (2005) 87.

[58] X. Tang, B. Zhang, Y. Li, Y. Xu, Q. Xin, W. Shen, Appl. Catal., A 288 (2005) 116.

[59] J. Xiaoyuan, L. Guanglie, Z. Renxian, M. Jianxin, C. Yu, Z. Xiaoming, Appl. Surf. Sci., 173 (2001) 208.

[60] P. Arnoldy, J. A. Moulijn, J. Catal., 93 (1985) 38.

[61] L. Ji, J. Lin, H. C. Zeng, J. Phys. Chem., B 104 (2000) 1783.

[62] T. Paryjczak, J. Rynkowski, S. Karski, J. Chromatogr., 188 (1980) 254.

[63] R. Brown, M. E. Cooper, D. A. Whan, Appl. Catal., A 3 (1982) 177.

[64] L. F. Liotta, G. Di Carlo, G. Pantaleo, A. M. Venezia, G. Deganello, Appl.Catal., B 66 (2006) 217.

[65] J. Nickl, D. Dutoit, A. Baiker, U. Scharf, A. Wokaun, Ber.Bunsenges. Phys. Chem., 97 (1993) 217.

[66] R. J. Gorte, Catal. Today, 28 (1996) 405.

[67] E. Jobson, A. Baiker, A. Wokaun, J. Chem. Sot. Faraday Trans., 86 (1990) 1131.

[68] C. D. Wagner, W. H. Riggs, L. E. Davis, J. F. Moulder, G. E. Muilenberg, Handbook of X-ray Photoelectron spectroscopy, Perkin Elmer, Palo Alto, CA, 1978.

Chapter – 3

PREFERENTIAL OXIDATION OF CO - CATALYTIC ACTIVITY STUDIES

3.1. INTRODUCTION

The catalysis research is mostly focused on establishing a relation between activity of the catalyst during a reaction under different reaction conditions with its composition and structure. The catalytic activity determined under a set of reaction conditions in combination with catalyst characterization could lead to useful information about reaction pathways, active sites on a catalyst and the reaction mechanisms.

The general introduction and literature survey about PrOx reaction is given in chapter 1. The catalytic activity in preferential oxidation of CO was carried out by using oxygen in air as an oxidizing agent on Pt-NaY, PtFe-NaY and Cu-Co-Ce-O mixed oxide catalysts prepared by ion exchange and co-precipitation methods. The catalytic activities of these catalysts have been correlated with their structural properties, studied by using an array of characterization methods described in chapter 2.

3.2. CATALYTIC ACTIVITY MEASUREMENTS

3.2.1. Experimental set up for catalytic reaction test

The catalytic tests were carried out in a fixed bed, down flow, glass reactor with a 15 mm i.d., as shown in Fig. 3.1. Two thermal mass flow controllers (MFC, Bronkhorst, Hi Tech) were used to control and monitor flow rates (GHSV = 10,000 - 30,000 h^{-1}) of reactant gases. One MFC was used to feed the dry synthetic mixture of reformate gas (H_2, CO, CH_4 and CO_2). The second MFC was used to feed oxygen in the form of air (O_2/CO = 0.5 - 2.0). The reactor was placed in an electrically heated split furnace (Geomechanique) manned by a PID programmer (Eurotherm 2404) to control and uniformly heat the catalyst bed. The exact temperature of the furnace, and the catalyst bed were monitored by using K-type thermocouples. The product gas mixtures (dry) was analyzed using an online gas chromatograph (CHEMITO 8610). The gas chromatograph (GC) is also equipped with a methanator loaded with a Ni catalyst, to detect sub-ppm level of CO. An IR Gas analyzer (Fuji Electric) was also used in series to estimate CO, CO_2, CH_4 and O_2 accurately.

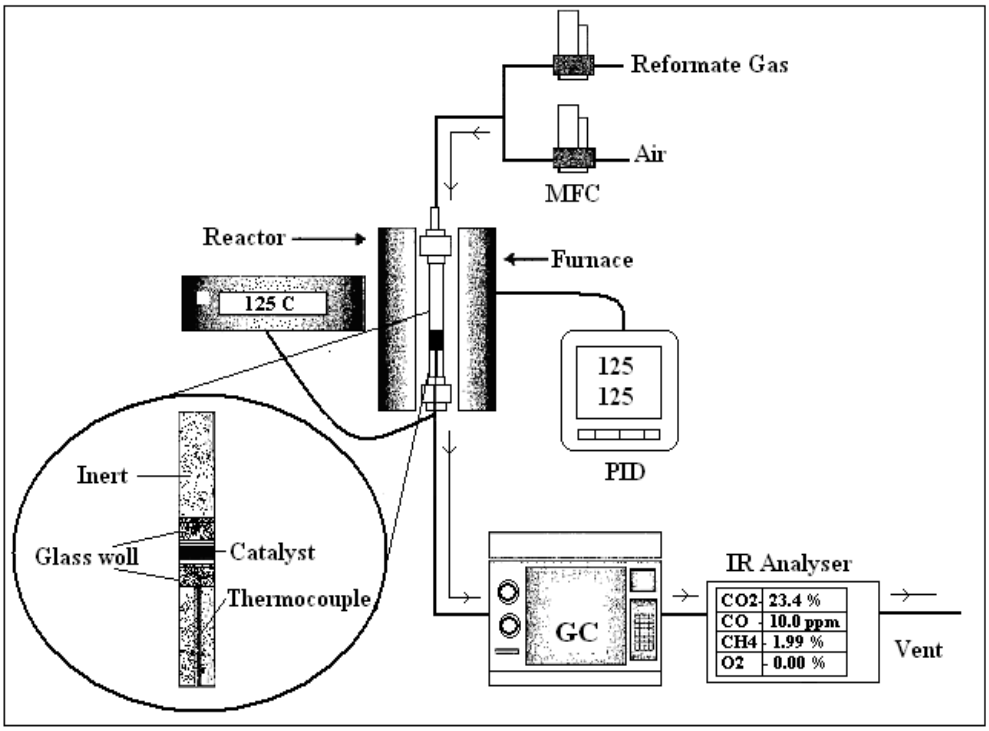

Fig. 3.1: *Reaction setup used for preferential oxidation of CO.*

The catalyst, in particle size range of 10-20 mesh was used, after crushing and sieving tablets of catalyst powder without any binder. These catalyst particles were sandwiched between two quartz-wool plugs in the reactor. Ceramic beads were used in the pre-heating zone above the catalyst bed to heat the gas mixture and water. For experiments involving steam (200 Torr), water was pumped to the pre-heater using a high precision syringe pump (ISCO 500D), wherein the feed gas is mixed with the steam.

3.2.2. Analytical methods

The gas mixture at the outlet of reactor was analyzed by using online GC (Chemito 8690), equipped with flame ionization detector (FID) as well as thermal conductivity detector (TCD). The product gas contains CO in ppm level, which is detected as a methane by sending through a methanation catalyst. For achieving better separation of nitrogen, hydrogen, CO, CO_2, methane and oxygen, Spherocarb column was used (1/8"dia, 8 feet length). An infrared-based gas analyzer (Fuji Electric) was also used in series for real time monitoring of CO, CO_2, CH_4 and O_2 accurately. For quantification of the gases, calibrated

gas mixture was used as reference. Conversions of CO and CO oxidation selectivity were calculated as;

$$\text{CO Conversion (Mole \%)} = \frac{\text{Moles of CO}_{in} - \text{Moles of CO}_{out}}{\text{Moles of CO}_{in}} \times 100$$

$$\text{CO Oxidation selectivity (Mole \%)} = \frac{\text{Moles of CO}_{in} - \text{Moles of CO}_{out}}{2(\text{Moles of O}_{2\,in} - \text{Moles of O}_{2\,out})} \times 100$$

$$\text{O}_2\text{ Conversion (Mole \%)} = \frac{\text{Moles of O}_{2\,in} - \text{Moles of O}_{2\,out}}{\text{Moles of O}_{2\,in}} \times 100$$

PART A: PREFERENTIAL OXIDATION OF CO ON Pt-NaY CATALYSTS

3.3. INTRODUCTION

There are two groups of catalysts, that are usually employed for CO oxidation: one is based on platinum group metals supported on passive supports and the other is based on metals supported on single or mixed transition metal oxides. This section describes the results of PrOx of CO in excess hydrogen using air as oxidizing agent on Pt-NaY zeolite catalyst. The reason for choosing Na form Y zeolite was the promoting role of Na in CO oxidation. Na was found to be a promoter, as it enhances both O_2 binding and $CO.O_2$ formation. The enhancement is mainly due to the formation of Na-O_2 bond [1, 2,]. Alkali metal addition to zeolite promotes oxidation activity mainly partial oxidation rather than complete oxidation [3]. Platinum, which is widely used for oxidation reactions, was supported on high surface area zeolite NaY. For this system, catalysts were activated by heating first in air at 350 ^{0}C for 3 h raising the temperature at a rate of 2 ^{0}C per minute to clean the catalyst surface as well as to remove the amine. Followed by this, it is reduced under hydrogen at 350 ^{0}C. Parameters such as metal concentration, temperature, space velocity, O_2/CO, water and CO content in the feed were studied.

The usual form in which oxygen is present in the gas phase is dioxygen O_2. One of the essential functions of the catalyst in oxidation reactions is the activation of oxygen. Generally the oxygen activation is considered to occur by its adsorption or incorporation

into the oxide crystal lattice, the surface atoms of which may also participate in the catalytic reaction [4]. Usually oxidation reactions are exothermic. In this study, we have used air that contains around 21 percent oxygen, as oxidant. This diluted oxygen is expected to help to control the temperature more effectively by dissipation of the heat generated during the reaction, thus avoiding the formation of hot spots.

3.4. RESULTS AND DISCUSSION

3.4.1. Effect of reaction temperature

Preferential oxidation of CO in excess of hydrogen was carried out using 0.5 cc catalyst. The gas mixture that contains H_2, 74.17 mole %; CO, 0.5 mole %; CH_4, 2.07 mole %; CO_2, 23.26 mole % was mixed with oxygen in the form of air to maintain the required O_2/CO ratio. The catalysts were tested in the temperature range 100 - 200 ^{0}C. Figures 3.2, 3.3, 3.4 show the mole % CO conversion, O_2 conversion and CO oxidation selectivity respectively at different temperatures on various Pt-NaY (Pt = 0.2, 0.5, 0.75, 1.0 wt %) catalysts.

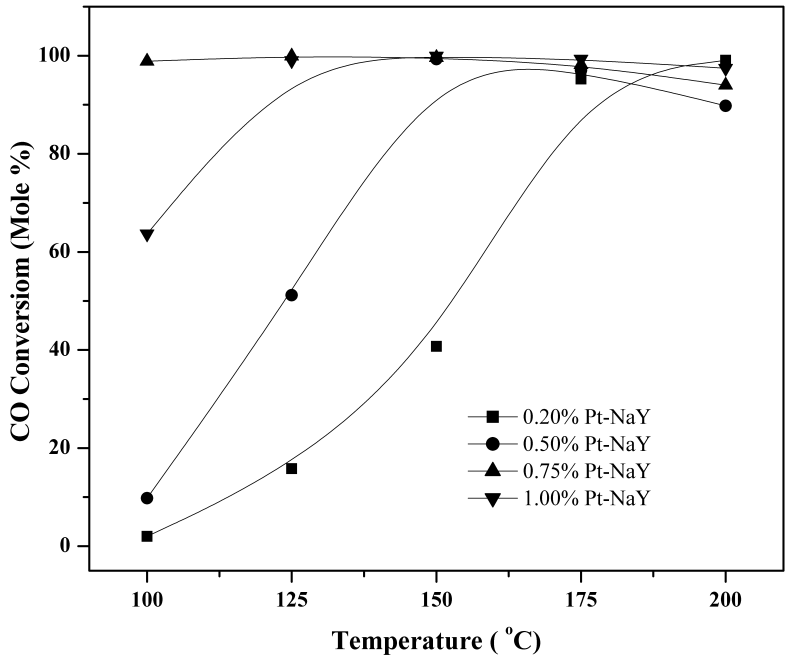

Fig. 3.2: *Effect of temperature on CO conversion over different Pt-NaY catalysts. Reaction conditions: Catalyst - 0.5 cc; O_2/CO ratio -1.0; GHSV - 10,000 h^{-1}; CO - 5000 ppm; TOS -5 h.*

The reaction was initiated at 100 ^{0}C and studied in 25 ^{0}C increments, with the analysis being carried out after 45-50 minutes on stream at each temperature to allow the reaction to stabilize. While, IR analyzer readings were monitored for every 10 minutes interval. The catalyst with 0.2 wt % Pt shows PrOx activity at higher temperatures as compared to other samples. Based on this, we can say that small amount Pt is enough to get active catalyst. But, better and steady CO conversion and CO oxidation selectivity at lower temperature can be achieved only on 0.75 wt % Pt sample, which was found to be optimum for the present system (Fig. 3.2 and 3.3). Catalyst with higher Pt shows low activity at low reaction temperatures, which may be due to the inferior dispersion of the platinum on the surface of the support [5, 6]. While the O_2 conversion and CO conversion increased with increase in temperature, fall in CO oxidation selectivity was noticed at higher temperature due to hydrogen oxidation. As a result, even a slight fall in CO conversion was observed at higher temperature showing that conversion passes through a maximum (Fig. 3.2 and 3.4.) The loss of CO oxidation selectivity at higher temperatures can also be explained based on the relative coverage of the surface by CO.

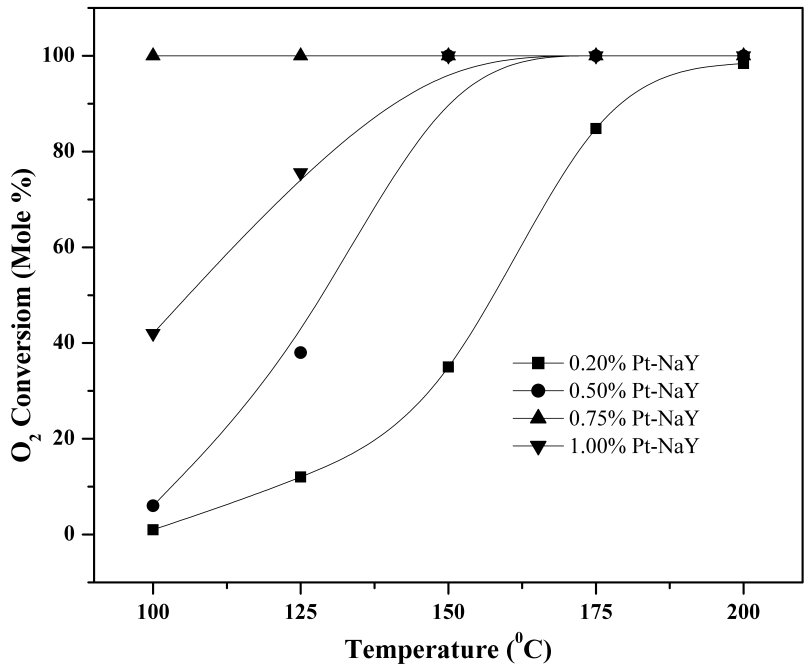

Fig. 3.3: *Effect of temperature on O_2 conversion over different Pt-NaY catalysts. Reaction conditions: Catalyst - 0.5 cc; O_2/CO ratio -1.0; GHSV - 10,000 h $^{-1}$; CO - 5000 ppm; TOS -5 h.*

When a mixture of CO and H_2 is subjected to oxidation, CO competes with H_2 for the reaction with O_2. In the absence of CO, hydrogen oxidation over a platinum catalyst is instantaneous, even at room temperature, which infact is difficult to control. A continuous fall in O_2 selectivity with increasing temperature shows that higher activation energy needed for H_2 oxidation is accomplished at higher reaction temperature [7]. It can be assumed that at lower temperatures, CO preferably covers the Pt metal surface and inhibits the hydrogen oxidation. In an adsorption study of CO on a Pt catalyst using FT-IR [8], full coverage of surface with CO was observed at temperatures below 200 ^{0}C even for 0.01 mole % CO containing gas mixture while 1 mole % CO is required for full coverage of CO at 300 ^{0}C. With increasing temperature, CO partially gets desorbed and the degree of CO coverage decreased. The partial coverage allows the hydrogen oxidation to proceed at a much faster rate than the CO oxidation, resulting in decreased CO oxidation selectivity with increasing temperature, as may be seen in Fig. 3.4.

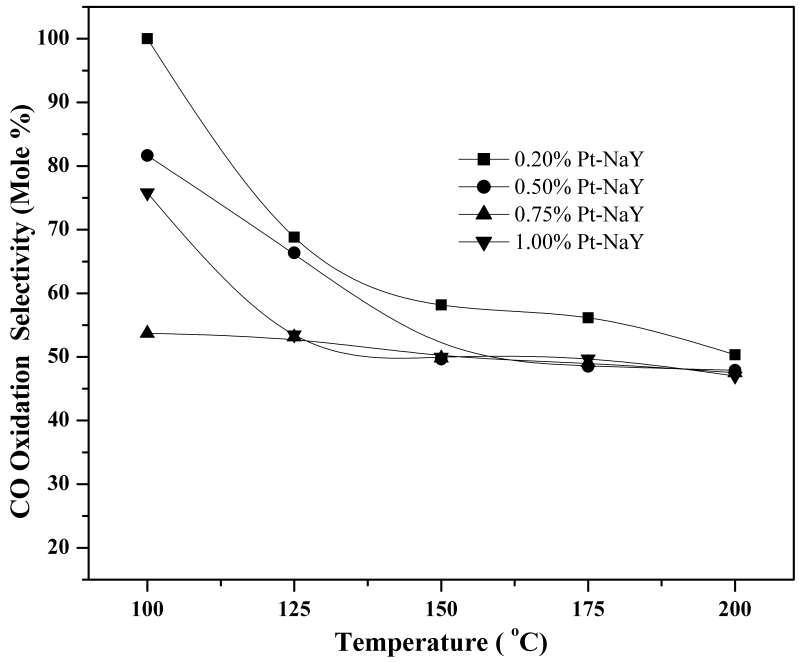

Fig. 3.4: *Effect of temperature on CO oxidation selectivity on different Pt-NaY catalysts. Reaction conditions: Catalyst - 0.5 cc; O_2/CO ratio - 1.0; GHSV - 10,000 h^{-1}; CO-5000 ppm; TOS - 5 h.*

The variation of oxidation selectivity in the low temperature region shows that there is a rapid decline of its value at initial stages, followed by steady high temperature

region. What is striking is that the slope of fall reduced with increasing Pt content in the sample. The results are in agreement with Watanabe et al. [9] and Kahlich et al [10]. This trend can be explained, as proposed by Kahlich et al [11], based on the assumption that H_2 and CO are co-adsorbed on the surface so that the selectivity for CO oxidation should be inversely proportional to θ_H/θ_{CO}. The lower adsorption energy of hydrogen compared to CO, leads to a reduction of the (small) hydrogen surface coverage with increasing temperature, while θ_{CO} remains close to saturation. This leads to a decrease in θ_H/θ_{CO}, which is equivalent with an increase of the selectivity of CO oxidation.

In this study, we have used gas streams with $O_2/CO = 1.0$ which is 100 mole % excess in oxygen than that required stoichiometrically for oxidation of CO. Thus, if O_2 conversion is complete, maximum CO oxidation selectivity that can be achieved is to 50 mole %. The excess oxygen is used for oxidation of hydrogen. It is reported that at higher temperatures, the CO with support (Al_2O_3) bond becomes weaker which leads to H_2 oxidation [11, 12]. Apart from this, H_2 oxidation and other side reactions such as CO methanation and reverse water gas shift reaction are also possible. However, these reactions were not observed for the present system [13, 14]. Not even trace content of methane was observed on any of the catalysts. For a better understanding of the system, correlation of characterization results with catalytic activity studies on 0.75 and 1 wt % Pt-NaY was done.

3.4.2. Influence of space velocity

In order to minimize the size and bring down the cost of the fuel processor, it is important to obtain high catalytic activity (good CO conversion and oxidation selectivity) at wide rage of contact times (1/SV, where SV is the space velocity).

Figure 3.5 shows the performance of 0.75Pt-NaY at different space velocities at a reaction temperature of 135 ^{0}C. Increase in the space velocity (decrease in contact time) led to a fall in CO and O_2 conversions, while CO oxidation selectivity improved at the same time in the 10,000 to 30,000 h^{-1} space velocity region. The decrease in CO and O_2 conversion with increasing space velocity shows that the drop in activity is due to reduced contact time. Kim et al. [14] observed that below 300 ^{0}C, the CO conversion decreased with the increasing total flow rate while the selectivity was more or less constant in the

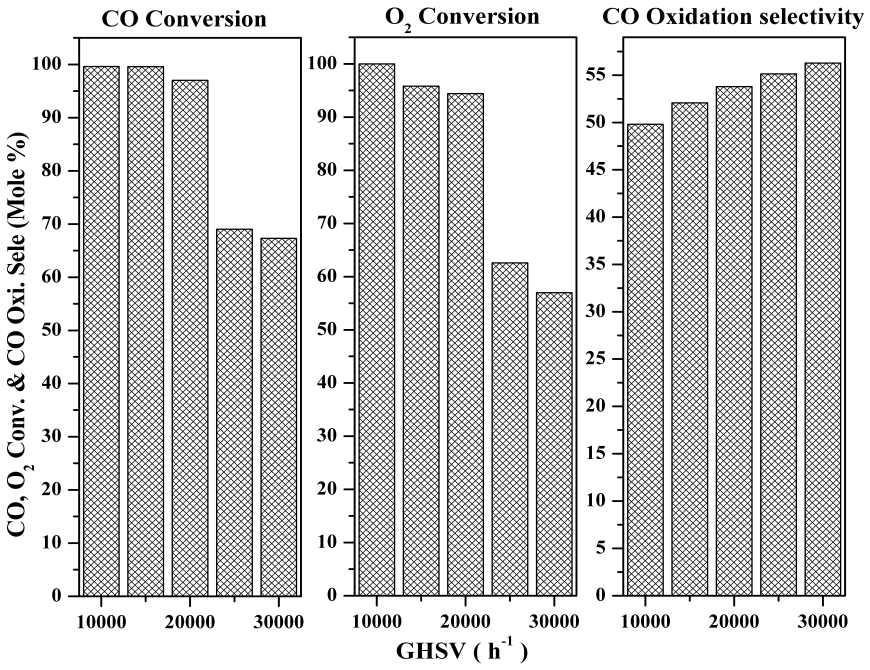

Fig. 3.5: *Effect space velocity on CO and O_2 conversion and CO oxidation selectivity on 0.75Pt-NaY.*
Reaction conditions: Catalyst - 0.5 cc; O_2/CO ratio -1.0; Temperature -135 ^{0}C, CO -5000 ppm; TOS 5 h.

3000-12,000 ml/h range over Pt/Al_2O_3 catalysts. There are some reports that the Pt catalyst works at very high space velocities [15 - 17] but the metal loading is on the higher side and in some cases it is more than 2 wt %. The higher is the metal loading and dispersion, more metal surface area is available for CO adsorption leading to higher activity. The increase in CO oxidation selectivity at higher space velocities could be attributed lower contact time that suppresses hydrogen combustion.

3.4.3. The effect of O_2/CO ratio

In the PrOx study, O_2/CO ratio is one of the most important factors, because excess oxygen can lead to undesired hydrogen consumption due to oxidation. Stiochiometrically, oxidation of one mole of CO requires one mole of oxygen. But, practically for this reaction, to get ~100 mole % conversion, excess oxygen is required, in-fact it is to the tune of double the content of CO. This may be attributed to the small activation energy difference between CO and H_2, as a result of which part of the O_2 is utilized for non-

selective oxidation of H_2. CO oxidation selectivity, CO and O_2 conversions with variation in oxygen (different O_2/CO) content over 0.75Pt-NaY are shown in Fig. 3.6.

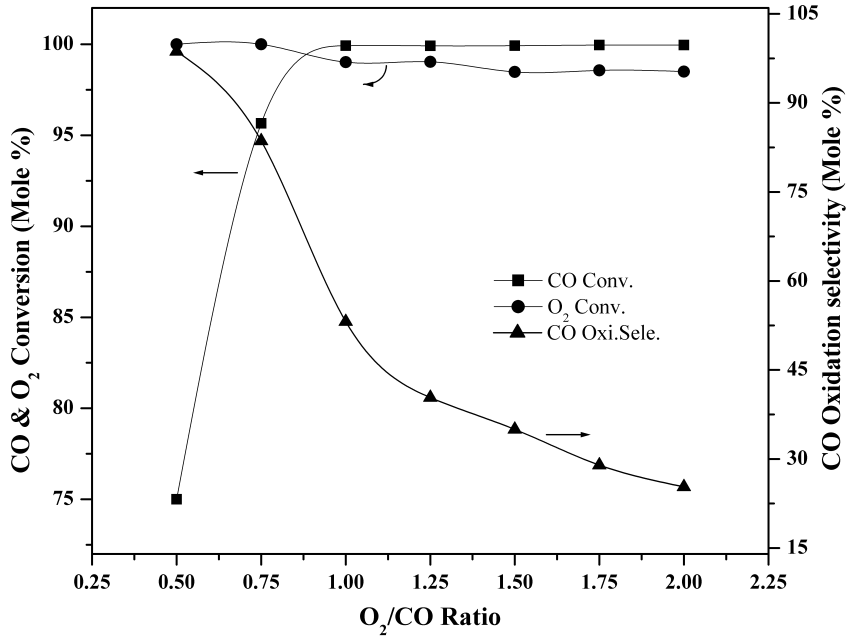

Fig. 3.6: *Effect of O_2/CO on CO and O_2 conversion and CO oxidation selectivity over 0.75Pt-NaY.*
Reaction conditions: Catalyst - 0.5 cc; GHSV-10,000 h^{-1}; Temp.-135 ^{0}C, CO-5000 ppm; TOS -7 h.

The CO and O_2 conversions increased with higher oxygen in the feed. However, a simultaneous parallel decrease in CO oxidation selectivity was observed. This observation indicates that though the catalyst is selective towards the oxidation of CO to CO_2; the hydrogen oxidation is favored in excess of oxygen. Ratio of O_2/CO = 1.0 should be enough for practical application for this class of catalysts. This catalyst is comparable in terms of the activity to those reported so far in literature, including catalysts such as Pt/Al_2O_3 and Pt/CeO_2 [18], Fe-promoted Pt/Al_2O_3 [19] and Ce-promoted Pt/Al_2O_3 [20].

3.4.4. The effect of H_2O in the feed

Reformate gas usually contains around 20 mole % of steam and 15-25 mole % CO_2. While most of the studies reportedly tried to achieve high CO conversion, the input stream did not contain either CO_2 and H_2O or either of it. Presence of CO_2 and H_2O lead to

a reduction in overall activity of the catalyst. If the gas mixture has CO_2, it may be methanated consuming valuable H_2, alternately it may promote reverse water gas shift reaction. Similarly, CO_2 in the feed can form some carbonate species that hampers reaction rates. Hence, study on the effect of H_2O and CO_2 on PrOx reaction is crucial for practical use. In the present study, the feed always contained CO_2. Figure 3.7 shows the effect of water on 0.75Pt-NaY at a reaction temperature of 135 ^{0}C. Decrease in CO and O_2 conversions were observed when H_2O was added (20 mol %) to the gas mixture. This may be attributed to the coverage of the metallic particles with H_2O resulting in the slow down of CO reaction rates. This may be partly attributed to the preferential sorption of water on the support (NaY), which is hydrophilic in nature. On the H_2O sorbed catalyst, the contribution of the Pt catalyst species outside the super cages increases, resulting in the lowering of CO oxidation selectivity [21]. This lowered PrOx activity was restored to original level by raising the temperature. Another possible explanation for this may be that the formation of bicarbonate in presence of water, which is more stable than that of carbonate.

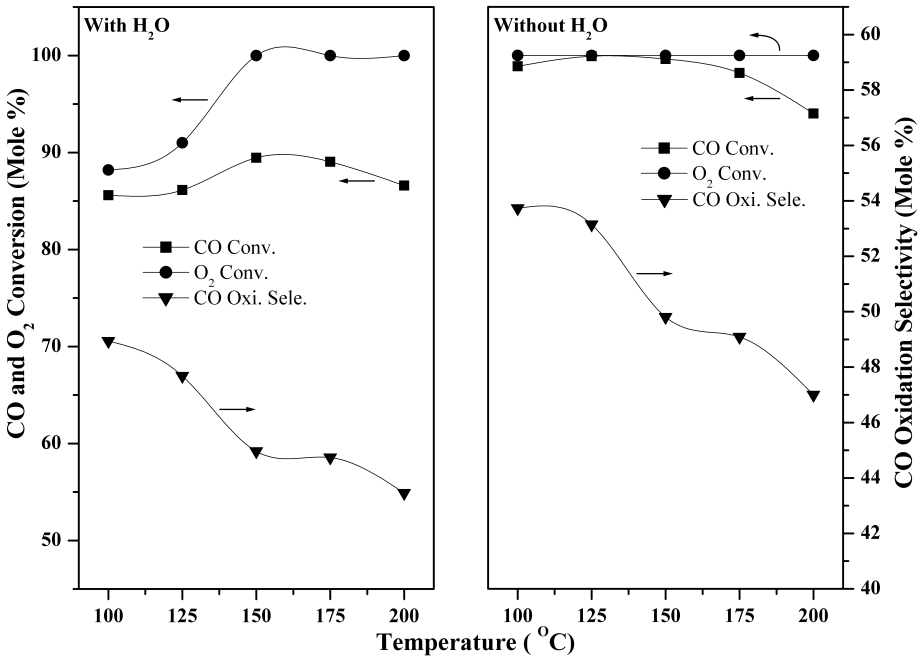

Fig. 3.7: *Effect of water on CO and O_2 conversions and CO oxidation selectivity at various temperatures on 0.75Pt-NaY.*
Reaction conditions: Catalyst-0.5 cc; GHSV-10,000 h^{-1}; Temperature-135 ^{0}C, CO-5000 ppm; pH_2O -200 Torr; TOS -5 h.

Effect of H_2O depends upon the support and active metal used for the reaction. In case of gold catalysts the H_2O reportedly enhances the activity through decomposition of carbonate formed during the reaction [22].

3.4.5. The effect of CO concentration

CO content in the feed influences the activity of the catalyst. The comparison of catalyst activity of 0.75Pt-NaY using two gas mixtures containing 5000 and 9500 ppm of CO respectively is shown in Fig. 3.8. The feed compositions used were H_2 , 73.37 mol %; CH_4, 1.93 mol %; CO_2, 23.75 mole %; CO, 0.95 mole % and H_2, 74.17 mole %; CH_4, 2.07 mol %; CO_2, 23.26 mole %; CO, 0.50 mole %.

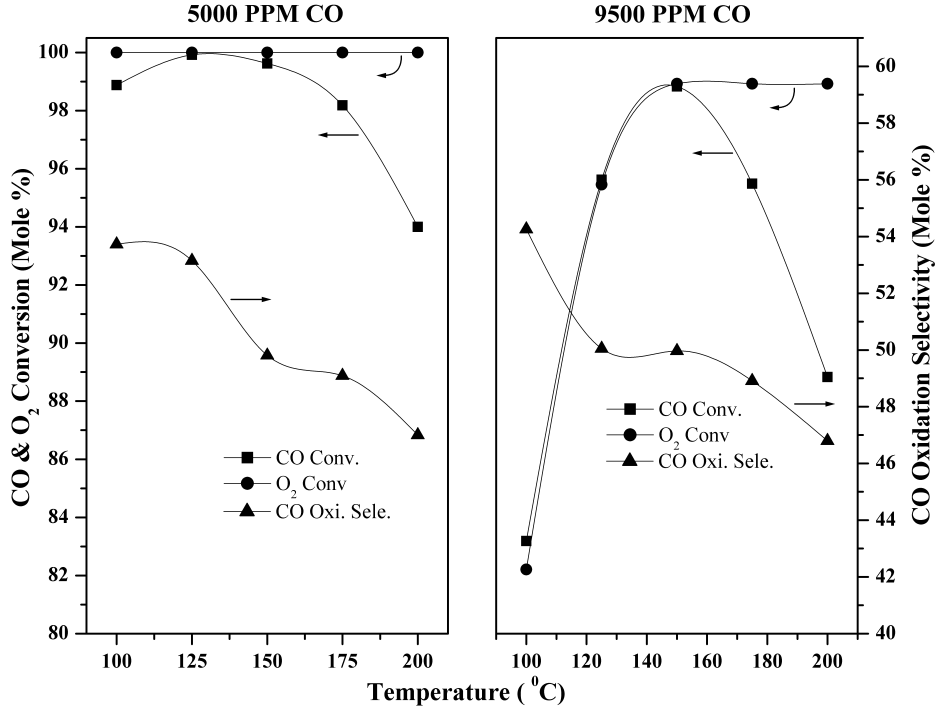

Fig. 3.8 *Effect of CO content in feed on CO conversion and oxidation selectivity over 0.75Pt-NaY.*
Reaction conditions: Catalyst-0.5 cc; GHSV-10,000 h^1; Temperature-135 ^{0}C, CO-5000 and 9500 ppm; O_2/CO ratio-1.0.

There was a fall in CO and O_2 conversions at higher CO concentration in the gas mixture, but the CO oxidation selectivity has slightly improved. This may be due competition between CO and H_2 for the available active sites, as a result higher content of

CO inhibits the H_2 chemisorption leading to increase in CO oxidation selectivity. This is also reflected in O_2 conversion for the feed containing 9500 ppm of CO. However, a raise in reaction temperature of about 10-15 ^{0}C is sufficient to restore the required activity.

3.4.6. Time on stream study

Based upon the above results, the reaction conditions were optimized and catalytic activity was studied for a longer duration. The time on stream study was carried out by using 5000 ppm CO; O_2/CO-1.0; GHSV-10, 000 h^{-1} at 135 ^{0}C for 30 h on 0.75Pt-NaY. The CO and O_2 conversion along with oxidation selectivity with reaction time is shown in Fig. 3.9. No change in CO or O_2 conversion was observed with time on stream, but a small increase in the CO oxidation selectivity after 10 h on stream was observed. Though longer-term durability test is essential for practical applications, we believe that observed stability demonstrates the high potential of the catalyst for applications in a fuel processor.

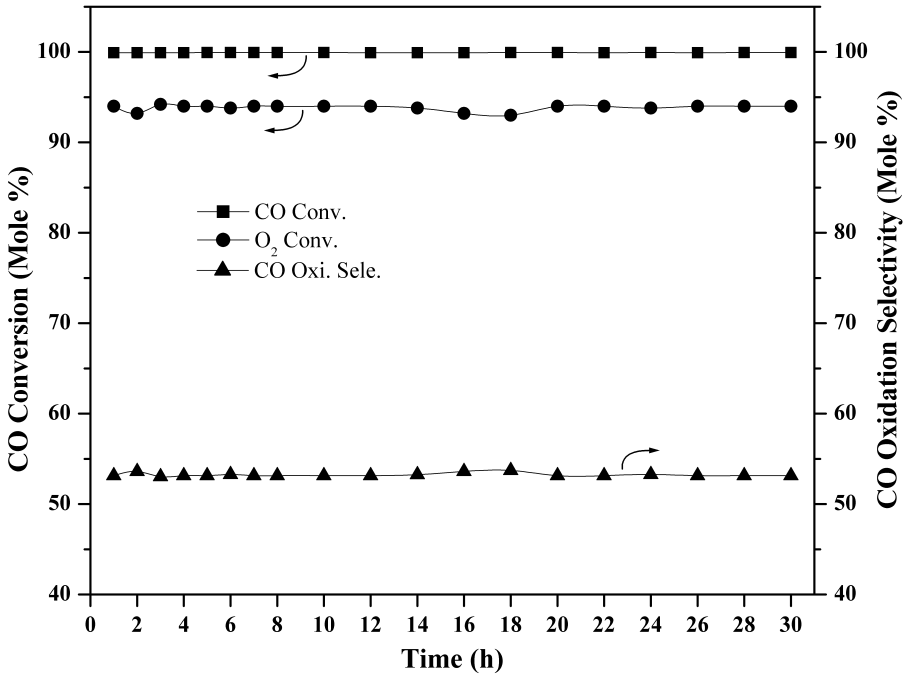

Fig. 3.9: *Effect of time on steam on 0.75Pt-NaY catalyst.*
Reaction conditions: Catalyst-0.5 cc; GHSV-10,000 h^{-1}; Temp.-135 ^{0}C, CO-5000 ppm; O_2/CO ratio - 1.0; TOS - 30 h.

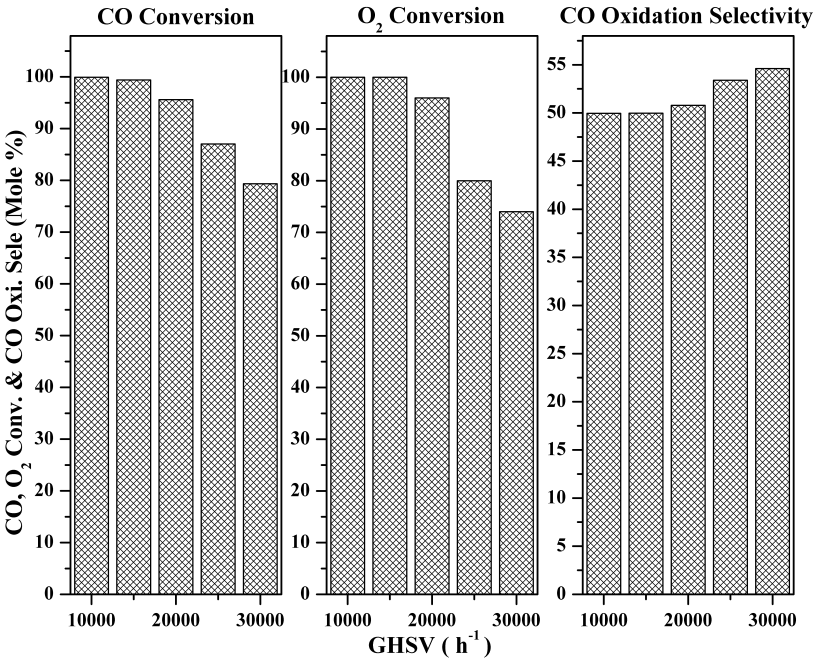

Fig. 3.10: *Effect of space velocity on PrOx activity selectivity over 1Pt-NaY. Reaction conditions: Catalyst-0.5 cc; O_2/CO ratio -1.0; Temp. - 135 ^{0}C, CO -5000 ppm.*

Table 3.1: Comparison of 0.75 and 1Pt-NaY for PrOx reaction

	0.75Pt-NaY			1Pt-NaY		
	CO Conv.	O_2 Conv.	CO Oxi. Sele.	CO Conv.	O_2 Conv.	CO Oxi. Sele.
CO = 5000 ppm	99.99	94.0	53.15	99.93	96.20	51.94
O_2/CO = 0.5	75.00	100.0	98.68	56.80	100.0	82.08
O_2/CO = 2.0	99.95	98.80	25.29	99.99	98.00	25.25
CO = 9500 ppm	99.90	99.8	50.50	99.89	100.0	49.94
* CO = 5000 ppm	88.38	94.00	47.01	97.38	98.40	49.48
After 30 hrs	99.93	94.00	53.15	99.92	96.20	51.93

Reaction conditions: Catalyst-0.5 cc; Temperature-135 ^{0}C; GHSV-10,000 h $^{-1}$.
** In presence of H_2O (steam).*

A similar study was carried out for 1Pt-NaY catalyst, which also shows similar results. However, this catalyst shows little improvement in activity with H_2O, though it is more active, at higher space velocities, compared to 0.75Pt-NaY (Fig. 3.10.). It also shows

better activity for streams containing 9500 ppm of CO. Comparison of these two catalysts is shown in table 3.1, while effect of space velocity on 1Pt-NaY catalyst is shown in Fig. 3.10.

PART- B: PREFERENTIAL OXIDATION OF CO ON Pt-NaY PROMOTED BY OTHER METALS

3.5. INTRODUCTION

There were several reports in the literature showing that the PrOx at low temperatures could be achieved with the addition of a suitable 2nd metal such as Ce [20], Fe [16, 23], Co [24 - 28], Ni [25], Mn [20] and alkali metals to Pt [29, 30]. Though each catalyst has proved its superiority over corresponding Pt catalyst, it is difficult to assess each catalyst as different reaction conditions are used. On a Pt catalyst, CO and H_2 oxidation occur by a Langmuir–Hinshelwood reaction mechanism [16, 31, 32]. However, CO strongly adsorbs on Pt surfaces [16, 24, 31, 33, 34], inhibiting O_2 adsorption. One way to overcome this problem is to promote the Pt catalyst with another metal to activate surface oxygen species. In this study, iron was used as a promoter for Pt [24]. The role of Fe is to provide an alternative site for O_2 adsorption because iron oxide does not adsorb CO as readily as O_2 [23, 35, 36]. It is believed that Fe in intimate contact with Pt will facilitate CO oxidation by creating a non-competitive, dual-site reaction mechanism [24].

In this section, we report the importance of the Pt promoted NaY catalysts and their catalytic activity for PrOx reaction, in addition to synergic effect of Pt with different metals like Fe, Au and Co on Pt catalyst.

3.6. RESULTS AND DISCUSSION

3.6.1. Effect of addition of cobalt, gold and Iron in Pt-NaY

Figure 3.11 shows the effect of cobalt, gold and iron with platinum on PrOx performance. As discussed in the previous section gold and cobalt based catalysts are effectively used for PrOx reaction. However, when we added these metals to Pt they do not show any improved activity compared to Pt-Fe based catalysts. There could be two possibilities (i) the expected synergic effect between these metals (Co, Au) and Pt may not

be there (ii) the Co and Au similar to the Pt strongly adsorb CO which inhibits O_2 sorption. Whereas iron may offer alternative site for O_2 adsorption facilitating duel site mechanism. O_2 and CO compete for same platinum site as in this system, support is inactive for the PrOx reaction.

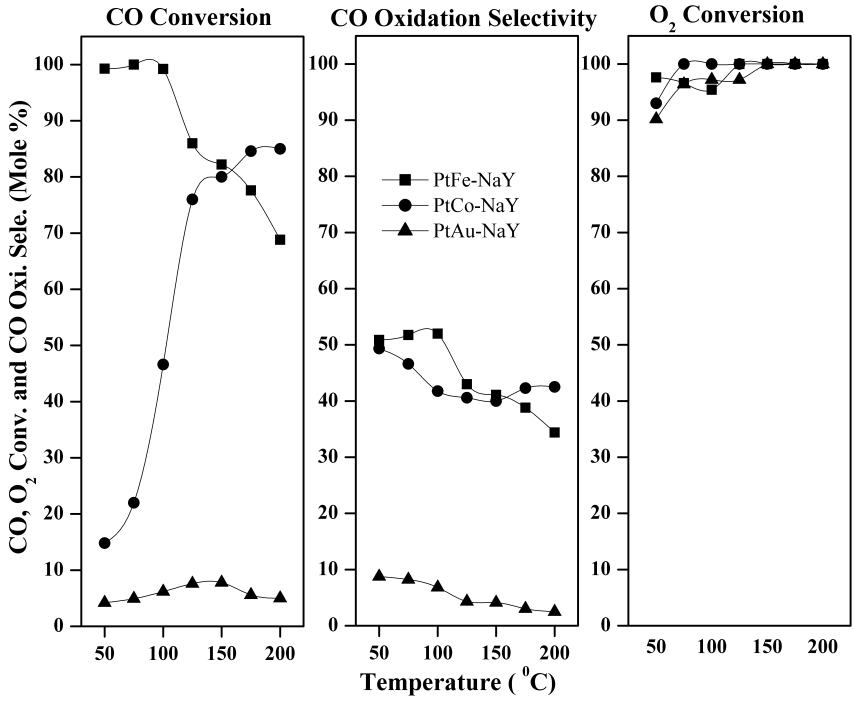

Fig. 3.11: *Effect of Fe, Co and Au addition to Pt-NaY on catalytic activity and selectivity. Reaction conditions: Catalyst - 0.5 cc; O_2/CO ratio -1.0; GHSV-10,000; CO-5000 ppm.*

Metal composition used for this study was 0.75:0.38 Pt-M-NaY (M = Au, Co and Fe), which was found to be optimum. PtFe-NaY and PtCo-NaY catalyst were activated by heating in air at 400 ^{0}C followed by reduction in hydrogen at 400 ^{0}C, whereas, Pt-Au-NaY was heated in air followed by reduction at 350 ^{0}C for getting good PrOx activity. The results shown in Fig. 3.11 are chosen from best activity obtained after activating at different temperatures. Complete CO and O_2 conversions were achieved at 75 ^{0}C , while it is 135 ^{0}C for Pt-NaY, under similar reaction conditions. At increased reaction temperatures, CO conversion fell due to hydrogen oxidation. Above results show that iron catalyst shows better activity than gold and cobalt. Hence, further studies were conducted on this catalyst by varying metal composition and activation temperature on this catalyst.

3.6.2. Effect of reaction temperature on Pt, Fe and PtFe-NaY

Comparison of catalytic activity on Pt-NaY, Fe-NaY with PtFe-NaY is shown in Fig. 3.12. Fe-NaY shows hardly any activity in the temperature range of 50 - 200 ^{0}C.

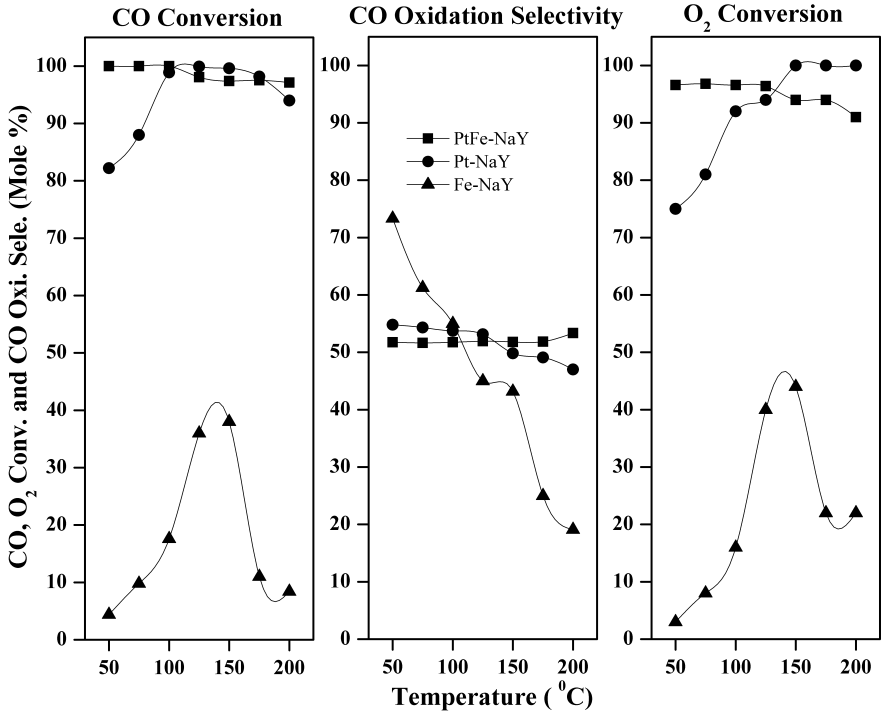

Fig. 3.12: *Comparison of Pt-NaY, Fe-NaY and PtFe-NaY with respect to CO, O_2 conversion and CO oxidation selectivity.*
Reaction conditions: Catalyst-0.5 cc; O_2/CO ratio -1.0; GHSV-10,000h $^{-1}$; CO-5000 ppm; TOS -7 h.

CO conversion of close to 100 mole % was observed at 75 ^{0}C for PtFe-NaY catalyst, whereas similar activity was obtained at 135 ^{0}C for the Pt-NaY catalyst. The behavior of PtFe-NaY catalyst was same as Pt-NaY, the only difference being the reaction temperature. This proves that Fe facilitates O_2 adsorption, which leads to more coverage for CO on platinum surface. To corroborate this, chemisorption of CO and O_2 were performed on Fe/Al_2O_3, Ir/Al_2O_3 and Ir/Fe/Al_2O_3. It was found that Fe/Al_2O_3 could not adsorb CO as compared to other samples. On the other hand, Fe promoted Ir catalyst shows much more O_2 uptake as compared to Ir supported Al_2O_3. These results clearly suggest that the role of Fe is to adsorb and activate O_2 [37, 38]. Metal loading in Fe-NaY

and Pt-NaY was 0.75 wt % whereas in case of PtFe-NaY, the metal loadings were 0.75 and 0.38 wt % for Pt and Fe respectively.

3.6.3. Variation in iron content

The catalytic behavior of bimetallics is influenced by the size and composition of metal nanoparticles, interaction with support and interaction between metal components.

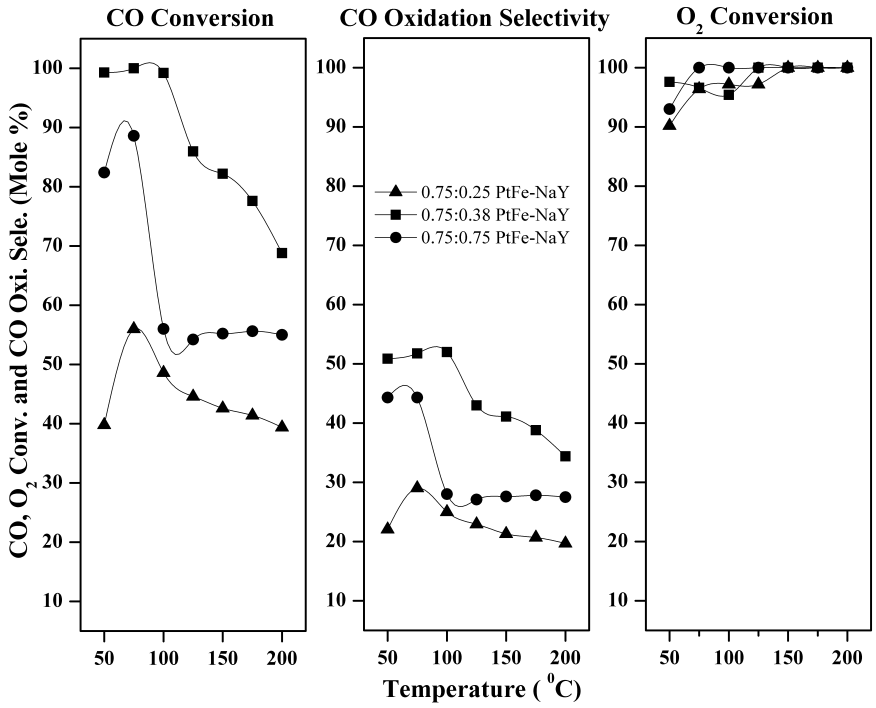

Fig. 3.13: *Effect of Fe content on CO and O_2 conversions and CO oxidation selectivity on PtFe-NaY catalyst.*
Reaction conditions: Catalyst-0.5 cc; O_2/CO ratio -1.0; GHSV-10,000; CO -5000 ppm.

The effect of Fe content (Fe - 0.25, 0.38, 0.75) on PrOx reaction was examined as a function of temperature by keeping Pt content at 0.75 wt %. As shown in Fig. 3.13, the catalyst containing 0.38 wt % Fe showed better performance (CO, O_2 conversion and CO oxidation selectivity) in the temperature range of 50 - 200 ^{0}C.

Increase in iron content led to a reduction in the overall activity of the reaction; proving that the metal composition plays an important role in achieving better results for PrOx reaction [35]. Probably at low Fe loading, the metallic particles are mostly in the

cages, whereas outside the cages at higher Fe loading, which may be the reason for fall in activity. This was proved by H_2-TPR results.

3.6.4. Effect of calcination temperature

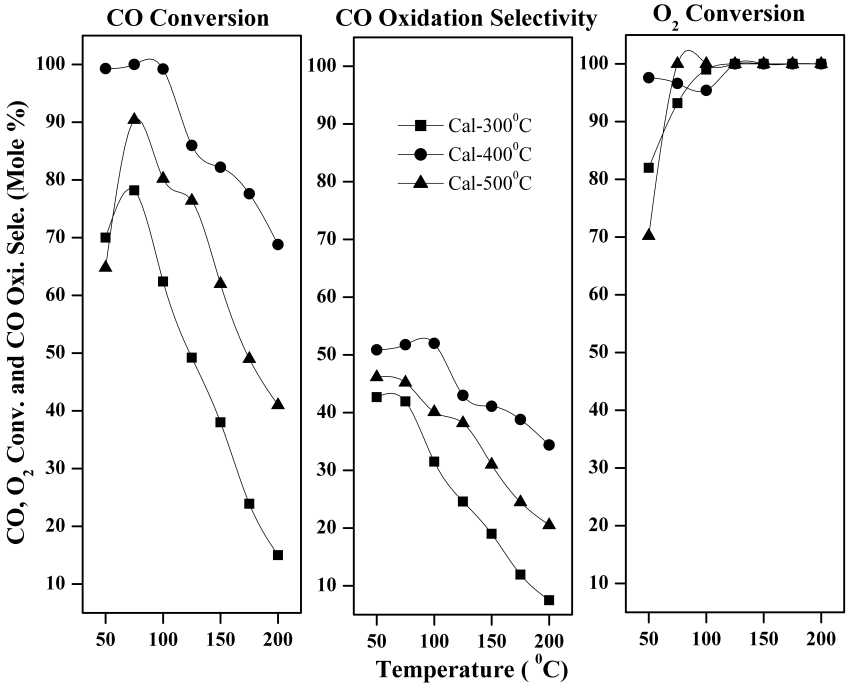

Fig. 3.14: *Effect of calcination temperature on CO, O_2 conversions and CO oxidation selectivity on PtFe-NaY catalyst.*
Reaction conditions: Catalyst-0.5 cc; O_2/CO ratio -1.0; GHSV-10,000 h^{-1}; CO-5000 ppm.

Calcination temperature is important as it plays vital role in promoting interaction between various metal oxide catalyst, in this particular case for obtaining bimetallic oxide phase of Pt and Fe [35]. In this study the catalyst was calcined at different temperatures and reaction results are shown in Fig. 3.14. The results show that the bimetallic oxide phase may be forming at 400 ^{0}C temperature. It is very difficult to get this phase identified by powder XRD because the metal content is very low as no peak for platinum or iron was observed, as discussed in chapter 2. These reaction results were also supported by TEM of samples calcined at different temperatures, Better dispersion and uniform particle size were observed for samples calcined at 400 ^{0}C. The 500 ^{0}C calcined samples gave bigger particles, which resulted in decreased PrOx activity.

3.6.5. Time on stream study

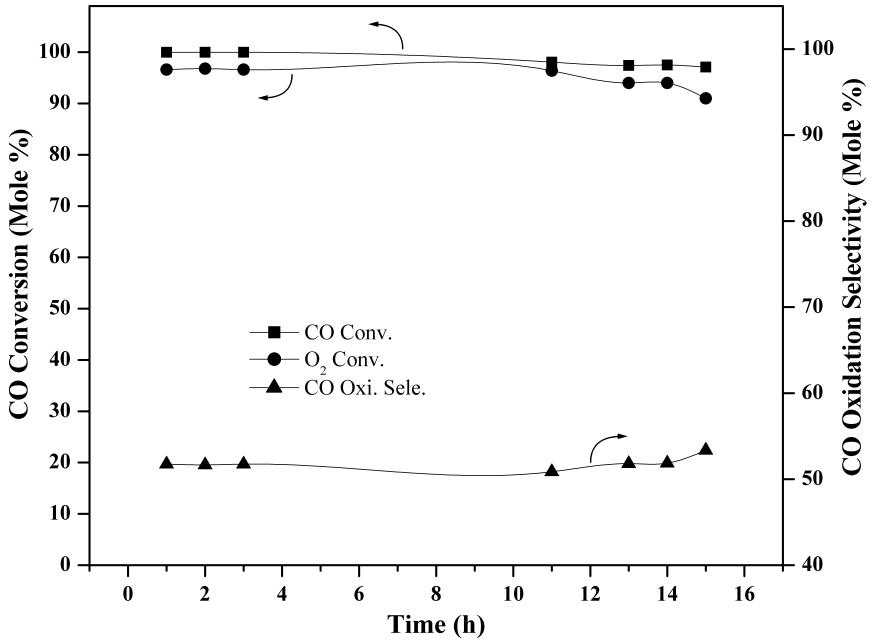

Fig. 3.15: *Effect of time on stream on CO, O_2 conversion and CO oxidation selectivity on PtFe-NaY catalyst.*
Reaction conditions: Catalyst-0.5 cc, O_2/CO-, GHSV-10,000 h^{-1}, CO-5000 ppm, Temperature- 75 ^{0}C; TOS -15 h.

Activity and selectivity in PrOx reaction in terms of long-term stability is strongly influenced by the choice of support material, active metal component and the promoter as well. Apart from this, the method of preparation, precursor used, metal content, activation temperature etc. also play important role in the long-term stability. Most of the studies to date suggest that the activity is highly sensitive to the preparation procedure and the testing conditions particularly composition of the inlet gas mixture, for catalyst evaluation.

Carbon dioxide, which is called an acid gas can affect the activity of the catalysts containing base metals like Fe, Cu, Cr, Ni, Zn, Co etc. by blocking catalytic sites through carbonate formation as carbonates are stable at low temperature at which PrOx reaction has to take place.

Stability test of PtFe-NaY at 75 ^{0}C was carried out for 15 h. The results in Fig. 3.15 shows that conversion was steady initially without any deactivation but the activity started falling after 10 h, with CO conversion reduced to 99.07 from 99.99 mole % at the same

time whereas a slight increase in oxidation selectivity from 50.76 to 51.94 mole % was observed. This may be due the formation of carbonate species on iron (basic in nature) surface because the feed contains more than 20 mole % CO_2 that act as acid gas. The presence of CO_2 in the feed induces a loss in the catalytic performance. This effect was reportedly more pronounced as the CO_2 partial pressure in the feed increases and could be explained through adsorption of CO_2 on the iron surface as carbonate [14]. This interpretation is supported by the fact that by increasing the temperature to 135 ^{0}C, the results obtained were essentially same as observed for Pt-NaY.

3.7. SUMMARY OF PART - A AND PART B

In part A, the catalytic properties of Pt-NaY catalyst with different platinum loadings under various reaction conditions were evaluated for preferential oxidation of CO in hydrogen rich gas stream. The CO oxidation selectivity increased with increase in metal content, maximum activity was obtained at metal loading of 0.75 wt %. At higher metal loading, the activity was low particularly at low temperature this may be due to the higher particle size and poor dispersion at higher metal loading. Detailed studies like space velocity, O_2/CO ratio, water effect and CO concentration on 0.75Pt-NaY and 1Pt-NaY was carried out and compared. Increase in space velocity led to a decrease in the CO and O_2 conversions, whereas, CO oxidation selectivity improved at the same time. As O_2/CO increases, the activity goes up and remains a plateau, whereas CO oxidation selectivity increases up to 50 mole % at O_2/CO ratio equal to one and goes down above one.

Since, the reformate gas in reality contains around 20 mole % water, a study was carried out by introducing steam in the reaction mixture. A decrease in the activity was observed on introduction of the steam. Also, studies were carried out by using different CO concentrations (5000 and 9500 ppm CO) and its activity compared. Higher CO content in the gas mixture led to decrease in activity, whereas better activity was observed for samples with higher Pt content (1Pt-NaY). Stability tests were carried out, by using optimum reaction conditions derived from above studies, no change in activity and CO oxidation selectivity were observed for upto 30 h. These results show that Pt-NaY catalyst is the promising candidate for PrOx reaction in hydrogen rich streams.

In part B, the results of samples of modified platinum catalyst by introducing second metals like Fe, Co and Au were discussed, PtFe-NaY catalyst has shown better activity than platinum only catalyst. The detailed studies like iron content, activation temperature and stability test were carried out. The catalyst with metal composition 0.75:0.38 for PtFe-NaY shows better activity at a temperature 75 ^{0}C. The best calcination temperature was found to be 400 ^{0}C. Time on stream study was carried out for 15 h; the catalyst started deactivating after 10 h only.

PART - C: PREFERENTIAL OXIDATION OF CO ON Cu-Co-Ce-O MIXED OXIDE CATALYSTS

3.8. INTRODUCTION

Preferential Oxidation of CO in excess hydrogen has been studied over supported Pt metal catalysts with the addition of second metals such as Fe, Co, Au, etc, as discussed in part A and B. These Pt catalysts supported on NaY proved to be good catalyst for selective CO oxidation in the presence of hydrogen. However, the high cost of the precious metals make it imperative to develop alternative catalysts. The use of base metal oxides as a catalyst, such as Cu, Co, Ni, Fe, Mn alone or in combinations [39 - 42] has been reported. Similarly, there were extensive reports on $CuCeO_2$ [42- 45] catalysts.

The well-known enhancement of oxidation activity of CuO, when supported on reducible oxides such as CeO_2, was attributed to "synergistic" effect [42, 46]. It was proposed that well dispersed CuO on CeO_2, which is reducible at lower temperatures with respect to bulk CuO, could easily adsorb CO. As a result, this catalyst exhibited high activity / CO oxidation selectivity for low temperature CO oxidation [47 - 49]. Additionally, it was demonstrated that the redox processes corresponding to the CO oxidation involved the reduction and oxidation of both the copper and the ceria species [50 - 53]. It was postulated that the presence of copper enhances the redox behavior, the oxygen storage capacity and thermal stability of ceria [42, 54].

Ceria is an interesting oxide with unique properties namely its ability to shift easily between Ce^{3+} to Ce^{4+} states ($Ce^{3+} \leftrightarrow Ce^{4+}$) and accommodate variable levels of bulk and surface oxygen vacancies. It plays multiple role in various catalyst systems and also

promotes noble metal dispersion and increased thermal stability. These characteristics make CeO_2 a good support. It promotes CO removal through oxidation by employing its lattice oxygen, by storing and releasing oxygen under lean and rich conditions.

In this section, we report the importance of CeO_2 in combination with Cu and Co mixed oxides. A series of Cu-Co-Ce-O mixed oxide catalysts were prepared by the co-precipitation method and their catalytic performance was tested for PrOx of CO in H_2-rich gas streams. These catalysts exhibited good catalytic activity and selectivity for the PrOx reaction in the presence of carbon dioxide.

3.9. RESULTS AND DISCUSSION

3.9.1. Effect of reaction temperature

The evaluation of the $Cu_xCo_{(1-x)}Ce_2O_{4-\delta}$ (x = 0, 0.15, 0.25, 0.50, 0.75, 1.0) mixed oxide catalysts as a function of temperature in terms of CO, O_2 conversions and CO oxidation selectivity is presented in figures. 3.16, 3.17 and 3.18 respectively.

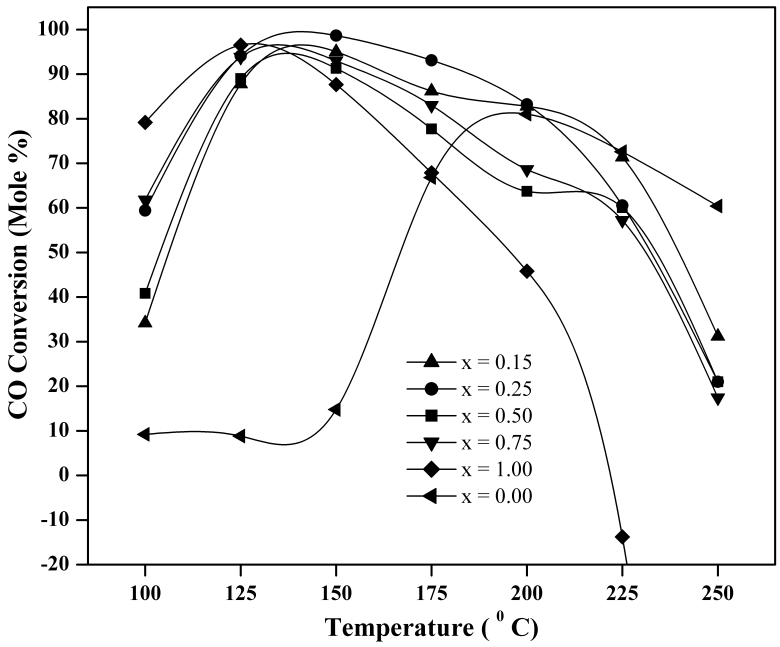

Fig. 3.16: *Effect of catalyst composition on CO conversion at different temperatures on $Cu_xCo_{(1-x)}Ce_2O_{4-\delta}$.*
Reaction conditions: Catalyst-0.5 cc; O_2/CO ratio -1.0; GHSV-10,000 h^{-1}; CO-5000 ppm.

The low temperature CO oxidation activity was evaluated with variation Cu content in the catalysts. The activity has increased sharply with increasing temperature for all samples with Cu content in the x = 0.15 – 1.0 range. The catalyst with copper content x = 0.25 showed relatively better activity than other compositions. The CO conversion reaches maximum at 150 ^{0}C (Fig. 3.16) and complete oxygen conversion at around 175 ^{0}C (Fig. 3.17). Oxygen and CO conversions behave in a similar fashion in the temperature range of 100 - 150 ^{0}C. Increase in CO conversion led to a decrease in CO oxidation selectivity. However, above 175 ^{0}C the combustion of hydrogen becomes dominant leading to a fall in both CO conversion and CO oxidation selectivity.

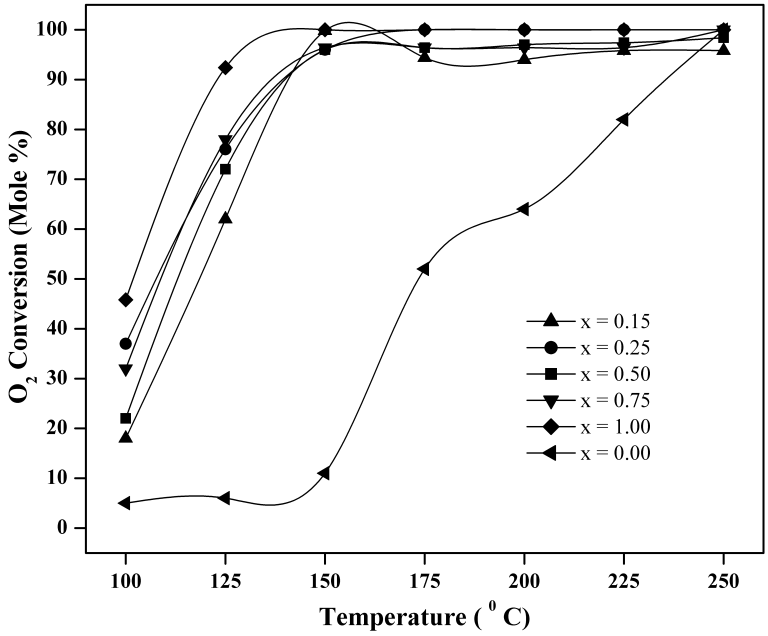

Fig. 3.17: *Effect of catalyst composition on O_2 conversion with respect to temperature on $Cu_xCo_{(1-x)}Ce_2O_{4-\delta}$.*
Reaction conditions: Catalyst-0.5 cc; O_2/CO ratio -1.0; GHSV-10,000 h^{-1}; CO-5000 ppm.

Oxygen conversion also follows a trend similar to that of CO conversion. It reaches close to 100 mole % conversion on all catalyst containing copper. The catalyst that has only cobalt (x = 0) was not much active at lower temperatures, however the CO conversion was achieved at higher temperature. Still, it is not similar to the one that obtained over copper-cobalt catalysts. But complete conversion of oxygen was noticed at 250 ^{0}C. This shows that the cobalt shows poor activity for CO oxidation [14].

Copper ceria catalyst (x = 1) that has no cobalt is more active at lower temperature giving 96.50 mole % CO conversion and 92.40 mole % O_2 conversion. As temperature increases, there is drastic fall in the CO conversion, which may be attributed to the reverse water gas shift reaction, that was observed when x = 1. The reverse water gas shift (RWGS) reaction would result in the formation of CO from CO_2 and H_2 and brings down the net CO conversion that could have been attained. To evaluate whether the RWGS reaction takes place over the $3CuCeO_2$ catalysts, CO_2 - H_2 mixture (25 mole % CO_2, 25 mole % H_2 and 50 mole % N_2) was fed to the reactor. Low content of CO due to RWGS above 200 ^{0}C has been reported [14]. In our case up to 1.4 mole % CO was detected in the product stream, under PrOx reaction conditions, which is more than that of the inlet concentration of CO. These results suggest that the RWGS reaction was suppressed by the addition of cobalt in the copper ceria sample, as drastic change in CO conversion was not observed on our catalysts, except a steady fall in CO conversion due to hydrogen oxidation at higher temperatures.

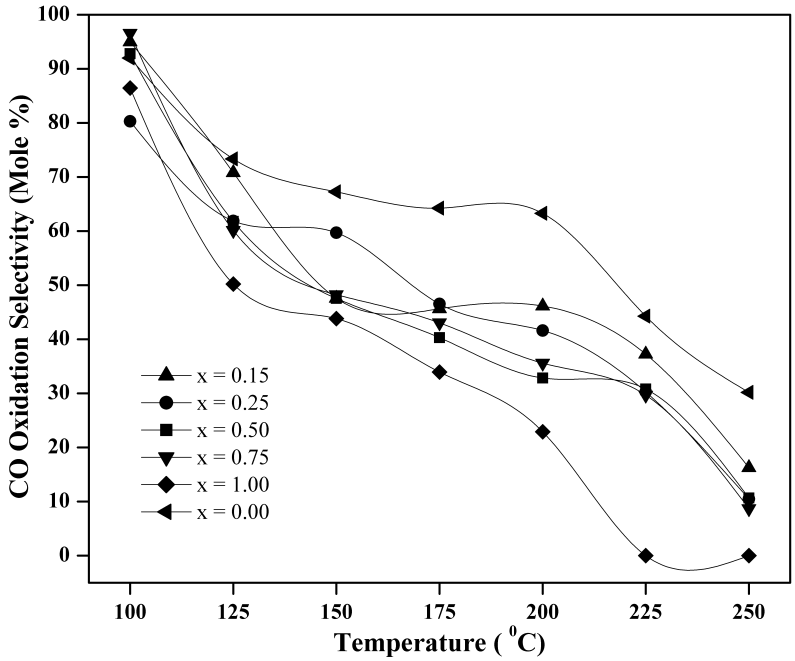

Fig. 3.18: *Effect of Composition on CO oxidation selectivity with respect to temperature on $Cu_xCo_{(1-x)}Ce_2O_{4-\delta}$.*
Reaction conditions: Catalyst - 0.5 cc; O_2/CO ratio-1.0; GHSV-10,000 h^{-1}; CO-5000 ppm; TOS - 7 h.

To evaluate whether the RWGS reaction takes place over these catalysts, we performed some additional experiments by feeding CO_2 and H_2 mixture to the reactor. The feed composition was 25 mole % CO_2 with 76 mole % H_2. The CO concentration at the reactor outlet at different temperature (same temperatures used for PrOx reaction study) is plotted in Fig. 3.19. As it may be seen, the catalyst with composition x = 0 and 0.25 were not active for RWGS under the experimental condition studied. But $Cu_xCo_{(1-x)}Ce_2O_{4-\delta}$ (x = 1.0) shows RWGS at temperatures above 175 ^{0}C, with CO present in the reaction product. The RWGS reaction is not in thermodynamic equilibrium [14]; as the expected maximum content of CO at 250 ^{0}C is only 0.65 mole %. Based on these results, we can conclude that RWGS reaction is kinetically controlled but not at thermodynamic equilibrium. This can be explained by self-poisoning of the active sites by the adsorbed CO_2 species.

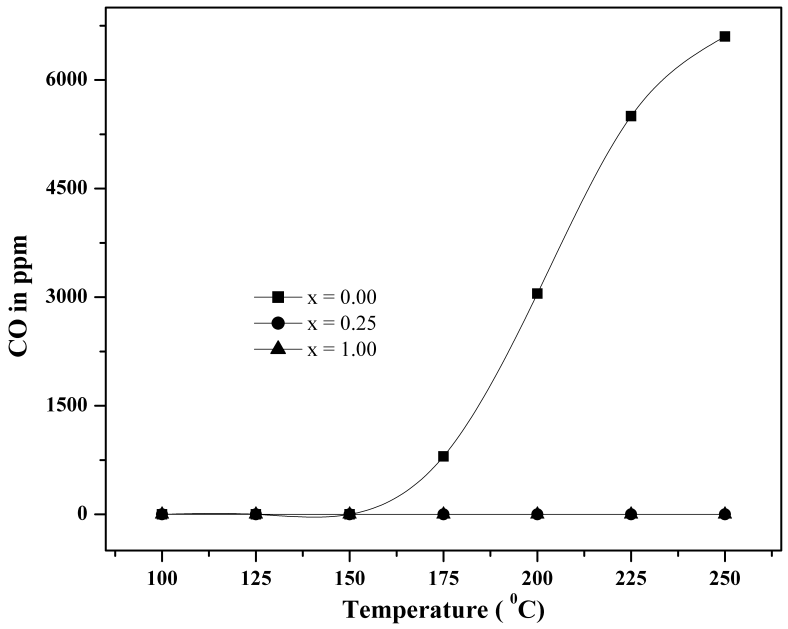

Fig. 3.19: *Effect of catalyst composition on reverse water gas shift reaction with respect to temperature on $Cu_xCo_{(1-x)}Ce_2O_{4-\delta}$.*
Reaction conditions: Catalyst - 0.5 cc; GHSV - 10,000 h^{-1}; Feed CO_2 = 25 mole %, H_2= 75 mol %.

Ceria alone also shows the catalytic activity for the oxidation of CO and H_2. But its activity was considerably lower than the copper or cobalt catalysts [49]. Hydrogen oxidation takes place on both the metal and the support [54, 55].

In addition to RWGS, methanation of CO may also take place on these catalysts. Particularly on copper containing cobalt rich catalysts. This can lead to reduction in hydrogen content in the reformate. We did not observe any formation of methane on Cu containing catalysts at any temperature. Hence, both CO and CO_2 methanation was ruled out on these catalyst. Ni, Ru and Rh catalysts used for oxidation of CO in the presence of hydrogen usually show methanation activity under PrOx conditions [14, 56]. There were reports that cobalt containing catalysts promote methanation reaction when supported on alumina, silica and titania [57]. Not even trace amount of methane was observed at the reaction temperature on $Cu_xCo_{(1-x)}Ce_2O_{4-\delta}$ with x = 0 and $Cu_xCo_{(1-x)}Ce_2O_{4-\delta}$ with x = 1 samples. But, in the presence of copper, with increase in cobalt from x = 1 to 0.15, methane was observed above 175 ^{0}C as shown in Fig. 3.20. This may be the evidence for the strong synergism between copper and cobalt supported on ceria catalyst.

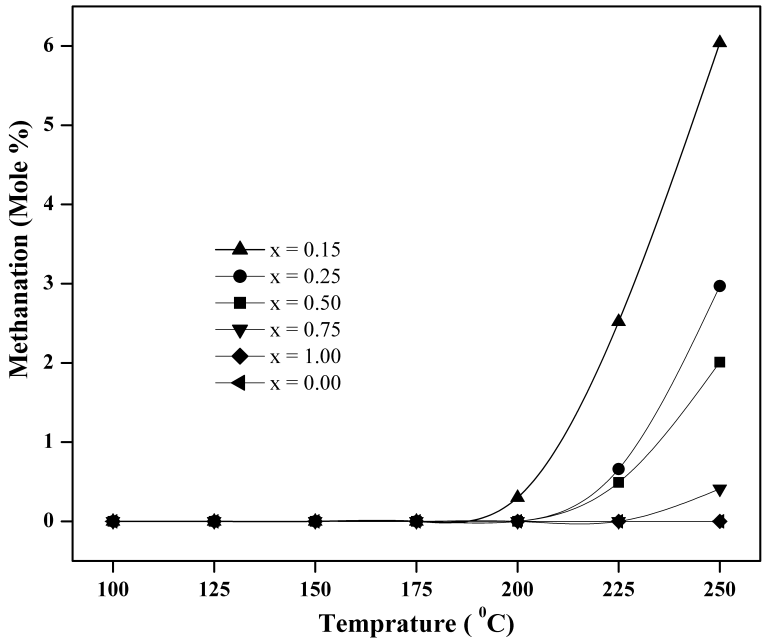

Fig. 3.20: *Effect of catalyst composition on CO and CO_2 methanation with respect to temperature on $Cu_xCo_{(1-x)}Ce_2O_{4-\delta}$.*
Reaction conditions: Catalyst-0.5 cc; O_2/CO ratio-1.0; GHSV-10,000 h^{-1}; CO -5000 ppm; TOS-7 h.

3.9.2. Influence of space velocity

It was reported in the literature, that the increase in space velocity or decrease in contact time leads to loss in activity and improvement in CO oxidation selectivity. In contrast to this, Cu-Co-Ce-O mixed oxide system shows improved oxygen conversion and a fall in CO oxidation selectivity with increase in space velocity, as shown in Fig 3.21. Increase in space velocity leads to hydrogen oxidation, as a result fall in CO oxidation selectivity takes place. In effect, the oxygen was utilized for hydrogen oxidation instead of CO oxidation. Cobalt may be promoting the hydrogen oxidation at high space velocities, whereas copper at high space velocity provides less coverage for CO [58]. This explanation can be supported by comparing the result obtained over $Cu_xCo_{(1-x)}Ce_2O_{4-\delta}$ with x = 0.25 and x = 1 plotted in Fig. 3.21 and 3.22 respectively.

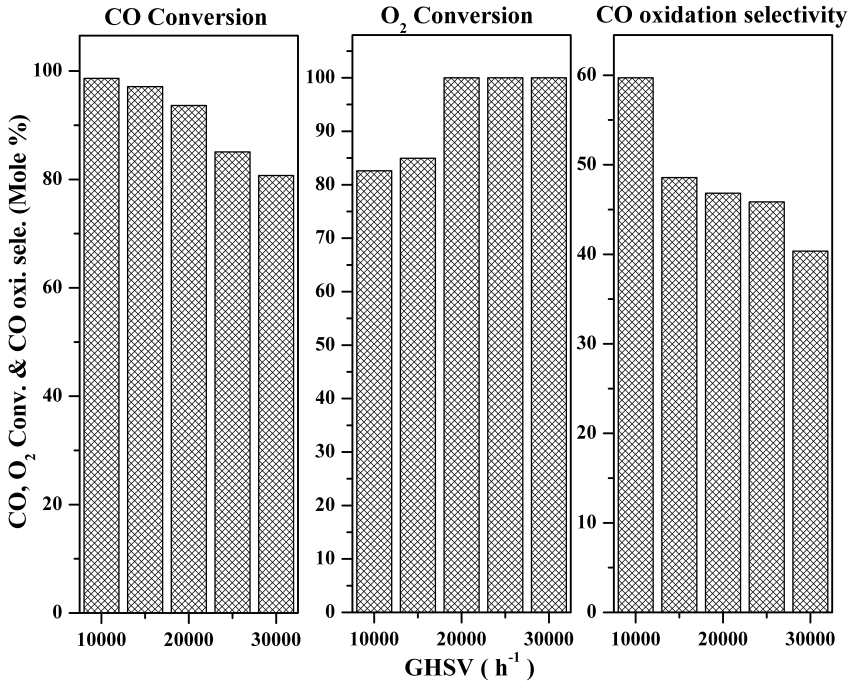

Fig. 3.21: *Effect space velocity on CO and O_2 conversion and CO oxidation selectivity on $Cu_xCo_{(1-x)}Ce_2O_{4-\delta}$ (x = 0.25).*
Reaction conditions: Catalyst - 0.5 cc; O_2/CO ratio - 1.0; Temperature - 150 ^{0}C, CO - 5000 ppm; TOS – 5 h.

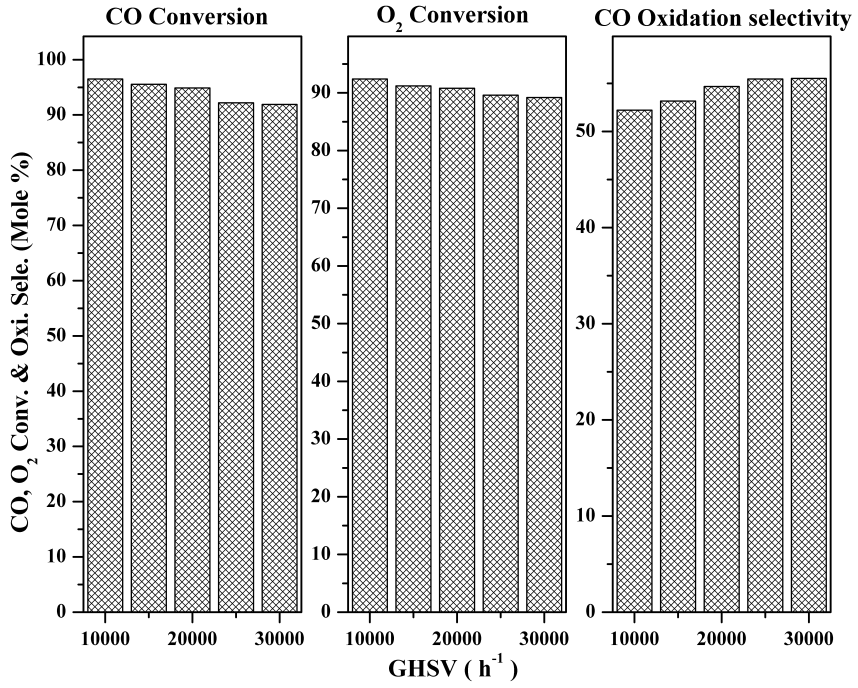

Fig. 3.22: *Effect space velocity on CO, O_2 conversion and CO oxidation selectivity over $Cu_xCo_{(1-x)}Ce_2O_{4-\delta}$ (x = 1).*
Reaction conditions: Catalyst-0.5 cc; O_2/CO ratio -1.0; Temperature-125 ^{0}C, CO-5000 ppm; TOS -5 h.

Effect of space velocity on x = 1 was done at 125 ^{0}C, the optimum condition for obtaining maximum activity, whereas other parameters were kept same as x = 0.25.

3.9.3. The effect of O_2/CO ratio

The effect of O_2/CO ratio was monitored on CO, O_2 conversion and CO oxidation selectivity as shown in Fig. 3.23. Parallel decrease in CO oxidation selectivity with O_2 conversion was observed, whereas CO conversion increased steadily and reaches plateau with increasing O_2/CO ratio. This shows that the catalyst is selective towards the oxidation of CO to CO_2. Ceria acts as an oxygen buffer, as a result the available oxygen concentration remains constant up to a certain oxygen inlet concentration when the maximum oxygen storage capacity (OSC) of ceria is exceeded. It must be noted that the product of total conversion does not directly result in the CO conversion. The oxygen excess must be taken into account, which gives O_2 conversion.

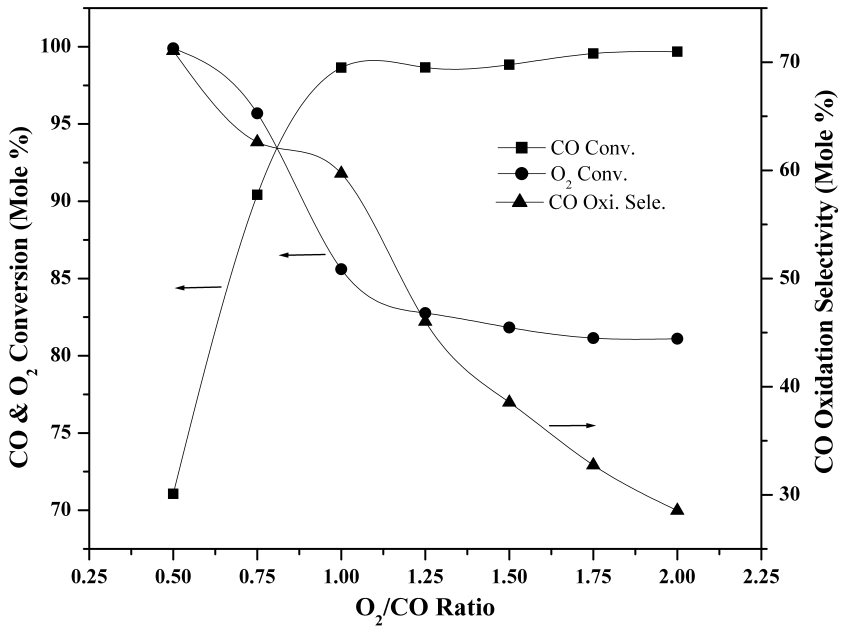

Fig. 3.23: *Effect of O_2/CO ratio on CO, O_2 conversion and CO oxidation selectivity on $Cu_xCo_{(1-x)}Ce_2O_{4-\delta}$ (x = 0.25).*
Reaction conditions: Catalyst-0.5 cc; GHSV - 10,000 h^{-1}; Temperature-150 ^{0}C, CO -5000 ppm; TOS -7 h.

3.9.4. The effect of H_2O

The effect on CO, O_2 conversion and CO oxidation selectivity with and without water is compared and plotted in Fig. 3.24 as a function of temperature. $CuCeO_2$ catalyst was found to be highly sensitive to the steam in the reaction feed. The fresh oxidized catalyst was deactivated after exposure to water with the light-off temperature increasing from 30 to 70 ^{0}C [58]. A large amount of small $Cu(OH)_2$ nanocrystals in the size of 1– 4 nm were observed in the exposed catalyst in this study, rather than the copper oxide clusters proposed in the literature [58]. The active sites are generally assumed to be fine copper or copper oxide clusters highly dispersed on CeO_2 support. The catalysts apparently adsorbed a large amount of water after exposure at room temperature. CeO_2 powders can absorb a large quantity of water, by monitoring effluent gas using a quadruple mass spectrometer on CeO_2 samples the weight loss and water evolution profiles were observed. Among them, 5 mole % was released at 100 ^{0}C and below, which is considered to be physically adsorbed water. Additional 1 mole % was released between 100 and 150 ^{0}C,

and the rest 1 mole % was released at 150 - 300 ^{0}C [58]; the continuous release of H_2O at temperatures over 200 ^{0}C indicates the strong chemical bonding between H_2O and the catalyst.

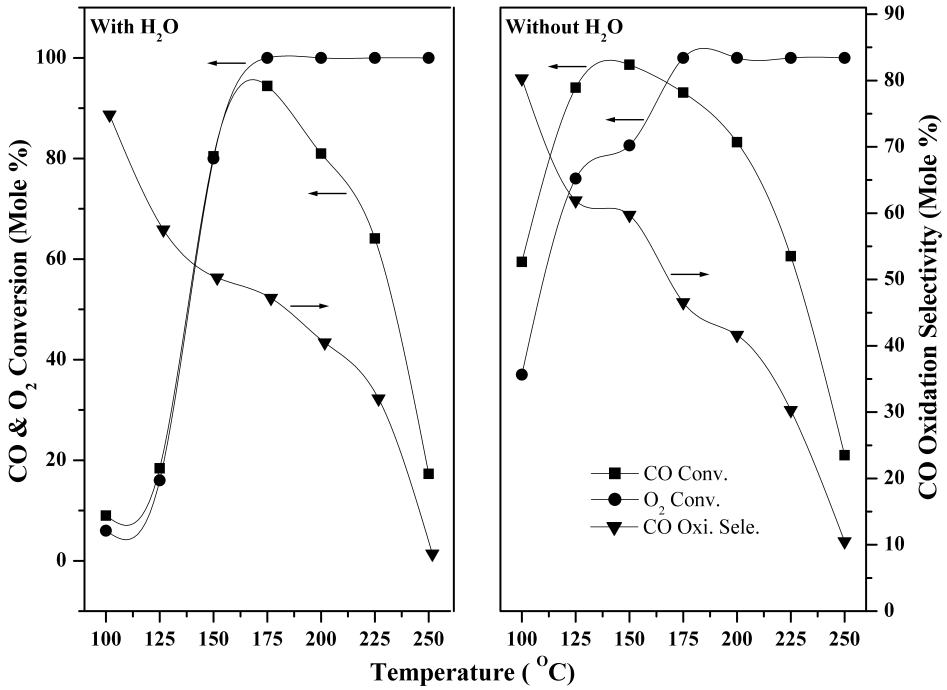

Fig. 3.24: *Effect of water on CO and O_2 conversion and CO oxidation selectivity on $Cu_xCo_{(1-x)}Ce_2O_{4-\delta}$ (x = 0.25).*
Reaction conditions: Catalyst-0.5 cc; GHSV-10,000 h^{-1}; Temperature-150 ^{0}C, CO – 5000 ppm; O_2/CO ratio –1.0; water- p (H_2O)-200 Torr; TOS -5 h.

The decomposition temperature of bulk $Cu(OH)_2$, which is formed after addition of water, in the range of 130 - 180 ^{0}C. In the bulk form, copper oxide is more stable than $Cu(OH)_2$. However, the surface energy of CuO is larger than that of $Cu(OH)_2$ [59]. Therefore, $Cu(OH)_2$ would become the more stable phase when the particle sizes are small enough that surface energy is an important contribution to the free energy [59]. To further confirm the effect of moisture on the catalytic activity, the catalysts were tested for PrOx reaction after preheating at 200 ^{0}C in the flow of air to get original activity.

3.9.5. The effect of CO content in the feed

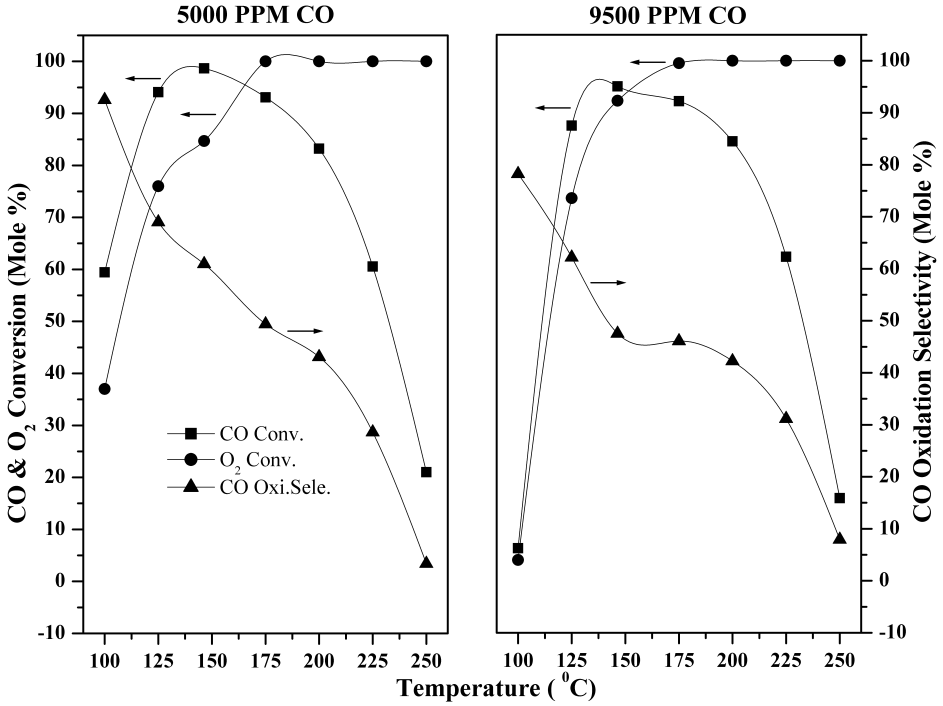

Fig. 3.25: *Effect of CO content in the feed on CO and O_2 conversion and CO oxidation selectivity on $Cu_xCo_{(1-x)}Ce_2O_{4-\delta}$ (x = 0.25).*
Reaction conditions: Catalyst-0.5 cc; GHSV-10,000 h^1; Temperature -150 ^{0}C, CO - 5000 and 9500 ppm; O_2/CO ratio -1.0.

The influence of CO content in the feed was studied by using gas mixture containing 5000 and 9500 ppm CO in addition to CH_4, CO_2 and hydrogen at 150 ^{0}C These results are shown in Fig. 3. Loss of activity was noticed at higher concentration of CO, however the activity could be (CO and O_2 conversion) regained by raising the temperature.

From the above results it is clear that high temperatures are required for feed containing high concentration of CO, to achieve optimum activity.

3.9.6. Time on stream study

The activity of freshly calcined catalysts towards PrOx reaction in excess hydrogen is shown in Fig. 3.26. It was found that O_2 conversion has increased while CO oxidation selectivity fell after few hours of reaction. Though CO oxidation remained stable over long periods, there was a slight fall in its value with time on stream. Possible reasons for

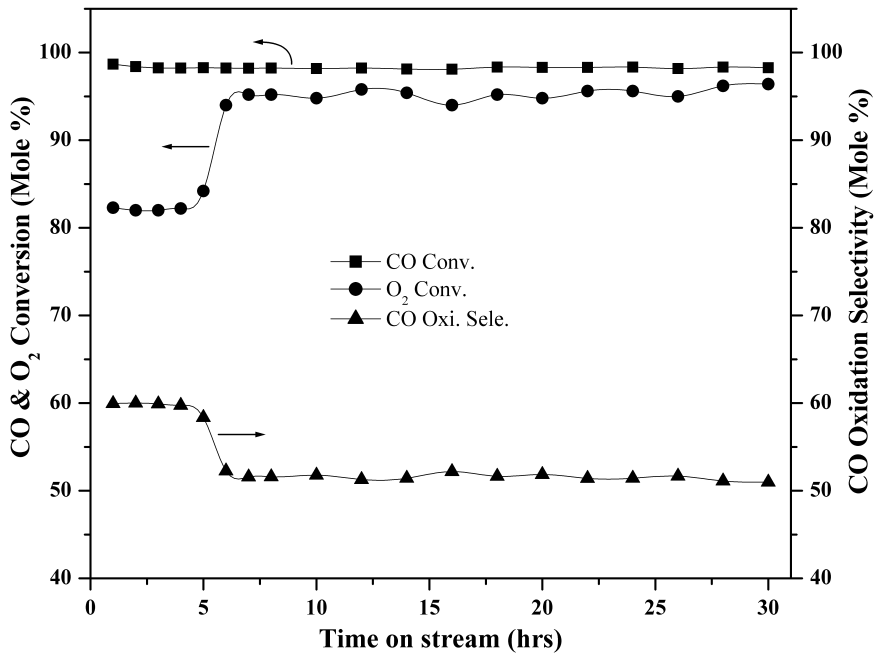

Fig. 3.26: *Effect of time on stream on $Cu_xCo_{(1-x)}Ce_2O_{4-\delta}$ (x = 0.25).*
Reaction conditions: Catalyst-0.5 cc; GHSV-10,000 h^{-1}; Temperature -150 ^{0}C, CO-5000 ppm; O_2/CO ratio -1.0; TOS -30 h.

catalyst deactivations are: poisoning, coking and solid-state transformation of catalyst. Coking of the catalyst was rejected, because no carbon-containing species were found on the catalyst surface, gray/brown color of the catalyst remained unchanged after 30 hrs run, catalyst poisoning by any components present in the feed would decrease the CO conversion monotonously to zero in most of the cases. The presence of H_2O in the reactor feed formed by hydrogen oxidation reportedly has no influence on the long-term stability of a similar type of catalyst that was prepared by co-precipitation [60, 61]. In some of the systems containing copper and ceria, the activity and CO oxidation selectivity increases which may be due to the small amount of water which is formed by the hydrogen oxidation, the participation of water derived species, such as – OH, act as a promoter in the reaction mechanism, which decomposes the reaction intermediate –COOH to CO_2 [61, 62].

No methanation or other side reactions like reverse water gas shift reaction was observed in the stability measurement on this catalyst apart from hydrogen oxidation for the duration of reaction studied (30 h).

Table 3.2 gives comparison of catalytic activity for PrOx of CO on $Cu_xCo_{(1-x)}Ce_2O_{4-\delta}$ catalysts with x = 0.25 and x = 1.0 for a better appreciation of this study.

Table 3.2: Comparison of $Cu_xCo_{(1-x)}Ce_2O_{4-\delta}$ for x = 0.25 and x = 1 for PrOx reaction

	x = 0.25			x = 1.0		
	CO Conv.	O_2 Conv.	CO Oxi. Sele.	CO Conv.	O_2 Conv.	CO Oxi. Sele.
CO = 5000 ppm	98.68	84.0	58.73	97.12	91.80	52.89
O_2/CO = 0.5	71.06	100.0	71.06	83.94	94.60	94.10
O_2/CO = 2.0	99.68	66.0	30.02	97.70	36.60	35.76
CO = 9500 ppm	91.54	73.6	62.18	96.24	85.00	56.61
* CO = 5000 ppm	40.12	41.6	48.22	14.18	28.20	25.14
After 30 h	98.28	96.4	50.97	96.48	91.80	52.54

Reaction conditions: Catalyst - 0.5 cc; Temperature - 150 and 125 ^{0}C for x = 0.25 and x = 1.0 respectively; GHSV-10,000 h^{-1}.
** In presence of H_2O (steam).*

3.10. SUMMERY OF PART C

PrOx catalysts prepared using prohibitively expensive precious metals (Pt, Pd, Ru, and Rh) supported on Al_2O_3 operate at higher temperatures (150 – 200 ^{0}C) with low oxidation selectivity. In order not to lose hydrogen and keep the overall energy conversion process as efficient as possible, the CO oxidation must be highly selective. In order to lower the cost and improve the oxidation selectivity, $CuCeO_2$ catalyst for the selective low-temperature oxidation of CO in excess H_2 was intensively studied.

In this section, we have studied catalytic properties of $Cu_xCo_{(1-x)}Ce_2O_{4-\delta}$ (x = 0, 0.15, 0.25, 0.5, 0.75, 1) for preferential oxidation of CO in excess hydrogen. The copper-cobalt supported on ceria with x = 0.25 gave best results. Only cobalt containing catalyst (x = 0) does not offer good activity at low temperatures, while the targeted CO conversion was achieved at higher temperature. However, complete conversion of oxygen was noticed at 250 ^{0}C. Catalyst only with Cu (x = 1) is more active at low temperature, but CO oxidation selectivity was low as compared to x = 0.25 at 125 ^{0}C. As temperature increases,

there is drastic fall in the CO conversion, this fall may be due to the addition of CO by reverse water gas shift reaction which was observed in only x = 1 catalyst. These results suggest that the RWGS reaction was suppressed by the addition of cobalt to the copper-ceria sample, because the drastic change in CO conversion was not observed in other catalysts except steady fall in CO conversion due to hydrogen oxidation at higher temperatures. No methane formation was observed under these reaction conditions on $Cu_xCo_{(1-x)}Ce_2O_{4-\delta}$ with x = 0 and $Cu_xCo_{(1-x)}Ce_2O_{4-\delta}$ with x = 1 samples, but with increase in cobalt from x = 1 to 0.15, methane was detected at reaction temperature above 175 ^{0}C.

In contrast to the $Cu_xCo_{(1-x)}Ce_2O_{4-\delta}$ for x = 1.0, the sample with x = 0.25 shows increase in O_2 conversion and decrease in CO oxidation selectivity at higher space velocities. Decrease in CO oxidation selectivity with steady CO conversion was noted with increase in O_2/CO ratio. Water affects the overall activity of the catalyst. For gas mixtures containing 5000 ppm CO, higher activity was observed than when CO in the feed was 9500 ppm. The activity of freshly calcined and in situ oxidized catalyst in PrOx reaction was monitored and it was found that CO oxidation selectivity fell with increase in O_2 conversion in the first few hours. No poisoning, coking or solid-state transformation of catalyst was observed up to 30 h of reaction time.

3.10. REFERENCES:

[1] P. Broqvist, L. M. Molina, H. Grönbeck, B. Hammer, J. Catal., 227 (2004) 217.

[2] C. Kwak, T. J. Park, D. J. Suh, Appl. Catal., A 278 (205) 181.

[3] M. Genta, S. Nishiyama, S. Tsuruya and M. Masai, J. Chem. Soc., Faraday Trans., 92-7 (1996) 1267

[4] Oxygen in catalysis, Adam Bielanski and Jerzy Haber.

[5] I. H. Son, M. Shamsuzzoha and A. M. Lane, J. Catal., 210 (2002) 460.

[6] D. H. Kim, M. S. Lim, Appl. Catal., A 224 (2002) 27.

[7] A. Luengnaruemitchai, S. Osuwan, E. Gulari, Int. J. Hydrogen Energy, 29 (2004) 429.

[8] O. Dulaurent, D. Bianchi, Appl. Catal., A 196 (2000) 271.

[9] M. Watanabe, H. Uchida, K. Ohkubo, H. Igarashi, Appl. Catal., B 46 (2003) 595.

[10] M. J. Kahlich, H. A. Steiger, R. J. Behm, J. Catal., 171 (1997) 93.

[11] M. J. Kahlich, H. A. Gasteiger, and R. J. Behm, J. Catal., 182 (1999) 430.

[12] O. Korotkikh and R. Farrauto, Catal. Today, 62 (2000) 249.

[13] S. H. Oh and R. M. Sinkevitch. J. Catal., 142 (1993) 254.

[14] F. Marin, C. Descorme, D. Duprez, Appl. Catal., B 58 (2005) 175.

[15] M. M. Schubert, M. J. Kahlich, H. A. Gasteiger, R. J. Behm, J. Power Sources, 84 (1999) 175.

[16] O. Korotkikh, R. Farrauto, Catal. Today, 62 (2000) 249.

[17] J. C. Trocciola, C. R. Schroll, R. R. Lesieur, US Patent, 5,330,727 issued 19/7/1994.

[18] A. Wootsch, C. Descorme, D. Duprez, J. Catal., 225 (2004) 246.

[19] Y. Choi, H. G. Stenger, J. Power Sources, 129 (2004) 246.

[20] I. H. Son, A. M. Lane, Catal. Lett., 76 (2001) 151.

[21] M. Kotobuki, A. Watanabe, M. Watanabe. Appl. Catal., A 307 (2006) 275.

[22] M. Haruta, A. Ueda, S. Tsubota, R. M. Torres Sanchez, Catal. Today, 29 (1996) 443.

[23] A. Sirijaruphan, J.G. Goodwin Jr. and R.W. Rice, J. Catal., 224 (2004) 304.

[24] X. Liu, O. Korotkikh and R. Farrauto, Appl. Catal., A 226 (2002) 293.

[25] D. J. Suh, C. Kwak, J. H. Kim, S. M. Kwon and T. J. Park, J. Power Sources, 142 (2005) 70.

[26] C. Kwak, T. J. Park and D. J. Suh, Chem. Eng. Sci., 60 (2005) 1211.

[27] C. Kwak, T. J. Park and D. J. Suh, Appl. Catal., A 278 (2005) 181.

[28] E. Y. Ko, E. D. Park, K. W. Seo, H.C. Lee, D. Lee, and S. Kim, J. Nanosci. Nanotechnol., 6 (2006) 3567.

[29] S. H. Cho, J. S. Park, S. H. Choi and S. H. Kim, J. Power Sources, 156 (2006) 166.

[30] C. Pedrero, T. Waku and E. Iglesia, J. Catal., 233 (2005) 242.

[31] A. Bourane, D. Bianchi, J. Catal., 209 (2002) 114.

[32] R. H. Venderbosch, W. Prins, W. P. M. van Swaaij, Chem. Eng. Sci., 53 (1998) 3355.

[33] A. Manasilp, E. Gulari, Appl. Catal., B 37 (2002) 17.

[34] D. H. Kim, M. S. Lim, Appl. Catal., A 224 (2002) 27.

[35] M. Watanabe, H. Uchida, K. Ohkubo, H. Igarashi, Appl. Catal., B 46 (2003) 595.

[36] M. M. Schubert, S. Hackenberg, A. C. van Veen, M. Muhler, V. Plzak, R. J. Behm, J. Catal., 197 (2001) 113.

[37] W. Zhang, A. Wang, L. Li, X. Wang, T. Zhang, Catal. Lett., (2007)

[38] P. Chin, X. Sun, G. W. Roberts, J. J. Spivey, Appl. Catal., A 302 (2006) 22.

[39] W. Liu, A. Sarofin, M. Flytzani-Stephanopoulos, Appl. Catal., B 4 (1994) 167.

[40] T. Huang, T. Yu, Appl. Catal., 72 (1991) 275.

[41] S. Zhang, W. Huang, X. Qiu, B. Li, X. Zheng, S. Wu, Catal. Lett., 80 (1/2) (2002) 41.

[42] G. Avgouropoulos, T. Ioannides, H. K. Matralis, J. Batista, S. Hocevar, Catal. Lett., 73 (2001) 33.

[43] Y. Teng, H. Sakurai, A. Ueda, T. Kobayashi, Int. J. Hydrogen Energy, 24 (1999) 355.

[44] G. G. Xia, Y. G. Yin, W. S. Willis, J. Y. Wang, S. L. Suib, J. Catal., 185 (1999) 91.

[45] C. D. Dudfield, R. Chen, P. L. Adcock, Int. J. Hydrogen Energy, 26 (2001) 763.

[46] J. B. Wang, W. H. Shih, T. J. Huang, Appl. Catal., A 203 (2000) 191.

[47] J. Xiaoyuan, L. Guanglie, Z. Renxian, M. Jianxin, C. Yu, Z. Xiaoming, Appl. Surf. Sci., 173 (2001) 208.

[48] M. Luo, Y. Zhong, X. Yuan, X. Zheng, Appl. Catal., A 162 (1997) 121.

[49] P. Ratnasamy, D. Srinivas, C. Satyanarayana, P. Manikandan, R. Senthil Kumaran, M. Sachin, V. Shetti, J. Catal., 221 (2004) 455.

[50] A. Martinez-Arias, M. Fernandez-Garcıa, J. Soria, J. Conesa, J. Catal., 182 (1999) 367.

[51] A. Martinez-Arias, M. Fernandez-Garcıa, O. Galvez, J. Coronado, J. Anderson, J. Conesa, J. Soria, G. Munuera, J. Catal., 195 (2000) 207.

[52] J. Wang, S. Lin, T. Huang, Appl. Catal., A 232 (2002) 107.

[53] G. Jernigan, G. Somorjai, J. Catal., 147 (1994) 567.

[54] S. Kacimi, J. Barbier Jr., R. Taha, D. Duprez, Catal. Lett., 22 - 4 (1993) 343.

[55] X. Zheng, X. Zhang, S. Wang, S. Wu, Appl. Catal., A 295 (2005) 142.

[56] K. Yaccato, R. Carhart, A. Hagemeyer, R. K. Grasselli and C. Brooks Appl. Catal., A 296 (2005) 30.

[57] V. Froseth, S. Storsater, O. Borg, E. A. Blekkan, M. Ronning and A. Holmen, Appl. Catal., A 289 (2005) 10.

[58] W. J. Zhang, S. P. Dey, S. Deevi, Appl. Catal., A 295 (2005) 201.

[59] P.W. Schindler in: W. Stumm (Ed.), Equilibrium Concepts in Natural Water Systems, ACS (1967) 196.

[60] W. Liu, M. Flytzani-Stephanopoulos, J. Catal., 153 (1995) 304.

[61] W. Liu, M. Flytzani-Stephanopoulos, Chem. Eng. J., 64 (1996) 283.

[62] H. H. Kung, M. C. Kung and C. K. Costello, J. Catal., 216 (2003) 425.

[63] G. C. Bond and D. T. Thompson, Gold Bull., 33(2) (2000) 41.

Chapter - 4

PREPARATION AND CHARACTERIZATION OF Mo/Hβ AND Mo/Fe-Zn-O CATALYSTS

4.1. INTRODUCTION

Methane is the most inert amongst hydrocarbons and hence its activation at low temperature (< 600 ^{0}C) is highly challenging. Earlier studies showed that at low temperatures, methane could be activated in the presence of higher hydrocarbons over modified zeolites [1-3]. Not many reports are available using zeolite as support for the active component. There is no catalyst system found that showed high activity and selectivity without the formation of undesired carbon oxides (CO, CO_2). Several supported oxide catalysts have been employed for this reaction at atmospheric pressure, among them are supported MoO_3 catalysts, which have been reported to be one of the most active and selective for the production of oxygenates [4-13]. Silica as a support has been widely used for metal oxide catalysts for methane partial oxidation and a number of reports have illustrated that silica itself shows discernible activity for formaldehyde formation [14 -16].

Direct conversion of methane to methanol or any other useful products [17] would reduce the number of reaction steps required and thus save greatly on capital cost in a commercial plant. For this reason, a large number of studies have focused in the area of selective oxidation of methane to oxygenates. However, till this date none has succeeded in demonstrating the required combination of high conversion, selectivity and catalyst stability, which would be useful to make direct conversion competitive to the existing multi step route.

Here, in this section, for partial oxidation of methane (POM), beta zeolite was used as a high surface area support for better dispersion of molybdenum oxide. Mo/Al_2O_3 and Mo/SBA-15 were also studied to compare the effect of surface properties of these high surface area oxides with that of Mo/Hβ. This chapter also includes characterization of the molybdenum supported on mixed oxide system (Fe-ZnO) studied for partial oxidation of methane.

The catalysts used in this study were prepared by co-precipitation and dry-impregnation method with different molybdenum contents. These samples were characterized by various physico-chemical methods such as powder X-ray diffraction, UV-visible, FTIR, Raman, ICP-AES, BET surface area, SEM, TEM, TPR-TPD, XPS, chemisorption of pyridine by IR spectroscopy etc. The various characterization techniques used for the present study are briefly described in this chapter.

4.2. PREPARATION OF Mo/Hβ CATALYSTS

Molybdenum based catalysts were reportedly prepared using various routes. These methods were proposed to obtain highly dispersed molybdenum oxide species at lower coverage, with good interaction between molybdenum precursor and the support material. Aqueous impregnation of zeolite with ammonium heptamolybdate followed by calcination has been widely used [18, 19]. Direct ion exchange of molybdenum from solution on zeolite is difficult, due to the absence of simple salts of molybdenum.

The Mo/Hβ catalyst with different metal content (1, 3, 5, 10 wt %) were prepared by dry impregnation method as discussed in the preparation method of catalysis in chapter 1. The catalysts were prepared by impregnating Hβ (Si/Al=14, BET surface area-580 m^2/g) with aqueous solution of ammonium heptamolybdate, $(NH_4)_6Mo_6O_{24}.4H_2O$ (Loba-chemie., AR grade) at a pH of ~2.9, followed by slow drying at 80 ^{0}C and 100 ^{0}C under constant stirring. Followed by impregnation and drying, the samples were calcined in air at 500 ^{0}C for 4 h.

Table 4.1. Characteristics of Hβ supported molybdenum catalysts

Sample name	Molybdenum Concentration (Wt %) *	Crystallinity (%) **	Surface area m^2/g	H_2 Consu. #	NH_3 Desorb. ϕ	Pore volume (cc/g) Ψ
				μmole/g		
Hβ	0	100	580	0.00	1070	0.253
1Mo/Hβ	1.01 (0.92)	87.80	572	320	980	0.234
3Mo/Hβ	2.98 (2.49)	71.55	521	NA	1010	0.214
5Mo/Hβ	4.81 (4.28)	69.07	507	1450	1160	0.208
10Mo/Hβ	10.10 (7.22)	55.53	463	2940	1150	0.184

** Determined by ICP-AES.*
( ) for Spent catalysts.
*** Calculated by considering crystallinity of Hβ as 100 %.*
 # Calculated from H_2-TPR.
ϕ Calculated from NH_3-TPD.
Ψ By BJH method.

4.3. CHARACTERIZATION RESULTS OF Mo/Hβ CATALYSTS

The characteristics of beta and modified beta catalysts, namely specific surface area and pore size were studied by nitrogen physisorption and the data is given in table 4.1. Pore size and pore volume were also obtained from the N_2 sorption data. There was continuous fall in surface area with increase in Mo loading. The reduction in surface area was also accompanied by reduction in pore size and pore volume. These results show that the molybdenum is not only present on the out side of the pores, but also penetrated into the pores of the beta. The reduction in pore volume with increased molybdenum content was reported by others [20-22]. The decrease in surface area indicates that there is strong interaction between the molybdenum species and the Hβ support, as a result there was some loss of framework of Hβ [23]. The chemical analysis was carried out for fresh as well as spent catalysts. Some loss in molybdenum was noticed in spent catalysts, probably due to sublimation of molybdenum, given in table 4.1.

4.3.1. Powder X-ray diffraction

Figure 4.1 shows the XRD patterns of Hβ without Mo and with different Mo contents (1, 3, 5, 10 wt %). The X-ray diffraction pattern of the as-prepared Hβ sample shows same features as described in references [23-26]. After impregnation of molybdenum followed by calcinations, shows only the characteristic peaks of Hβ zeolite and no peaks pertaining to MoO_3 phase were observed even for molybdenum loading upto 10 wt %.

When catalysts contain more than 15 wt % Mo, intense peaks at 2θ = 12.9, 23.4, 25.8 and 27.4 corresponding to α-MoO_3 were observed, while β-MoO_3 phase was reportedly unstable above 500 ^{0}C [27, 28]. No α-MoO_3 or β-MoO_3 phases were observed in our samples. The crystallinity of the Hβ zeolite decreased continuously with the increase in Mo loading, as revealed by the X-ray pattern. This shows that MoO_3 was highly dispersed on the surface of Hβ. The same results were observed when we impregnated different transition metals like Cu, W, Fe and V on Hβ; no phases of these metals were detected in the PXRD. The metal content for these samples was 3 wt % prepared by dry impregnation method and calcined at 500 ^{0}C for 5 hours.

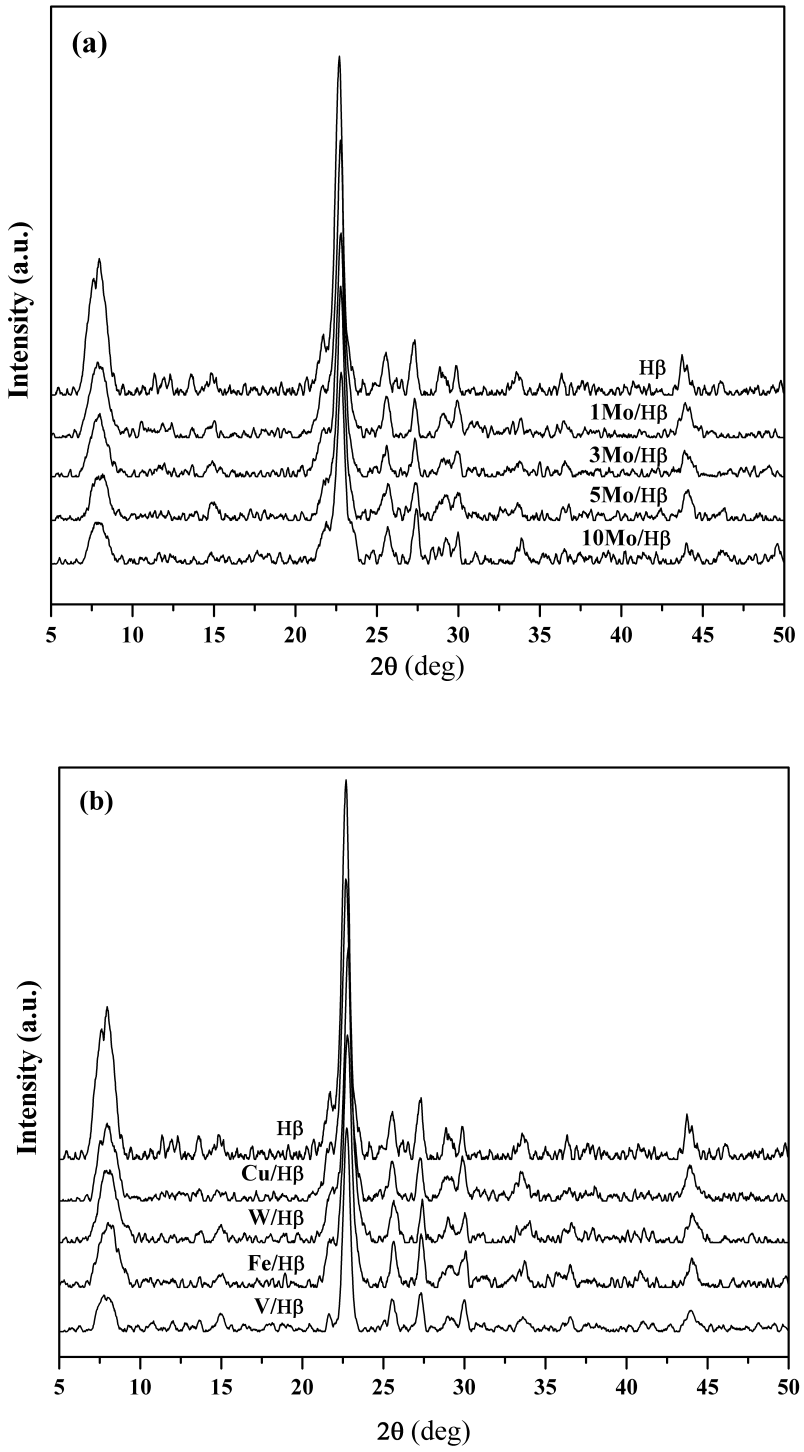

Fig. 4.1: *Powder X-ray diffraction pattern of (a) Hβ with different molybdenum content, (b) different metals impregnated on to Hβ.*

4.3.2. Infrared spectroscopy

Infrared spectroscopy studies were carried out to investigate the nature of metal oxide species present in the supported molybdenum oxides. Mainly two types of stretching modes are possible for this system, viz; stretching of O–Mo–O and Mo=O. Figure 4.2 gives the IR spectra of Hβ support as well as different molybdenum containing Hβ samples. The bands at 956 and 910 cm^{-1} are usually assigned to terminal Mo=O stretching and Mo–O–Si stretching in silicomolybdic acid (SMA) [29,30]. In the present study, we have observed bands at 954 and 912 cm^{-1} for Mo=O and Mo–O–Si in case of MoO_3, the stretching mode for Mo–O–Mo can be assigned at around 862 cm^{-1} [31, 32] and also it has been reported that the spectra for pure MoO_3 shows absorption bands at 996, 869, 824 and 546 cm^{-1} [33]. However, two additional bands at 810 and 572 cm^{-1} were also observed on our Mo/Hβ samples. These results show that not only SMA but also MoO_3 phase might be present in our samples.

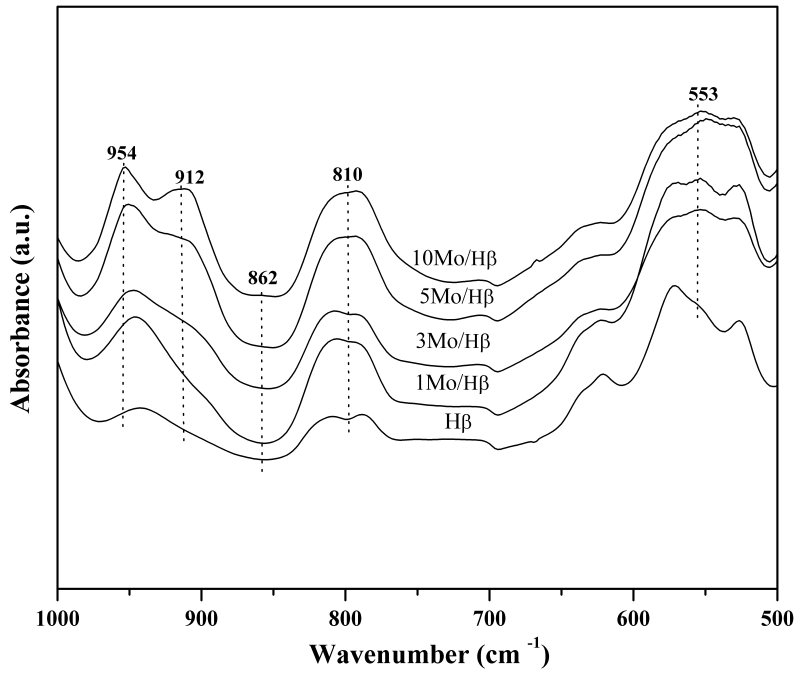

Fig. 4.2: *Diffuse reflectance IR (DR-IR) of Hβ and different Mo containing Hβ samples.*

Infrared studies were carried out on $3Mo/Al_2O_3$ prepared by dry impregnation method for comparison purpose with Mo/Hβ. No M=O species were recorded on these

samples, which are responsible for the formation of methanol or formaldehyde by partial oxidation of methane.

4.3.3. Laser Raman spectroscopy

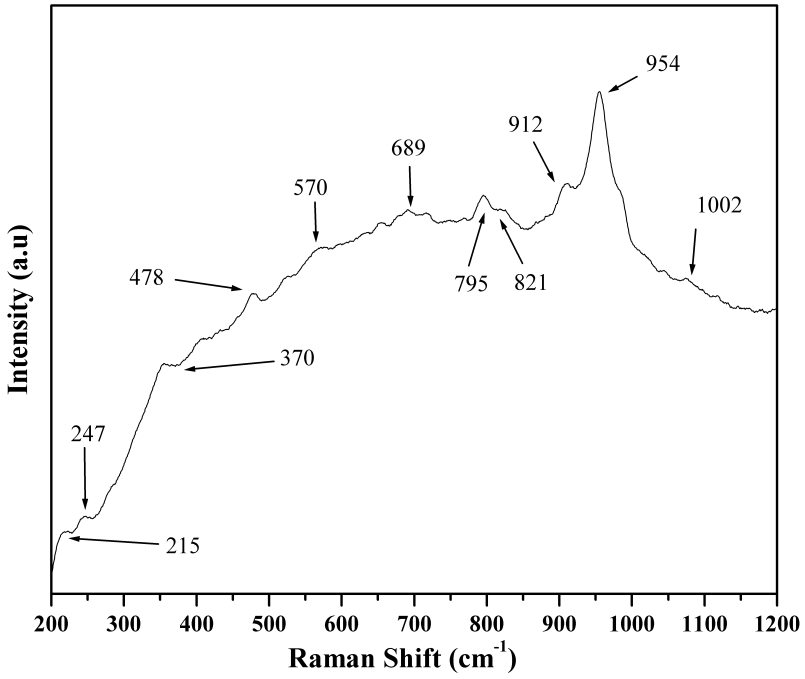

Fig. 4.3: *Laser Raman spectra of 3% molybdenum containing Hβ sample.*

Laser Raman spectroscopy is one of the most effective tools to identify α phase and β phase of MoO_3 and the presence of SMA on the catalyst surface. It is known that MoO_3 has two forms, α phase and β phase, and the assignment of IR bands of these phases is difficult. As discussed in section 4.3.1, β phase is not stable above 500 ^{0}C. Since, we calcined the samples at 500 ^{0}C, the material is expected to have only α phase. The presence of SMA on this kind of catalysts has been reported to be effective for partial oxidation of methane to formaldehyde and also for the oxidation of methanol to formaldehyde [34-36]. The formation of SMA was reportedly observed when the Mo loading is below 5 wt %, above 10 wt % it decreases to zero [37]. Figure 4.3 shows Raman spectra of molybdenum containing Hβ catalyst (3Mo/Hβ). Four characteristic bands were observed in the range at 160-290, 340-467, 504-680 and 900-1000 cm^{-1}. These are

assigned to Mo–O–Mo deformation mode, Mo=O bending mode, symmetric Mo–O–Mo stretching mode, and symmetric Mo=O terminal stretching mode, respectively [38]. Less intensity bands at 1002 and 370 cm^{-1} are due to the formation of $Al_2(MoO_4)_3$ [39, 40], a species resulting from the interaction of molybdenum with the support.

4.3.4. Diffuse reflectance UV-visible spectroscopy

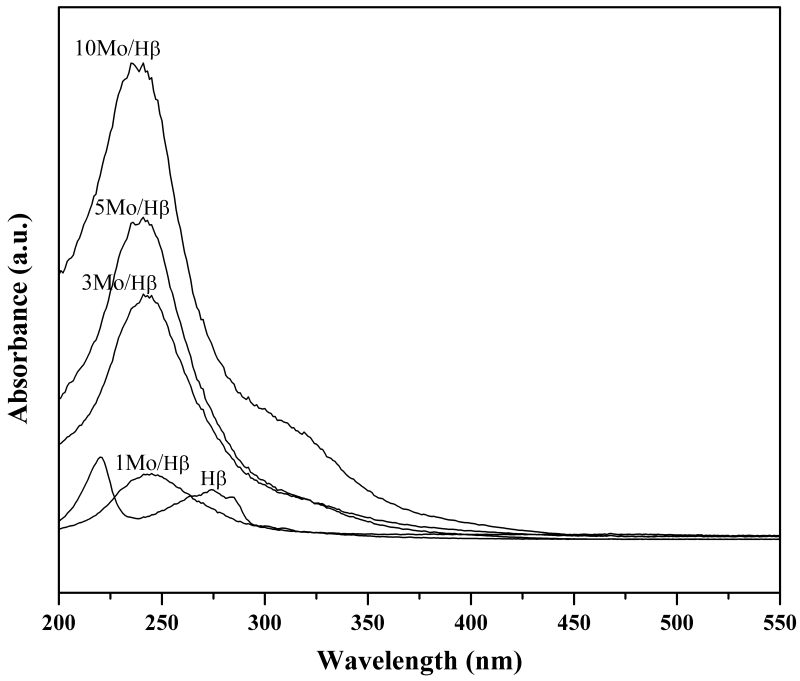

Fig. 4.4: *Diffuse reflectance UV-visible spectra molybdenum containing Hβ catalyst.*

Figure 4.4 depicts diffuse reflectance spectra of Hβ and various Mo/Hβ catalysts in UV-visible region. For all the samples, their spectra consist of two overlapping bands at about 237-250 and 305 nm. According to Cacers [41], the expected range of absorption for tetrahedrally coordinated Mo (VI) is 200-300 nm, while that of octahedrally coordinated Mo (VI) is 260-400 nm. The band at 320 nm is assigned to Mo-O-Mo bridges in octahedral coordination [42-44]. It can be seen from Fig. 4.4 that the intensities of both the bands increased with the increase in molybdenum loading. However, the concentration of tetrahedral species was more dominant as compared to that of octahedral species with increase in molybdenum concentration. At 5 wt % molybdenum content, the spectra hardly

show the presence of second peak, suggesting that the Mo-O-Mo octahedral species is present only at high molybdenum loadings.

4.3.5. Scanning electron microscopy

Figure 4.5 shows SEM pictures of Hβ and 3Mo/Hβ of samples calcined at 500 ^{0}C. The morphology of the sample shows some changes post Mo loading. Though not much change was observed, difference in particle size was observed on Mo loading. Increase in the particle size of 3Mo/Hβ was observed as a result of aggregation of the Mo particles. Similar results were reported on Mo/Al_2O_3 catalysts [45].

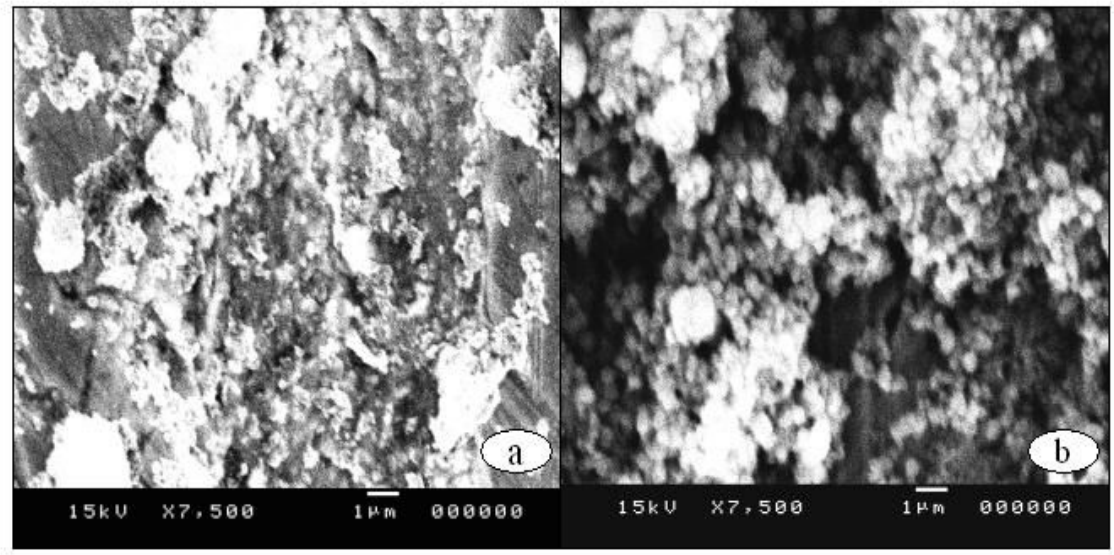

Fig. 4.5: *SEM pictures of (a) Hβ and (b) 3Mo/Hβ samples.*

4.3.6. Transmission electron microscopy

TEM images of Hβ support and different Mo containing samples are shown in the Fig. 4.6. Clean surface with particle size in the range 50-80 nm were seen in the case of Hβ (e and f), whereas the clusters of Mo nanoparticles can been seen for Mo containing samples. The cluster size increased at higher metal loading. The size of the clusters is initially around 50 nm and increased to more than 100 nm for samples with 5 and 10 wt % Mo content.

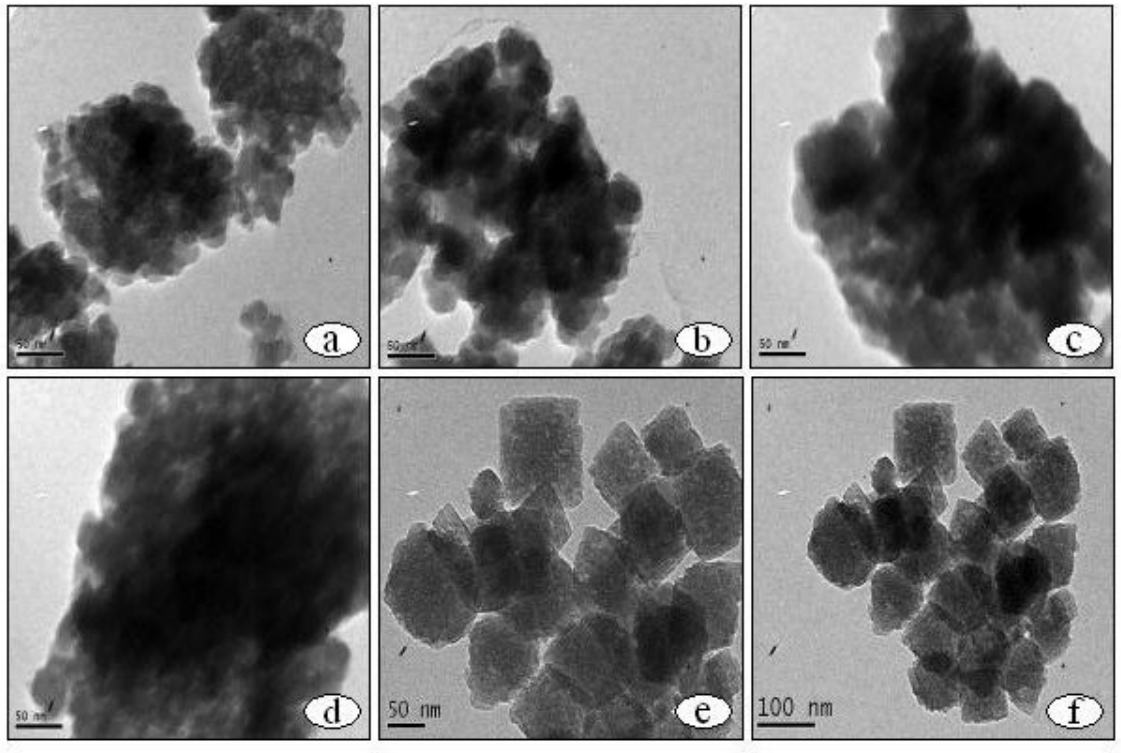

Fig. 4.6: *TEM images of Hβ with (a) 1wt% Mo, (b) 3wt% Mo, (c) 5wt% Mo, (d) 10wt% Mo, (e & f) Hβ.*

This shows that at higher metal loading particle size increases leading to lower dispersion, which is responsible for the formation of clusters. This eventually can affect the catalytic activity.

4.3.7. Temperature programmed reduction

The interaction between Mo and the Hβ support was investigated by temperature programmed reduction in the presence of H_2 (H_2-TPR). The H_2-TPR profiles of Mo/Hβ samples with different Mo contents are shown in Fig. 4.7. As one would expect, no H_2 reduction peak was observed for Hβ sample. Three peaks, centered at about 325, 555 and 805 ^{0}C were observed on the 10Mo/Hβ catalyst. According to literature reports [46-50], these peaks correspond to the reduction of polymolybdate or multilayered Mo oxide to MoO_2, $Al_2(MoO_4)_3$ or microcrystalline MoO_3 to MoO_2 and MoO_2 to Mo.

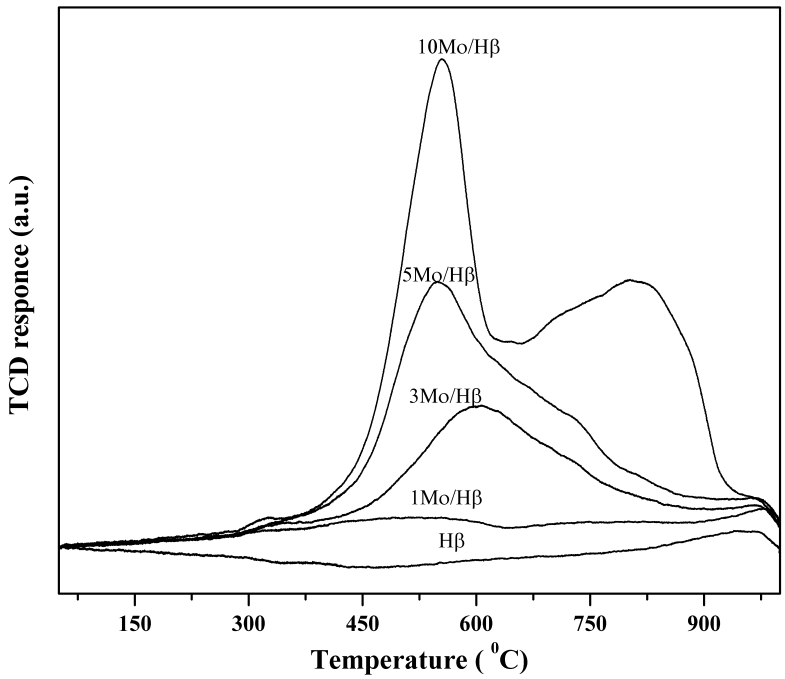

Fig. 4.7: *Temperature programmed reduction profiles of Hβ and different Mo containing Hβ samples.*

The low temperature peak shifts further down with increase in metal content. Two peaks with maxima at 325 and 555 ^{0} C were observed in the TPR profile, which in accordance with the literature data [51-53] are interpreted for the reduction of the octahedrally coordinated Mo^{VI} ions and to the consecutive reduction of the tetrahedrally coordinated Mo^{VI}, the later being harder to reduce.

The reduction of Mo^{VI} should take place in two stages: $Mo^{VI} \rightarrow Mo^{IV}$ and $Mo^{IV} \rightarrow Mo^{0}$. At low loading of around 8 wt % of Mo on SiO_2, the Mo oxide species were highly dispersed as shown by XRD. If these highly dispersed Mo^{VI} are reduced to Mo^{0}, superfine metal particles are expected to be formed. But such particles are extremely unstable [49], so it is believed that Mo^{VI} is reduced to Mo^{IV} [50], which corresponds to only one reduction peak at around 710 ^{0}C. But in our case we have observed three peaks, showing that Mo is getting reduced to the Mo ^{0} in multiple states. The amount of H_2 consumption increases with the increase in molybdenum loading on the Hβ support as given in table 4.1.

4.3.8. Acidity

Acidity of the zeolites is very important as they determine their catalytic activity. Information of the acid centers, their location and relative strength is crucial to understand the catalytic performance. In the present study, acidity of the Hβ zeolite with different Mo loadings was determined by NH_3-TPD and IR of pyridine chemisorption.

4.3.8.1. Temperature programmed desorption of ammonia (NH_3-TPD)

For acidity determination, TPD of base is a good technique, where ammonia is used as a probe molecule. Being small in size ammonia can penetrate into the pores of zeolite and interact with Bronsted and Lewis acid sites. Hence, TPD of ammonia is a good technique for rapid characterization of acidity of zeolite as well as oxides. Figure 4.8 shows the NH_3-TPD of the parent Hβ and the Mo/Hβ catalysts. For the Hβ, two peaks were observed in the NH_3-TPD profile at 187 and 305 ^{0}C. The low temperature peak was assigned to desorption of NH_3 on weak acid sites [54], whereas, the high temperature peak was assigned to desorption of the chemisorbed NH_3 from strong Bronsted acid sites [55-57]. The low temperature (about 183 ^{0}C) peak area increased and high temperature peak area (about 410 ^{0}C) reduced when the Mo loading increased. (Expanded part in Fig. 4.8).

As described earlier in the section 4.3.1, there was a loss in strong acidity. For the 10Mo/Hβ, the peak at high temperature almost disappeared. This disappearance of high temperature peak indicates that the molybdenum oxides migrated into the channels of the Hβ zeolite and preferentially interacted with the bridging hydroxyl groups, which are generally considered as strong acid sites [58-61].

The Mo species inside the channel of Hβ interacted with the strong Bronsted acid sites, hence, the concentration of strong acid sites decreased with increase in MoO_3 loading. At the same time, the low temperature peak at 183 ^{0}C shifted to 188 ^{0}C and high temperature peak at 345 to 403 ^{0}C. According to the reports in literature [59-61], the acid sites of medium strength can be generated with increased Mo loading. Our results show that with the increase in the acid sites of medium strength, the peak at low temperature shifted slightly to higher temperature.

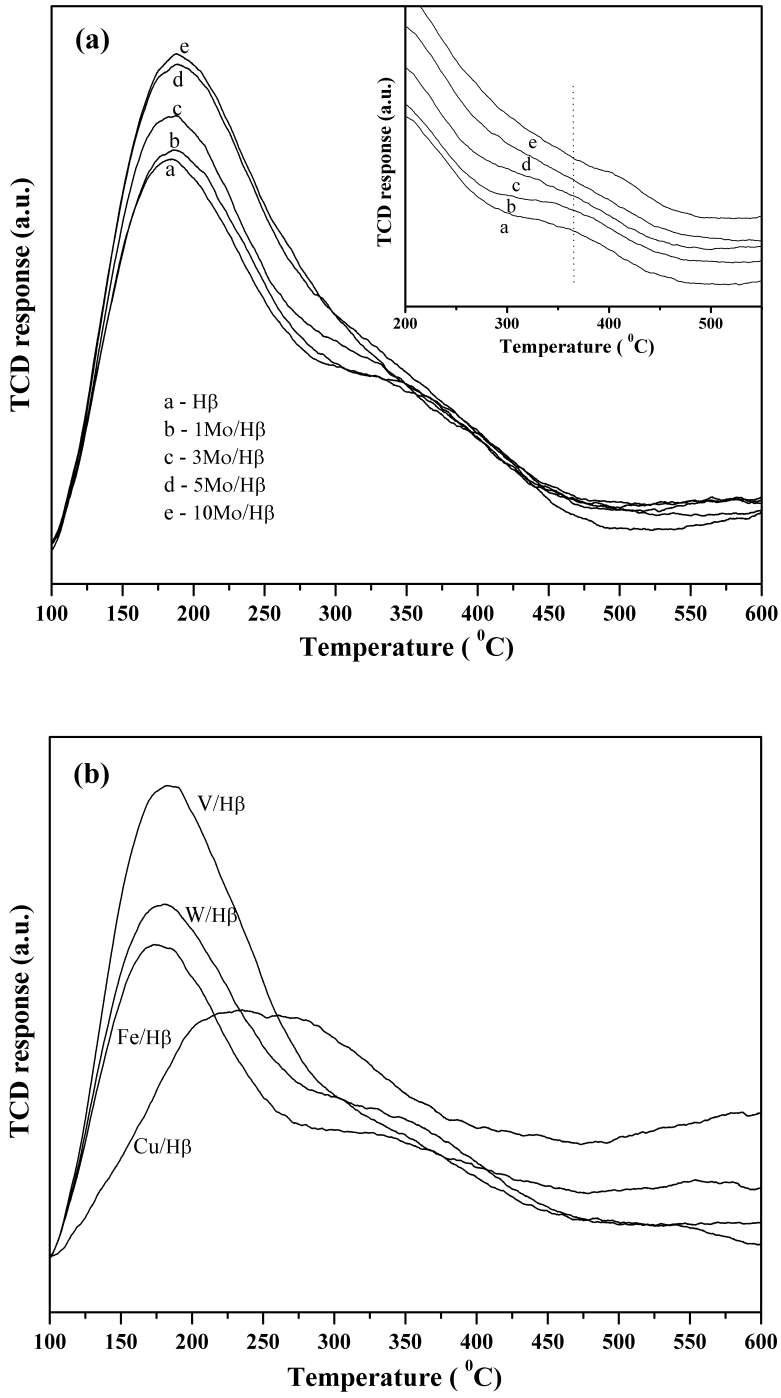

Fig. 4.8: *NH_3-TPD plots of (a) Hβ and Mo/Hβ with different molybdenum contents, (b) Hβ impregnated with different metals.*

The total number of acid sites of the catalysts measured by NH_3-TPD increased as the Mo species loading increased. Figure 4.8 b shows NH_3-TPD studies of different metal

containing Hβ. The total acidity of these samples increased in the order Cu < Fe < W and < V. The total acidity was compared for the samples with 3 wt% metal content.

4.3.8.2. IR studies of Chemisorption of pyridine on Mo/Hβ and Mo/Al_2O_3 (P-IR)

In this study, chemisorbed pyridine was studied by using IR. About 70 mg (~25 mm diameter) of sample (self supported wafer) was prepared and placed in an aluminum holder, which is in contact with K-type thermocouple. Samples were heated for 8-10 h at 280-300 ^{0}C under vacuum (~1×10^{-3} Torr) prior to pyridine adsorption experiments. For acidity measurements, samples were exposed at 100 ^{0}C to multiple doses of pyridine until it reached to the saturation coverage. A gas mixture containing nitrogen saturated with pyridine was used for this purpose. The gas pressure in the IR cell was monitored with the help of a digital capacitance manometer. IR spectra were plotted after an equilibration time of 15-20 minutes. Final spectra were recorded to distinguish between the weak and strong acidity after evacuation at 100 ^{0}C for 30 minutes. A total of 300 scans were co-added for obtaining spectra with good S/N ratio at a resolution of 4 cm^{-1}.

Though the NH_3-TPD is a good technique for determination of acidity of solid acids, it cannot distingwish between Lewis and Bronsted acid sites. Infrared spectroscopy is a powerful technique for studying acidity of zeolites, as adsorbed pyridine clearly distinguishes between Bronsted and Lewis acidity. Figure 4.9 and 4.10 show the infrared spectra of the pyridine ring vibration region after pyridine is desorbed at various temperatures for Mo/Hβ and Mo/Al_2O_3 respectively. It is known that the pyridinium ions associated with Bronsted acid sites show three additional vibration frequencies. Of these, N^+-H stretching vibration is not seen due to broadness of the bands. The other two vibrations appear at 1545 and 1490 cm^{-1}. Coordinately bound pyridine exhibits infrared bands at 1450 and 1490 cm^{-1}. As a result, three bands are observed due to chemisorbed pyridine at 1450-1455 cm^{-1}, 1490 and 1545-1547 cm^{-1} with the simultaneous disappearance of hydroxyl bands [62] on pyridine chemisorption. The band near 1450 cm^{-1} is due to pyridine chemisorbed at Lewis site and the one at 1545 cm^{-1} is due to pyridine at Bronsted site, while 1490 cm^{-1} band represent both Lewis and Bronsted acidity. However,

the 1490 cm^{-1} band is not useful for quantitative determination of individual Bronsted and Lewis acidity as it is common for both Bronsted and Lewis species [63].

All molybdenum based beta catalysts with different molybdenum content shows increase in the B/L ratio with increasing evacuation temperature. This shows that the intensity of the infrared band at 1450 cm^{-1}, associated with coordinately held pyridine decreases rapidly as the temperature is raised, implying that Lewis acidity is not that strong when compared to Bronsted acidity on these modified zeolites. The variation in relative B/L ratio with increasing evacuation temperature is given in table 4.2 for Hβ and Mo/Hβ samples. The B/L ratio for Hβ increase with evacuation temperature as Lewis pyridine is desorbed. Though a similar trend was observed for molybdenum beta samples, the rate of increase in B/L ratio was much higher for samples with 1 and 3Mo compared to either Hβ or for that matter with the 5 or 10 wt % Mo samples. These results show that the Bronsted acid sites are stronger on 1 and 3 wt % Mo containing samples.

Figure 4.10 gives IR of desorbed pyridine on alumina at different temperatures. This experiment was carried out to compare the results on H-beta sample. Alumina gave only one peak for Lewis acidy. Decrease in intensity of this Lewis acidity peak was noticed with increase in the evacuation temperature on Al_2O_3 as well as $3Mo/Al_2O_3$ beta samples.

Table 4.2. Bronsted to Lewis acidity (B/L) ratios of various Mo/Hβ catalysts

Temp (^{0}C)	B/L ratio				
	Hβ	**1Mo/Hβ**	**3Mo/Hβ**	**5Mo/Hβ**	**10Mo/Hβ**
100	1.63	0.47	0.79	0.42	0.68
150	1.78	0.72	0.84	0.50	0.75
200	1.99	1.07	1.43	0.65	0.85
250	2.03	1.12	1.38	0.84	0.99

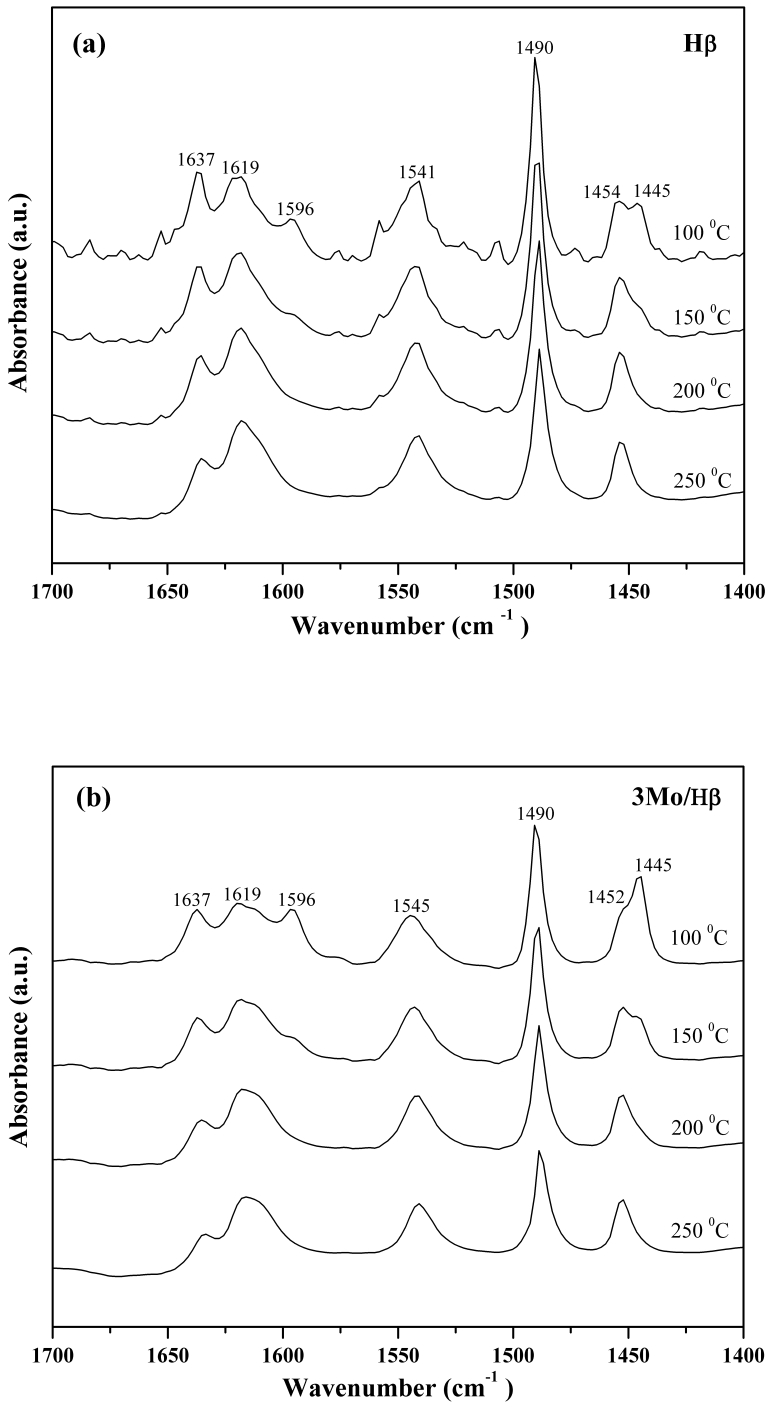

Fig. 4.9: *FT-IR spectra of pyridine chemisorbed on (a) Hβ and (b) 3Mo/Hβ after desorption at different temperatures.*

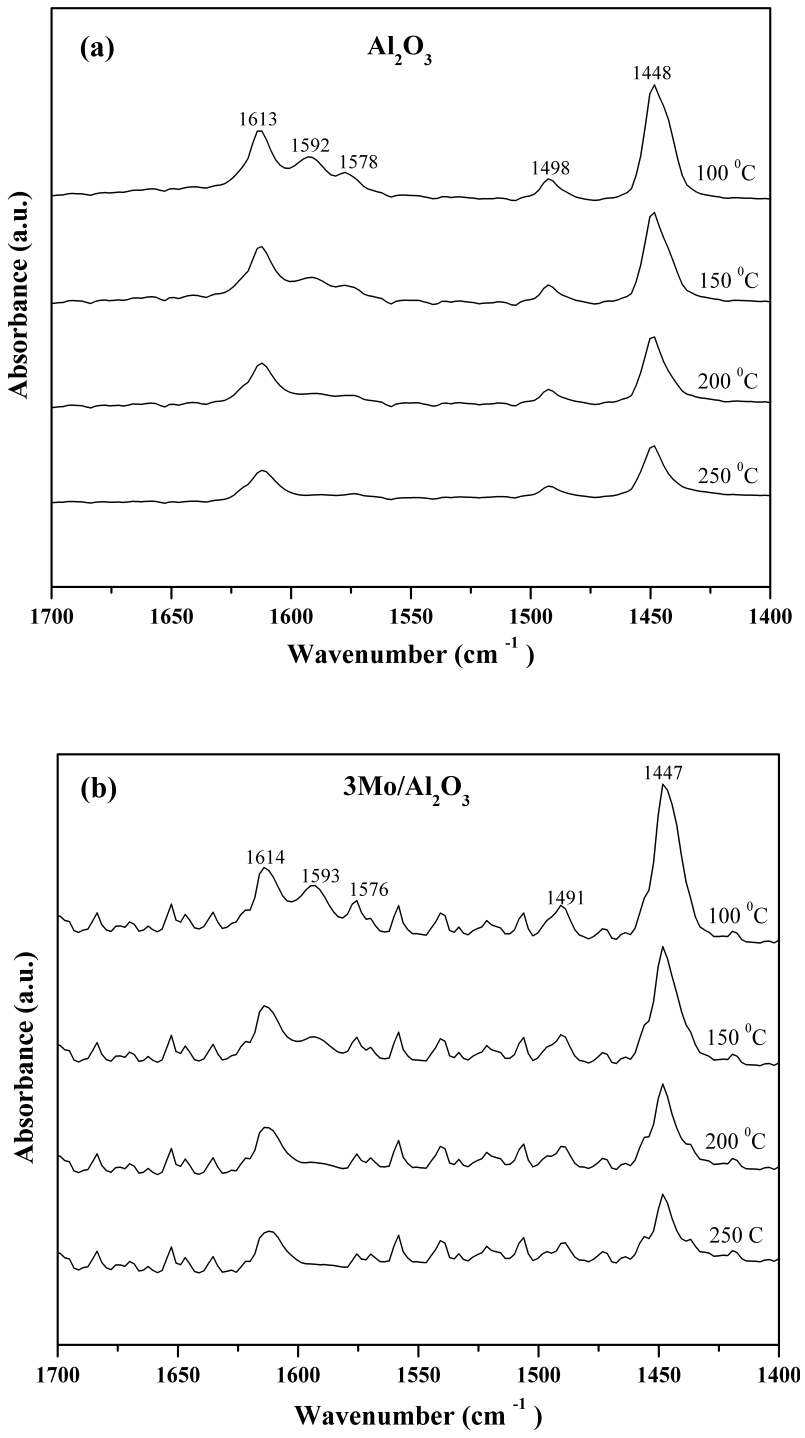

Fig. 4.10: *FT-IR spectra of pyridine chemisorbed on (a) Al_2O_3 and (b) $3Mo/Al_2O_3$ after desorption at different temperatures.*

4.3.9. X-ray photoelectron spectroscopy

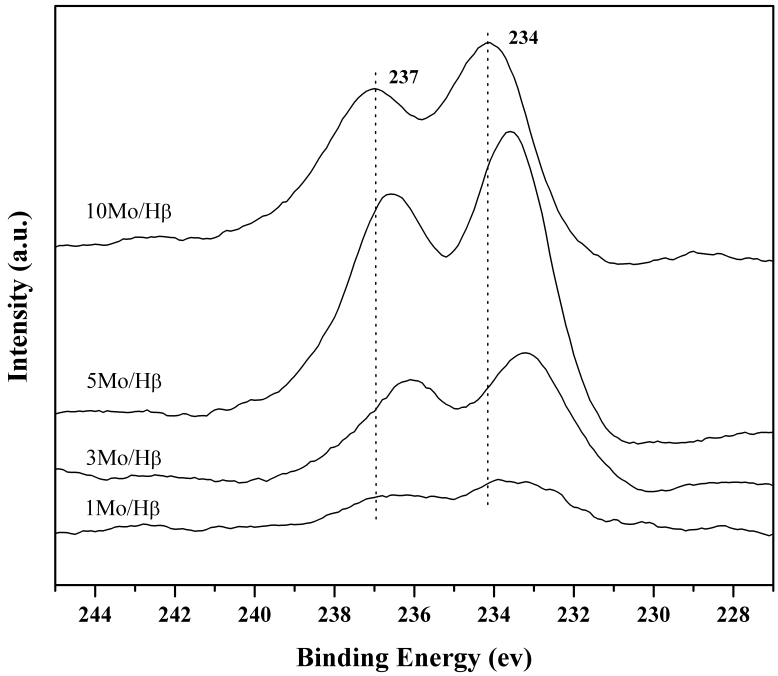

***Fig. 4.11**: Mo3d XPS spectra of different Mo containing Hβ samples.*

The Mo3d XPS spectra of different Mo containing Hβ samples are shown in Fig. 4.11. It shows the presence of Mo3d in more than one oxidation state with peaks in the region of 233-234 and 236-237 eV. It is reported that, the peak at 236 eV corresponds to Mo^{6+}, which is characteristic of oxidized Mo resulting from passivation step [64] and the peak at 233 eV is probably attributed to Mo^{5+} and Mo^{4+} species [65].

No peaks that correspond to Mo atoms or metallic molybdenum at 228 eV were detected [66]. On increasing the molybdenum content on Hβ, the position shifted to higher binding energy, indicating that there might be strong effect on chemical environment of Mo or may be due to the change in the interaction of different Mo species.

4.4. PREPARATION OF Mo/Fe-Zn-O MIXED OXIDE CATALYSTS

We have also prepared Mo/Fe-Zn-O catalysts for this reaction. It involved two-steps. In the first step, Fe-Zn-O with different iron contents (2.5, 5, 10 wt %) was prepared, by co-precipitation method, following the same procedure, used for Cu-Co-Ce-O mixed

oxide in chapter 2. Solutions of $Zn(NO_3)_2.6H_2O$, $Fe(NO_3)_2$, (s.d. fine-chem, AR grade) and KOH (Loba Chemie) were used to prepare these catalysts. Final pH of the resulting solution was adjusted to around 9.5 by adding metal solution slowly to KOH solution. Aging of the precipitate was carried out for 3 hours and then washed thoroughly with demineralized water till pH is around 7.5. The precipitate was filtered and dried at 100 ^{0}C in an oven for about 12 hours. The dried materials were powdered and calcined at 500 ^{0}C. In second step the Fe-Zn-O supported catalysts with different molybdenum content (1, 3, 5, 10 wt %) were prepared by dry impregnation method. The samples after loading were dried at 100 ^{0}C for 12 h followed by calcination in air at 500 ^{0}C for 4 h.

4.5. CHARACTERIZATION RESULTS OF Mo/Fe-Zn-O MIXED OXIDE CATALYSTS

Table 4.3 gives structural information of Fe-Zn-O support and supported molybdenum catalysts, such as BET surface area, crystallite size, hydrogen consumption in H_2-TPR and ammonia desorbed during NH_3-TPD of calcined samples. The molybdenum content was estimated through ICP-AES and found to be close to that of targeted. Loss in molybdenum content was noticed in spent catalysts as compared to the fresh catalysts.

Table 4.3: Characteristics of Fe-Zn-O support and Mo/Fe-Zn-O catalysts

Catalyst name	Metal Content (Wt %) by ICP-AES *			Crystallite size (nm) of Fe-Zn-O **	Surface area m^2/g	H_2 Consu. #	NH_3 Desorb. ϕ
	Fe	Zn	Mo			μmole/g	
2.5Fe-ZnO	2.5	97.5	0	22.06	28	----	2.21
5Fe-ZnO	4.9	95.1	0	22.05	29	----	3.01
10Fe-ZnO	10.1	89.1	0	20.65	37	----	8.20
1Mo/Fe-ZnO	NA	NA	1.14 (1.09)	20.66	25	850	4.31
3Mo/Fe-ZnO	NA	NA	2.98 (2.68)	20.66	21	1010	4.89
5Mo/Fe-ZnO	NA	NA	5.06 (4.44)	19.48	19	1290	6.28
10Mo/Fe-ZnO	NA	NA	10.09 (9.2)	19.47	16	1570	6.45

** Determined by ICP-AES, ( ) for Spent catalysts.*
*** Calculated by using Debye-Scherrer equation.*
 # H_2 consumption from H_2-TPR.
ϕ NH_3 Desorbed from NH_3-TPD.

It was observed that specific surface area decreases with molybdenum as well as iron content. Increase in total acidity with the molybdenum was observed on these samples as given in table 4.3.

4.5.1. Powder X- ray diffraction

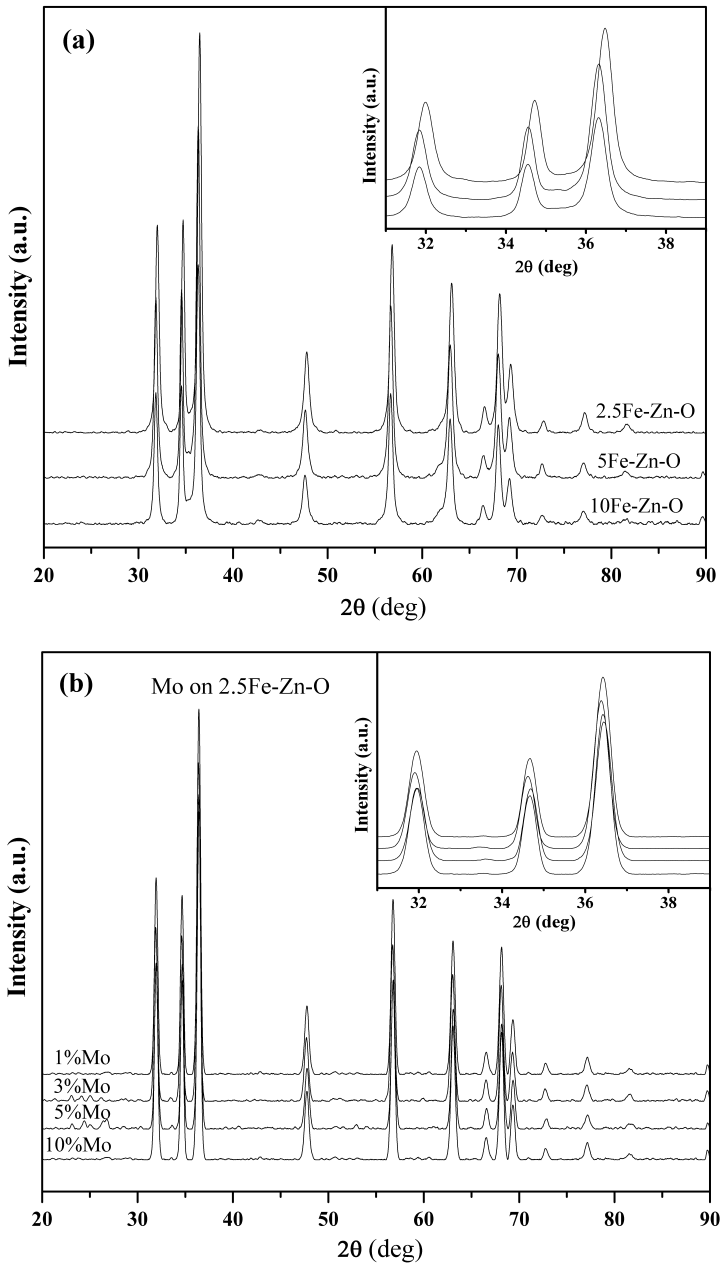

Fig. 4.12: *Powder X-ray diffraction pattern of (a) Fe-Zn-O with different Fe contents, (b) different Mo containing catalyst on 2.5% Fe-Zn-O.*

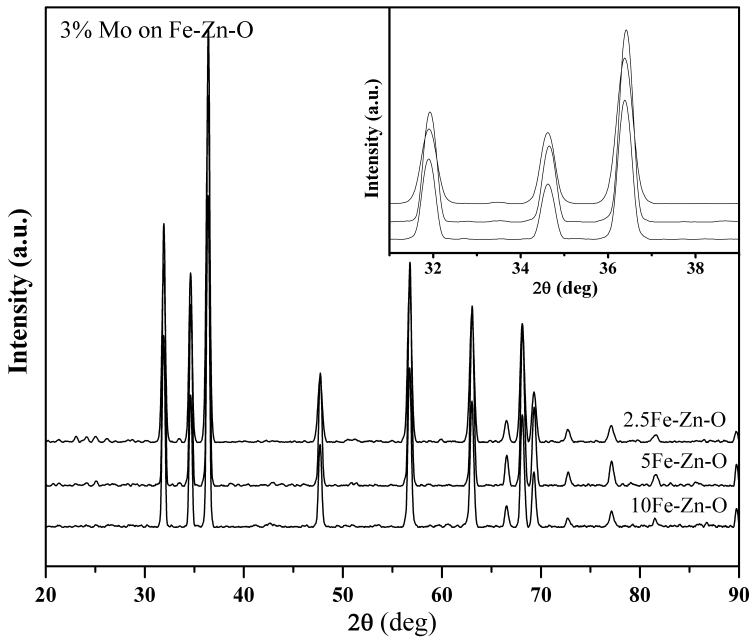

Fig. 4.13: *Powder X-ray diffraction pattern of 3% Mo impregnated catalysts supported on different Fe containing Fe-Zn-O oxides.*

Powder XRD pattern of different iron containing Fe-Zn-O are plotted in Fig. 4.12 (a), all diffraction peaks could be identified as belonging to Zn-O phase with hexagonal wrutzite crystal lattice [67-70]. Peaks related to iron oxide were not observed in these samples, suggesting that iron was either well dispersed on Zn-O, hence their low content was bellow detection or at least part of Fe is substituted into Zn-O lattice. The XRD pattern of different Fe-Zn-O samples has been blown up in the region 31-39 as shown in Fig. 4.12 (a). A clear shift of peaks towards lower 2θ is clearly seen indicating as increase in 'd' values. Figure 4.12 (b) shows the XRD pattern of different Mo loaded samples on 2.5Fe-Zn-O. The X-ray diffraction pattern of the as-synthesized Mo/Fe-Zn-O sample shows almost the same features as described and shown below in Fig. 4.12 b. After addition of MoO_3, the corresponding pattern show only the characteristic peaks of Fe-Zn-O and no MoO_3 crystallite peaks were observed on any of the samples. On the other hand, the crystallinity of the samples decreased slightly with the increase in Mo loading, leading to a drop in the intensities of peaks belonging to Fe-Zn-O. This indicates that MoO_3 was well

dispersed on the surface of support [42]. Shift in the XRD peak of zinc was observed with Fe and Mo, which indicates the formation of solid solution.

Similar results were obtained with 3 wt% Mo on different Fe containing Zn-O samples as shown in Fig. 4.13. No peaks corresponding to molybdenum phase or iron were observed. The crystalline size obtained by Debye-Scherrer equation is given in table 4.3. Crystallite size decreased with increase in iron as well as molybdenum content, which may be due to the extra phases of Mo and Fe formed.

4.5.2. Infrared spectroscopy

Figure 4.14 shows IR spectra of Fe-Zn-O as well as different Mo containing Fe-Zn-O catalysts. As it was discussed earlier for IR studies of Mo/Hβ (Section 4.4.2), absorption bands of the two types of stretching O–Mo–O and Mo=O at 910 and 956 cm^{-1} can be studied for this system.

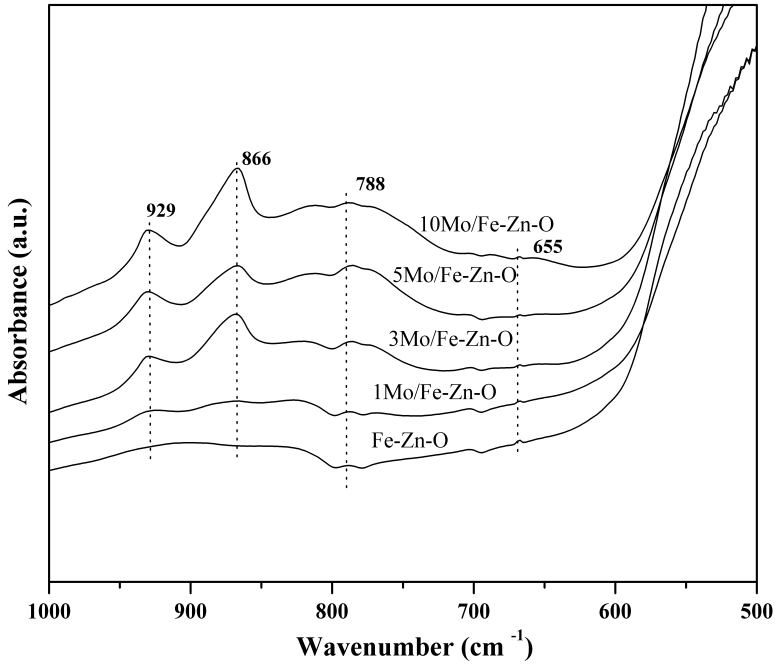

Fig. 4.14: *Diffuse reflectance infrared spectrum (DR-IR) of Mo/Fe-Zn-O samples.*

We have observed two absorption bands at 929 and 866 cm^{-1}, which may be due to the Mo=O and O–Mo–O stretchings of MoO_3 respectively [31]. From these results it can

be concluded that molybdenum is present in these samples as MoO_3 phase. The band at 788 and 655 cm^{-1} are assigned to the stretching of metal to oxygen bond in Zn-O [32].

4.5.3. Laser Raman spectroscopy

Figure 4.15 presents the Laser Raman spectra of molybdenum containing samples supported on 2.5Fe-Zn-O, which were calcined at 500 ^{0}C. Raman spectra could determine the Mo species on the surface of the catalyst within a depth of 2 nm. As discussed for Mo/Hβ system, LRS is used to identify the phase of MoO_3 and SMA. Three bands at 329, 940 and 967 cm^{-1} were observed in samples containing 1-5 wt % Mo. But at higher Mo loading (10%), more peaks can be seen. Strong bands at 941, 896, 360 and 219 cm^{-1} are characteristic of octahedral molybdenum species [67, 71], while peaks at 932, 352 and 220 cm^{-1} are usually assigned to tetrahedral molybdenum species [39]. Raman spectra of the different molybdenum containing samples (except for 10Mo/Fe-Zn-O) were similar, which suggests that the same species existed on the surface of these samples. But with increasing Mo loading, stronger bands of Raman were observed more clearly.

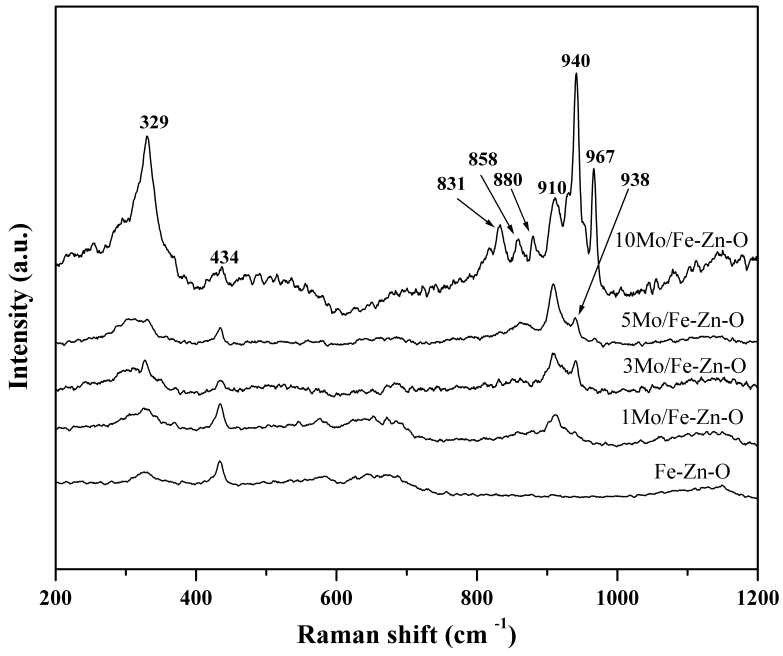

Fig. 4.15: *Laser Raman spectra of various molybdenum containing 2.5Fe-Zn-O.*

The bands at 329, 940 and 967 cm^{-1} seen in this region of molybdenum containing Fe-Zn-O samples are assigned to the octahedral species of molybdenum, whereas the bands at 910 and 938 cm^{-1} are assigned to tetrahedral species of molybdenum. From these results it is clear that both Td and Oh species are present in these samples, which is supported by the results of UV-vis, IR and H_2-TPR. Octahedral molybdenum species concentration found to increase with higher loading of molybdenum. Band at 434 cm^{-1} was observed in only Fe-Zn-O sample; the intensity of these bands goes down with increase in molybdenum content. This band at 434 cm^{-1} attributed to Zn-O [40].

4.5.4. Diffuse reflectance UV-visible spectroscopy

The UV-vis spectra of the Mo-containing Fe-Zn-O composite powders and Fe-Zn-O were recorded in diffuse reflectance mode. $BaSO_4$ was used as a reference for all the measurements. Figure 4.16 shows the dependence of the absorption spectra on Mo content in Fe-Zn-O supported samples.

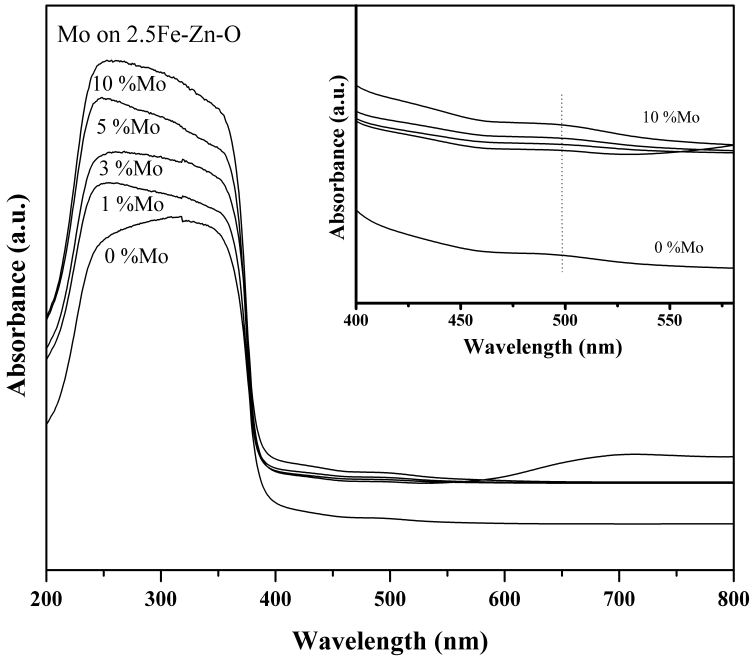

Fig. 4.16: *Diffuse reflectance UV-visible spectra of different Mo supported on 2.5Fe-Zn-O.*

As discussed for Mo/Hβ catalysts (Section 4.3.4), according to Cacers [34], the range of absorption band of tetrahedrally co-ordinated Mo(VI) is 200-300 nm, while that of octahedrally coordinated Mo(VI) is 260–400 nm, whereas the UV absorption edge at about 385 nm was ascribed to the fundamental absorption of Zn-O [72]. From Fig. 4.16, it may be seen that mainly two maxima are observed at 250 and 353 nm. The 250 nm peak corresponds to tetrahedrally coordinated Mo (VI) whereas 350 nm peak may belongs to Zn-O or octahedrally coordinated Mo (VI). Less intense small absorption edge was observed in visible range 500 nm, which may be due to iron present on the support.

4.5.5. Transmission electron microscopy studies

Transmission electron microscopy helps to confirm the average particle size calculated using XRD results. The TEM images of different Mo containing Fe-Zn-O are given in Fig. 4.17. Hexagonally shaped crystallites of zinc oxide are visible in these samples (indicated by arrow), which expose the polar Zn-O surface [73].

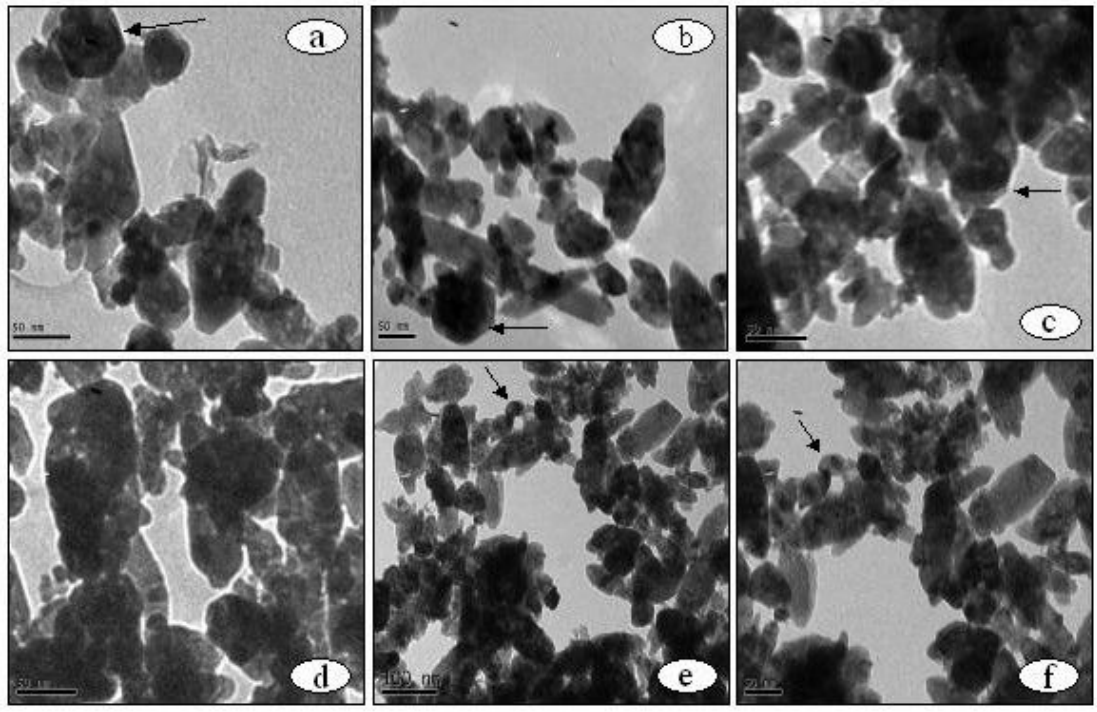

Fig. 4.17: *TEM images of different molybdenum supported 2.5Fe-Zn-O samples (a) 1%Mo, (b) 3% Mo, (c) 5% Mo, (d) 10% Mo, (e & f) 2.5Fe-Zn-O.*

Hexagonally shaped crystallites are not easily found in these materials, particularly in the mixed oxide. From these results, we were not able to find the Mo particles and since we could not carry out electron diffraction studies, it was not possible to carry out the elemental mapping of the agglomerates.

4.5.6. Temperature programmed reduction

The H_2-TPR profiles of Mo/Fe-Zn-O samples with different Mo contents are shown in Fig. 4.18 included that of only Fe-ZnO, which is used as support. The TPR was carried out from 50 to 1000 ^{0}C, but plotted only in the region of 100 from 800 ^{0}C. Zinc oxide does not consume any hydrogen during the TPR experiment as it does not undergo any reduction in the given temperature of 800 ^{0}C [74]. But introduction of iron promotes reduction of the zinc species to some extent. A broad reduction peak of Fe-O and Zn-O was observed at 605 ^{0}C [75].

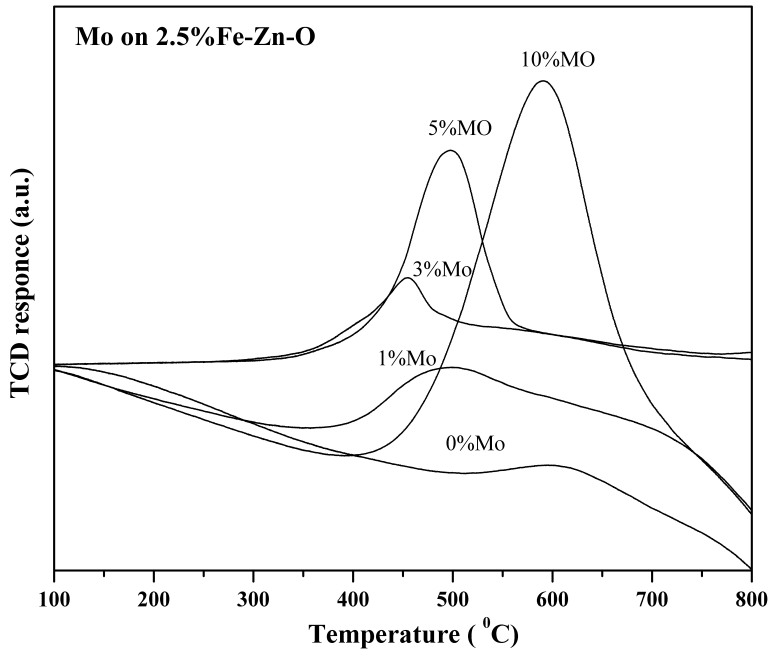

Fig. 4.18: *Temperature programmed reduction profile of Fe-Zn-O and different Mo content Fe-Zn-O.*

We have observed only one reduction peak in case of TPR of molybdenum loaded samples. Whereas one would expect three peaks as was the case with Mo/Hβ system. No

XRD peaks for Mo-O or Fe-O were observed suggesting that Mo and Fe are highly dispersed on zinc oxide, which was also observed by the TEM. If these highly dispersed Mo reduced to zero valance state, superfine metal particles would form which are extremely unstable. So above results show that Mo^{VI} is reduced to Mo^{IV} [50], which gives a maxima between 490 to 590 ^{0}C. It is to be noted that the T_{max} of the reduction peak of the Mo depends upon concentration of the Mo, which shift towards higher temperature with increase in Mo content indicating that higher temperature is required for the reduction of Mo species. Hydrogen consumption increases with increase in molybdenum content. No reduction peak for 2.5Fe-Zn-O was noticed for the amount of sample used for this experiment under our reaction conditions.

4.5.7. Acidity

Temperature-programmed desorption of ammonia is widely used in the study of zeolites as well as other solid acids. However, an important drawback of this technique is that ammonia cannot distinguish between to Brønsted and Lewis acid sites [76]. Adsorption on non-Brønsted acid sites (referred to as Lewis acid sites) may also be stronger. In this respect, Juskelis et al. [77] demonstrated that ammonia adsorbs more strongly on CaO than it does on USY zeolite. However, they provide a valuable fingerprint of the overall nature and distribution of the acid sites (weak or strong) in the calcined and steamed zeolites, and a quantification of the density of total acid sites [78,79]. This technique is particularly useful when it is complemented by FTIR spectroscopy of adsorbed pyridine; as the latter is able to discriminate between different types of acid sites. Due to transmission of samples, we could not record the pyridine IR spectra for the Mo containing Fe-Zn-O samples; hence the total acidity was calculated by using NH_3-TPD studies.

4.5.7.1. Temperature programmed desorption of ammonia

Figure 4.19 shows NH_3-TPD profiles of the iron containing zinc oxide sample (a) and different molybdenum containing samples supported on 2.5Fe-Zn-O (b). The high temperature desorption peak corresponds to strong acidity while low temperature peak

corresponds to weak acidity. The acidity (both strong and weak) of the sample increased with increase in iron content as shown in Fig. 4.19.

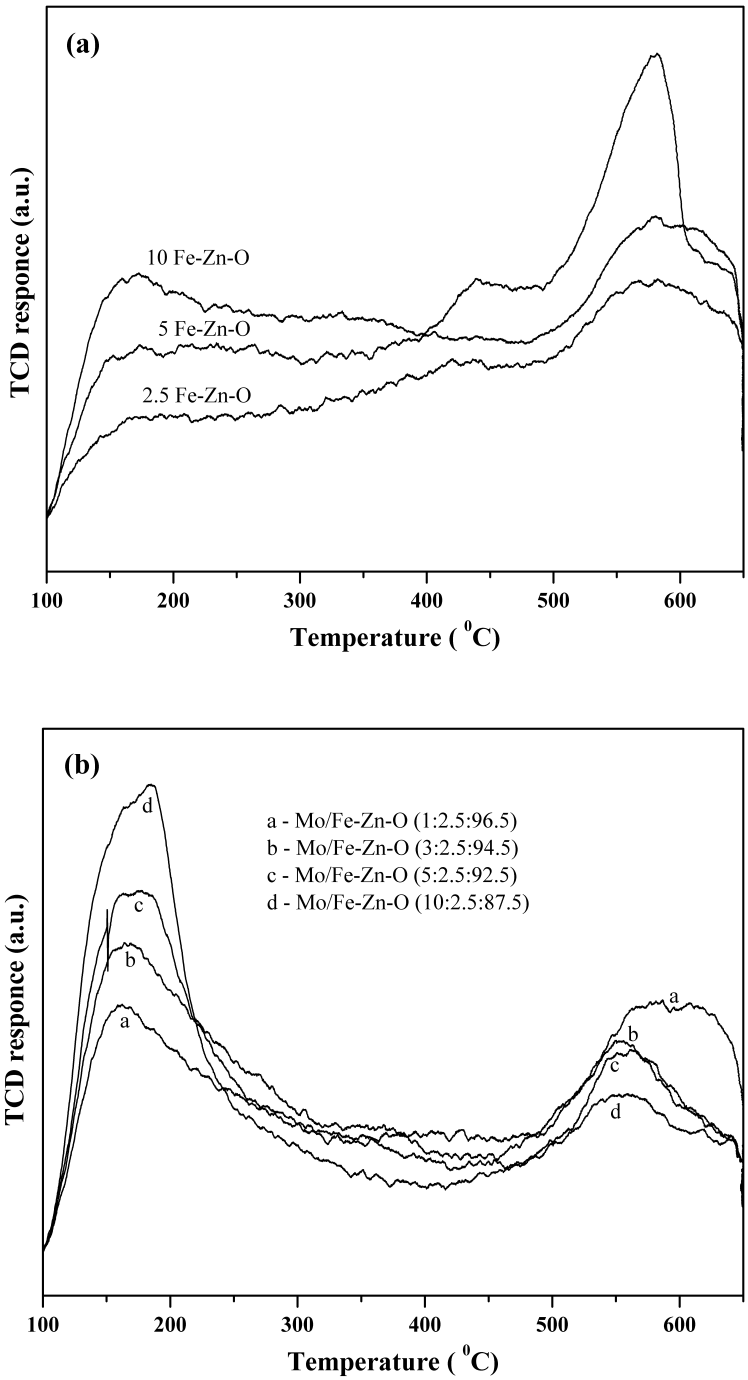

Fig. 4.19: *NH_3 -TPD profiles of (a) different Fe containing Zn-O, (b) Different Mo samples supported on 2.5% Fe-Zn-O.*

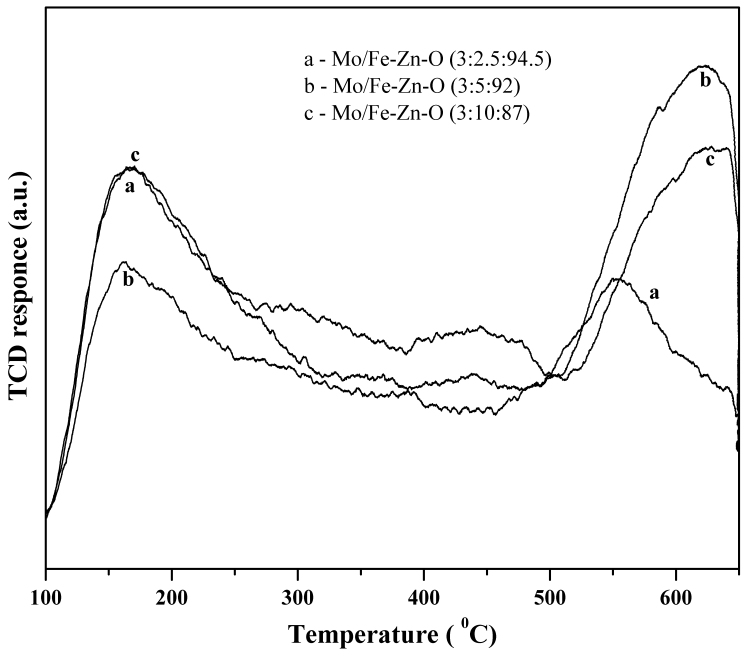

Fig. 4.20: *NH_3 -TPD profile of 3% Mo supported on different Fe containing supports.*

The maximum acidity was observed for 10Fe-Zn-O sample with 10 wt Fe. The low temperature peak was observed at around 168 ^{0}C whereas high temperature peak shifted from 575 to 582 ^{0}C for Fe-Zn-O samples. The ammonia consumption for all these samples is given in table 4.3. NH_3-TPD profile of various molybdenum samples supported on 2.5Fe-Zn-O is shown in Fig. 4.19 (b). These samples show two peaks for the two types of acidity, weak and strong present in the samples. As molybdenum content increased, the intensity of week acidity peak increased showing that week acidity is enhanced, while the strong acidity decreased simultaneously [62]. Temperature shift was noticed for low temperature peak from 161 to 184 ^{0}C, while not much difference was observed in case of high temperature peak. However, sample with 1 wt % Mo requires higher temperature to desorb ammonia. So from above observations it can be said that a higher number of weak acid sites are generated with increased Mo content, while strong acidity reduced relatively. Figure 4.20 gives NH_3-TPD for 3 wt % Mo on iron zinc containing support. 2.5Fe-Zn-O and 10Fe-Zn-O shows more weak acid sides, whereas 5Fe-Zn-O shows relatively strong acidity. The maximum acidity was observed on the 5Fe-ZnO calculated from the desorbed ammonia on these catalysts as given in the table 4.3.

4.6. SUMMARY

Catalysts with different molybdenum contents supported on H-beta and Fe-ZnO mixed oxides were prepared by wet impregnation and characterized using various physico-chemical techniques such as powder X-ray diffraction, ICP-AES, BET surface area measurements, SEM, TEM, TPR/TPD, XPS, chemisorption of pyridine by IR and LRS. These characterizations revealed that the molecular structure of molybdenum species depends on the molybdenum loading on the support i.e. Hβ and Fe-Zn-O. Monomeric molybdenum species are predominant at low molybdenum contents, while polymeric molybdenum species concentration increased with molybdenum loading. FTIR and laser Raman studies show the formation of silicomolybdic acid on Mo/Hβ catalyst. The presence of Mo=O and Mo-O–Mo species were confirmed by FTIR, LRS, H_2-TPR and UV-visible. The acidity measurement of these catalysts was done using NH_3-TPD. The acidity (both strong and weak) of the samples increased with increase in iron content. The maximum acidity was observed for 10Fe-ZnO sample with 10 % iron. For the Mo/Fe-Zn-O samples as molybdenum content increased the week acidity has increased, while the strong acidity decreased at the same time. No MoO_3 crystallites were observed even for a Mo loading as high as 10 wt% on Mo/Hβ samples by PXRD. All diffraction peaks identified in Mo/Fe-Zn-O by PXRD were Zn-O phase with hexagonal wrutzite crystal structure with average crystallite size of 22 nm prepared by dry impregnation and co-precipitation methods. No peaks for Fe and Mo were observed. Only one reduction peak in case of TPR of molybdenum-loaded Mo/Fe-Zn-O samples was observed whereas in case of Mo/Hβ, three peaks were observed. Hexagonally shaped crystallites of zinc oxide were visible in the all Mo containing Fe-Zn-O samples, which expose the polar Zn-O surfaces. Specific surface area and crystallite size of Fe-Zn-O and Mo/Fe-Zn-O samples decreased with molybdenum as well as iron content. The molybdenum content was estimated through ICP-AES and found to be close to the targeted value. Loss in molybdenum content was noticed in spent catalysts as compared to the fresh catalysts due to sublimation of molybdenum, which is likely to be happening at above 600 ^{0}C. Studies like NH_3-TPD), H_2-TPR, UV-visible and others techniques used for characterization of these materials is discussed in detail in this chapter.

4.7. REFERENCES

[1] M. J. Brown and N. D. Parkyns, Catal. Today, 8 (1991) 305.

[2] R. Burch, G. D. Squire and S. C. Tsang, J. Chem. Soc., Faraday Trans. I, 85 (1989) 3561.

[3] N. R. Hunter, H. D. Gesser, L. A. Morton, P. S. Yarlagadda and D. P. C. Fung, Appl. Catal., 57 (1990) 45.

[4] R. G. Herman, Q. Sun, C. Shi, K. Klier, C. B. Wang, H. Hu, I. E. Wachs and M. M. Bhasin, Catal. Today, 37 (1997) 1.

[5] S. H. Taylor, J. S. J. Hargreaves, G. J. Hutchings, R. W. Joyner and C. W. Lembacher, Catal. Today, 42 (1998) 217.

[6] H. Berndt, A. Martin, A. Bruckner, E. Schreier, D. Mulller, H. Kosslick, G. U. Wolf and B. Lucke, J. Catal., 191 (2000) 384.

[7] M. R. Smith and U. S. Ozkan, J. Catal., 141 (1993) 124.

[8] M. A. Banares, J. L. G. Fierro and J. B. Moffat, J. Catal., 142 (1993) 406.

[9] K. Aoki, M. Ohmae, T. Nanba, K. Takeishi, N. Azuma, A. Ueno, H. Ohfune, H. Hayashi and Y. Udagawa, Catal. Today, 45 (1998) 29.

[10] A. de Lucas, J. L. Valverde, L. Rodriguezl, P. Sanchez and M. T. Garcia, Appl. Catal., A 203 (2000) 81.

[11] H. F. Liu, R. S. Liu, K. Y. Liew, R. F. Johnson and J. H. Lunsford, J. Am. Chem. Soc., 106 (1984) 4117.

[12] S. Irusta, E. A. Lombardo and E. E. Miro, Catal. Lett., 29 (1994) 339.

[13] T. Takemoto, K. Tabata, Y. Teng, L. Dai and E. Suzuki, Catal. Today, 71 (2001) 47.

[14] N. D. Spencer, J. Catal., 109 (1988) 187.

[15] S. Kasztelan and J. B. Moffat, J. Chem. Soc., Chem. Commun., (1987) 1663.

[16] K. Vikulov, G. Martra, S. Coluccia, D. Miceli, F. Arena, A. Parmaliana and E. Paukshtis, Catal. Lett., 37 (1996) 235.

[17] O. V. Krylov, Catal. Today, 18 (1993) 209.

[18] M. W. Anderson, J. Klinowski, Zeolites, 6 (1986) 455.

[19] J. H. de Boer, B. G. Linsen, T. J. Osinga, J. Catal., 4 (1964) 643.

[20] B. Michalkiewicz, Appl. Catal., A 277 (2004) 147.

[21] Y. Xu, S. Liu, L. Wang, M. Xie, X. Gue, Catal. Lett., 30 (1995) 135.

[22] L. Chen, L. Lin, Z. Xu, X. Li, T. Zang, J. Catal., 157 (1995) 190.

[23] X. Li, W. Zhang, S. Liu, X. Han, L. Xu, X. Bao, J. Mol. Catal., A 250 (2006) 94.

[24] P. Caullet, J. Hazm, J. L. Guth, J. F. Joly, J. Lynch, F. Raatz, Zeolites, 12 (1992) 240.

[25] A. P. Stevens, P. A. Cox, J. Chem. Soc. Chem. Commun., (1995) 343.

[26] K. S. N. Reddy, B. S. Rao, V. P. Shiralkar, Appl. Catal., A 95 (1993) 53.

[27] T. M. Huong, K. Fukushima, H. Ohkita, T. Mizushima, N. Kakuta, Catal. Comm., 7 (2006) 127.

[28] A. Kido, H. Iwamoto, N. Azuma, A. Ueno, Catal. Surv. Jpn., 6 (2002) 45.

[29] M. S. Kasprzak, G. E. Leroi, S.R. Crouch, Appl. Spec., 36 (1982) 285.

[30] C. Li, Q. Xin, K. L. Wang and X. X. Guo, App. Spec., 45-5 (1991) 874.

[31] T. M. Huong, K. Fukushima, H. Ohkita, T. Mizushima, N. Kakuta, Catal. Comm., 7 (2006) 127.

[32] R. Moleski, E. Leontidis, F. Krumeich, J. of Colloid and Interface Sci., 302 (2006) 246.

[33] L. Chen, L. Lin, Z. Xu, X. Li and T. Zhang, J. Catal., 157 (1995) 190.

[34] J. M. Tatibouet, M. Che, M. Amirouche, M. Fournier, C. R. Deltcheff, J. Chem. Soc., Chem. Commun., (1988) 1260.

[35] T. Sugino, A. Kido, N. Azuma, A. Ueno, Y. Udagawa, J. Catal., 190 (2000) 118.

[36] A. Kido, H. Iwamoto, N. Azuma, A. Ueno, Catal. Surv. Jpn., 6 (2002) 45.

[37] Y. Barbaux, A. R. Elamrani, E. Payen, L. Gengembre, J. P. Bonnelle, B. Gbzybowska, Appl. Catal., 44 (1988) 117.

[38] G. Mestl, T. K. K. Srinivasan, Catal. Rev. Sci. Eng., 40 (1998) 451.

[39] J. Zhang, Y. Wang, L. Chang, Appl. Catal., A 126 (1995) 205.

[40] M. L. Tu, Y. K. Su, C. Y. Ma, J. Appl. Phy., 100(2006) 53705.

[41] C. V. Cacers, Preparation of catalysis III. P 333 Elsevier, Amstradam, 1993.

[42] A. Duan, G. Wan, Z. Zhao, C. Xu, Y. Zheng, Y. Zhang, T. Dou, X. Bao, K. Chung, Catal. Today, 119 (2007) 13.

[43] T. Klimova, M. Calderon, J. Ramırez, Appl. Catal., A 240 (2003) 29.

[44] M. Cheng, F. Kumata, T. Saito, T. Komatsu, Appl. Catal., A 183 (1999) 199.

[45] R. Maiti, M. Chakraborty, J. of Alloys and Compounds, April 2007 article in press.

[46] S. Liu, S. Huang, W. Xin, J. Bai, S. Xie, L. Xu, Catal. Today, 93 - 95 (2004) 471.

[47] S. Rajagopal, H. J. Marini, J. A. Marzari, R. Miranda, J. Catal., 147 (1994) 417.

[48] R. Lopez Cordero, F. J. G. Llambias, A. L. Agudo, Appl. Catal., A 74 (1991) 125.

[49] M. R. Smith, U. S. Ozkan J. Catal., 142 (1993) 226.

[50] Q. Zhang, D He, Z. Han, X. Zang, Q. Zhu, Fuel, 81 (2002) 1599.

[51] J. Brito, J. Laine, J. Catal., 139 (1993) 540.

[52] J. Brito, J. Laine, Polyhedron, 5 (1986) 179.

[53] H.C. Yao, J. Catal., 70 (1981) 440.

[54] N.Y. Topsoe, K. Pedersen, E.G. Derouane, J. Catal., 70 (1981) 41.

[55] C. V. Hidalgo, H. Itoh, T. Hattori, M. Niwa, Y. Murakami, J. Catal., 85 (1984) 362.

[56] N. R. Meshram, S. G. Hegde, S. B. Kulkarni, Zeolites, 6 (1986) 434.

[57] L. J. Lobree, I. Ch. Hwang, J. A. Reimer, A. T. Bell, J. Catal., 186 (1999) 242.

[58] Y. Shu, D. Ma, X. Bao, Y. Xu, Catal. Lett., 66 (2000) 161.

[59] L. Balkrishnan, B. S. Rao, S. G. Hedge, A. N. Kotasthane, S. B. Kukarni, P. Ratnaswamy, J. Mol. Catal., 17 (1982) 261.

[60] Y. Xu, W. Liu, S. Wong, L. Wang, X. Guo, Catal. Lett., 40 (1996) 207.

[61] A. P. V. Soares, M. Farinha Portela, A. Kiennemann, L. Hilaire, J. M. M. Millet, Appl. Catal. A., 206 (2001) 221.

[62] N. Y. Topsqe, K. Pedersen, E. G. Derouane, J. Catal., 70 (1981) 41.

[63] E. P. Parry, J. Catal., 2 (1963) 371.

[64] K. Oshikawa, M. Nagai, S. Omi, J. Phys. Chem., B 105 (2001) 9124.

[65] M. Xiang, D. Li, W. Li, B. Zhong, Y. Sun, Catal. Comm., 8 (2007) 503.

[66] T. P. S. Clair, S.T. Oyama, D. F. Cox, S. Otani, Y. Ishizawa, R. L. Lo, K. Fukui, Y. Iwasawa, Surf. Sci., 426 (1999) 187.

[67] C. P. Cheng, G. L. Schrader, J. Catal., 60 (1979) 276.

[68] L. Wang, W. K. Hall, J. Catal., 66 (1980) 251.

[69] Z. Yin, N. Chen, Y. Fei, S. Song, C. Chai, Z. Jun, H. Qian, K. Ibrahim, Solid State Commun., 135 (2005) 430.

[70] T. C. Damen, S. P. S. Porto and B. Tell, Phys. Rev., 142 (1966) 570.

[71] D. S. Kim, K. Segawa, T. Soeya, I. E. Wachs, J. Catal., 136 (1992) 539.

[72] D. Li, H. Haneda, J. Photochem. Photobio. A 160 (2003) 203.

[73] H. Wilmer, M. Kurtz, K.V. Klementiev, O. P. Tkachenko, W. Grumery, O. Nrichsen and M. Muhler. Phy. Chem. Chem. Phy., 5 (2003) 4736.

[74] P. L. D. Cola, R. Glaser, J. Weitkamp, Appl. Catal., A 306 (2006) 85.

[75] M. Vijayaraj, C. S. Gopinath, J. Catal., 241 (2006) 83.

[76] R. J. Gorte, Catal. Lett., 62 (1999) 1.

[77] M. V. Juskelis, J. P. Slanga, T. G. Roberi, A. W. Peters, J. Catal., 138 (1992) 391.

[78] E. Alsdorf, M. Feist, H. Fichtner-Schmittler, Th. Gross, H. J. Jerschkerwitz, U. Lohse, and B. Parlitz, Adsorp. Sci. Technol., 5 (1988) 127.

[79] P. A. Parikh, N. Subramanyam, Y. S. Bhat and A. B. Halgeri, Catal. Lett., 14 (1992) 107.

Chapter - 5

PARTIAL OXIDATION OF METHANE - CATALYTIC ACTIVITY STUDIES

5.1. INTRODUCTION

Methane is the main constituent of natural gas, coal bed gas and biogas. Natural gas is an abundant resource in various parts of the world. Direct conversion of methane to methanol, formaldehyde or other oxygenates, not only yields liquid products, it is most preferred because it is energetically more efficient. In this process, the oxidation is intercepted at the stage of initial oxidation to avoid complete combustion of methane to CO_2 and H_2O.

Formaldehyde is produced during controlled oxidation of methane, and has been reported to be present in trace quantities during studies on the complete catalytic oxidation of methane. Industrially, direct conversion of methane to formaldehyde in a single stage would be a desirable goal as around half of the world's methanol production is used to convert it into formaldehyde for use in paint and polymer industries [1,2]. Standard industrial catalysts for oxidation of methanol to formaldehyde are based either on silver or Fe/Mo/oxides supported on silica and other oxides.

Numerable studies of partial oxidation of methane to formaldehyde have been carried out at atmospheric pressure over silica supported MoO_3 or V_2O_5 [2] over zeolites [3] as catalysts. The catalysts most widely studied for the oxidation of methane to methanol or formaldehyde are those based on molybdenum (MoO_3, ZnO-MoO_3, Fe_2O_3-MoO_3, UO_2-MoO_3, Cu-MoO_3, VO_2-MoO_3) at pressures up to 50 bar [4]. MoO_3 when supported on aluminosilicates proved to be selective catalyst for production of formaldehyde [5]. The yield of oxygenates increases with the CH_4/O_2 ratio and strongly dependent on loading of molybdena. The addition of water strongly inhibited the production of CO but decreased the conversion of methane [5].

Nearly all reported studies have used oxide catalysts, pure metals are considered to be specific towards complete oxidation. The activities of different oxides were investigated and correlated with electronegativity of the respective cations [6] based on which a scheme for methane oxidation was proposed as in equation 4.1. It required abstraction of hydrogen in step 1 and insertion of oxygen in step 2, which would require different catalytic sites.

$$\mathbf{CH_4 \xrightarrow{1} CH_{4-X} \xrightarrow{2} HCHO \xrightarrow{3} CO, CO_2} \qquad \text{Equation 4.1.}$$

The highest activity for methane conversion to products, including CO and CO_2 was achieved on Ga_2O_3 and Bi_2O_3. These metals lie in the middle of the electronegativity plot. On the other hand maximum HCHO yield and selectivity implies minimizing the rate of step 3 compared to step 2, which was mostly facilitated by highly electronegative oxides of W, Nb, Ga, and Bi etc.

The use of nitrous oxide as oxidant may have some merit, as it has milder oxidizing power compared to the dioxygen, may yield partially oxidized products. However, there is no evidence to support this proposition. Molybdenum oxide containing catalysts have been used almost exclusively with N_2O as an oxidant. In the work done by Spencer [7, 8], where he used a MoO_3 catalyst supported on silica, obtained rather higher yield of HCHO with oxygen than any other group obtained with N_2O. It is reported that [9] N_2O actually gives O^- species on MoO_3 leading to total oxidation, O^{2-} from oxygen on the other hand is active for partial oxidation of methane to formaldehyde.

In this study we have used molybdenum supported on beta zeolite and Fe-Zn-O for partial oxidation of methane to formaldehyde using air (oxygen) as oxidant.

5.2. CATALYTIC ACTIVITY MEASUREMENTS

5.2.1. Experimental set-up for catalyst evaluation

The catalytic tests were carried out by using fixed bed, down flow, quartz reactor with 12 mm i.d., which is shown schematically in Fig. 5.1. Such an assembly was designed to prevent the deep oxidation of methane by using quartz reactor instead of metallic reactor. The set up used was fully equipped to perform the experiment with full control of reaction parameters (temperature, flow of gases etc) by using methane and air as an oxidant. Two thermal mass flow controllers (MFC, Bronkhorst, Hi Tech) were used to obtain specific flow rate (GHSV = 36,000-82,000 h^{-1}), with one used to feed methane; while the other used to feed air (oxygen) (Air/CH_4 = 0.80-2.0) in to the reactor. The reactor was placed in an electrically heated furnace (Geomechanique) controlled with PID temperature programmer (Eurotherm 2404) for controlled and uniform heating of the catalyst bed. The exact temperature of the furnace and the catalyst bed were monitored by K-type thermocouples. The catalyst particles, of size 10-20 mesh, crushed and sieved after pelletization, were sandwiched between two quartz-wool plugs. Wet gas meter was

connected in series with GC, before venting the gaseous products. Ice cool condenser was placed in between GC and wet gas meter to condense the water and formaldehyde to avoid blocking of the vent line.

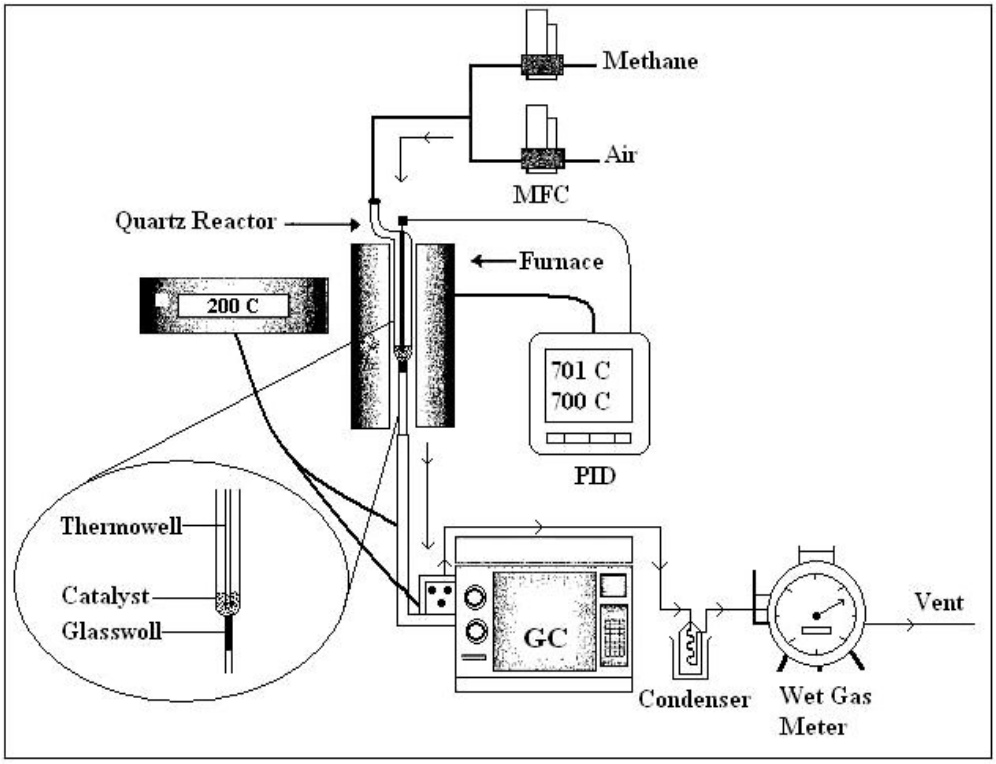

Fig. 5.1: *Reactor setup used for atmospheric partial oxidation of methane.*

5.2.2. Analytical methods

Outlet gases of the reactor were analyzed using an online Shimandzu 15A gas chromatograph (GC), equipped with flame ionization detector (FID) as well as thermal conductivity detector (TCD) to analyze all the gas and liquid products. The line used for online detection, from reactor to GC as well as sampling valve were heated at 180-200 ^{0}C to avoid condensation of water as well as liquid products. Methane, air, water were analyzed on TCD while formaldehyde, methanol and other hydrocarbons along with unconverted methane were analyzed using FID by using Porapac-Q column and helium as a carrier in a combined analysis. Spherocarb column (1/8"dia, 8 feet length) and argon as a carrier were used with Chemito 8610 GC to analyze CO on TCD. For quantifying the

gases like air, methane, CO_2 and CO calibrated gas mixture with known composition was used as reference to estimate the concentration of gases. All product gases with unconverted methane and air were quantified by injecting gas mixture containing Air- 38.39 mole %, CH_4-1.48 mole %, H_2- 45.10 mole %, CO_2 -15.12 mole % and vaporized formaldehyde solution (formaldehyde- 40 wt %, methanol -10 wt % and water- 50 wt %).

Methane conversion, selectivity (formaldehyde and methanol) and formaldehyde yield were calculated as below:

$$\text{Methane conversion (Mole \%)} = \frac{\text{Moles of } CH_{4\,in} - \text{Moles of } CH_{4\,out}}{\text{Moles of } CH_{4\,in}} \times 100$$

$$\text{Formaldehyde selectivity (Mole \%)} = \frac{\text{Moles of HCHO}}{\text{Moles of all carbon containing products}} \times 100$$

$$\text{Methanol selectivity (Moles \%)} = \frac{\text{Moles of } CH_3OH}{\text{Moles of all carbon containing products}} \times 100$$

$$\text{Formaldehyde Yield (Mole \%)} = \frac{\text{Methane conversion} \times \text{Formaldehyde selectivity}}{100}$$

PART - A: PARTIAL OXIDATION OF METHANE ON Mo/Hβ CATALYSTS

5.3. INTRODUCTION

Direct oxidation of methane to methanol and formaldehyde holds considerable potential for producing liquid fuels and petrochemicals from natural gas. The yield and selectivity for methanol or formaldehyde reported catalysts were too low for commercialization. Several groups have investigated heterogeneous partial oxidation of methane by using oxygen (3-7 mole %.) as an oxidant in the feed. In most of the reports, the methanol selectivity varies from 30 to 70 mole %, while using molybdenum or vanadium oxide as catalysts. This shows considerable activity for methanol or formaldehyde formation (oxygenates). Several supported oxide catalysts have been reported to be effective and selective for oxygenate production. Silica as a support has been widely used in metal oxide catalysts for partial oxidation of methane. That makes

zeolites as an interesting and useful support to be considered for this reaction [2,3]. Zeolites provide not only a higher surface area but also the acidity, which play very important role in the reaction. The nature and the dispersion of metal oxide phase on the support have a great influence on catalyst behavior. Here in this part of study, we have used Hβ zeolite as the support for the molybdenum oxide, which was found to be effective for the partial oxidation of methane to formaldehyde. It was found that at low metal loading, the predominant species were silicomolybdic species with terminal Mo=O which were found to have better selectivity for formaldehyde. But at higher loading polymolybdate species with Mo–O–Mo bridges begin to be generated at the expense of Mo=O sites that catalyzed the complete oxidation of methane.

Here in this study we have studied partial oxidation of methane over Mo/Hβ catalysts to show the specificity of the monomeric molybdenum oxo-species for the production of formaldehyde from methane. The use of Hβ as a support is very interesting due to three reasons; it's thermal stability, high surface area that enables high metal oxide loading, dispersion and the acidity that could lead to formation and stabilization of active metal oxide species.

5.4. RESULTS AND DISCUSSION

The partial oxidation of methane using oxygen as oxidizing agent was carried out in a fixed bed continuous flow quartz reactor (Fig. 5.1), at ambient pressure. Catalytic study was carried out with air to methane ratio of 0.80 (O_2/CH_4 ratio-0.16), at a space velocity of 32,000 h^{-1} for comparison. Other parameters like composition of catalyst, space velocity (32,000-82,000 h^{-1}), temperature (500-700 ^{0}C), variation of metal (copper, iron, tungsten, vanadium and molybdenum) were explored. Detailed study on Mo/Hβ was carried out which was found to have better catalytic activity than compared to metal catalyst studied for partial oxidation of methane.

5.4.1. Effect of temperature

Figures 5.2, 5.3, 5.4 and 5.5 represent methane conversion, formaldehyde selectivity, methanol selectivity and formaldehyde yield respectively at different reaction temperatures.

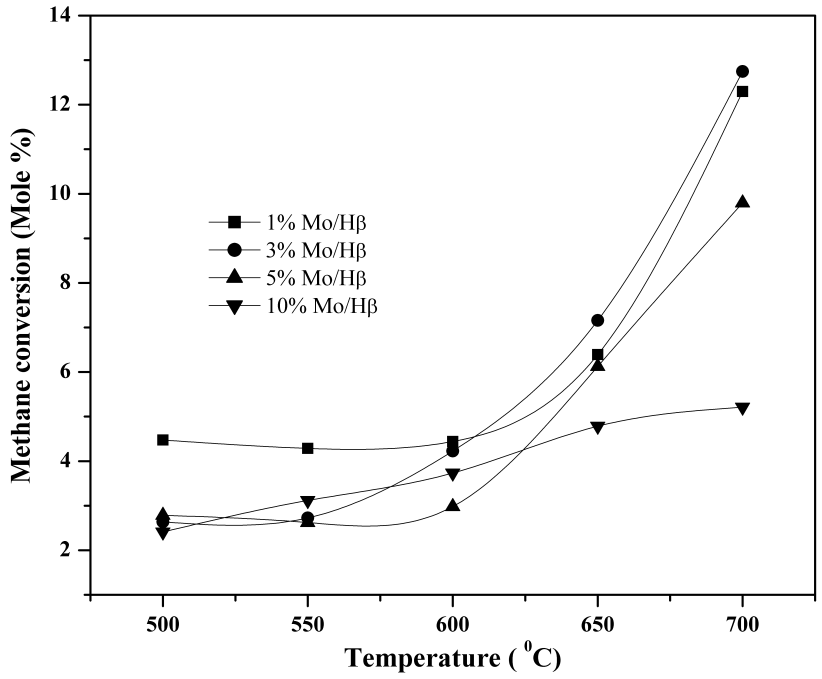

Fig. 5.2: *Influence of reaction temperature on methane conversion over different Mo/Hβ catalysts.*
Reaction conditions: Catalyst - 0.5 cc; GHSV-32,000 h^{-1}; Air/CH_4 ratio - 0.8; TOS-5 h.

The products observed were HCHO, CO_2, CO, H_2O in addition to unconverted methane and trace amount of C_2H_6 and C_2H_4. The conversion of methane was very low at 500 ^{0}C, which was increased with temperature to 12 mole % at 700 ^{0}C on 1 % and 3 wt % Mo/Hβ catalysts.

At low reaction temperature, conversion of O_2 was low, hence only trace contents of formaldehyde were observed. The amount of methane reacting with oxygen increased with temperature, implying that the temperature enhanced the methane as well as oxygen conversion. Both 1 wt % and 3 wt % Mo/Hβ samples gave similar methane conversion at higher temperature; the selectivity to HCHO was much higher on later catalyst. In fact, at both 650 and 700 ^{0}C, formaldehyde selectivity was much higher on 3Mo/Hβ catalyst as compared to all other catalysts. Hence most of the methane was converted into the product at higher temperature, which can be observed from Fig. 5.2. It is generally believed that partial oxidation of methane is initiated through the abstraction of hydrogen and addition of oxygen [10] to it for the production of formaldehyde.

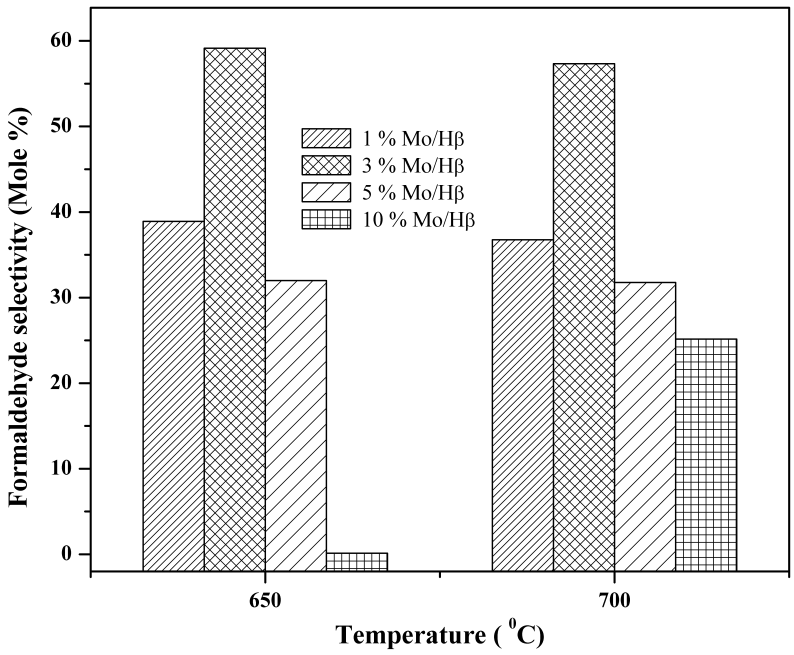

Fig. 5.3: *Effect of reaction temperature on formaldehyde selectivity over different Mo/Hβ catalysts.*
Reaction conditions: Catalyst - 0.5 cc; GHSV-32,000 h^{-1}; Air/CH_4 ratio - 0.8.

In most of the experiments, the selectivity of methanol and formaldehyde were optimized in a certain temperature range where most of the oxygen was used up for the reaction. It was observed that formaldehyde or methanol selectivity decreased with increase in temperature. Not much difference in the formaldehyde selectivity was observed at 650 and 700 ^{0}C, but methanol selectivity decreased with increase in reaction temperature as well as with molybdenum content. These results indicate that at higher temperature methanol is further oxidized to formaldehyde, leading to increased selectivity and yield. This was further supported by the results carried out with low oxygen containing feeds.

Formaldehyde yield on different molybdenum containing beta catalysts at different temperatures is plotted in Fig. 5.5. Yield of formaldehyde increased with increase in temperature, 3 wt % metal containing sample gave better yield than higher metal loaded Hβ catalysts. This could be attributed to the formation of polymolybdic species at higher molybdenum loadings, which led to a decrease in formaldehyde selectivity as well as methane conversion. As a result the formaldehyde yield was much higher on 3 wt % Mo/Hβ at 700 ^{0}C.

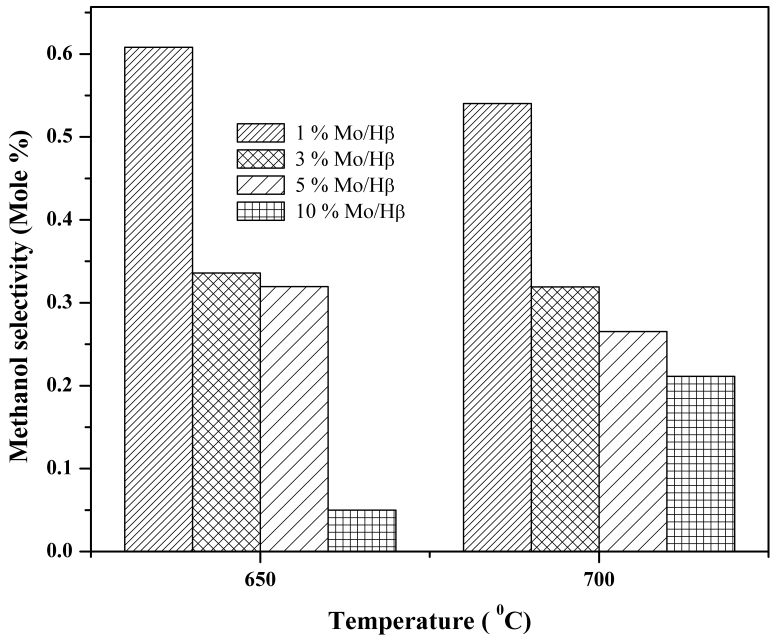

Fig. 5.4: *Effect of reaction temperature on methanol selectivity over Mo/Hβ catalysts. Reaction conditions: Catalyst - 0.5 cc; GHSV-32,000 h^{-1}; Air/CH_4 ratio - 0.8.*

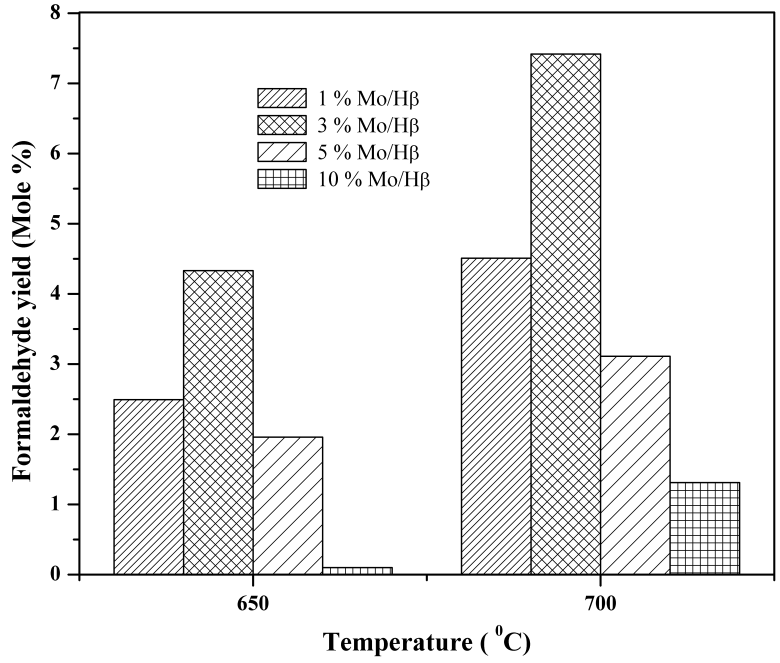

Fig. 5.5: *Effect of reaction temperature on formaldehyde yield over Mo/Hβ catalysts. Reaction conditions: Catalyst - 0.5 cc; GHSV-32,000 h^{-1}; Air/CH_4 ratio - 0.8.*

Figure 5.6 shows the effect of molybdenum content on Hβ on the methane conversion, formaldehyde selectivity and yield at 700 ^{0}C. Many studies have attempted to elucidate the Mo structures [11-14] involved in the reaction and their connectivity to molybdenum dispersion. At low Mo loadings, the formation of molybdates is thought to be induced by the presence of Na or Ca impurities on the silica surface [15]. As Mo increases, polymeric molybdenum oxide species becomes dominant, until the onset of bulk MoO_3 formation.

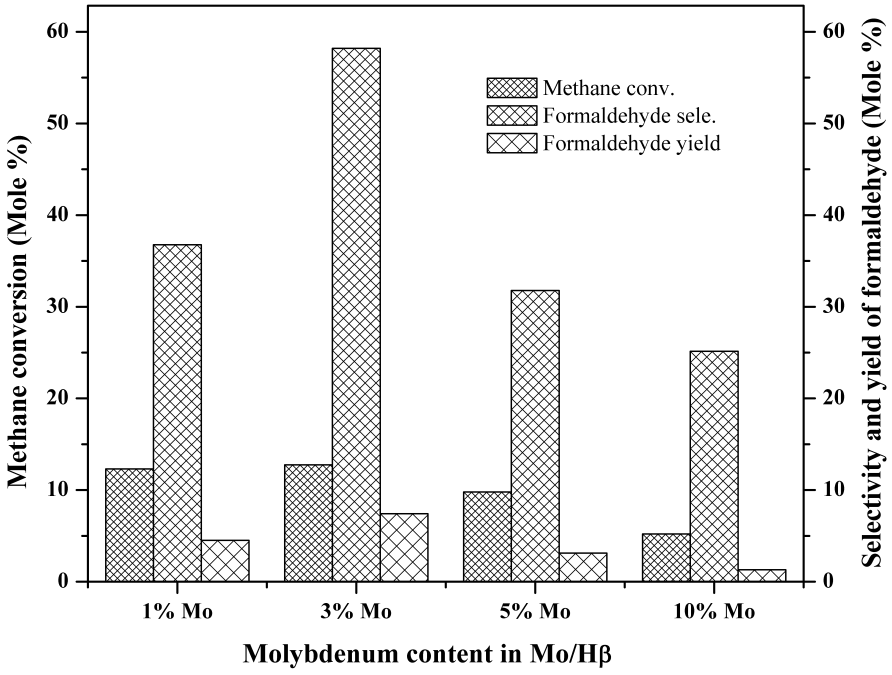

Fig. 5.6: *Methane conversion, formaldehyde selectivity and yield over different molybdenum containing Hβ catalysts.*
Reaction conditions: Temperature - 700 ^{0}C; GHSV - 32,000 h^{-1}; Air/CH_4 ratio - 0.8.

The involvement of different Mo species, in catalysts prepared with varying surface concentrations of Mo atoms, on the performance of methane partial oxidation was investigated by Banares and Fierro [12, 13]. They observed that CH_4 conversion and HCHO selectivity were found to depend on both Mo-loading and the pH of impregnation, which in turn governed the dispersion of molybdenum oxide.

From Fig. 5.6, it is seen that the methane conversion, formaldehyde selectivity as well as yield decreased with Mo loading from 3 to 10 wt %, which was in agreement with the results over Mo/HZSM-5 catalyst [16]. Compared to Hβ catalyst, methane conversion

and of formaldehyde selectivity highly improved when catalyst has certain amount of Mo on Hβ. The results confirmed the positive effect of Mo species on formaldehyde formation. Whereas, increase in Mo loading diminishes methane conversion and at higher loadings there seems to be some synergy between Mo species and Bronsted acid sites to form active centers for methane activation, while Bronsted acidity is passivated at higher Mo contents, it led to lower methane conversion [17]. At 1Mo/Hβ, the yield was low, as a result small amount of the metal loading which was not sufficient to activate the methane at studied temperature. From above studies it can be concluded that 3 wt % metal loading is better for obtaining not only better yield but also good methane conversion and formaldehyde selectivity.

Thus, Suzuki et al. [18] concluded that the well-dispersed molybdenum oxide clusters on SiO_2 support were the active species for the production of formaldehyde. Whereas, Smith and Ozkan [19, 20] proposed that the Mo=O sites present in the MoO_3 crystals were catalytically active while the Mo–O– Mo bonds accelerate the deep oxidation of methane. However, the reactivity of supported molybdenum oxide differs from bulk MoO_3 and no direct extrapolation can be done.

In our studies methanol yield was not considered, as the yield was very low compared to the formaldehyde yield. Plain Hβ was also studied for this reaction, which was not at all active for the formation of formaldehyde.

5.4.2. Effect of different metals

The partial oxidation of methane to methanol and formaldehyde using nitrous oxide as an oxidant has been studied extensively on Mo/SiO_2 [10, 21] and V_2O_5/SiO_2 [22] catalysts. Very few attempts were successful at getting methanol or formaldehyde, when nitrous oxide is replaced with air as the oxygen source [23, 24]. The effect of different metal oxides on Hβ such as copper, iron, vanadium, tungsten and molybdenum were studied for partial oxidation of methane (Fig. 4.5). The purpose was to determine an active and selective catalyst for synthesizing formaldehyde. All catalysts were prepared by dry impregnation method with 3 wt % metal loading using relevant metal salts as precursors. The activity and selectivity for each product depends, of course, on the catalyst and temperature. The catalytic evaluation as a function of temperature with respect to methane

conversion, selectivity (formaldehyde and methanol) and formaldehyde yield obtained over different catalysts as shown in Fig. 5.7.

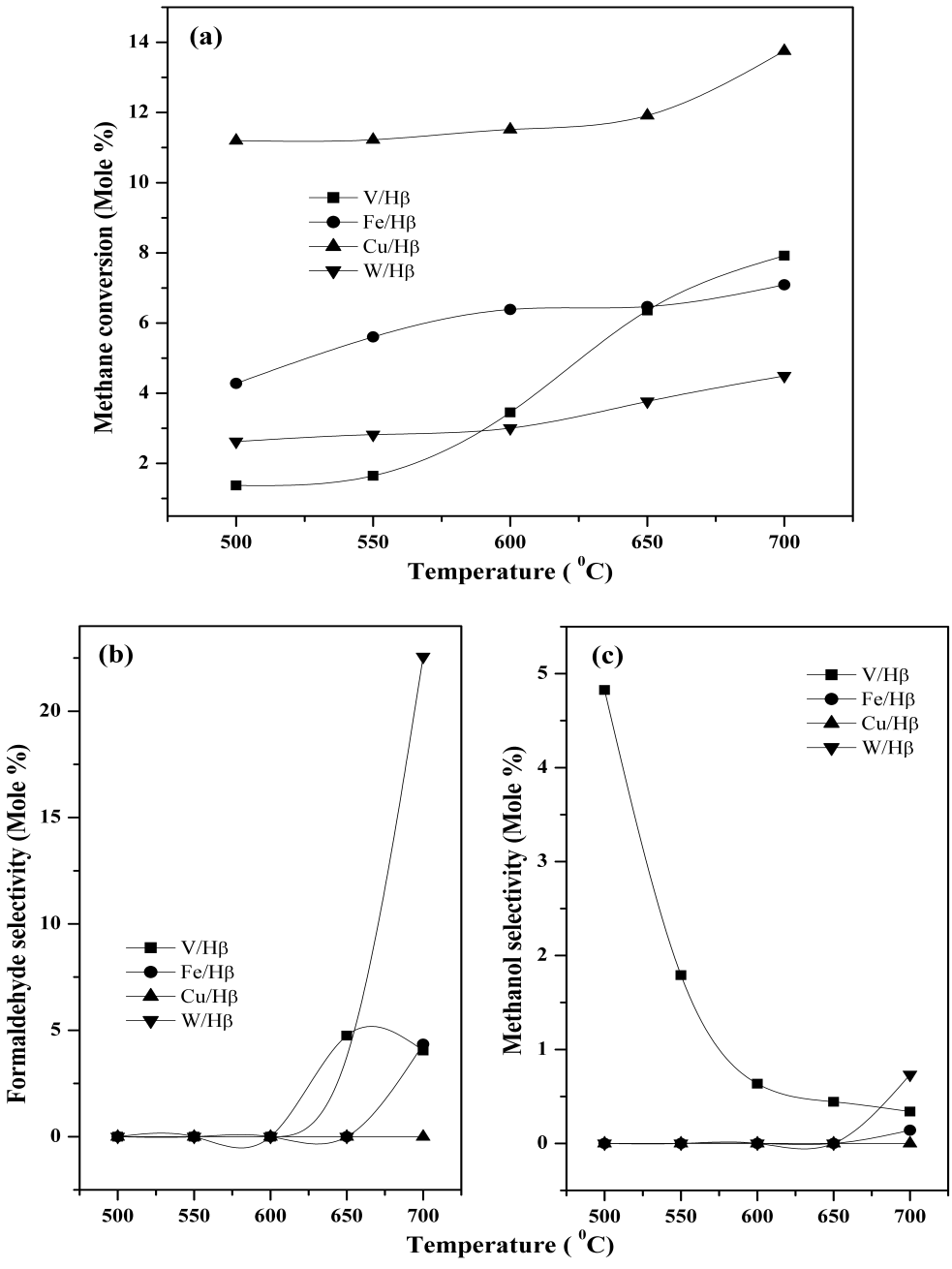

Fig. 5.7: *Influence of different metal on (a) methane conversion, (b) formaldehyde selectivity and (c) methanol selectivity over 3M/Hβ catalysts at different temperatures (M - Cu, Fe, W and V).*
Reaction conditions: Catalyst - 0.5 cc; Temperature - 700 ^{0}C; GHSV-32,000 h^{-1}; Air/CH_4 ratio - 0.8; TOS-5 h.

Copper catalyst showed maximum conversion of methane, but to mostly carbon dioxide and water. Not even trace content of formaldehyde or methanol was observed. Tungsten gave good selectivity towards formaldehyde with 1 mole% yield of formaldehyde at 700 ^{0}C, whereas vanadium showed better selectivity towards methanol at low temperature, which falls at higher temperature.

However the methane conversion was low on these catalysts at lower temperatures. Iron showed moderate activity towards methane to formaldehyde as compared to other metals. Formaldehyde yield with respect to different metals on Hβ is given in table 5.1. The best results were obtained only on molybdenum containing beta catalyst; hence only molybdenum system was further explored in detail for partial oxidation of methane.

Table 5.1: Methane conversion and formaldehyde yield on different metal loaded Hβ catalysts

Catalyst name	Methane conversion (Mole %)		Formaldehyde yield (Mole %)	
	At 650 ^{0}C	At 700 ^{0}C	At 650 ^{0}C	At 700 ^{0}C
V/Hβ	6.35	7.92	0.30	0.32
Fe/Hβ	6.47	7.09	0.00	0.31
W/Hβ	3.77	4.49	0.00	1.01
Cu/Hβ	11.91	13.75	0.00	0.00
Mo/ Hβ	7.33	12.76	4.33	7.32

Reaction conditions: Catalyst - 3M/Hβ (0.5 cc), where M - Mo, Cu, Fe, W and V; Temperature - 650 and 700 ^{0}C; GHSV-32,000 h^{-1}; Air/CH_4 ratio - 0.8.

5.4.3. Influence of space velocity

Figure 5.8 shows the variation of space velocity (32,000-82,000 h^{-1}) on methane conversion, methanol and formaldehyde selectivity's and formaldehyde yield at 700 ^{0}C. The feed rate (methane and air) was changed in these experiments, keeping the amount of the catalyst constant, to vary the space velocity. In partial oxidation of methane, contact time (space velocity) plays a very important role in obtaining better selectivity with

reasonable methane conversion. As shown in Fig. 5.8, space velocity distinctly affects the catalytical activity of 3Mo/Hβ catalyst.

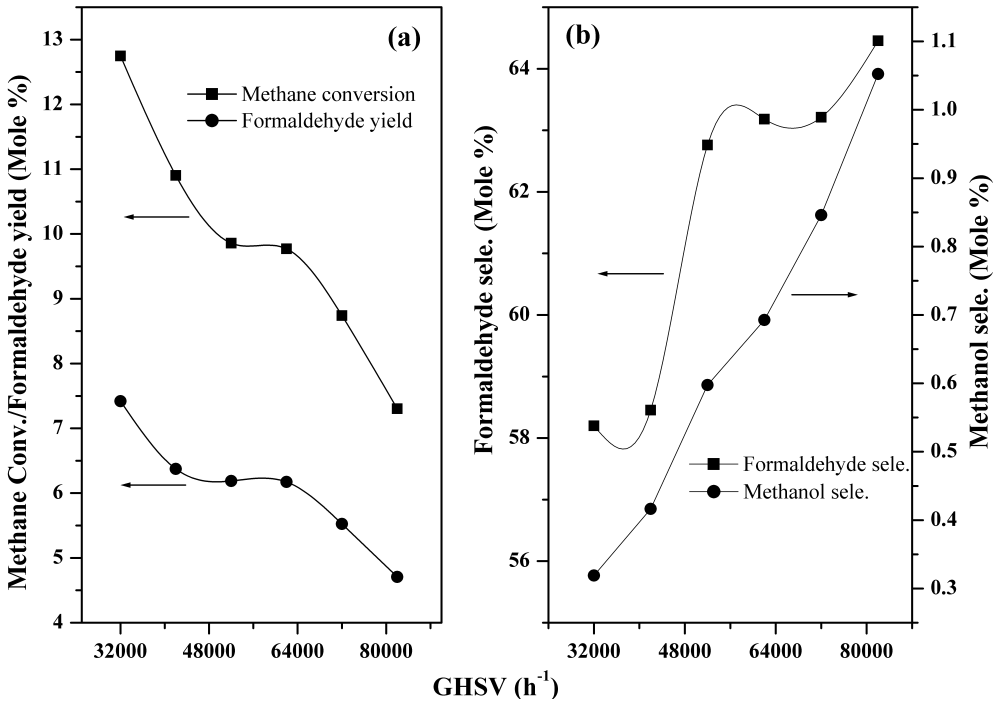

Fig. 5.8: *Influence of space velocity on (a) methane conversion and formaldehyde yield, (b) methanol and formaldehyde selectivity's over 3Mo/Hβ catalyst.*
Reaction conditions: Catalyst - 0.5 cc; Temperature -700 ^{0}C; Air/CH_4 ratio - 0.8; TOS-6 h.

Higher methane conversion and selectivity was observed when space velocity was 32,000 h^{-1}, which was optimum for this system. With increase in space velocity, the methane conversion decreased gradually due to reduction in contact time. Formaldehyde selectivity improved significantly from 58.45 to 64.45 mole % while formaldehyde yield from 7.4 to 4.7 mole % as space velocity increased from 32,000 to 82,000 h^{-1}.

When contact time, is decreased, it minimizes undesired products like carbon monoxide and carbon dioxide. Trace amounts of ethane and ethene were observed in this study. Ethane has increased with a simultaneous decrease in ethene as space velocity increased. The increase in formaldehyde yield with increasing space velocity, stabilized at higher space velocity and a marginal improvement was observed on further increase of space velocity. It is suggested that shorter residence time transports the formaldehyde from

the catalyst surface rapidly decreasing the probability of consecutive reaction of formaldehyde to CO_2 and water [25,26].

5.4.4. Influence of Air/CH_4 ratio

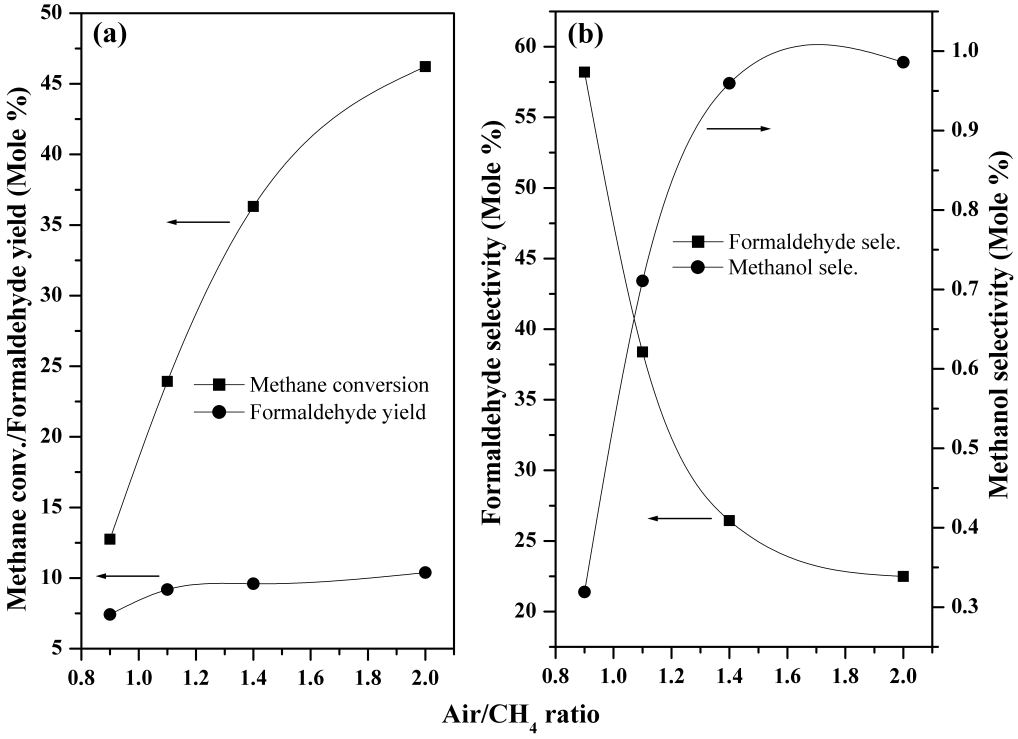

Fig. 5.9: *Influence of Air/CH_4 ratio on (a) methane conversion and formaldehyde yield, (b) methanol and formaldehyde selectivity's over 3Mo/Hβ catalyst.*
Reaction conditions: Catalyst - 0.5 cc; Temperature- 700 ^{0}C; GHSV- 32,000 h^{-1}; TOS-4 h.

The influence of air to methane ratio (excess of oxygen) on the performance of 3 Mo/Hβ catalyst was investigated. Methane conversion, formaldehyde yield, selectivity of formaldehyde and methanol with respective to air to methane ratio is plotted in Fig. 5.9. The methane to air ratio had marginal effect on the product distribution and methane conversion. There is significant increase in conversion of methane when oxygen content was increased. However higher air to methane ratio lowered formaldehyde selectivity with slight improvement in formaldehyde yield as a result of higher methane conversion. Higher oxygen concentrations in the feed the lowers oxygenates selectivity [27], which suggests the influence of oxygen concentration in the gas phase partial oxidation of methane to

formaldehyde or methanol [28-33]. Burch et al. reported that oxygen (O_2/CH_4 ratio) concentration had little effect on product distribution in the range of 2.5 to 6.6 mole% [34], which was obvious to notice with the ratio they adopted in their work. But the ratios used in our study were higher than those reported, which are closer to the explosion limits of methane and oxygen mixture.

5.4.5. Time on stream study

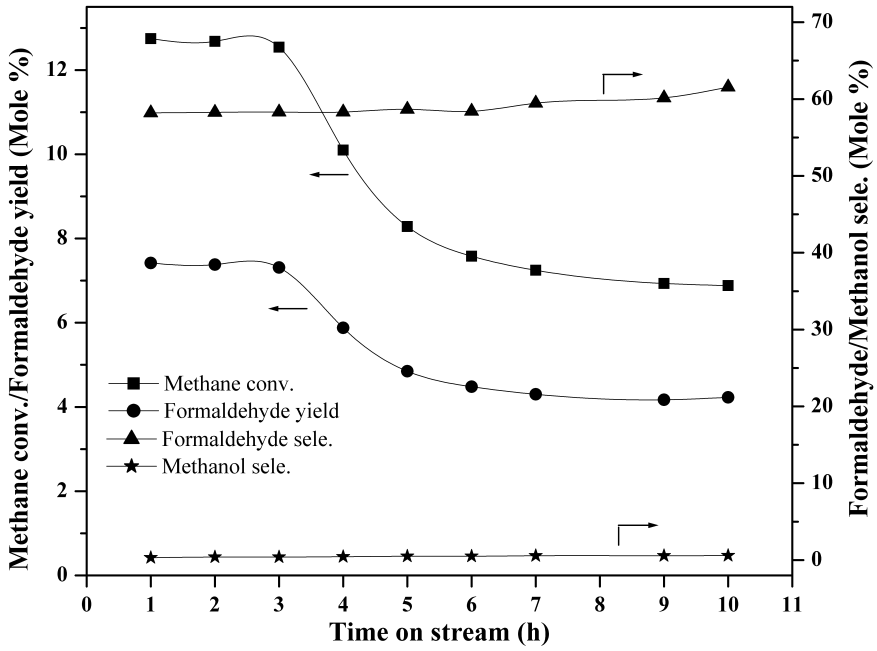

Fig. 5.10: *The activity and selectivity behavior of 3Mo/Hβ catalyst in air atmosphere as a function of time on stream.*
Reaction conditions: Catalyst -0.5 cc; Temperature -700 ^{0}C; GHSV-32,000 h^{-1}; Air/CH_4 ratio - 0.8; TOS-10 h.

The activity, selectivity and formaldehyde yield of 3Mo/Hβ catalyst was studied as a function of time on stream in order to investigate the change in catalyst activity over time. The results of the reaction conducted at 700 ^{0}C using 3Mo/Hβ with space velocity 32,000 h^{-1} and Air/CH_4 ratio 1.15 is shown in Fig. 5.10. Slow and steady fall in the conversion of methane in initial hours was observed with time, after six hours it was stable at around 7.0 mole % conversion of methane. This initial fall in activity may be due to the sublimation of molybdenum. Studies have been carried out on molybdenum-loaded

catalysts to investigate the loss of MoO_3 due the sublimation, which is likely to occur at >600 ^{0}C [21]. Reduction in activity was observed with fall in selectivity, whether the decline in activity was due to poisoning or loss of MoO_3 through volatilization was not cleared. The changes in selectivity also indicate deactivation process through selective poisoning of surface sites rather than the loss of molybdenum. Not much variation was observed on 3Mo/Hβ when the reaction was carried out over 10 h. Thus the reaction was believed to be mostly steady state except for initial fall in its catalytic activity.

5.4.6. Partial oxidation of methane in presence of nitrous oxide

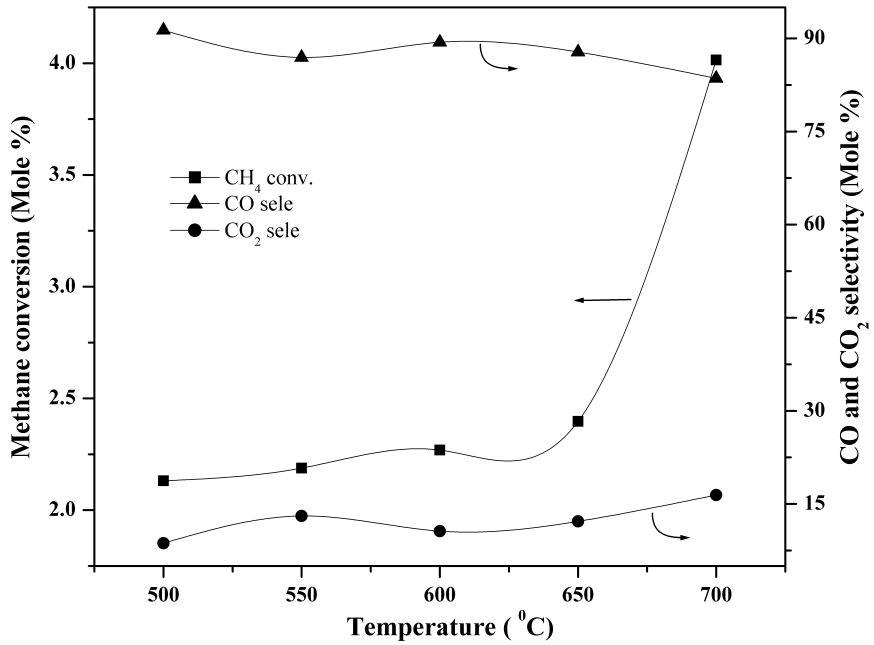

Fig. 5.11: *Influence of N_2O as an oxidant on methane conversion, CO and CO_2 selectivity on 3Mo/Hβ catalyst.*
Reaction conditions: Catalyst - 0.5 cc; GHSV- 32,000 h^{-1}, CH_4: N_2O: He (80:10:180).

To compare the effectiveness of nitrous oxide as an oxidant, the catalytic activity of 3Mo/Hβ catalyst was investigated using nitrous oxide as oxidizing agent. Nitrous oxide, a mild oxidant, should be a good solution for getting better yield and selectivity towards formaldehyde. With either nitrous oxide or oxygen, the products of the reaction are predominately CO_2, CO, HCHO, CH_3OH with trace amounts of ethane and ethene. But on 3Mo/Hβ catalyst, the major products were CO and CO_2. It is reported that [9] N_2O actually

gives O^- species on MoO_3 which lead to total oxidation of methane, whereas O^{2-} species from oxygen on the other hand was found to be active for partial oxidation of methane to formaldehyde. It has been observed that increase in temperature is reflected in the improvement of methane as well as N_2O conversions. The product distribution was affected in the sense that increase in the conversion level of methane followed by decrease in selectivity of CO. Figure 5.11 shows the methane conversion at different temperatures in nitrous oxide atmosphere for 3Mo/Hβ. The major products detected were CO_2 and H_2O with trace amount of hydrocarbons (ethane and ethene), small concentration of methanol and formaldehyde at lower temperature.

5.4.7. Partial oxidation methane on Mo/Al_2O_3 and Mo/SBA-15 catalysts

For better understanding the role of support on this reaction for partial oxidation of methane, studies were carried out over Mo/Al_2O_3 and Mo/SBA-15 to compare their performance with 3Mo/Hβ catalyst. Both the systems (Mo/Al_2O_3 and Mo/SBA-15) were not active for production of formaldehyde. No catalytic activity on Al_2O_3 and SBA-15 was recorded for this reaction. The products were only CO, CO_2 and H_2O with trace amount of hydrocarbons. But at higher reaction temperatures, trace content of formaldehyde was observed on Mo/Al_2O_3, while the same was true for Mo/SBA-15 at lower temperature, while the quantity was minimal in both the cases. From above results, it is clear that the Mo/Al_2O_3 and Mo/SBA-15 are not active probably due to the absence of M=O species, which confirmed by FTIR spectroscopy.

Figure 5.12 gives the effect of temperature on methane conversion, CO_2 and CO selectivity. The CO_2 selectivity increased with increase in temperature, but not much increase in CO selectivity was observed. Whereas, methane conversion has increased to 6.27 mole % when temperature is raised from 500 to 700 ^{0}C.

Figure 5.13 gives the effect of temperature on methane conversion as well as CO and CO_2 selectivity. Increase in temperature led to decrease in CO_2 selectivity with simultaneous increase in CO selectivity and methane conversion. Based on these results over Mo/Al_2O_3 and Mo/SBA-15, we can conclude that, these catalysts drive the reaction to complete oxidation (combustion) of methane to CO_2 and water with small amount of CO.

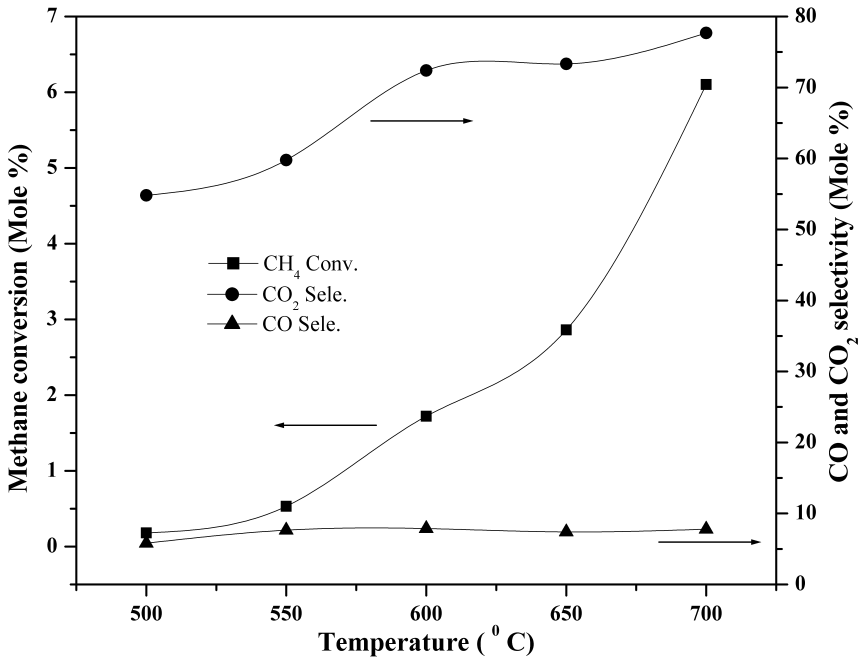

Fig. 5.12: *Effect of reaction temperature on methane conversion, CO and CO_2 selectivity on $3Mo/Al_2O_3$ catalyst.*
Reaction conditions: Catalyst - 0.5 cc; GHSV-32,000 h^{-1}; Air/CH_4 ratio - 0.8; TOS-5 h.

The catalytic activity of Mo/SiO_2 for the partial oxidation of methane using N_2O has been reported by many authors [35, 36], which gives methane conversion of around 12 mole% with 2 mole% formaldehyde yield. It has been proposed that highly dispersed monomeric species of molybdenum oxide are active sites for the formaldehyde formation [37], while Suzuki et al. [18] concluded that well-dispersed molybdenum oxide clusters on SiO_2 support are the active species. On the hand, Smith and Ozkan [38] proposed that Mo=O sites present in the MoO_3 crystals are catalytically active while Mo-O-Mo accelerates the deep oxidation. From all above results, the Mo species formed with silica is responsible for obtaining methanol or formaldehyde from methane through partial oxidation. Mo/Al_2O_3 and Mo/SBA-15 were not active for production of formaldehyde, whereas Mo/SiO_2 shows good activity towards formaldehyde, which suggest that surface area does not play any role for getting better activity in the partial oxidation of methane to oxygenates.

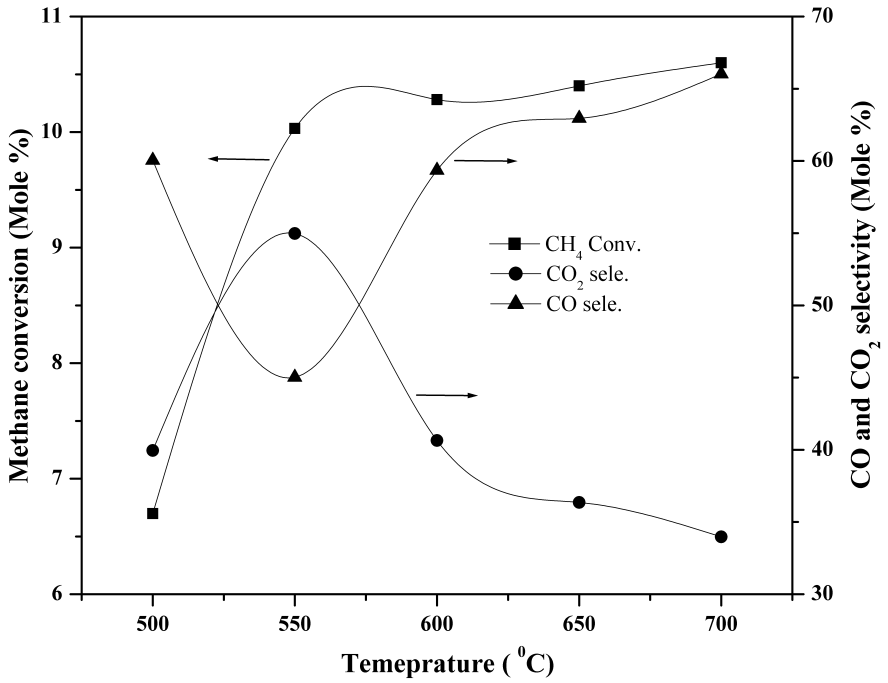

Fig. 5.13: *Effect of reaction temperature on methane conversion with CO and CO_2 selectivity on 3Mo/SBA-15.*
Reaction conditions: Catalyst - 0.5 cc; GHSV - 32,000 h^{-1}; Air/CH_4 ratio - 0.8; TOS-5 h.

5.5. SUMMARY OF PART – A

The catalytic properties of Mo/Hβ catalysts with different metal loadings (1-10 wt %) were evaluated for the partial oxidation of methane to oxygenates using air as an oxidant. The influence of mild oxidants like nitrous oxide was also studied to understand its influence on methane conversion, selectivity and yield of oxygenates. The structural characterization of these molybdenum-supported catalysts has been discussed in chapter 4. The results indicate that isolated molybdenum species are predominant at a metal loading of 3 wt % molybdenum and these species play a prominent role for the formation of oxygenates, particularly formaldehyde. With increase in metal loading, formation of polymolybdate species was observed. These polymolybdate species are responsible for combustion of methane which leads to not only lower conversion of methane but also selectivity and yield of formaldehyde. Hence the methane conversion was found to increase with molybdenum loading, reaching maximum at 3 wt % metal loading, while the conversion reduced when the loading was increased to 10 wt %. The products observed

were HCHO, CO_2, CO, H_2O with unconverted methane and traces of C_2H_6 and C_2H_4. The conversion of methane was low at 500 ^{0}C, which raised with temperature. The effect of different metal oxides on Hβ support as copper, iron, vanadium and tungsten was also studied for partial oxidation of methane to look for an active and selective catalyst for oxygenates formation. Space velocity (contact time) distinctly influences the catalytic activity. High methane conversion and good oxygenate selectivity were observed at 32,000 h^{-1} space velocity. It is suggested that shorter residence time moves the product (formaldehyde) from the catalyst, thus enabling better yield and selectivity of formaldehyde, minimizing its decomposition to carbon dioxide and water. An increase in conversion of methane with increased flow rate of oxygen was observed. Slow and steady decrease in the conversion of methane in the initial hours of reaction was observed with time, which may be due to the sublimation of molybdenum.

PART – B: PARTIAL OXIDATION OF METHANE ON Mo/Fe-Zn-O MIXED OXIDE CATALYSTS

5.6. INTRODUCTION

The first part of this chapter (Part-A) discusses the results of partial oxidation of methane to oxygenates on molybdenum-supported zeolite catalysts. Here in this section partial oxidation of methane is reported on Mo supported on mixed oxides. The experimental set up and analytical procedure used was same as described in earlier sections of this chapter.

The partial oxidation of methane has been carried out above 500 ^{0}C due to the high C-H bond energy. But these conditions result in poor selectivity as the partial oxidation product, such as methanol and formaldehyde, were unstable and get oxidized to CO_2. [1]. Chemical processes on metal oxide surfaces have been of great interest for long time, due to their relevance in the field of heterogeneous catalysis. Perfect oxide surfaces usually show little or no activity. It is widely believed that the high activity of the oxide results from the presence of small number of active sites [39]. Due to interesting bulk and surface properties of zinc, its oxide is widely employed in several applications. For example mixed oxide catalyst containing zinc oxide and chromia were used for high temperature and high

pressure methanol synthesis. $Fe_2(MoO_4)_3$ was supported to be the most active and selective catalyst among several molybdates for the partial oxidation of methane to formaldehyde at atmospheric pressure. The addition of metals like Li, Zn or Ce to $Fe_2(MoO_4)_3$ greatly enhance the formaldehyde formation. These additives inhibit oxidation of formaldehyde to CO and H_2O [40], while pure Fe_2O_3 yielded complete oxidation of methane to CO_2 [41]. Therefore, it is important to understand the role of active species and the promoter in the oxidation catalyst to minimize the decomposition of reaction intermediates, while maximizing the yield of formaldehyde or methanol. Here in this section, Fe containing zinc oxides were prepared by co-precipitation method. Molybdenum was supported on these oxides and used for partial oxidation of methane to oxygenates. These catalysts were characterized using technique such as powder XRD, BET surface area, UV-visible, FTIR, NH_3-TPD/H_2-TPR, TEM and Raman spectroscopy.

5.7. RESULTS AND DISCUSSION

The commercial catalyst for formaldehyde synthesis from methanol partial oxidation, Mo/SiO_2, is also known for methane partial oxidation [42-49]. Oxidation of methane has been generally performed above 500 ^{0}C as a result of high C-H bond energy of 105 kcal. Here in this part we report the effect of iron and molybdenum on zinc in the partial oxidation of methane.

Partial oxidation of methane on Fe-Zn-O and Mo/Fe-Zn-O was carried out using air as an oxidant. Different iron and zinc containing (2.5, 5.0 and 10 wt %) mixed oxides were prepared by co-precipitation method, which were further modified by dry impregnation of molybdenum. Process parameters like temperature (500-700 ^{0}C), metal content (1-10 wt %), influence of support, time on stream and nitrous oxide as oxidant were carried out on these catalysts for partial oxidation of methane to formaldehyde.

5.7.1. Effect of temperature

The effect of reaction temperature on methane conversion and formaldehyde yield is plotted in Fig. 5.14, whereas selectivity of formaldehyde and methanol is shown in Fig. 5.15. The methane conversion as well as formaldehyde yield has improved with

temperature in the range (500-700 ^{0}C) chosen for the study. Maximum conversion of methane was observed at 700 ^{0}C.

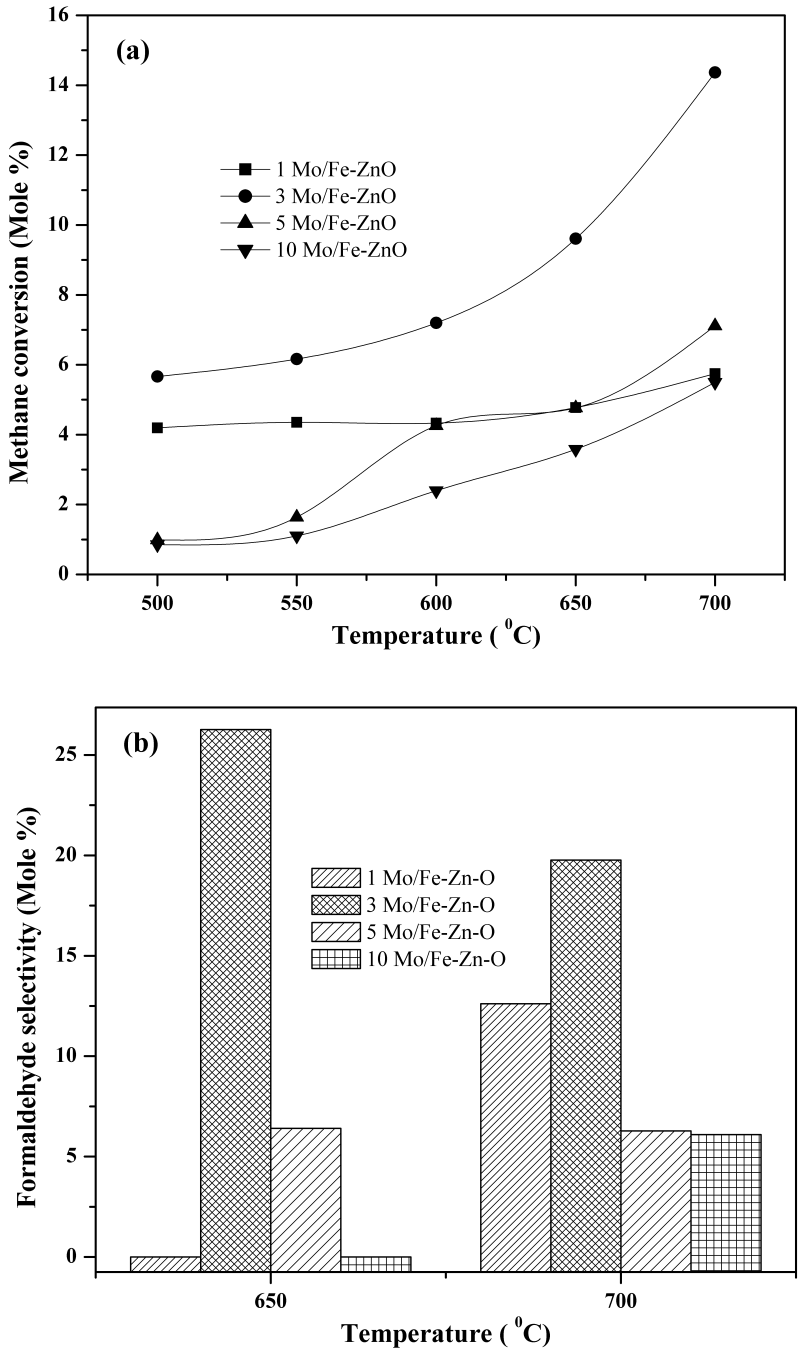

Fig. 5.14: *Effect of reaction temperature on (a) methane conversion and (b) formaldehyde selectivity over different molybdenum containing 2.5Fe-Zn-O catalysts.*
Reaction conditions: Catalyst - 0.5 cc; GHSV-32,000 h^{-1}; Air/CH_4 ratio - 0.8.

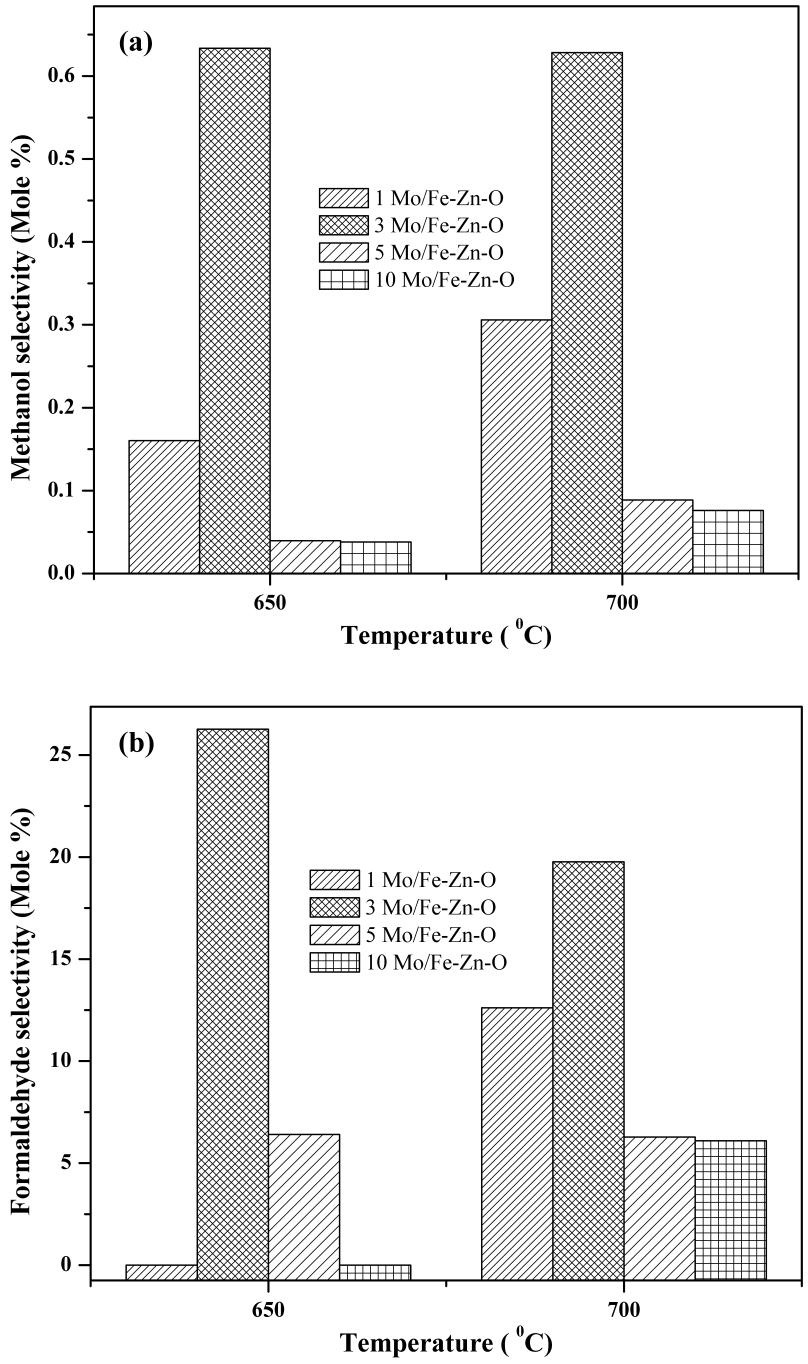

Fig. 5.15: *Effect of reaction temperature on methanol selectivity (a) and formaldehyde yield (b) over 2.5Fe-Zn-O with different molybdenum content.*
Reaction conditions: Temperature - 650 and 700 ^0C; GHSV-32,000 h^{-1}; Air/CH_4 ratio - 0.8.

Catalyst 3Mo/Fe-Zn-O showed better activity in the studied temperature range as compared to other molybdenum loaded Fe-Zn-O catalysts. The selectivity of formaldehyde

and methanol as a function of temperature is shown in Fig. 5.15. Increase in temperature leads to decrease in formaldehyde selectivity but it improves the methanol selectivity to a small extent, while a similar trend was noticed with increase in molybdenum loading.

Formaldehyde was the major notable liquid product in addition to CO_2 on Mo/Fe-Zn-O catalysts. The results on these catalysts prove synergistic effects between iron and molybdenum in Mo/Fe-Zn-O for the production of formaldehyde by methane partial oxidation. The role of Fe and Mo in the Mo/Fe-Zn-O could be that Fe may be the catalytic site for C-H activation to generate reaction intermediates, and Mo accounts for the transformation of intermediates into formaldehyde [50].

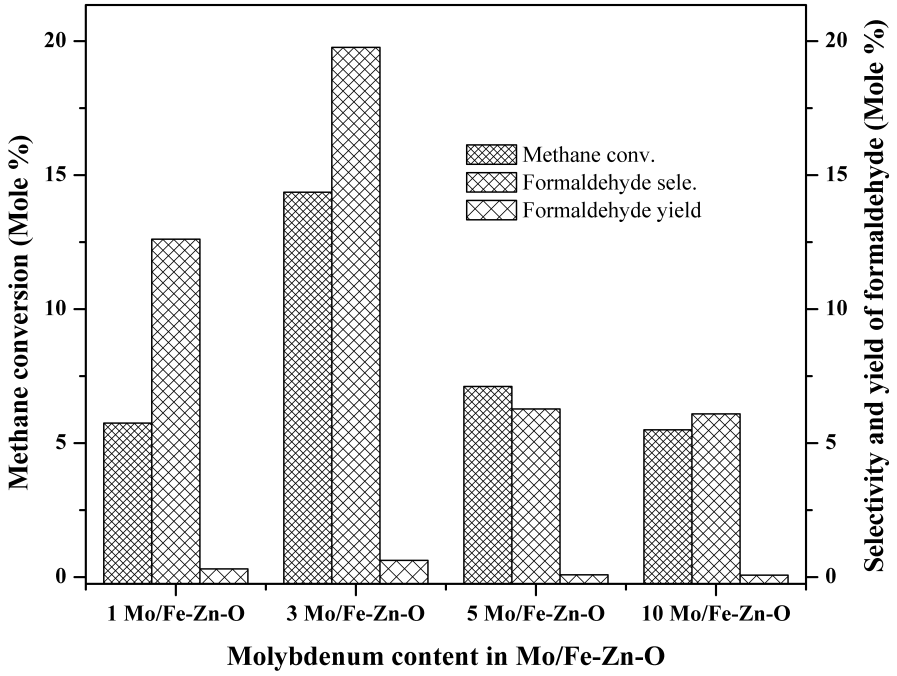

Fig. 5.16: *Relationship between conversion of methane, formaldehyde selectivity, and formaldehyde yield over different molybdenum containing samples.*
Reaction conditions: Temperature - 700 ^0C; GHSV-32,000 h^{-1}; Air/CH_4 ratio - 0.8.

Molybdenum content plays very important role in activity and selectivity for partial oxidation of methane, which is discussed in detail in part - A for Mo/Hβ catalyst. Figure 5.16 shows the effect of molybdenum content on 2.5Fe-Zn-O catalysts. The concentration of the molybdenum in the catalyst influences methane conversion, yield and selectivity to formaldehyde. It is clear that initially with increasing molybdenum content, both methane

conversion and formaldehyde selectivity improves, but higher molybdenum content beyond 3 wt % has an adverse effect. From the results obtained on these Mo/Fe-Zn-O catalysts, 3 wt % Mo containing 2.5Fe-Zn-O was found to be better.

5.7.2. Effect of Fe content

Above results show that optimum molybdenum loading for obtaining better formaldehyde yield and selectivity with reasonably good methane conversion is around 3 mole %. By using different iron loaded zinc oxide as a support with 3 wt % molybdenum, the system was further explored for this reaction. The best results were obtained on Fe-Zn-O support compared to other iron loaded zinc catalysts. Figure 5.17 shows the effect of methane conversion, selectivity and yield of formaldehyde of different iron loaded zinc with 3 wt % molybdenum over catalysts at a temperature of 700 ^{0}C. The data indicate that Fe addition of around 2.5 wt % is better, while higher loading leads to decrease in overall activity.

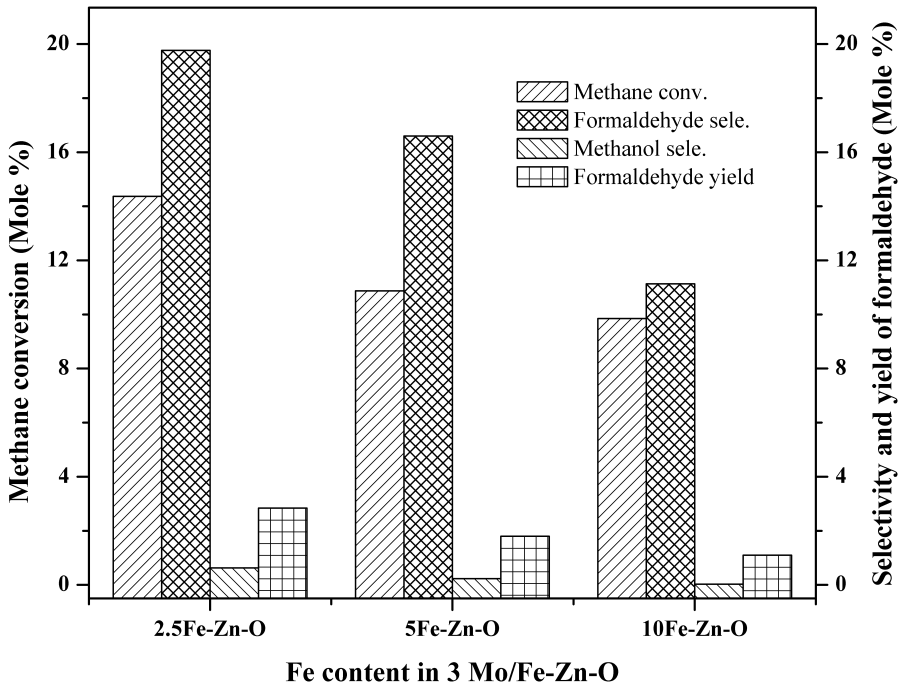

Fig. 5.17: *Effect of Fe content in Fe-Zn-O on methane conversion, selectivity and yield of formaldehyde over 3 % molybdenum catalysts.*
Reaction conditions: Temperature - 700 ^{0}C, GHSV-32,000 h^{-1}; Air/CH_4 ratio - 0.8.

Higher iron content reportedly led to non-selective oxidation, producing oxides of carbon [51]. Molybdenum containing zinc oxide (3Mo/ZnO) gave 4.8 mole % methane conversion with trace amount of formaldehyde at higher temperature, which shows that addition of iron promotes the partial oxidation of methane to oxygenates. Recently, it has been reported that Fe^{3+} ions in trigonal bipyramidal coordination on silica supported $FePO_4$ catalysts are easily reducible providing highly reactive oxygen species for C-H activation in partial oxidation of methane [52].

Otsuka et al. [53] claimed that Fe^{3+} sites in various oxide systems, owing to the Bronsted acidity induced in the surrounding surface groups; enhance the formation of O_2^{2-} species, which are responsible for the activation and the partial oxidation of the methane molecule.

5.7.3. Partial oxidation of methane on Fe-Zn-O

Partial oxidation of methane was studied on iron-loaded zinc, the support used for Mo/Fe-Zn-O catalysts. No formaldehyde or methanol was detected on these samples. These catalysts drive complete oxidation of methane to CO_2 and H_2O. The methane conversion, CO and CO_2 selectivity are plotted in Fig. 5.18 and 5.19 at different reaction temperatures. Increase in iron content has increased the methane conversion with a small decrease in CO_2 selectivity, while CO selectivity goes up at the same time in the temperature range studied.

Only trace content of formaldehyde was observed on 10Fe-Zn-O above 650 ^{0}C but the yield was very low. Figure 5.20 shows the effect of iron content in Fe-Zn-O support on methane conversion, and CO and CO_2 selectivity at 700 ^{0}C. As it may be seen, increase in Fe content improves the methane conversion with increase in CO selectivity and little fall in CO_2 selectivity. The increment in methane conversion at 700 ^{0}C with the addition of iron, indicates the active participation of the iron component in the C-H activation of methane [12].

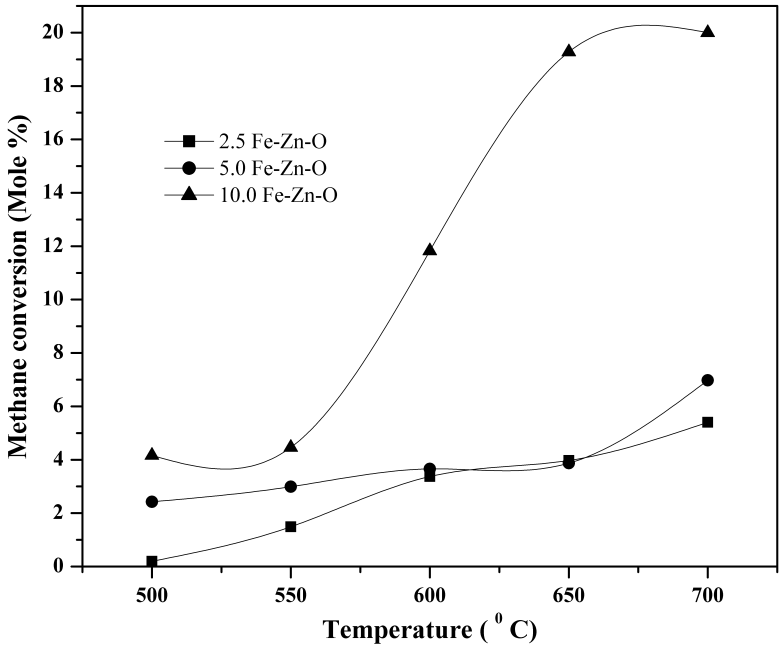

Fig. 5.18: *Influence of reaction temperature on methane conversion over different iron loaded Zn-O catalysts.*
Reaction conditions: Catalyst - 0.5 cc; Air/CH_4 ratio - 0.8; GHSV-32,000 h^{-1}.

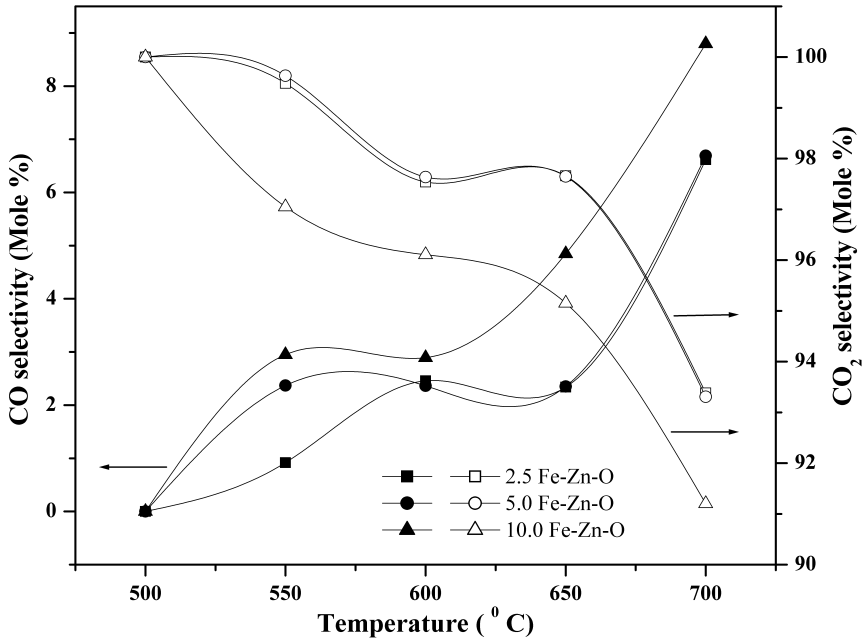

Fig. 5.19: *Variation of CO and CO_2 selectivity with respect to temperature over different iron loaded Zn-O catalysts. (Legends: Filled - CO selectivity and Empty - CO_2 selectivity).*

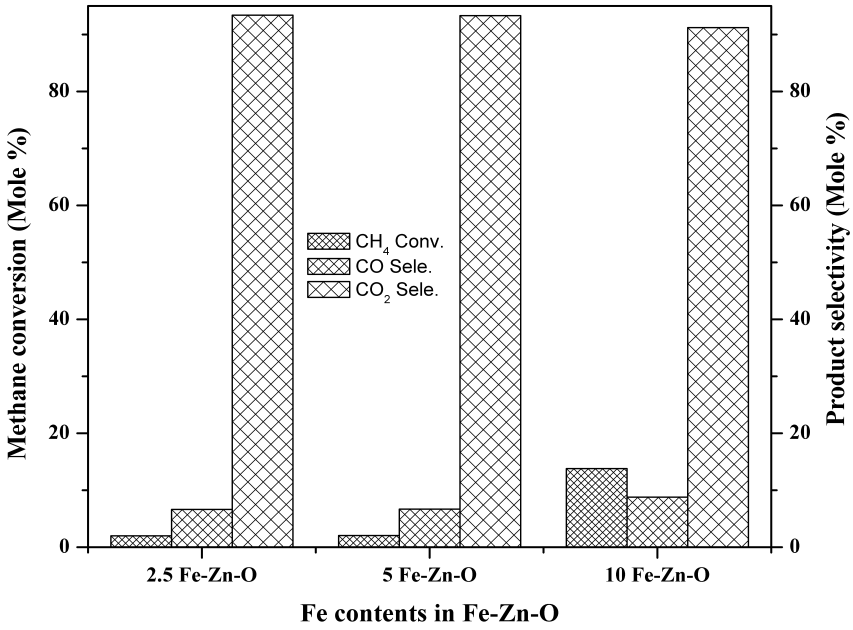

Fig. 5.20: *Variation of CO, CO_2 selectivity and methane conversion over different iron loaded Zn-O (without Mo) at 700 ^{0}C.*
Reaction conditions: Catalyst - 0.5 cc; Air/CH_4 ratio - 0.8; GHSV-32,000 h^{-1}.

5.7.4. Methane partial oxidation in nitrous oxide

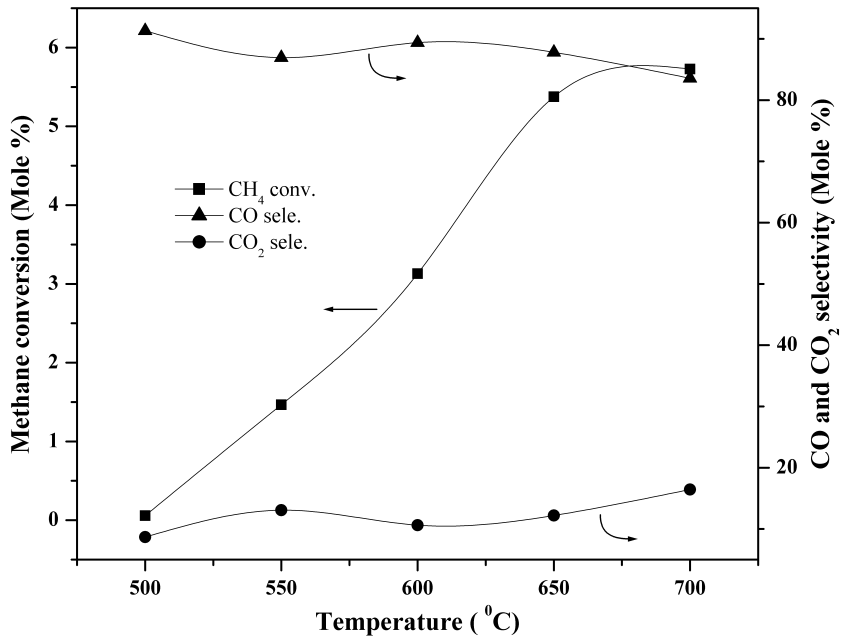

Fig. 5.21: *Partial oxidation of methane in N_2O, methane conversion, CO & CO_2 selectivity over 3Mo/2.5Fe-Zn-O.*
Reaction conditions: Catalyst-0.5 cc; GHSV- 32,000 h^{-1}, Feed - CH_4:N_2O:He (80:10:180).

The products were mainly CO and CO_2 with trace amount of ethane, ethene and below detectable quantities of formaldehyde and methanol. The major product was CO, which slightly reduced with increasing temperature. The maximum methane conversion was observed at 700 ^{0}C temperature.

5.7.5. The time on stream study

Time on stream activity and selectivity for partial oxidation of methane over 3wt % molybdenum containing 2.5Fe-Zn-O catalyst is shown in Fig. 5.22 at reaction conditions optimized earlier. The reaction was carried out for 10 h. Rapid fall in methane conversion was observed with time; as the conversion reduced from 14.00 to 7.00 mole %, with simultaneous increase in formaldehyde selectivity and small decrease in methanol selectivity. The yield was initially stable and started falling down only after 6 hours. This continuous drop in the conversion of methane may be attributed to sublimation of molybdenum at higher temperatures.

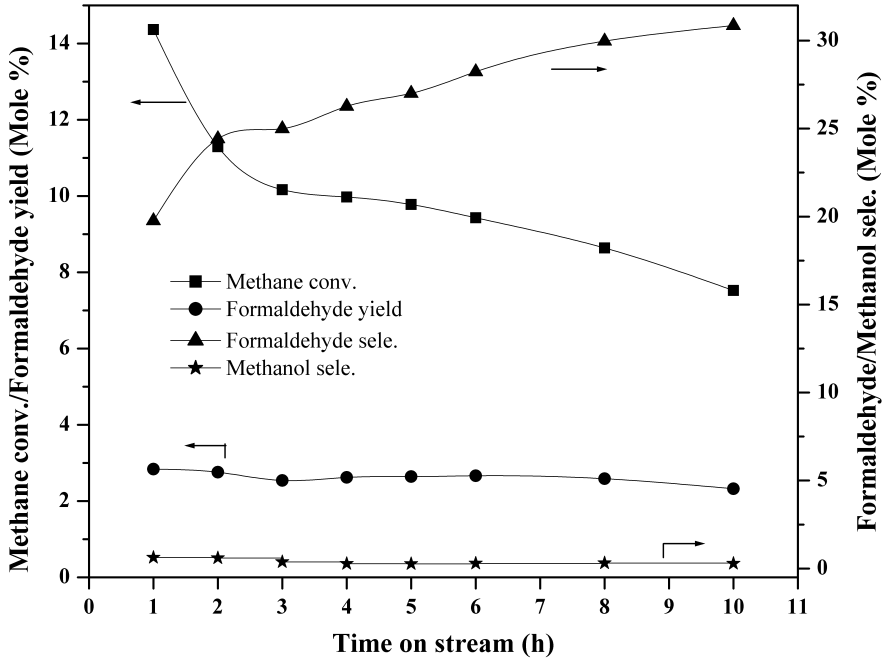

Fig. 5.22: *Time on stream activity and selectivity behavior for partial oxidation of methane over 3Mo/2.5Fe-Zn-O.*
Reaction conditions: Temperature-700 ^{0}C; GHSV-32,000 h^{-1}; Air/CH_4 ratio-0.8; TOS-10 h.

These results can be supported by the chemical analysis values obtained by ICP-AES. No coke formation was observed on the surface of these catalysts, which might be due to the high temperature and presence of oxygen in the feed.

5.8. SUMMARY OF PART – B

Since the formation of CH_3OH, CHOH and CO_2 are formed consecutively, it appears that if we can block some of the reaction pathways by suitable means, the selectivity to various oxygenates can be improved. In this section, zinc oxide is promoted with iron, which is used for supporting molybdenum to investigate the performance in the partial oxidation of methane to oxygenates. The catalytic properties of these catalysts with different molybdenum and iron loadings were evaluated for partial oxidation of methane to oxygenates. No activity towards formation of formaldehyde was observed on Fe-Zn-O and Mo/Zn-O in the temperature range studied. Only CO, CO_2 and H_2O were observed in the products in the case of Fe-Zn-O. Conversion of methane to formaldehyde increased with molybdenum loading, reached maximum at 3 wt %, while it has decreased when the loading was raised to 10 wt %. The results show that 3 wt % molybdenum loaded on 2.5Fe-Zn-O was found to be better in activity. The activity towards formation of formaldehyde with air as an oxidant was better when compared to N_2O as oxidant. Continuous drop in conversion of methane was noticed with time on stream, which is attributed to sublimation of molybdenum at high reaction temperatures.

5.9. REFERENCES:

[1] M. J. Brown and N. D. Parkyns, Catal., Today, 8 (1991) 305.

[2] A. Parmaliana, F. Frusteri, Stud. Surf. Sci. Catal., 119 (1998) 551.

[3] G. I. Panov, V. I. Sobolev, Kinet. Catal., 39-6 (1998) 792.

[4] D. A. Dowden and G. T. Walker, UK Patent 1, 244, 001 (August 25, 1971).

[5] R. Pitchai and K. Kiler, Catal. Rev., Sci. Eng., 28 (1986) 13.

[6] K. Otsuka and M. Hatano, J. Catal., 108 (1987) 252.

[7] N. D. Spencer, U.S. Patent, 4 127(1986) 607.

[8] N. D. Spencer, J. Catal., 109 (1988) 117.

[9] Y. Barbaux, A. R. Elmrani, E. Payen, L. Gengembre, J. P. Bonnelle and B. Grzybowska, Appl. Catal., 44 (1988) 117.

[10] H. F. Liu, R. S. Liu, K. Y. Liew, R. E. Johnson and J. H. Lunsford, J. Am. Chem. Soc., 106 (1984) 4117.

[11] S. Kasztelan, E. Payen, J. B. Moffat, J. Catal., 112 (1988) 320.

[12] M. A Banares, J. L. G. Fierro, Ann. Quim., 87 (1991) 223.

[13] M. A. Banares, J. L. G. Fierro, Catal. Lett., 17 (1993) 205.

[14] Y. Barbaux, A. R Elmrani, E. Payen, I. Gengembre, J. B Bonnelle, B. Grzybowska, J. Catal., 44 (1988) 117.

[15] M. A. Banares, N. D. Spencer, M. D. Jones, J. Catal., 146 (1994) 546.

[16] A. de, Lucas, J. L. Valverde, L. Rodriguezl, P. Sanchez and M. T. Garcia, Appl. Catal., A 203 (200) 81.

[17] S. Miao, L. Liu, Y. Lian, X. Zhu, S. Zhou, Y. Wang and X. Bao, Catal. Lett., 97 (3-4) (2004) 209.

[18] K. Suzuki, T. Hayakawa, M. Shimizu, K. Takehira, Catal. Lett., 30 (1993) 167.

[19] M. R. Smith, L. Zhang, S. A. Driscoll, U. S. Ozkan, Catal. Lett., 1 (1993) 19.

[20] M. R. Smith, U. S. Ozkan, J. Catal., 124 (1993) 141.

[21] M. M. Khan and G. A. Somorjai, J. Catal., 91 (1985) 263.

[22] K. J. Zhen, M. M. Khan, C. H. Mak, K. B. Lewis and G. A. Somorjai, J. Catal., 94 (1985) 501.

[23] G. I. Golodets, V. A. Borko, V. I. Gomonai, Theoretical Experimental Chemistry,

20 (1984) 311.

[24] R. Pitchai and K. Klier, Catal. Rev. Sci. Eng., 28 (1986) 13.

[25] T. Shimamura, K. Okumura, K. Nakagawa, T. Ando, N. O. Ikenga, T. Suzuki, J. Mol. Catal., A 211 (2004) 97.

[26] G. Du, S. Lim, Y. Yang, C. Wang, L. Pfefferle, G. L. Haller, Appl. Catal., A 302 (2006) 48.

[27] K. Tabata, Y. Teng, T. Takemoto, E. Suzuki, M. A. Banares, M. A. Pena and J. L. G. Fierro., Catal Rev., 44 (1) (2002) 1.

[28] H. D. Gesser, N. R. Hunter, C. B. Prakash, Chem. Rev., 85 (4) (1985) 235.

[29] J. C. Mackie, Catal. Rev. Sci. Eng., 33 (1/2) (1991) 169.

[30] D. W. Rytz, A. Baiker, Ind. Eng. Chem. Res., 30 (1991) 2287.

[31] K. Omata, N. Fuluoka, K. Fujimoto, Ind. Eng. Chem. Res., 33 (1994) 784.

[32] P. S. Casey, T. McAllister, K. Foger, Ind. Eng. Chem. Res., 33 (1994) 1120.

[33] M. J. Foral, Prepr. Am. Chem. Soc. Div. Pet. Chem., 37 (1) (1992) 34.

[34] R. Burch, G. D. Squire, S. C. Tsang, J. Chem. Soc., Faraday Trans., Part I., 85 (10) (1989) 3561.

[35] D. A. Dowden, C. R. Schnell, G. T. Walker, in: Proceedings of the Fourth International Congress on Catalysis, (1968) 201.

[36] H. F. Liu, R. S. Liu, K. Y. Liew, R. F. Johnson, J. K. Lunsford, J. Am. Chem. Soc., 106 (1984) 4117.

[37] M. A. Banares, N. D. Spencer, M. D. Jones and I. E. Wachs, J. Catal., 146 (1994) 204.

[38] M. R. Smith, U. S. Ozkan, J. Catal., 142 (1993) 226.

[39] V. E. Henrich, P. A. Cox, The surface Science of Metal Oxides, Cambridge University Press, 1996.

[40] K. Otsuka and M. Hatano, J. Catal., 108 (1987) 187.

[41] G. Kastanas, G. Tsigdinos, A. Sachdev and J. Schwank, 11th N. A. Meeting of the Catal. Soc., Dearborn, MI, 1989, Abstr. No. PF07.

[42] R. S. Liu, M. Iwamato and J. H. Lunsford, J. Chem. Soc. Chem. Commun., 78 (1982).

[43] H. F. Liu, R. S. Liu, K. Y. Liew, R. E. Jonson and J. H. Lunsford, J. Am. Chem.

Soc., 106 (1984) 4117.

[44] S. Kasztelan and J. B. Moffat, J. Catal., 106 (1987) 512.

[45] S. Kasztelan and J. B. Moffat, J. Catal., 112 (1988) 54.

[46] N. D. Spencer, J. Catal., 109 (1988) 187.

[47] Q. Sun, R. G. Hermann and K. Klier, Catal. Lett., 16 (1992) 251.

[48] F. Arena, F. Frusteri, A. Parmaliana and N. Giordano, Appl. Catal., 125 (1995) 39.

[49] M. Faraldos, M. A. Banares, J. A. Anderson, H. Hu, I. E. Wachs and J. L. G. Fierro, J. Catal., 160 (1996) 214.

[50] X. Yang, K. D. Jungb, S. H. Cho, O. S. Joo, S. J. Uhm and S. H. Han, Catal. Lett., 64 (2000) 185.

[51] A. Parmaliana, F. Arena, F. Frusteri, A. Martınez-Arias, M. Lopez Granados, J. L. G. Fierro, Appl Catal., A 226 (2002) 163.

[52] G. O. Alptekin, A. M. Herring, D. L. Williamson, T. R. Ohno, R. L. McCormick, J. Catal., 181 (1999) 104.

[53] K. Otsuka, I. Yamanaka, Y. Wang, Stud. Surf. Sci. Catal., 119 (1998) 15.

Chapter - 6

SUMMARY AND GENERAL CONCLUSIONS

6.1. SUMMARY

This thesis describes preparation, characterization and study of two catalytic reactions, preferential oxidation of CO and partial oxidation of methane on supported metal oxides as well as metals supported on zeolites. Platinum exchanged NaY, iron promoted platinum NaY and ceria supported copper-cobalt catalysts were explored for preferential oxidation of CO. For partial oxidation of methane to oxygenates, H-beta supported molybdenum and iron-zinc oxide supported molybdenum catalysts were used. These H-beat supported catalysts were found to be selective towards formation of formaldehyde with trace amount of methanol. This chapter presents a brief summary drawn based on the work described in previous chapters and suggestions for further research with general conclusions.

Chapter 1 presents general introduction to heterogeneous catalysis. It describes briefly about zeolites as well as mixed metal oxides. Among the oxides, mixed metal oxides and their acid-base properties in catalysis have been discussed. Similarly, in regard to zeolites, their special feature like acidity is discussed in detail. A brief description of various modification methods involved in the preparation and characterization of active and selective catalysts is described. The role of transition metals in selective oxidation on metals like Mo, Pt and Cu has been described. It mainly discuses the published literature on the preparation, structure and catalytic aspects of oxides and modified zeolites. It gives introduction to preferential oxidation (PrOx) of CO and partial oxidation of methane. For PrOx reaction, the probable mechanism is discussed. Other methods for the removal of CO and their limitations were covered with brief description to fuel cells. In case of partial oxidation of methane, classification of natural gas, use of natural gas for the production of value added products as well as chemicals, current industrial process for the production of formaldehyde is discussed. Methane activation by other means particularly using nitrous oxide is also discussed. This chapter mainly reviews literature on these topics. At the end of this chapter the scope of the thesis has been discussed in detail.

Chapter 2 describes preparation and characterization of Pt-NaY, promoted Pt-NaY and Cu-Co-Ce-O as catalysts, which were evaluated for preferential oxidation of CO. These materials were characterized by PXRD, SEM, TEM, AAS, surface area (BET),

FTIR, UV-visible, XPS, NH_3-TPD, H_2-TPR and H_2-Chemisorption. General introduction to the physico-chemical characterization techniques, theory and experimental procedures used are described briefly in this chapter.

Pt-NaY and promoted Pt-NaY catalysts were prepared by ion exchange method with different platinum contents. These catalysts were characterized by using techniques such as powder XRD, BET surface area, TEM, H_2-Chemisorption and H_2-TPR. All platinum samples were activated at 350 ^{0}C except Pt sample modified with other metals, which were activated at 400 ^{0}C. Powder XRD does not show any phases belonging to platinum or other metals used for exchange like Fe, Co and Au. Temperature programmed reduction results reveal that platinum undergoes reduction in two-steps, one at lower temperatures other at higher temperature. Iron promoted platinum samples show better dispersion of platinum when compared to only platinum samples calculated by H_2-Chemisorption. These results were supported by TEM, which shows small and well dispersed Pt particles of around 4 nm. A number of well-dispersed platinum particles on the support can be seen in the TEM picture with a fairly even size distribution. The average particle size of the platinum was found to be 8 nm (± 2 nm) for samples with only platinum, whereas 4 nm (± 2 nm) for PtFe-NaY samples.

This chapter also describes the characterization of Cu-Co-Ce-O mixed oxide samples, with general formula $Cu_xCo_{(1-x)}Ce_2O_{4-\delta}$ (x = 0, 0.15, 0.25, 0.50, 0.75, 1.0). These catalysts were prepared by co-precipitation method, with various copper contents (5-15 wt %). It was observed for these samples, that the surface area decreased with cobalt content, which may be due to the formation of new phases of cobalt or may be due to the blocking of pores of ceria by clusters of cobalt. Techniques such as UV-visible, FTIR and PXRD reveal that copper species are present in tetrahedral sites with cobalt in octahedral sites. These materials were also characterized by using H_2-TPR, TEM, HRTEM and chemical analysis by AAS.

Chapter 3 describes the investigation of preferential oxidation of CO in excess hydrogen over Pt-NaY, promoted Pt-NaY and Cu-Co-Ce-O mixed oxide catalysts. This chapter has three parts. Part - A describes the evaluation of Pt-NaY catalyst for PrOx of CO, the effect of various reaction parameters such as catalyst composition, reaction

temperature, space velocity, O_2/CO ratio, CO concentration and water on CO conversion, O_2 conversion and CO oxidation selectivity. 0.75Pt-NaY with 0.75 wt% platinum exhibited good activity than other platinum NaY catalysts.

Part - B discusses PrOx of CO on platinum promoted NaY catalysts. These catalysts were prepared by ion exchange method by using different metals like Fe, Co and Au in addition to Pt. The effect of these transition metals with platinum on catalytic activity and influence of various parameters like composition, reaction temperature, activation temperature and time on stream is reported. The best results were obtained on PtFe-NaY catalyst with 0.75 wt % platinum and 0.38 wt % iron at 75 ^{0}C, whereas for catalyst with only platinum, a reaction temperature of 135 ^{0}C is required under similar reaction conditions and feed composition.

Particle size and support plays an important role for getting better activity for PrOx reaction. The addition of second metal helps in achieving better dispersion and catalytic activity towards selective CO oxidation. But the catalyst containing Co and Au along with platinum does not offer improved activity as in case with Fe promoted Pt-NaY. Two possibilities may arise, one the synergic effect between this metal will be less on NaY or second possibility may be the Co, Au and Pt are similar metals that compete for adsorption of CO which inhibits O_2 adsorption. But, iron appears to offer alternative site for O_2 adsorption rather than CO, which is less reactive than O_2. Oxygen and CO compete for same platinum site because in this (Pt-NaY) system, support is inactive for the PrOx reaction; it only facilitates better dispersion and high surface area.

Part - C presents catalytic activity over Cu-O-Ce-O mixed oxide samples, for the PrOx reaction. Studies similar to the one carried out on Pt-NaY were carried out and discussed in this part. The copper-cobalt containing ceria sample with x = 0.25 gave best results. Catalyst with only cobalt (x = 0) was not much active at low temperatures. However, the CO conversion was achieved at higher temperature, but not similar to the one that obtained over copper-cobalt catalysts. The reverse water gas shift reaction (RWGS) was observed in only copper containing ceria samples (x = 1) but it was totally suppressed by the addition of cobalt in the copper ceria sample. Methane formation was observed on copper-cobalt containing ceria samples at higher temperatures except on copper ceria and cobalt ceria catalysts.

Chapter 4 describes preparation and characterization results of Mo/Hβ and Mo/Fe-ZnO catalysts. Catalysts with different molybdenum loading were prepared by dry impregnation and characterized by powder X-ray diffraction, ICP-AES, surface area measurements, SEM, TEM, TPR/TPD, XPS, FTIR adsorption of pyridine and laser Raman spectroscopy. These characterization results revealed that the molecular structure of molybdenum species depends on the coverage of molybdenum. Monomeric molybdenum species are predominant at low molybdenum content, while polymeric molybdenum species increased with increase in molybdenum loading. FTIR and laser Raman studies showed the formation of silicomolybdic acid on Mo/Hβ catalyst. No MoO_3 phase was observed even for Mo loading as high as 10 wt % for Mo/Hβ samples by powder XRD. All diffraction peaks identified in Mo/Fe-Zn-O were for ZnO phase with hexagonal wrutzite crystal structure with average crystalline size of 22 nm. No diffraction peaks for Fe or Mo were observed by XRD in the case of Mo/Fe-Zn-O samples. Study of acidity (NH_3-TPD), H_2-TPR, UV-visible and others techniques used for characterizing these materials are discussed in detail in this chapter.

Chapter 5 describes the investigation of partial oxidation of methane to formaldehyde using oxygen in the form of air on Mo/Hβ and Mo/Fe-Zn-O catalysts. As observed, both the systems show good activity and selectivity towards formaldehyde with 3 percent metal loading. In general, the activity increases with reaction temperature and contact time with 9.25 mole % of oxygen in the feed, which is within the range of flammable limit (Flammable limit 5-15 mole % of oxygen). Space velocity, air/methane ratio, time on stream and effect of alternative oxidants like N_2O were the parameters studied by choosing best possible reaction conditions. The selectivity towards formaldehyde has decreased with increase in molybdenum content, which may be due to the polymeric molybdenum species, which may be responsible for combustion of methane. Variation of reaction temperature, iron and molybdenum content in Mo/Fe-Zn-O catalysts was explored and reported in this chapter.

For better understanding and correlation of the reaction data with characterization results this reaction was carried out on Mo/Al_2O_3 and Mo/SBA-15 prepared by the same procedure as used for Mo/Hβ. These results prove that the molybdenum species and the

acidity of the samples play an important role for partial oxidation of methane to formaldehyde, but not the surface area.

Finally, chapter 6 summarizes the conclusion arrived based on the above results and offers suggestion for further research.

6.2. GENERAL CONCLUSIONS

Preferential oxidation of CO is among the simplest, least expensive and most effective method for CO clean up from the H_2 rich reformates as compared to other methods used. It has been observed that platinum supported catalysts are highly active for the preferential oxidation of CO in excess hydrogen and these catalysts are also widely applied for several oxidation reactions. Here in this work active support like CeO_2 and non-active support like NaY were studied in detail. In PrOx reaction, the reactants are CO and O_2, while Pt and Cu metal species are most suited for their adsorption followed by the reaction. At low metal loading, the dispersion of these species was higher, hence better activity was observed. However, the activity was low at higher metal loading due to poor dispersion and bigger particle size. Addition of second metals like Ce, Fe, Co, Au and Ni is expected to reduce the reaction temperature. CO strongly adsorbs on Pt surface, inhibiting O_2 adsorption, so the addition of second metal (which adsorbs O_2 strongly rather than CO) should provide an extra site, that facilitate CO oxidation by creating a non-competitive, dual-site reaction mechanism. The activities of copper and cobalt supported on ceria were comparable to the performances of noble metal samples classically used for the PrOx reaction.

Though numerous studies on catalytic partial oxidation of methane to oxygenates have been undertaken, overall conversions and more importantly oxygenate selectivities are still uneconomical (except for those reported recently by Gesser and coworkers and Feng). Though this work on partial oxidation of methane to formaldehyde by using oxygen (air) as an oxidant, we show that the production of formaldehyde is feasible. The reaction can be carried out at atmospheric pressure at moderate temperature, which makes this process highly energy intensive. For this reaction, molybdenum based catalyst were studied in detail. The catalytic performance is very sensitive towards the structure of molybdenum species. As previous studies and reports suggest that the surface species

formed on the support play very important role on reactivity and selectivity. It is found that at low metal loading of Mo, predominant species were M=O, whereas at higher loading Mo-O-Mo species began to form at the expense of Mo=O sites. The tetrahedral molybdenum species with Mo=O sites were reported to be better for selective formation of formaldehyde than polymolybdate species with Mo-O-Mo bridging sites. The same results were observed in our studies.

6.3. SUGGESTIONS FOR FURTHER RESEARCH

This study shows that preferential oxidation of CO in excess of hydrogen using molecular oxygen is promising as an alternate method for conventional process used for removal of CO through methanation in industrial processes. The catalysts for this reaction are mostly prepared with alumina as support using precious metals like Pt, Pd, Ru and Rh with high metal loading (around 2 wt %). Hence these systems require extensive studies to reduce the precious metal content. Here in this work, we were successful in minimizing the metal loading. This reaction is very sensitive towards catalyst as well as reaction temperature. The catalyst structure has to be optimized by varying different parameters like preparation method, promoters etc. Studies proved that in PrOx reaction, metal crystallite size and dispersion of active metal play very important role for obtaining better CO conversion and CO oxidation selectivity. This can be achieved by using different supports such as zeolites as well as oxides, which helps for better dispersion and small particle size. Here in this work we studied NaY by adding different promoters like Au, Co and Fe with Pt, out of this PtFe-NaY shows better activity but it deactivates within few hours probably due to the formation of carbonate species. The formation of carbonates can be avoided by addition of other metals like Ce, Mn or Ru to the support. The supports play an important role in oxidation reaction, like ceria, which provides high oxygen storage capacity. We have evaluated ceria supported copper and cobalt catalysts for PrOx reaction. The activities of these materials were comparable to the performance of noble metal catalysts used for the PrOx reaction. The catalytic activity has gone down a little in the presence of water on these catalysts. Hence, there is a need for some improvement to these systems to sustain activity even in presence of water. Reducible supports like Fe_2O_3, TiO_2, MnO_2 etc. can be

used for this reaction to improve CO oxidation selectivity along with sustainability of activity in presence of water.

The vast worldwide reserves of natural gas, of which methane is the chief constituent, tempts to focus on the possibility of converting it directly to fuels and chemical intermediates in single step. The need for a process to convert methane to methanol and formaldehyde has been long perceived. At present the method for synthesis of methanol involves converting methane to synthesis gas, followed by selective synthesis of methanol with high efficiency. But the process is relatively costly and energy intensive. The method of direct conversion i.e. partial oxidation of methane to methanol or formaldehyde would be highly attractive, if this could be achieved economically. The present study shows that partial oxidation of methane using oxygen (air) is a promising method for the synthesis of formaldehyde. However, this is a preliminary study in laboratory scale and a lot need to be done for developing a viable process. Only Hβ and Fe-ZnO supports were examined in the current study while many other oxides as well as different zeolites with variable molybdenum content can be used as catalysts. The activity and selectivity of these molybdenum catalysts are significantly affected by the properties of support as well as molybdenum loading. For example, the activity in the oxidation of methanol to formaldehyde varies by several orders of magnitude among the following supports: Al_2O_3, Nb_2O_5, TiO_2, ZrO_2, CeO_2. Hence the effect of different support on the catalytic performance should be further studied.

In the present study, catalysts were prepared by dry impregnation and co-precipitation method. However, the effect of other preparation methods needs to be studied. Molybdenum sublimes at a temperature around 600 ^{0}C; this can be minimized by adding promoters like Co, W and Ni for the stabilization of molybdenum, which has to be investigated in detail. The formaldehyde selectivity of the system has to be improved. One significant problem observed with both the systems for selective oxidation of methane is deactivation. Further work need to be carried out to optimize the catalyst, probably with the help of promoters to zero-in on a good catalyst.

LIST OF PUBLICATIONS:

1) Influence of the support on the preferential oxidation of CO in hydrogen rich reformates over the $CuO-CeO_2-ZrO_2$ system. *J. Catal,. Vol - 221, 2 (2004) 454-465.* P. Ratnasamy, D. Srinivas, C. V. V. Satyanarayana, P. Manikandan, R. S. Senthil, **M. Sachin,** Vasudev N. Shetti.

2) Oxidative dehydrogenation of ethylbenzene over $Cu_{1-x}Co_xFeO_4$ catalyst system influence of acid-base property. *Catal. Lett., Vol - 91 (2003) 217-224.* Thomas Mathew, **Sachin Malwadkar**, Shivanand Pai, N. Sharanappa, C. P. Sebastian, C.V.V. Satanarayana and V. V. Bokade.

3) Low temperature water gas shift reaction on combustion synthesized Pt/CeO_2 Catalyst. *Catal. Lett., Vol-96, Nos 3-4 (2004) 213-218.* Parthasarthi Bera, **Sachin Malwadkar,** Arup Gayen, C.V.V.Satanarayana, B. S. Rao and M. S. Hegade.

4) Au-Pt - Bimetallic nanoparticals in MCM-41 material: Application in CO preferential oxidation. *Stud. Surf. Sci. Catal., Vol-146, 573-576.* Satyanarayana Chilukuri, Trissa Joseph, **Sachin Malwadkar,** S. B. Halligudi, Murali Sastry and Paul. Ratnasamy.

5) $CuCeO_2$ mixed oxides supported on Al-PILC: Effect of method of preparation on catalytic activity in the preferential oxidation of carbon monoxide (PROX). *Appl. Catal., B (29 February 2008, article in press)*. Veda Ramaswamy, **Sachin Malwadkar** and Satyanarayana Chilukuri.

6) Platinum nano catalyst by oleic acid method for low temperature oxidation of CO in excess of hydrogen for PEM fuel cells. *(Communicated).* **Sachin Malwadkar,** Tanushree Bala, B. L. V. Prasad and Satyanarayana Chilukuri.

7) Hydrogen purification for fuel cell: Preferential Oxidation of CO over Pt, Au- Pt Zeolite. *(Communicated).* **Sachin Malwadkar,** Anjali Gupta, Satyanarayana Chilukuri.

8) Gas-phase oxydehydrogenation of ethylbenzene with nitrobenzene to produce styrene and aniline on $Ni-CeO_2$ catalyst. *(Manuscript under preparation).* **Sachin Malwadkar** and Satyanarayana Chilukuri.

9) Synergistic effect of cobalt on preferential oxidation of CO over $CuCeO_2$ catalysts. *(Manuscript under preparation).* **Sachin Malwadkar**, S. P. Mirajkar and Satyanarayana Chilukuri.

10) Partial oxidation of methane to formaldehyde on molybdenum supported beta catalysts. *(Manuscript under preparation).* **Sachin Malwadkar**, Anil Kinage and Satyanarayana Chilukuri.

Awards:

"Best Poster Award" in 17 National Symposium of catalysis, 18 to 20 January 2005, CSMCRI, Bhavangar.

"Award of Senior Research Fellowship (SRF)" for 2005-2008 yrs. by CSIR, Govt. of India, New Delhi.

Workshop:

1) SERC Summer School of Fuel Cell.
   4th to 16th July 2005. Indian Institute of Technology, Pawai, Bombay.

2) National workshop on current opportunities and new directions in catalysis.
   8th to 10th February 2007. Bangalore Institute of Technology, Bangalore.

3) National workshop on Futuristic materials for catalysis and adsorbents.
   18th to 20th February 2008. Institute of Minerals and Material Technology, Bhubhaneswar.

SYMPOSIA AND CONFERENCES:

Oral presentations:

1) Paper Presented in 17 National Symposium of catalysis, 18 to 20 January 2005, CSMCRI, Bhavangar. ***Sachin Malwadkar,*** *Anjali Gupta and C. V. V. Satyanarayana.*

2) Paper presented in National seminar on Fuel Cell - Material, system & Accessories, 25 to 26 September 2003 NMRL, Ambernath. *C. V. V. Satyanarayana, H. S. Potdar,* ***S. Malwadkar,*** *N. Sharanappa, V. V. Bokade, P. Ratnasamy.*

Poster presentations:

1) Poster Presented in 17 National Symposium of catalysis, 18 to 20 January 2005, CSMCRI, Bhavangar. *R. A. Shaikh,* ***Sachin Malwadkar*** *and C.V.V. Satyanarayana.*

2) Poster Presented in National Science Day, 22 February 2007, NCL, Pune.
   Sachin Malwadkar, *Sivaram Pradhan, N. K. Rao and C. V. V. Satyanarayana.*

3) Poster presented in International Symposium of catalysis, February 16 to 18, 2007, IIP Dehradhun. ***Sachin Malwadkar,*** *Sivaram Pradhan, Atul Bansode, N. K. Rao and C. V. V. Satyanarayana.*

4) Poster presented in International Symposium of North American Congress on catalysis, 17 to 22 June 2007, Houston, USA. ***Sachin Malwadkar,*** *C.V.V. Satyanarayana and Veda Ramaswamy.*

5) Poster presented in National Symposium of catalysis, February 18 to 20 2008, IMMT Bhubhaneswar. ***Sachin Malwadkar,*** *Richa Nagarkar, N. K. Reji, Satyanarayana Chilukuri.*